HOLM OAK DECLINE IN HUMAN-SHAPED SAVANNAHS

PHYSIOLOGICAL AND ECOLOGICAL BASIS

MANUEL ENCINAS VALERO

PHD THESIS 2023

eman ta zabal zazu

Universidad del País Vasco

Euskal Herriko Unibertsitatea

¿Qué le pasa a una encina al defoliarse?

Podría estar horas intentando explicarlo con palabras y aun así no conseguiría que lo entendieras. Igualmente podrías leer la tesis y tampoco conseguiría que lo entendieras. Todo este cuarto de ideas está cerrado con llave e impide que salgan. Pero ¿por qué hemos de usar esa llave? No me gustaría mirar esta tesis en el futuro y ver un taco de doscientas páginas de palabras, sino algo que hablase sin siquiera abrir la puerta. Así no hace falta llave y así es como las veo en la dehesa.

Ilustración de portada: Vicky Ilhe (ilustradora)

Concepto: Manuel Encinas

BASQUE CENTRE FOR CLIMATE CHANGE
Klima Aldaketa Ikergai

eman ta zabal zazu
Universidad del País Vasco
Euskal Herriko Unibertsitatea

Holm oak decline in human-shaped savannahs: Physiological and ecological basis

Ph.D. Thesis

Manuel Encinas Valero

May 2023

Thesis supervisors

Prof. Jorge Curiel Yuste

Prof. Raquel Esteban Terradillos

Manuel Encinas Valero was funded by the Spanish Government through the IBERYCA project (CGL2017-84723-P), its associated FPI scholarship BES- 2014-067971. It was further supported by the BC3 María de Maeztu excellence accreditation ref. CEX2021-001201-M funded by MCIN/AEI/10.13039/501100011033; by the Basque Government through the BERC 2022-2025 program; and by the UPV/EHU-GV IT-1648-22 (from the Basque Government).

In addition, this work was also supported in by the Royal Botanic Garden at Kew, RGB, Fungal-Plant Interaction programme; the 'Juan de la Cierva programme' (IJCI-2017-34640; the Spanish Government); and one project funded by the Romanian Ministry of Research, Innovation and Digitization through UEFISCDI (REASONING,PN-III-P1-1.1-TE-2019-1099).

A Mamá,

Siempre caminas a mi lado

Acknowledgements

En el mundo de la ciencia son famosas las analogías que uno oye a cerca de lo que parece un doctorado. “Parece una montaña rusa” ¿Quién no se ha emocionado con unos resultados que luego resultaban ser erróneos? ¿Quién no se ha pasado una tarde entera bloqueado intentando relacionar ideas inconexas, frustrarse y diez minutos antes de volver casa todo cobraba sentido? ¿Por qué si hoy estás en el fondo de un pozo mañana estás en la cima? “Es como un embarazo” Algo que acabas amando, pero a veces pesa tanto. “Una mochila que llevas a todas partes” “Es todo un espectáculo”.

Pues ya que esto va de encinas, yo diría que es como un árbol. Como si fuese una bellota que encierra un proyecto rigurosamente redactado para convertirse en árbol, un plan de tesis empieza con un código genético de instrucciones planeadas para llegar a ser tesis. Pero ¿quién le dice a la bellota que no encontrará contratiempos? ¿Quién le dice al plan que va a crecer recto? Una tesis es un árbol, un potencial proyecto, flexible, modelado por las condiciones ambientales, que crece, cae, se retuerce, se defolia, rebrota y vuelve a elevarse. Y esa es la belleza del árbol, que no sabes en qué dirección crecerá mañana, ni que forma tomará. Cada nudo de su tronco es una batalla. A veces me pregunto cómo hubiera sido esta historia si no hubiera sido yo quien la hubiese escrito, qué ramas distintas hubieran crecido o cómo lo habrían contado. Y sin embargo, habría tenido el mismo inicio. Podrían haber sido miles de historias diferentes, miles de formas diferentes, pero me tocó a mí coger esa bellota y germinar…

Y este inicio no tiene detrás ninguna historia a cerca de perseguir el sueño de ser científico. Recuerdo que me solían preguntar al inicio del muestreo ¿te gusta la ciencia? ¿por qué te has metido a hacer el doctorado? a lo que dije de manera ingenua “Yo solo quiero salvar los árboles” Por eso quiero agradecer a mis dos directores de orquesta, de manera especial a **Jorge C.** el haberme entregado esa bellota y sobre todo el haberla cuidado. A **Raquel E.** de la que tanto he aprendido, aun siendo tan distintos. Finalmente, a **Ana H.** por contestarme que no olvidase nunca aquella respuesta y por todas las risas que vinieron después. Tenías razón, ha sido todo un espectáculo.

A mis colegas de grupo por ser los mejores compañeros que uno podría haber deseado. A **Leti P.** por todas las risas que nos hemos echado en la ofi y por ser la compañera que le da esa alegría especial al grupo. A mi hermano pequeño de tesis **Oti**, a quien deseo todo el éxito y la paciencia del mundo. A **Celine M.** por escucharme tanto y a **Phil M.** por ser la mente más brillante del grupo. A **Borja A.** el trabajazo que hizo con nosotros.

Thank you so much to my collegue of the Royal Botanic Garden at Kew. Specially to **Laura M.** for her patience. I will always remember those evening in the British pub having white wine and chips after the lab chaos one hour ago. Thanks to **Sophie L,** I hadn´t survive in the lab without you. Thanks to **Ricardo A.** and all the shared tips from a PhD expert to a PhD novice. Thank you very much to **Elena A**. Also thank you very much to **Julia** and all her enthusiasm and willingness to help in all aspects. Very special thanks to all my sportmates at Richmond canoe club, specially to **Eva, Tony** and **Sue**. I was always excited to train and have a great time with you all, particularly after a day of very hard work looking for mycorrhizae. Here is where

I really begin to learn how to paddle. You all made my stay in London one of the most valuable periods in this thesis.

Y que hubiera sido de mí sin los Junior researchers, o ECR de BC3. Ah! me llega un slack de que han vuelto a cambiarle el nombre al grupo. Bueno, de los JRERCYHCNFUR. Especialmente a mis compis de la generación del 19. A mis primeros compañeros de oficina: **María R**, **Estíbaliz S.** que junto a **Ana H.** aquello era de todo menos una oficina. A mis compis de fuera de la ofi a quienes he considerado como si fueran familia. Gracias A **Esti B.** y **Julia B.** por ese intento de secuestro milimétricamente ejecutado con el fín de acabar comiendo pollo en una cervecera. Gracias a **Patri M** y a **Nico**, sobre todo por no enfadaros a la hora de la comida. Ya sabéis porqué lo digo. Gracias A **Maria Mar S,** puede que no te lo creas, pero también has sido clave en esta tesis. Gracia también a **Elena L, Asun R, Itxaso R, Asma J, Alessandro S, Celina A, Nerea B, Alba M, Julia L, Dani C, Javi P, Luz D, Rubén S, Manuel T y Kevin P**. Gracias a **Guille JL**, podría escribir páginas enteras con nuestras chorradas, pero prefiero irme a vender cocos a Tailandia. Que suerte haberme sentado a tu lado.

A mis compañeros del laboratorio de fisio vegetal, especialmente a **Irati A** y a **Jon M** quienes me apoyaron en los peores momentos.

A mis amigos de Albacete y de Murcia: **Pedro J**, **Esther A**, **Adri G**, **Isa J** y **Miguel B**. Las vueltas a la tierra siempre se celebran a lo loco, pero ya vamos teniendo una edad y no aguanta el cuerpo tanto. Pero mientras podamos, a seguir disfrutando. Gracias a **Guille G**, pues, aunque sigan pasando los años siempre encontramos un sitio entre medias para vernos. Gracias a ti también **Jesús B**, por encontrar siempre un rato para charlar. Espero que sigamos muchos años más.

A mis compañeros de Barrika Piragua Taldea. **Ane R**, **Aitor B**, **Gema** y **Kerman**. A **Txomin V.** por acabar en el agua partiéndome de la risa con sus ocurrencias. Recuerda “no es paja, es ciencia.

Gracias a **Zhou Xin C.** y a **Cynthia L.** por atiborrarme a comida hasta hartarme.

Todos son de alguna forma coautores de esta tesis, pero si hay alguien que merece ir en la posición que le corresponde al “jefe” de la publicación eres tú **Cris M**. No existe nadie que sepa mejor cómo he vivido la tesis. Has venido a por mí a sujetarme en los peores momentos y has celebrado como si fuesen tuyos mis éxitos. Gracias por esa seguridad que me transmites, por leerte mis artículos, por perderte conmigo por esos laberintos en la dehesa de Siruela y sobre todo por acompañarme en este camino de la vida.

Con esta tesis no sé si habré salvado algún árbol, pero espero haber contribuido.

Contents

Abstract

The decline of holm oak trees in Iberian anthropic savannahs (dehesas) is a syndrome caused by the interaction of multiple stressors such as climate change-related events (i.e., extreme droughts), invasive pathogens and changes in dehesa use and management. These stressors are pushing Iberian oak dehesas to the brink of collapse. Holm oak decline is characterized by the loss of leaves (i.e., defoliation), however, the biochemical and physiological mechanisms that precede and follow defoliation and decline remain elusive. In addition, there is also a gap in our understanding of the functional role that soils, particularly soil microbial communities play in holm-oak decline. Soil microbial communities are, among other things, major responsible for making all essential nutrients (e.g. nitrogen or phosphorous) available for plant consumption. Therefore, exploring the relationship between the tree health and the associated soil microbial community, as well as the potential tree-soil feedback effects that arise during holm oak decline may help us to identify which soil conditions enhance holm oak health and improve its resilience to ongoing environmental stress. Hence, a holistic view of the problem is needed to predict, prevent and mitigate holm oak decline.

In this dissertation, we conducted a regional study in 9 dehesa sites to characterize the physiological (i.e., leaf-level photoprotective responses, photochemical efficiency and carbon allocation patterns), morphological (crown phenotype and root system structure) and ecological (i.e., plant-soil microbial community continuum and soil chemistry) responses underlying the declining process observed on holm oak.

Our findings demonstrated the holm oak ability to acclimate to the prevailing environmental conditions by maintaining homeostasis through the adjustments of the photoprotective compounds (i.e., total xanthophylls, VAZ and total tocopherols). In this regard, we proposed VAZ and tocopherols as early stress indicators of holm oak decline as these compounds increased before declining symptoms (i.e., defoliation) were evident. However, once the stress exceeded certain limits, we observed an evident sign of defoliation. This was associated with the identification of a physiological threshold for total tocopherol that indicated a point beyond which the tree was unable to cope with the current stress conditions and defoliation symptoms appear. This point, coincided with a shift in tree energy allocation (i.e., non-structural carbohydrates) to optimize soil resource acquisition by developing and maintaining a high fine root phenotypic plasticity. The shift towards a high plastic root system was done at the expense of maintaining leaves (defoliation).

The progressive loss of tree health was further reflected in the relation of the tree with the soil microbial community responsible for nutrient mineralization. Indeed, our results showed how the loss of crown health was strongly related with the upregulation of certain biogeochemical steps, mainly denitrification and phosphorus solubilisation, responsible for the downregulation of soil nutrients (i.e., N and P), essentials for maintaining a healthy crown. Thus, we described a tree soil feedback loop in which the holm oak declining process led to net losses of soil nutrients which, in turn, was associated with the loss of tree vigour.

All these results shed light on previously unknown aspects of holm oak decline by characterizing, firstly, those factors that define tree health at the leaf and organismal level, secondly, by describing some of the key mechanisms behind the loss of tree health, and thirdly, by identifying different levels of tree responses to stress, including how trees interact with soils and soil microbial communities. The knowledge obtained in this thesis could be of special relevance to facilitate the implementation of practices aimed at predicting, preventing and mitigating the decline of holm oak trees in the Iberian dehesa..

Resumen

El decaimiento de la encina en la dehesa es un síndrome causado por la interacción de múltiples factores de estrés como son los fenómenos relacionados con el cambio climático (por ejemplo, sequías extremas), patógenos alóctonos o cambios en el uso y gestión de las dehesas. Estos factores representan una seria amenaza para la continuidad de la dehesa. El decaimiento de la encina se manifiesta por la pérdida de vigor y follaje, sin embargo, los mecanismos bioquímicos y fisiológicos que se desencadenan antes y durante el proceso de decaimiento no son muy conocidos. Además, también es limitado el conocimiento acerca del papel funcional que desempeñan los suelos, en particular las comunidades microbianas, en el decaimiento de la encina. Las comunidades microbianas del suelo desempeñan un papel clave al ser las responsables de la disponibilidad de los nutrientes esenciales (como el nitrógeno o el fósforo) para el crecimiento y desarrollo de las plantas. Así pues, investigar la relación existente entre la salud del árbol y la comunidad microbiana del suelo asociada, así como los potenciales efectos recíprocos que surgen durante el decaimiento de la encina, puede ayudarnos a identificar qué condiciones del suelo mejoran la salud de la encina y su resiliencia frente al estrés ambiental. En este contexto, se requiere de una visión holística de la situación con el fin de predecir, prevenir y mitigar el decaimiento de la encina en la dehesa.

En esta tesis doctoral, se llevó a cabo un estudio regional en nueve dehesas con el objetivo de describir las respuestas fisiológicas (respuestas fotoprotectoras a nivel foliar, eficiencia fotoquímica y patrones de redistribución de carbono no estructural), morfológicas (estructura de la copa y del sistema radicular) y ecológicas (es decir, continuum de la comunidad microbiana planta-suelo y química del suelo) asociadas al decaimiento de la encina en la dehesa.

Nuestros resultados demostraron la capacidad de la encina para aclimatarse a las condiciones ambientales de la dehesa y mantener la homeostasis a través de ajustes en los compuestos fotoprotectores (pigmentos del ciclo de la vioaxantina, VAZ y tocoferoles totales). Así, propusimos el contenido en VAZ y en tocoferoles como indicadores tempranos decaimiento de la encina, ya que estos compuestos aumentaron antes de que los síntomas de decaimiento se manifestasen. Sin embargo, una vez el estrés superó ciertos límites, observamos signos evidentes de defoliación. Esto se asoció con la identificación de un umbral fisiológico en el tocoferol total que supuso un punto de inflexión a partir del cual el árbol no era capaz de hacer frente a las condiciones de estrés de la dehesa y aparecían síntomas de defoliación. Este

punto, también coincidió con un cambio en la reedistribución de los sustratos energéticos que el árbol emplea para su desarrollo (carbohidratos no estructurales). Este proceso presumiblemente optimiza la adquisición de recursos del suelo mediante el desarrollo y mantenimiento de una alta plasticidad fenotípica en las raíces finas. El cambio hacia un sistema radicular de alta plasticidad se producía a costa del mantenimiento del follaje. Además, la pérdida progresiva de la salud del árbol afectó a la relación recíproca del árbol con la comunidad microbiana responsable de la mineralización de nutrientes del suelo. Así, las observaciones demostraron cómo la pérdida de salud de la copa estaba vinculada con la intensificación de ciertos pasos biogeoquímicos, principalmente la desnitrificación y la solubilización de fósforo. Estos pasos eran responsables de reducir los nutrientes del suelo (es decir, N y P), esenciales para mantener una copa sana. De esta manera, se describió un proceso de retroalimentación del sistema árbol-suelo en el que el decaimiento de la encina provocaba pérdidas de nutrientes del suelo y esta a su vez a su vez, ocasionaba la pérdida de vigor del árbol.

En definitiva, estas observaciones revelan aspectos desconocidos a cerca del decaimiento de la encina en la dehesa, al caracterizar, en primer lugar, aquellos factores que definen la salud del árbol a nivel foliar y de organismo; en segundo lugar, al describir algunos de los mecanismos que se desencadenan durante el proceso de pérdida de salud del árbol; y, en tercer lugar, al incluir cómo interactúa el árbol con el suelo y las comunidades microbianas. Los conocimientos obtenidos en esta tesis podrían ser de especial relevancia para facilitar la implementación de prácticas encaminadas a predecir, prevenir y mitigar el decaimiento de las encinas en la dehesa ibérica.

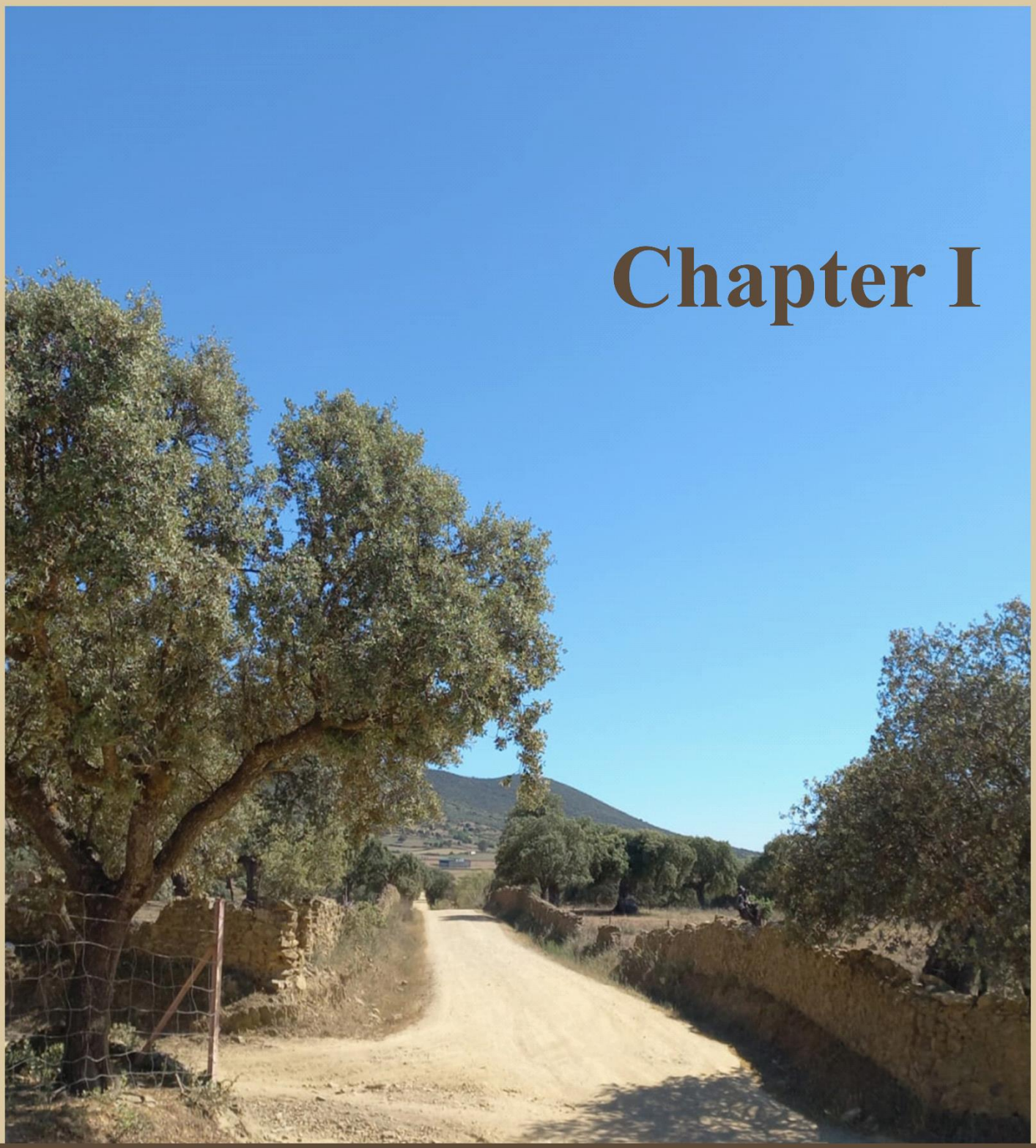

Chapter I

General Introduction

1.1. Forest decline as a global phenomenon

Tree decline and mortality are signs of climate stress that forest ecosystems have experienced in the last decades due to climate change (Vicente-Serrano *et al.*, 2013; IPCC, 2014; Cailleret *et al.*, 2019). All over the world, climate-model projections, both for short- and long-terms, estimate warming and drying trends, extreme temperatures and precipitations, ocean acidifications and other natural disturbances, such as damaging cyclones and floodings. These estimations are expected to have an important impact on forest ecosystems (IPCC, 2014). Tree mortality triggered by climate change-related events is a major concern and since the 1960s an increasing number of studies have pointed out this issue as a global phenomenon. The first global systematic review that assessed tree decline and mortality due to increasing temperature and drought was published more than a decade ago (Allen *et al.*, 2010). Nevertheless, this phenomenon has been updated over the years (Allen *et al.*, 2015; Hammond *et al.*, 2022; Hartmann *et al.*, 2022), increasing the number of reported sites and species that experienced climate-induced tree decline and mortality. Drought induced-tree mortality, also termed "tree die-off", refers to events when tree mortality affects a considerable number of individuals within a population in forests. It is usually related to tree decline or die-back, however, this last term is used in cases where only partial mortality occurs in some part of the tree (Martínez-Vilalta *et al.*, 2012). Understanding the relationship between environmental conditions and tree decline and mortality is of paramount importance to link die off-events to causal climate drivers and predict this phenomenon in the future (Allen *et al.*, 2010). Hence, Hammond *et al.*, (2022) identified a global hotter-drought fingerprint from the peer-reviewed studies published since the 1970s that reported tree mortality (**Fig. 1**). This fingerprint revealed that the forests experienced climate-induced die-off were closely related to the unusually higher temperature and water deficit not only in the year when die-off event occurred but also one year prior and after the event.

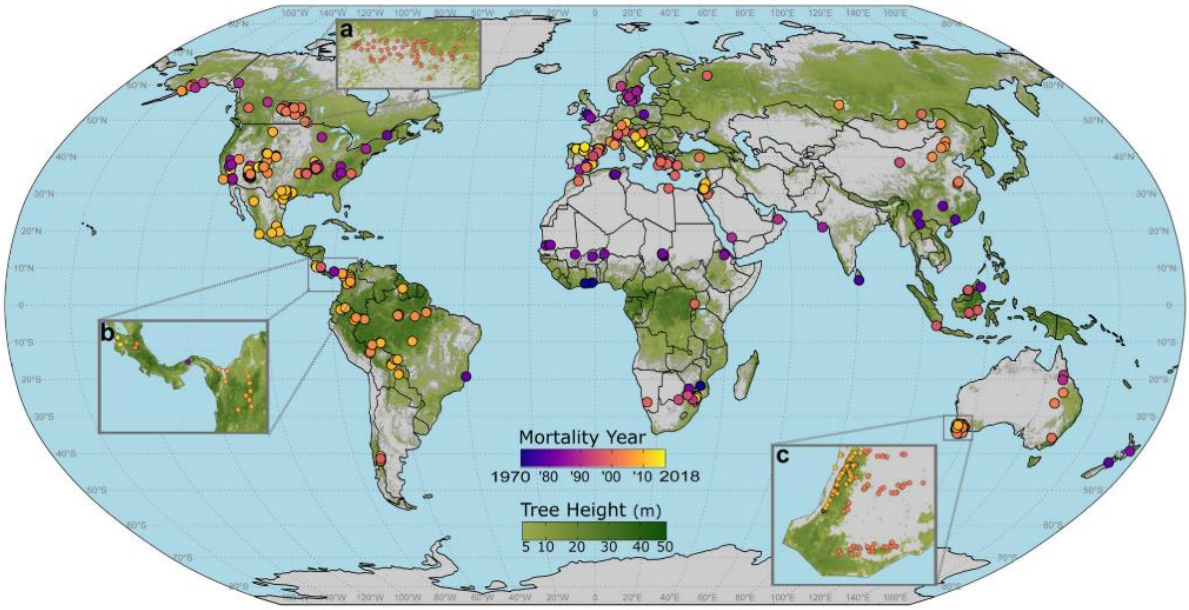

Figure 1. Global locations of the hotter-drought tree mortality plots (n=1303). The colour of the dot indicates the tree mortality year. The background layer in green indicates canopy height. (Hammond et al., 2022)

1.2. What are the declining patterns in the Mediterranean basin?

The Mediterranean basin is one of the global regions with the highest risk to be affected by climate change. Over the last century, abnormal increases in temperature along with reductions in precipitations have been observed (Cramer *et al.*, 2018). Despite presenting well-adapted vegetation to the harsh environmental condition (García-Plazaola *et al.*, 2008; Fernández-Marín *et al.*, 2017) studies have put into perspective the potential risk that these sorts of events may have even in typically drought-resistant species (Peñuelas *et al.*, 2001; Vicente-Serrano *et al.*, 2013). Mediterranean region is considered to be especially vulnerable to forest die-offs. In the Iberian Peninsula, the drought and heatwaves occurred (i.e.,1990-1995, 2000, 2003, 2005) resulted in severe crown defoliation in Mediterranean tree species such as evergreen oaks (*Quercus ilex* L., *Quercus suber* L., *Quercus faginea* Lam.), pines (*Pinus pinea* L., *Pinus halepensis* Mill.) or Spanish juniper (*Juniperus thurifera* L.) (Carnicer *et al.*, 2011). These recurrent drought events reduce tree resilience and its ability to recover an efficient functional crown, increasing the risk of mortality (Bréda *et al.*, 2006; Gazol *et al.*, 2018).

1.3. The focus of this work: Holm oak (*Quercus ilex* L. subsp. *ballota* (Desf.) Samp.) decline in dehesas

Holm oak decline is common in the Mediterranean basin. This phenomenon has been observed in; Spain and Portugal (Brasier, 1992; Camilo-Alves *et al.*, 2013; Corcobado, 2013), Italy (Frisullo *et al.*, 2018; Pasquini *et al.*, 2023), Morocco, Algeria (Mahamedi *et al.*, 2020); or Croatia; (Pernek *et al.*, 2022). Since the 1990s an increasing trend in holm oak defoliation and decline have been observed, being nowadays the most defoliated tree in Europe (Forest Europe, 2020; Sánchez-Cuesta *et al.*, 2021; López-Ballesteros *et al., in press*). However, the different land use practises (i.e., coppices or dehesas) to which holm oak is subjected determine its performance to drought conditions and the causes of the decline (Gazol *et al.*, 2021; López-Ballesteros *et al., in press*).

1.3.1. Dehesas, exclusive agrosilvapastoral systems

In this thesis, we investigate climate change induced-holm oak decline and mortality in the Spanish woodland, commonly named "*dehesa*" (and stated as this hereafter). Dehesas are exclusive agrosilvopastoral systems as the result of the autochthonous Mediterranean forest management and transformation (by ploughing and clearing shrubs and evergreen trees, such as holm and cork oaks) to obtain "defended grazing areas" (**Fig. 2**). In Spanish documents of the XII century, the term *deffesa* referred to a defended or restricted land against the open grazing transhumant herds of La Mesta (Arias Sánchez, 2015). Thus, dehesas constituted privately owned farms where the landlord obtained cropping or livestock benefits. This land use and management allowed higher tree development (i.e., wider canopy and trunk diameter) compared with trees growing in the autochthonous Mediterranean forest (Moreno & Pulido, 2009; García-Angulo *et al.*, 2020) and consequently higher acorn production (Pulido & Díaz, 2005). In recent years, the term dehesas has been used in the academic context to refer to a land characterized by scattered oak trees with a cropped or grazed understory that integrates livestock grazing, crops and in some cases wood production. Nevertheless, treeless grasslands as a consequence of complete deforestation are also considered a dehesa. (Díaz & Pulido, 1997).

The dehesas cover a vast area of 4.1 million hectares in the Iberian Peninsula, converting them in the largest European farming system with high nature value (Plieninger *et al.*, 2021). These ecosystems are included in the pan-European network of protected areas, Natura 2000, and contain a high level of biodiversity due to the diverse habitats that comprise

(Moreno *et al.*, 2016). Dehesas also provide provisioning services, such as cork, timber, acorn, crop and livestock benefits, as well as regulating ecosystem services like water fluxes regulation, carbon storage, and fire prevention (Bugalho *et al.*, 2018). In addition, the dehesa has been developed in the Iberian peninsula for centuries, becoming an integral part of the landscape and contributing to the cultural identity of the region (Álvarez, 2016). In fact, the stone walls that limited the old transhumance tracks and the dehesas can still be observed nowadays (cover photo of this chapter; Bugalho *et al.*, 2018). This constitutes a cultural heritage resulting from the constant struggles between the farmers and the herds of La Mesta (Rodríguez-Serrano, 2011)

Figure 2. Dehesas are a unique ecosystem in the south-western of the Iberian Peninsula characterized by a savannah-like landscape with scattered oak trees and grazing livestock (Image by Raquel Esteban).

1.3.2. Current threats to dehesa ecosystems

In the last decades, profound changes in land management have threatened dehesa ecosystems. Since the 1980s the rate of loss for this ecosystem has significantly increased (Plieninger, 2006). Several threats impact the sustainability of the dehesa. For example, the loss of rural population has led to the lack of maintenance in this ecosystem and has promoted shrubs encroachment that competes with the tree layer for resources. Overexploitation such as a more intensive grazing regime and changes in crop cultivation (Moreno *et al.*, 2007) have led to soil degradation and the lack of tree regeneration, preventing seedlings and saplings (Moreno-Fernández *et al.*, 2019). Additionally, the conversion of the land use through the removal of the oaks to a new land system compromises the future of the dehesa (Plieninger *et al.*, 2021). These substantial changes have been accompanied by climate change-related events

such as drought and heat waves inducing tree decline and mortality (Sánchez-Cuesta *et al.*, 2021) and reducing its density and cover in dehesas (Díaz & Pulido, 1997; López-Sánchez *et al.*, 2018; Plieninger *et al.*, 2021). Moreover, pathogen outbreaks such as *Phytophthora* spp root-rot (more details in the forthcoming section) and other opportunistic pathogens make trees more vulnerable to the ongoing stress induced by climate change.

1.3.3. The problem of an allochthonous pathogen

Phytophthora cinnamomi Rands was isolated from declining trees in the 1990s (Brasier, 1992, 1996) and since then it has been considered the main biotic factor associated with tree decline in dehesas (Gazol *et al.*, 2021). However, in the last years, studies of the soil microbiome have isolated several pathogens from declining trees apart from *P. cinnamomi* such as *P. quercinea* (Mora-Sala *et al.*, 2018), *P. psycrophila* (Ruíz-Gómez *et al.*, 2019a), *P. gonapodyides* (Corcobado *et al.*, 2010) or *P. megasperma* and *P. nicotianae* (Mora-Sala *et al.*, 2019). These species have different levels of virulence (Mora-Sala *et al.*, 2019) and studies have demonstrated that the co-infection of these species may alter the mortality rate of holm oak. For example, prior infection of the less virulent species (i.e., *P. gonapodyides*) increases the survival rate before the infection of the most virulent species (i.e., *P. cinnamomi*; (Corcobado *et al.*, 2017). This may support the hypothesis that soils with a high diversity of oomycetes decrease the ability of the most severe species to infect roots (Ruíz-Gómez *et al.*, 2019a).

The infective agent that initiates the plant disease is the motile biflagellate zoospores of the oomycete that allows it to move through soil water (Hardham & Blackman, 2018). This aspect is key during its asexual phase and provides it the capacity to infect in the short conductive periods of the Mediterranean climate (Cahill *et al.*, 2008). Hence, water condition is a significant component in root infection (Sánchez-Cuesta *et al.*, 2022). In this sense, Sánchez-Cuesta *et al.*, (2021) observed higher rates of holm oak decline and mortality in infected plots during wet years. When the infection body (i.e., zoospores, chlamydospores) reaches the host root surface, the haustorial structure is developed and hyphae penetrate epidermal cells, invading cortical and mainly phloem tissues (Redondo *et al.*, 2015). As a consequence of the infection, roots exhibit dark-brown spots, necrosis lesions, root softness and lack of secondary roots (Ruíz-Gómez *et al.*, 2018b). These results are in line with studies at field conditions that report a reduction of fine root density in declining holm oaks (Corcobado *et al.*, 2013b, 2014b). The reduction of the root mass fraction prevents holm oak to uptake soil resources (Redondo *et al.*, 2015). This fact makes holm oak more vulnerable to

the Mediterranean seasonal drought and climate change extreme events, contributing to holm oak decline and death (Ruíz-Gómez *et al.*, 2015, 2018b; Sánchez-Cuesta *et al.*, 2021).

1.4. How do declining factors interact?

Dehesas experienced tree mortality is considered a complex multifactorial phenomenon influenced by several biotic and abiotic factors. Drought and heatwaves-induced holm oak decline and mortality cannot be understood without accounting for the effect of land use and management, *Phythopthora* spp root infections, and the interaction with other factors present in dehesas (i.e., topography and soil conditions). All these factors and their interactions make it challenging to unravel the main driver of holm oak decline (Camilo-Alves *et al.*, 2013). According to the adapted Manion`s disease spiral (**Fig. 3**), these factors may include i) predisposing factors (i.e., *Phytophthora* spp, soil conditions and topography) that increase tree susceptibility and reduce its resilience to inciting factors (see below). The predisposing factors include those conditions that reduce root efficiency to uptake soil resources (i.e., water and nutrients) and increase tree susceptibility to drought. For instance, shallow and rocky soils or shrub encroachment are associated with a reduction in water availability and may promote tree decline (Augusta *et al.*, 2010). In addition, soil waterlogging conditions favoured by clay texture, soil compaction or stream bank locations favour root infection by *Phytophthora* spp (Corcobado *et al.*, 2013b,c). The inciting factors (i.e., drought legacies and heat waves), are the main drivers of declining symptoms that lead to death (Gea-Izquierdo *et al.*, 2021). Long-term monitoring studies in dehesas point out that the annual mean temperature is a good predictor of holm oak defoliation and decline (Sánchez-Cuesta *et al.*, 2021). Finally, contributing factors include opportunistic and secondary pathogens that affect trees already weakened, accelerating the declining process (Gentilesca *et al.*, 2017).

Overall, inciting factors are identified as the main driver of holm oak decline. Nevertheless, the absence of this stress may allow holm oak to recover from *Phytophthora* spp root infection (Ruíz-Gómez *et al.*, 2018). Thus, the expression of the symptoms depends on specific soil conditions that favour root rot infection (Gentilesca *et al.*, 2017). Adequate water and nutrient soil conditions, or site-specific locations and soil texture that avoid waterlogging or root infection allow trees to cope with drought and may prevent declining symptoms even when the pathogen is present (Manion, 1981; Camilo-Alves *et al.*, 2013; Serrano *et al.*, 2013; Ruíz-Gómez *et al.*, 2018; Sánchez-Cuesta *et al.*, 2022).

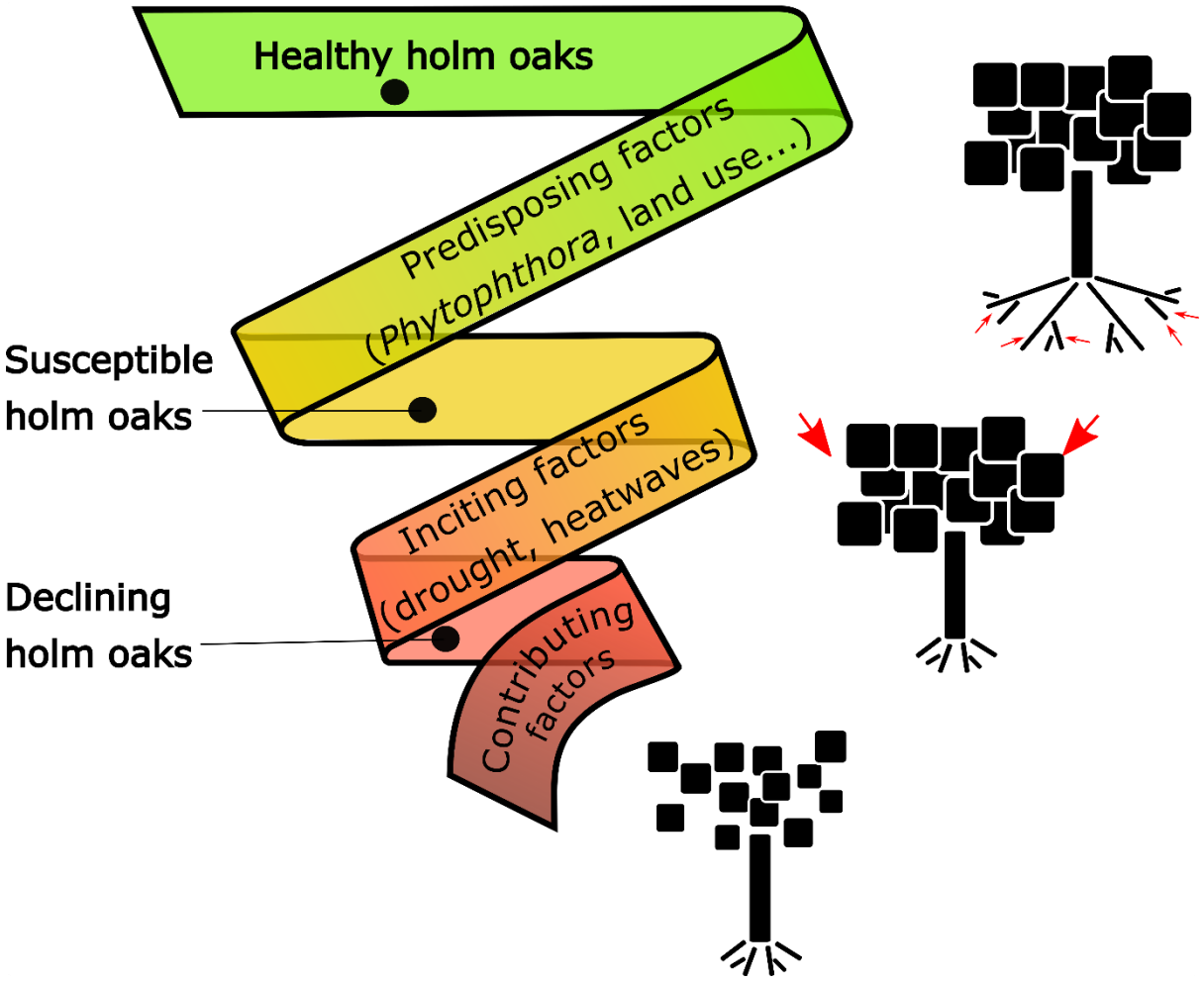

Figure 3. Adaptation of Manion's (1981) disease spiral (left) with the main driving factors associated with holm oak decline. Red arrows indicate the stress factors affecting a part of the tree. Redrawn from Camilo-Alves *et al*., 2013.

1.5. Declining symptoms: a scaling-down perspective

1.5.1. Declining symptoms at the ecosystem level

The nature of the holm oak decline and mortality in dehesas shows a particular pattern. "Healthy" (areas where trees showed no evident signs of defoliation) and "unhealthy" zones present a spatial separation (**Fig. 4a**). This patchy pattern is characterized by declining or unhealthy foci (Brasier, 1992, 1996; Cardillo *et al.*, 2021) where trees present declining symptoms (i.e., wilting, drying branches, defoliation) that decrease from the centre of the foci to the periphery (Sánchez *et al.*, 2002). The reason for this declining pattern is mainly due to the way *Phytophthota*-induced diseases spread within a stand. Studies have shown that the abundance of host trees and their proximity to the nearest infected tree are significant factors contributing to an increased risk of infection (Jules *et al.*, 2014). In addition, the distribution of unhealthy sites in dehesas responds to spatially preferred soils that *Phytophthora* spp exhibits

for certain specific conditions (water-holding soils such as fine-textured soils or stream banks; Augusta *et al.*, 2010; Gómez-Aparicio *et al.*, 2012; Corcobado *et al.*, 2013c).

1.5.2. Declining symptoms at the crown level

Holm oak declining symptoms at the crown level are unspecific and resemble those of water deficit. It has been described two types of syndromes: a progressive process of defoliation that may affect the whole crown or just some branches (i.e., branch dieback) and a sudden death characterized by chlorotic and wilted leaves that remain attached to the branches (Brasier, 1996; Sánchez *et al.*, 2002; Camilo-Alves *et al.*, 2013; Ruíz-Gómez *et al.*, 2018b; San-Eufrasio *et al.*, 2021). In both cases, these symptoms are followed by the death of the tree.

Crown dieback or defoliation indicates the tree´s inability to withstand adverse environmental conditions and is the main indicator of holm oak decline (**Fig. 4b**). These symptoms are the result of an accumulative process due to the long-term drought rather than an immediate response to adverse environmental conditions (Gea-Izquierdo *et al.*, 2021; Sánchez-Cuesta *et al.*, 2021). Defoliation is defined as the loss of leaf percentage compared to a reference optimum (Rodríguez-Calcerrada *et al.*, 2017) and may be a consequence of a premature leaf fall but also due to a limited crown development. For example, the number of new leaves and internodes formed within a bud is reduced in the year when drought occurred (Bréda *et al.*, 2006). Furthermore, when those buds flush the following year, drought reduces leaf area and shoot extensions (Bréda *et al.*, 2006). In this sense, this reduction in leaf area and the enhancement of crown transparency and defoliation have been used to assess tree health and vitality in a European forest and its trend in time and space (Forest Europe, 2020; Michel *et al.*, 2020).

Defoliation has been observed to increase for the last 30 years in holm oak, being nowadays the most defoliated tree in Europe (Forest Europe, 2020; Michel *et al.*, 2020). This defoliation assessment has been employed to evaluate the association between holm oak decline with root pathogens (Gallego *et al.*, 1999; Sánchez *et al.*, 2002; Corcobado *et al.*, 2010, 2017; Ruíz-Gómez *et al.*, 2019a), microbial soil functional groups (Corcobado *et al.*, 2015; García-Angulo *et al.*, 2020; Gómez-Aparicio *et al.*, 2022), soil conditions (Corcobado *et al.*, 2013b,c; Rodríguez *et al.*, 2016), biogeochemical cycles (Rodríguez *et al.*, 2019), climatic factors such as drought and heatwaves (Ogaya & Peñuelas, 2006; Forest Europe, 2020; Gea-Izquierdo *et al.*, 2021; Sánchez-Cuesta *et al.*, 2021), topography (López-Ballesteros *et al.*, *in*

press) and tree functional traits (Pollastrini *et al.*, 2016; Hornero *et al.*, 2021; Pasquini *et al.*, 2023) to determine the causes and effects of this syndrome.

1.5.3. Declining symptoms at the physiological level

The majority of studies evaluate declining symptoms at the physiological level in nursery conditions (i., seedlings). In these studies, the effects of the factors that presumably induce holm oak decline (drought treatment, inoculation with *Phytophthora* spp and its interaction) are evaluated. While it is difficult to extract a general response to translate to adult trees growing in the field, these studies agree that physiological symptoms observed, such as stomatal conductance, leaf water potential, CO_2 assimilation, quantum yield and water use efficiency reduction, are due to the individual effect of drought or *Phytophthora* spp and/or its interaction (Corcobado *et al.*, 2014a; Ruíz-Gómez *et al.*, 2018b, 2019b; San-Eufrasio *et al.*, 2021). These results are consistent with those reported by Corcobado *et al.* (2013b) at field conditions in which declining holm oaks exhibited symptoms of drought stress such as lower leaf water potential, lower stomatal conductance, and a reduced CO_2 assimilation (**Fig. 4b**). Furthermore, the physiological assessment at the stand and regional scale, using remote sensing techniques, also reported a reduction of quantum yield, as well as chlorophylls and carotenoids (Hornero *et al.*, 2021).

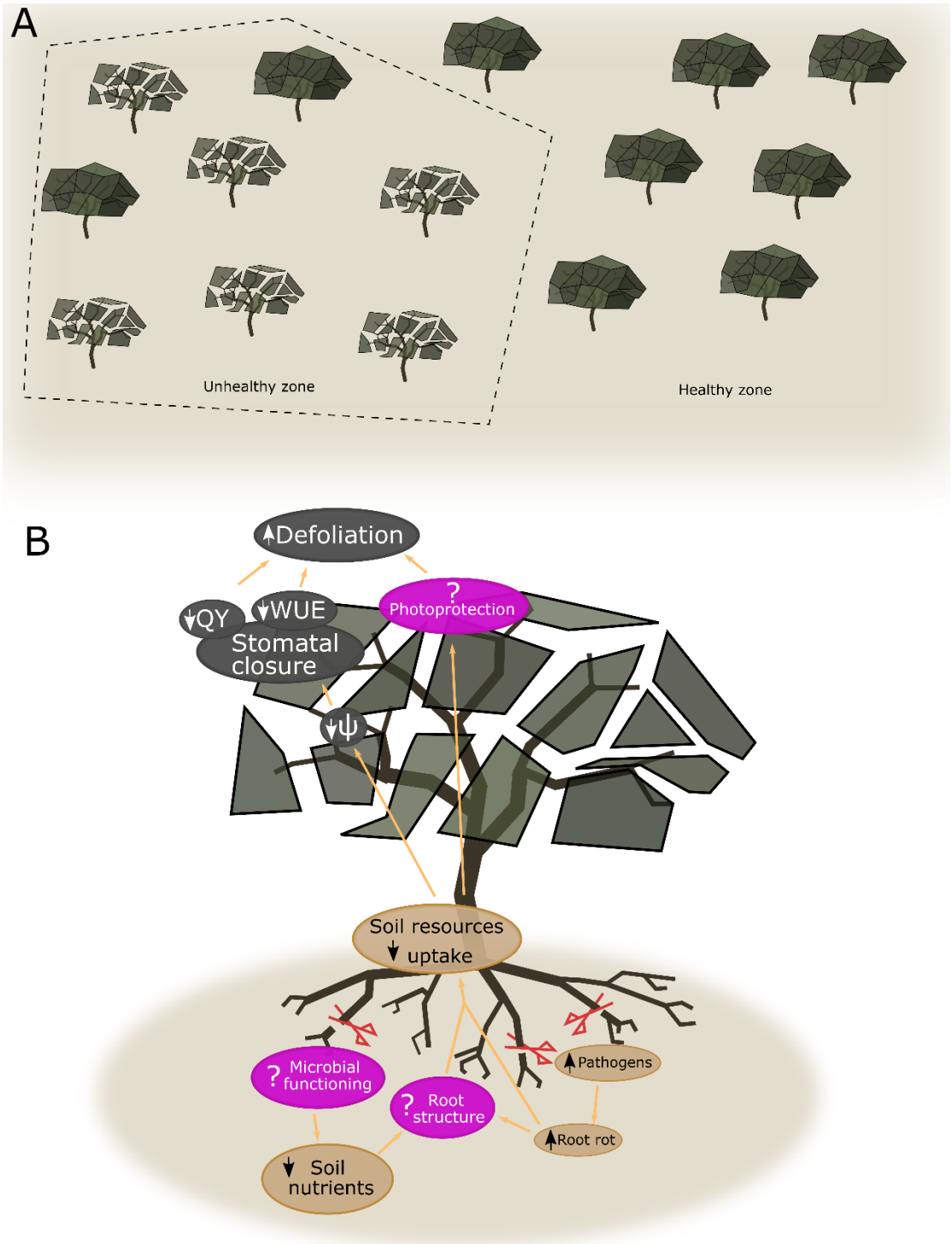

Figure 4. Conceptual depiction of the holm oak declining symptoms at: ecosystem level (panel A), tree level (panel B; including tree physiologicaland soil system level. Pink ellipses represent how the aims of this thesis align within the scheme. Leaf water potential, ψ; quantum yield of the photosystem II, QY; water use efficiency, WUE. Redrawn from Ruíz-Gómez *et al.*, 2019.

1.6. Physiological mechanism underlying tree mortality

In section 1.5., we explain the declining patterns observed in dehesa ecosystem, including those symptoms at the tree and physiological levels. When the environmental conditions that induce tree decline are prolonged, tree death may occur. Since the last decade's hydraulic failure (i.e., embolism) and carbon starvation (McDowell *et al.*, 2008) were two of the proposed mechanism underlying drought induced-tree decline and mortality. Both mechanisms are coupled by stomata closure and water use efficiency (Bréda *et al.*, 2006). The first mechanism proposed an irreversible xylem dysfunction once drought overcomes a physiological threshold while the second refers to a depletion of the storage carbohydrates pool as a result of the drought-induced-stomatal closure and photosynthesis limitation. Depending on the stomatal behaviour of each species, mortality would be triggered by hydraulic failure (i.e., anisohydric species as *Q. ilex*) or carbon limitation (i.e., isohydric species; McDowell et al., 2008). However, this hypothesis was questioned due to the lack of evidence that water stress consistently leads to carbon depletion (Sala *et al.*, 2010; Hartmann, 2015). For example, carbohydrate-related studies on oak trees reported contrasting results, as the carbohydrates pool decreased (Hartmann *et al.*, 2013) or did not change in response to drought (Villar-Salvador *et al.*, 2004; Sanz-Pérez *et al.*, 2009; Zang *et al.*, 2014). By contrast, xylem hydraulic failure is ubiquitous across different tree taxa subjected to drought (Adams *et al.*, 2017) and may be a more plausible mechanism underlying drought-induced tree mortality. Accordingly, recent investigations have related tree mortality with sequential changes in hydraulic conductivity. Before visual signals of tree mortality were evident, Preisler *et al.*, (2021) reported a stem shrinkage followed by a reduction in stem diurnal fluctuation and finally a cessation of sap flow. The reduction of this stem diurnal fluctuation is identified as a potential point of no return since these fluctuations, resulting from radial water flow in the morning and night did not recover the normal trend even after the drought was alleviated by precipitation (Preisler *et al.*, 2021).

1.7. Adaptation and tolerance mechanisms to environmental stress: an above and belowground perspective in holm oak.

Among the strategies to withstand water stress, acclimation/tolerance and avoidance are the most common. The first one allows plants to withstand a decrease in water potential and protect the cell against the damage arising from water stress, whereas, the second mechanism involves the maintenance of an adequate water status by regulating the water that leaves lose and the water that roots uptake (Fromm, 2019; Schulze *et al.*, 2019). Given the current and future threats in the context of the Spanish dehesa (i.e., climate change-induced drought and heatwaves, *Phytophthora* spp root infections and changes in dehesa use and management) the ability to withstand changing environmental conditions is essential for holm oak survival in these ecosystems.

To mitigate the effect of the environmental stresses that lead to tree decline and eventually to death, holm oak sets an array of morphological, physiological and biochemical responses to survive. Specifically, these responses include controlling stomata aperture to reduce water loss and prevent xylem cavitation (Quero *et al.*, 2008; Peguero-Pina *et al.*, 2018), implementing photoprotection mechanism to avoid photo-oxidative damage (Camarero *et al.*, 2012; García-Plazaola *et al.*, 2017), investing preferentially in root growth at expense of stem and leaf development; Ruíz-Gómez *et al.*, 2018b), executing changes in root structure to increase soil resource acquisition (León *et al.*, 2017; Łakomy *et al.*, 2019; Vivas *et al.*, 2021) or applying cell-level modification to prevent *Phytophthora* spp root infection (Ruíz-Gómez *et al.*, 2015). In the context of this thesis, we focused on some of these mechanisms (i.e., photoprotection and changes in root structure) and provide further information in the following lines.

1.7.1. Aboveground leaf biochemical adjustments: the leaf as the protagonist

In the range of conditions imposed by drought stress (between the water potential that induces stomatal closure and water potential that induces xylem cavitation), the energy of excited chlorophyll cannot be directed to the photosynthetic electron transport chain and reactive oxygen species (i.e, ROS as singlet oxygen, superoxide radicals, hydrogen peroxide or hydroxyl radicals) are generated if the excited chlorophyll state is extended (García-Plazaola

et al., 2017). To avoid these ROS photoprotection mechanisms allow Mediterranean species to prevent damage to the photosynthetic apparatus and acclimatize or even tolerate drought conditions (García-Plazaola *et al.*, 2008; Fernández-Marín *et al.*, 2017). These mechanisms operate in a hierarchical level: i) reducing the absorption of light, ii) enhancing energy dissipation iii), increasing the metabolic utilization of absorbed light energy iv) activating antioxidant mechanisms to quench ROS and v) repairing damaged structures (Camarero *et al.*, 2012; García-Plazaola *et al.*, 2017).

The first photoprotection mechanisms to reduce light absorption by chlorophylls include: morphological and anatomical leaf adjustments (i.e., reducing leaf area or changing leaf angle (Ogaya & Peñuelas, 2006) and increasing leaf reflectance by enhancing pubescence (Camarero *et al.*, 2012; Moles *et al.*, 2020) and epicuticular wax on the leaves (Paoletti *et al.*, 1998). The second mechanism consists in deactivating the excited electron of the chlorophyll to the ground state by i) light reemission (i.e., chlorophyll fluorescence), ii) dissipation of excess energy as heat, or iii) light use by phytochemistry. These three processes occur in competition, wherein any enhancement in the effectiveness of one will lead to a decline in the output of the remaining two. Consequently, by assessing the chlorophyll fluorescence yield, insights into photochemistry efficiency and heat dissipation can be obtained, being chlorophyll fluorescence emission a good proxy of the photosynthetic efficiency (Maxwell & Johnson, 2000) (further information is provided in Chapter III, General techniques) The heat emission, on the other hand, is associated to the xanthophyll cycles that include violaxanthin (VAZ) cycle and lutein epoxide-lutein (LxL) cycle (Esteban & García-Plazaola, 2014; García-Plazaola *et al.*, 2017). When the photosystem II is excited under high light irradiance, a proton gradient is created that decreases the pH of the thylakoid lumen (Szabó *et al.*, 2005). This activates the de-epoxidation of the violaxanthin (antheraxanthin as intermediate) to zeaxanthin and lutein-epoxide to lutein and the protonation of light-harvesting complex proteins (PsbS) (Schulze *et al.*, 2019). The association of the excited chlorophyll to the PsbS protein via zeaxanthin or lutein attenuates the energy transfer from the light-harvesting complex to the active centre of PSII thereby dissipating the excess energy as heat (**Fig. 5**; Schulze *et al.*, 2019; Navakoudis *et al.*, 2022).

The next mechanism against photo-oxidative damage is the induction of antioxidant compounds. As explained above, the generation of ROS may react and oxidize different molecules, including lipids, proteins, and sugars. Antioxidants defense compounds are categorized into enzymatic (i.e. superoxide dismutase and peroxidases) and non-enzymatic (i.e,

ascorbic acid, carotenoids and tocopherols). In this introduction, the focus will be done in the compounds that are studied in the thesis. These enzymatic and non-enzymatic antioxidants work together to maintain redox homeostasis, neutralize ROS, and protect plant cells from oxidative damage caused by various environmental stresses. Apart from their role in the thermal dissipation of excess energy, xanthophylls and carotenes mitigate the photo-oxidative stress by quenching singlet oxygen and other ROS (Havaux, 2013; Esteban *et al.*, 2015b). This process operates in conjunction with tocopherols (isoprenoids), in which electrons are donated to oxidized molecules such as lipid peroxyl radicals, preventing lipid peroxidation in thylakoid membranes (Munné-Bosch, 2005). The main form of tocopherol found and more biologically active form in plants is α-tocopherol (Munné-Bosch, 2007)In addition to the physical and chemical quenching, these lipophilic antioxidants regulate the fluidity of the thylakoid membranes acting as stabilizers against membrane disorganization induced by heat (**Fig. 5**; Havaux, 1998).

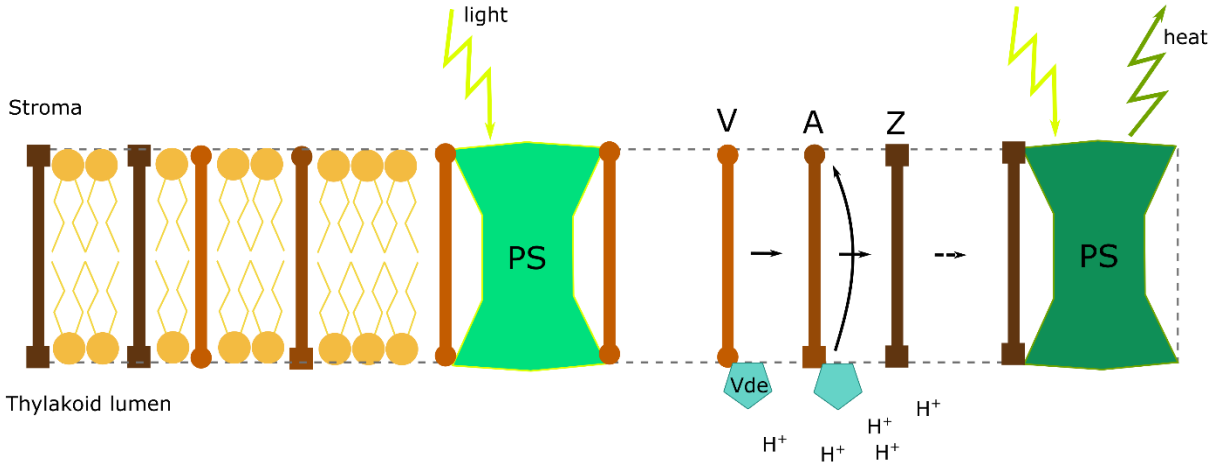

Figure 5. Schematic representation of the functions of the violaxanthin cycle pigments in the thylakoid membrane of the chloroplast. Left side figure represents the role of the dipolar carotenoids (V, A, Z) reducing the membrane fluidity and avoiding the disorganization induced by heat. Right side figure depicts the changes from light-harvesting (light green) to dissipating state (dark green) of the photosystem II (PS) once pH decreases in the thylakoid lumen and the violaxanthin de-epoxidase (Vde) de-epoxides violaxanthin (V) to zeaxanthin (Z) though antheraxanthin (A). Redrawn from Havaux 1998.

Changes in the photoprotective compounds have been observed in different Mediterranean evergreen *Quercus* species (Peguero-Pina *et al.*, 2008a, 2009; Grant *et al.*, 2010; García-Plazaola *et al.*, 2017) allowing them to withstand Mediterranean xeric conditions (Camarero *et al.*, 2012). Given the high responsiveness of the photoprotection mechanism (i.e., VAZ and tocopherol) against Mediterranean climatic stressors (García-Plazaola *et al.*, 2008; Fernández-Marín *et al.*, 2017), the application of these markers as early warning indicators of

tree health may provide a valuable insight (Hernández-Clemente *et al.*, 2019) to characterize the vulnerability status of the trees (Wujeska *et al.*, 2013). This may allow to identify and predict potential hotspots of tree decline and mortality and implement future action that counteracts this phenomenon (Hartmann *et al.*, 2018).

1.7.2. Morphological adjustments belowground: roots as protagonists

Root adjustment is another mechanism to tackle with climatic conditions. Mediterranean soils are characterised by low resource availability, a condition that has worsened due to climate change (Sardans & Peñuelas, 2004; Sardans *et al.*, 2008). These conditions have a negative impact on tree survival (Gessler *et al.*, 2017). To cope with such challenging conditions, the root system has evolutionarily acquired a varying degree of phenotypic plasticity reflected in morphological, architectural and physiological adjustments (i.e., by increasing root investment) to adapt to drought conditions and maintain their physiological status (Ramírez-Valiente *et al.*, 2018; Fromm, 2019).

In dehesas, the development of a deep and lateral root system is a key strategy for holm oaks to access soil resources and cope with the high variability of the Mediterranean climate (David *et al.*, 2004). Holm oak root extension in dehesas is estimated to be 33m horizontally and 5.2 m in depth (Moreno *et al.*, 2005). This makes the explored root surface to be seven times the projection of the canopy (Moreno et al., 2005). Within the root system, fine roots (<2 mm) are the most dynamic faction. In holm oaks, fine roots may be found in the upper layer (0-60 cm), decreasing while increasing depth (López *et al.*, 2001). Fine roots located in the upper soil layer are responsible for to uptake of mainly nutrients and water, whereas deeper fine roots would play a key role in extracting water in deep soil (Canadell *et al.*, 1992; Cubera & Moreno, 2007a). Hence, the fine root system is key to maintain tree water status by increasing water uptake under drought conditions (Schulze *et al.*, 2019), albeit is the most vulnerable part to pathogen root infection (León et al., 2017). For example, studies under controlled conditions reported root proliferation close to the surface (León *et al.*, 2017) and an increase in root investment at the expense of aboveground organs in response to *Phytophthora* spp root infections (Vivas *et al.*, 2021). However to the extent of our knowledge, few studies have studied the holm oak root system in the dehesas (Canadell *et al.*, 1992; Moreno & Pulido, 2009) or their role in the declining process (Corcobado *et al.*, 2013b, 2014b) under different soil nutrient availability.

1.8. The effect of the soil on holm oak decline

Soils are a key component of ecosystems because, among other things, they are the source of nutrients and water for plant development and growth. Soil properties such as pH, nutrient content, water availability, texture (e.g. clay content) or structure (e.g. physical properties such as compaction or water infiltration), may either favour decline or increase tree resilience under stressful conditions. In addition, the relationship between soil and tree physiology may be affected by factors such as climate change, land use, soil-borne pathogens and their interactive effects. This is specially true for dehesas, because the presence and virulence of the pathogens belonging to the genus *Phytophthora* are tightly linked to the presence of soil water (Gómez-Aparicio *et al.*, 2012). Understanding the edaphic factors, both physicochemical and biological, that can predispose the holm oak to be more vulnerable to climate change is of vital importance to prevent its decline.

1.8.1. The influence of soil nutrients in holm oak decline

Dehesas are characterized by low soil nutrient availability, a characteristic that may be aggravated by drought (Sardans & Peñuelas, 2004; García-Angulo *et al.*, 2020). Several studies have related soil nutrient availability with tree decline. In dehesas, phosphorus and nitrogen are the most altered soil nutrients in the declining process. In this regard, an increase in organic phosphorus and a decrease in assimilable phosphorus due to drought (Sardans & Peñuelas, 2004) or *Phytophthora*-driven tree mortality (Avila *et al.*, 2016, 2019) have been observed (**Fig, 4b**). This reduction may be also accompanied by higher rates of nitrogen mineralization that will promote the loss of nitrogen mineral forms for the tree by leaching and/or denitrification (Rodríguez *et al.*, 2016, 2019; García-Angulo *et al.*, 2020). Overall, the shortage of these nutrients may presumably hamper photosynthesis and water use efficiency, resulting in faster senescence (El-Madany *et al.*, 2021).

1.8.2. The influence of the microbial community on holm oak decline

Soil microbial communities, such as bacteria and fungi, play an important role in the health of the tree through carbon and nutrient cycling (Berendsen *et al.*, 2012). Microorganisms involved in biogeochemical cycling interact with the elements, transforming carbon, nitrogen, phosphorus, sulfur and iron and changing the physicochemical properties of the nutrients, making them available for plants (Berendsen *et al.*, 2012). Understanding microbial contribution to carbon and nutrient cycling may allow to identify potential limitations of nutrient availability essential for tree health. In the last years, studies exploring the contribution

of the microbial community on tree health have combined taxonomic and functional diversity and recently have used co-occurrence networks. In these studies, an increase in saprotrophs and pathogenic microorganisms has been observed in the last phases of tree decline (Denman *et al.*, 2018; Ginnan *et al.*, 2020; Pinho *et al.*, 2020; Gómez-Aparicio *et al.*, 2022) along with a low connectivity and high modularity in the topology of soil microbial networks (**Fig. 4b**; Fernández-González *et al.*, 2020; Gómez-Aparicio *et al.*, 2022). Nevertheless, further functional information needs to be provided to understand tree-soil microbial community functioning (White *et al.*, 2020). The use of soil microbial functional genes involved in nutrient cycling may allow us to understand how the functioning of soil microbial communities affects nutrient cycling and nutrient availability for trees. However, few studies have assessed the involvement of soil functional genes in the decline of oaks (Scarlett *et al.*, 2020) or dehesas (Shvaleva *et al.*, 2015) and their role as regulators of soil nutrient cycling .

.

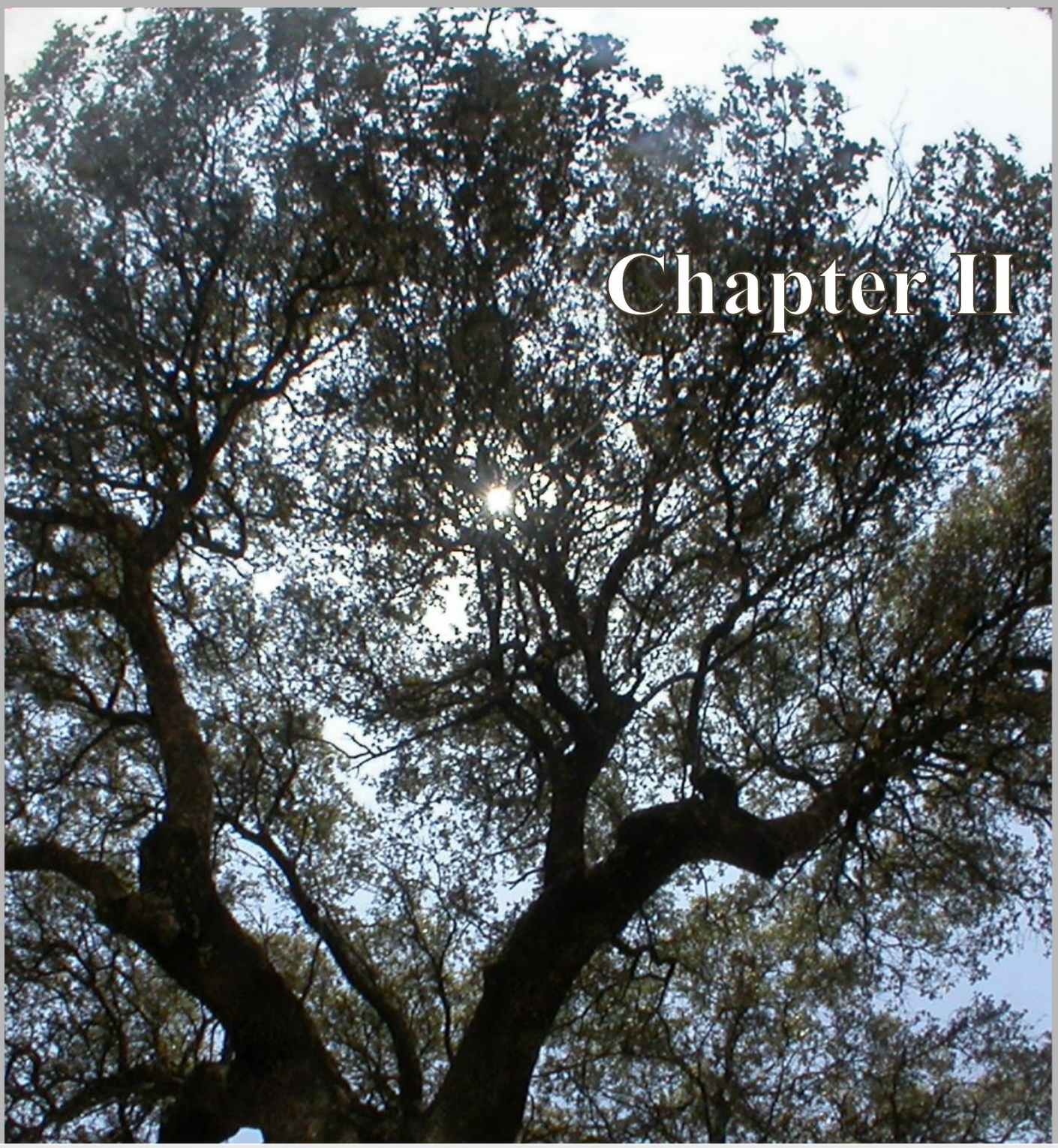

Chapter II

Aims

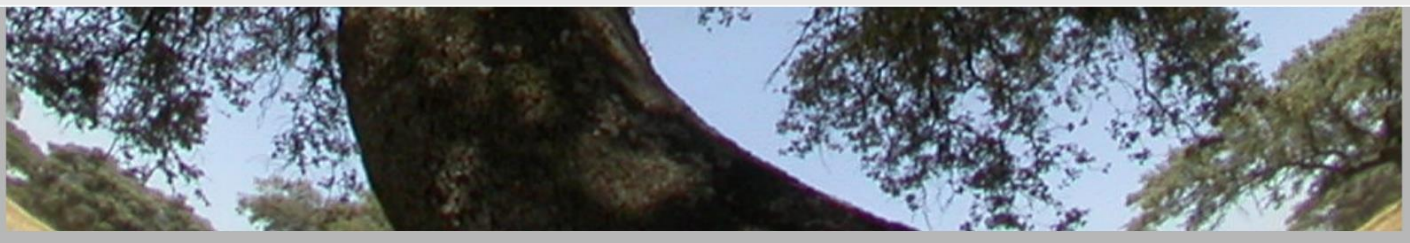

2.1. Why is it necessary to study holm oak decline?

Investigating holm oak decline is of paramount importance due to its dominance in the tree layer in dehesas. This ecosystem has been part of the Iberian landscape for many centuries (as it is explained in section 1.3). They harbour a high level of biodiversity and provide socio-ecological services, co-produced by the joint action of natural and human factors (Huntsinger & Oviedo, 2014). The decline and disappearance of the dehesas might carry enormous repercussions not only at the ecological level but also due to the ecosystem services that provide (Plieninger *et al.*, 2021). A common mistake about these ecosystems is the belief that they will provide and even enhance such services with the cessation of human activity (Huntsinger & Oviedo, 2014). However, both over-use and under-use have a negative impact on the ecosystem (Bugalho *et al.*, 2011). Sustainable management practices are needed to promote the conservation of the dehesas and the delivery of its ecosystem services. However, for the conservation of the dehesas and particularly holm oak in the current scenario of climate change, ***a profound understanding of the mechanisms that trigger holm oak during the declining process is needed***. Identifying the mechanisms that characterize the health of the tree and understanding how soil conditions contribute to the health of the trees may enable to target land management strategies aimed at promoting tree health. These practices may increase the resilience of the tree in the current climatic conditions.

In the last years, substantial progress has been made regarding the influence of soil conditions and the biotic component. In this sense, *Phytophthora* spp was identified as the main biotic factor that predisposes the tree to decline. While topography and soil conditions (i.e., texture, and nutrients) are also key contributors to its performance (Corcobado, 2013b), the histological assessment of the root infection may have some clues about the severity of the disease and the vulnerability of the tree (Ruiz-Gómez, 2018a). Additionally, recent breakthroughs have mapped declining patterns (Sánchez-Cuesta, 2022), allowing to unravel the ecological implications (García-Angulo, 2020) at stand even regional level. The physiological and ecological mechanism underlying the declining process is currently a trending subject (Hornero *et al.*, 2021). However, further research is required, therefore, to understand both, the physiology underlying holm oak decline and the role of the soils as a potential predisposing factor of its vulnerability. Some of the questions that we formulate are the following:

i) Which individuals within a population are more susceptible to decline and why?

ii) Which physiological threshold and traits may be employed to predict holm oak decline?

iii) Which soil conditions predispose holm oak to decline?

iv) How could we apply this knowledge to prevent holm oak decline?

2.2. The mission of this thesis: Shedding light on the previous questions

The ***general purpose*** of the present work was to characterize the physiological (i.e., leaf-level photoprotective responses, photochemical efficiency and carbon allocation patterns), morphological (crown phenotype and root system structure) and ecological (e.g., plant-soil microbial community continuum and soil chemistry) responses underlying the declining process observed on holm oak.

To achieve this main goal, we focused on:

i) The mechanisms previously described play an essential role in the survival of Mediterranean plant species (Esteban *et al.*, 2015a; García-Plazaola *et al.*, 2017; Fernández-Marín *et al.*, 2017). Specifically, we aimed to identify lipophilic photoprotective compounds in the photosynthetic organs that are activated before symptoms of decline become evident, serving as early stress indicators of holm oak decline. Furthermore, we aimed to associate these mechanisms with the loss of vigor, such as defoliation, to determine a physiological threshold beyond which the tree is unable to cope with the stress conditions.

ii) The above-belowground adjustments that occur at the tree level during the declining process, as well as, the different soil nutrient uptake strategies that the tree root system performs in different stages of the onset of decline.

iii) The reciprocating effect of the plant-soil microbial community system, particularly examining how the loss of crown health impacts nutrient-transforming microbial communities, and how these communities ,in turn, alter key soil nutrients that are essential for tree health.

2.3. A more in-depth perspective on the objectives and hypothesis.

Aim 1. To unveil early stress markers that precede crown defoliation and identify a physiological threshold in holm oak Chapter IV.

We aimed firstly: i) to study the leaf-level physiological adjustments (mainly VAZ-cycle pigments and total tocopherol pool) before the holm oak defoliation occurs as a consequence of the declining process. It is not totally understood which alterations in the photosynthetic apparatus are triggered at the early stages of the declining process and whether they constitute a physiological threshold beyond which defoliation occurs. We hypothesized that before declining symptoms are evident (i.e., tree defoliation), trees induce the synthesis and accumulation of photoprotective compounds at the leaf leaf-level to cope with drought/*Phytophthora* stress. We aimed secondly ii) to study the variation of photoprotective compounds (mainly VAZ and total tocopherol pool) along a quantitative gradient of tree decline (i.e., defoliation). We hypothesized that these photoprotective compounds pool will reach a concentration threshold that marked the onset of the declining phase in holm oaks. This will further result in tree defoliation. These issues are thoroughly addressed and explained in Chapter IV (**Fig. 1**).

A2. To describe root system structural changes during holm oak decline with an insight into structural carbohydrate dynamics Chapter V.

It is unclear which potential adaptations may trigger the root system to minimize the effect of the environmental conditions that lead to decline. Therefore, we aimed firstly: i) to investigate the changes in fine root phenotypic plasticity and its relationship with tree decline and soil nutrients. We hypothesized that both soil nutrients and the health status of the trees will determine the morphology and architecture of the fine root system. Furthermore, ii) we aimed to study the patterns of carbon allocation in fine roots and their relationship with tree health status. We hypothesized that the observed changes in the holm oak fine root system structure in response to the declining process are at the expense of available carbohydrates and foliage maintenance. These issues are thoroughly addressed and explained in Chapter V (**Fig. 1**).

A3. To advance in the understanding of the reciprocating effect in the tree-soil relationship in the context of holm oak decline, Chapter VI.

We aimed to explore the role of soils and their effect on the tree-soil microbiome relationships during the holm oak declining process. It is expected that plant-soil microbial community interactions might be affected as a result of the increase in belowground stress, albeit the direction of the cause and effects is still unclear. We hypothesized that in the tree-soil system, changes in the soil abiotic conditions resulting from holm oak decline affect the functioning of the microbial communities and their ability to mineralize key nutrients for plant health. These changes in soil nutrients will further affect the capacity of the tree to cope with stressful conditions Overall, the health and predisposition of holm oaks to decline depend on the tree-soil microbiome continuum and the feedback loops that ultimately control the availability of essential nutrients. These issues are thoroughly addressed and explained in Chapter VI (**Fig. 1**).

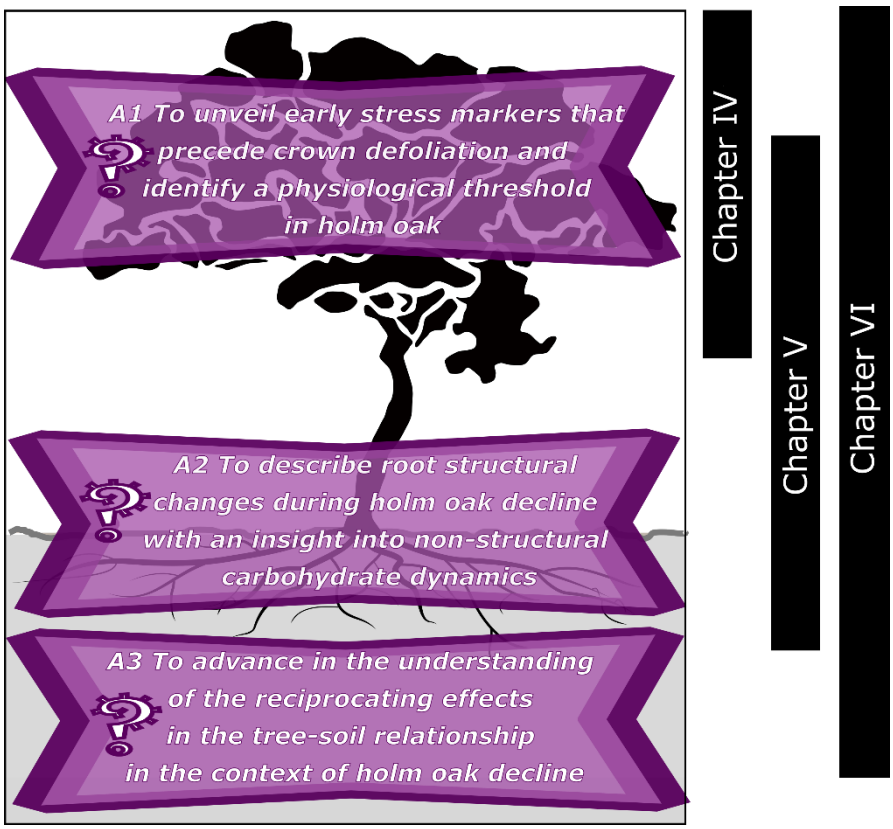

Figure 1. Depiction of the specific aims presented in this thesis. Note that the chapter where they are achieves is also indicated in the figure.

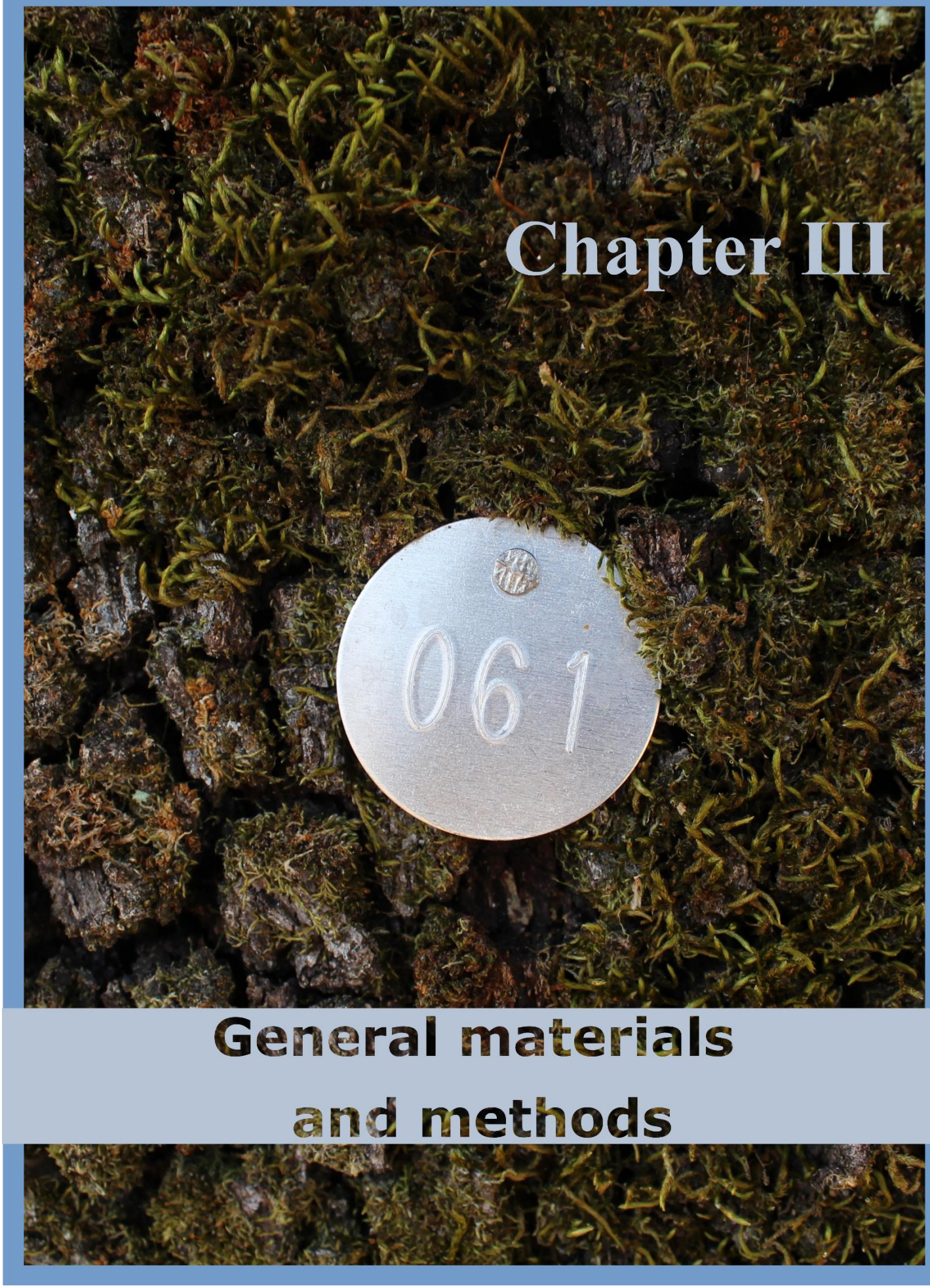

Chapter III

General materials and methods

3.1. The selected species: *Quercus ilex* L. subsp. *ballota* (Desf.) Samp.

Holm oak is a broadleaved evergreen tree or shrub and may grow up to 20 meters tall. The bark is dark-grey and deeply furrowed, with fissures that become more pronounced with age. The crown is broad and rounded. This tree is characterized by evergreen leaves with bright dark-green color on the upper side and hairy ashen green on the lower side (De Rigo & Caudullo, 2016). Their margins are waved or sinuate, but they can be dentate in young trees. Leaf lifespan varies between one to four years. The fruit is an oval-shaped acorn, brown in color with a length of 1.5 to 2.5 cm and a diameter of 1 to 2 cm. Mature acorns fall in November (De Rigo & Caudullo, 2016).

It may grow well in a wide variety of soil types in different Mediterranean climates. These climates may vary from semi-arid to very humid in terms of precipitation, and from warm to very cold at high altitudes, particularly when associated with low levels of rainfall (Barbero *et al.*, 1992). This versatility makes holm oak the most widely distributed *Quercus* species in Mediterranean woodland and maquis, covering from the western part of the Mediterranean basin (Iberian Peninsula, Morocco and Algeria) to the Aegean island and Turkey. It exists two subspecies *Quercus ilex* L. subsp. *ilex* and *Quercus ilex* L. subsp. *ballota* [Desf.] Samp. The main criterion to distinguish these two subspecies is the shape of the leaves. Whereas *Q.s ilex* subsp *ballota* exhibits more rounded and elliptical-shaped leaves (**Fig. 1**), Q. *ilex* subsp. *ilex* presents lanceolate-shaped leaves (Rivas-Martínez, 1987; Ferrer-Galego & Sáez, 2019). In the Iberian Peninsula, *Q. ilex* susp *ilex* colonizes temperate, subhumid and humid places in littoral or sublittoral areas, mountains or islands whereas Q. *ilex* subsp *ballota* occupies drier continental sites in the inner part of the Iberian Peninsula (Barbero *et al.*, 1992). Q. *ilex* subsp. *ballota* was selected as the focal species for investigating tree decline in the dehesa, as is the main species, along with *Quercus suber* L., that dominates the tree layer in dehesas (Moreno & Pulido, 2009).

Figure 1. Leaves and acorns from a mature holm oak in the dehesa

3.2. The selected study sites for this PhD. Thesis

The study area was located in the provinces of Cáceres and Toledo (Central-western part of the Iberian Peninsula). Nine dehesa sites located in the municipalities of Majadas de Tiétar, Aldeanueva del Camino, Salorino, Jaraicejo, Plasencia, Cáceres and Portaje (Cáceres province) and Oropesa and Velada (Toledo province) were selected. The location of these dehesas was based on previous studies (Corcobado, 2013a) that reported tree-experienced declining events. To select these sites, we used the following criteria: i) representative forests of the southwestern region of Spain, where dehesas abound (i.e., Cáceres and Toledo), ii) dehesas that contained holm oaks at various stages of decline, ranging from healthy to moderate defoliation (0 to 40% defoliation) iii) dehesas that contained two different zones, one predominantly healthy trees and the other with a mix of healthy and defoliated trees and iv) dehesas, where we had permission to conduct research and sampling (most of these dehesas were private properties).

The last issue was addressed considering the different challenges that imply conducting ecological research on private properties (Dyson *et al.*, 2019). In the process, a permanent channel of communication was established with the University of Extremadura at Plasencia. The Department of Plant Biology and Ecology at this University has extensive expertise in studying the decline of holm oak trees in dehesas. Hence: i) we established communication with the owners by both phone calls and emails, ii) we explained the main purpose of the research and the relevance of our study to the future of the dehesa, iii) we negotiated the access to the site and, vi) once in the field, we verbally reiterated the goal of the research of the study.

Finally, v) we conveyed the potential benefits and knowledge that this research could provide to counteract one of the main challenges that the owners face, the holm oak declining process. However, some concerns and problems were raised during the sampling campaign. This includes potential damage due to the sampling. For example, we try to minimize the impact of the digging sampling by refilling the pit once we collected enough samples or we stylized sampling tools such as the shovel or the hoe to avoid the spreading of tree pathogens. Additionally, we also had to face common problems such as rejections or non-responses to access requests (for instance in our second sampling, we could not access to one of the sites).

3.2.1. Climatic conditions of the sampling sites

We characterized the climatic conditions of each studied dehesa site by the Climatic Research Unit gridded Time Series dataset (CRU TS, Harris *et al.*, 2020) This dataset is annually updated to span 1901-2019. In detail, our sites presented a Mediterranean climate characterized by warm and dry summers and cold wet winters. The precipitation occurs mainly in autumn, winter and in April. **Fig. 2**). Further information on the climatic conditions may be found in Chapters IV, V and VI.

The Mediterranean climate is the result of the combination of different factors. The subtropical location of the basin, the presence of mountain ridges that surround the Mediterranean sea, the high-pressure systems during summer and the low-pressure systems during winter create wind and rain patterns in the different regions of the basin that determine the Mediterranean climate (Lionello *et al.*, 2006). This is characterized by dry and hot summers and wet and mild winters. Nevertheless, in regions out of the influence of the sea, the climate tends to be more extreme with hotter summers and colder winters

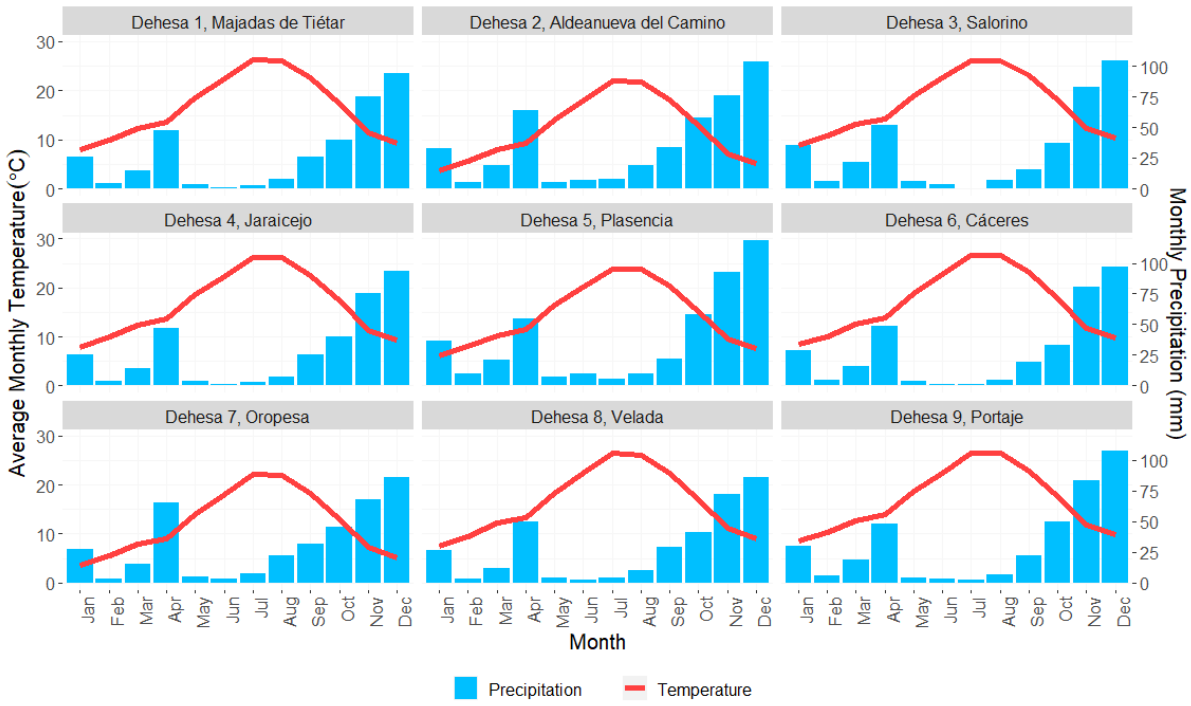

Figure 2. Average monthly temperature (ºC) and precipitation (mm) in the nine sampled dehesas in this study (CRU TS v.4; Harris et al. 2020, reference period 2019).

3.2.2. Land use and management of the sampling area.

The inappropriate land use and management affect the physicochemical and biotic soil properties that can increase the susceptibility of trees to drought and heatwaves (Camilo-Alves *et al.*, 2013). This implies that dehesas with an intense management footprint may be more vulnerable to current climatic conditions (Moreno-Fernández *et al.*, 2019), leading to a reduction in tree density and cover in these ecosystems (López-Sánchez *et al.*, 2018). A comprehensive understanding of land use and management is crucial to address tree decline in dehesas.

During the sampling campaign, a survey to landowners was carried out to describe the land use and management of each dehesa site. The following information was required: i) area of the dehesa, ii) livestock load, iii) number of months with livestock, iv) type of livestock, v) ploughing activities in the present or in the past, vi) treated trees for pests or pathogens and vii) pruning activities in the present or the past. With the information compiled a figure was created to have a general view of the land use and management (**Fig. 3)**. Briefly, a common factor of these dehesas is the presence of cow cattle the whole year (except in dehesa 1 and 4) and pruning activities in 2019 or previous years (i.e., 2004). Ploughing was also a common activity

for the majority of the dehesas. Dehesa 1 and 4 reported treated trees for foliage feeders or soil-borne pathogens respectively.

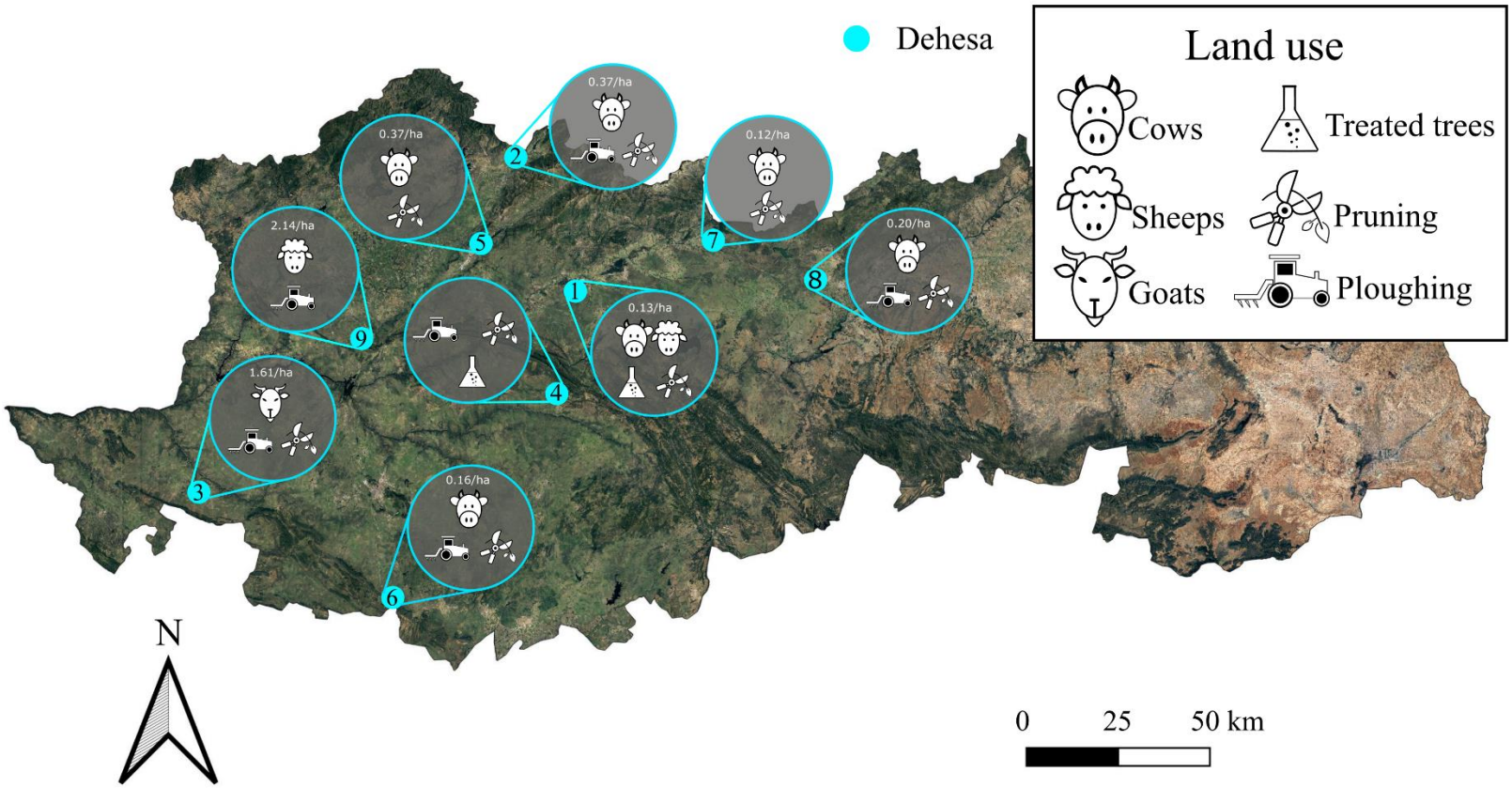

Figure 3. Depiction of the land use and management of the studied dehesas. The number above the livestock representation indicate livestock load per hectare. Icon redrawn from: Belloren, SBTS, Chanut is Industries, Orin Zuu, LutfI Gani Al Achmad, Vector Points (The Noun Project), accessed through (https://thenounproject.com/).

3.3. Experimental design to explore holm oak decline

The experimental design of this thesis was based on an initial expert-eye-based assessment in which we distinguished two different zones: i) healthy zones with no visible signs of holm oak decline and declining or unhealthy zones with evident signs of holm oak decline (i.e., these zones contained defoliated holm oaks) (**Fig. 4**). Additionally, in the declining zone we differentiated two distinct types of trees: i) trees with no signs of decline and ii) trees with evident signs of decline. This design provided us with a framework to test and answer our hypotheses at two different levels of spatial decline: i) at dehesa level to explore which are the common declining pattern in dehesas and ii) at zone level to identify why individuals within the declining zone exhibit different levels of vulnerability.

Hence, within each of the 9 dehesas, we sampled 6 trees in the healthy zone and 12 trees in the declining or unhealthy zone (i.e., 6 trees with no signs of decline and 6 trees with evident signs of decline). Overall we sampled 162 trees, 18 trees per dehesa. A more detailed description of the experimental design may be found in Chapters IV, V and VI.

Then, we categorized the sampled trees by health status. This status was assessed considering the zone where each tree was growing (healthy and declining) and by the visual assessment of the crown (detailed in the following sections) Consequently, the trees growing in the healthy zone were categorized as control or “healthy trees”. In the case of the declining zone, trees with no signs of decline were categorized as “non-declining trees” and trees with declining signs were categorized as “declining trees”. This classification was employed in Chapter IV. Nevertheless, we updated this classification for further chapters, according to the new results we obtained along Chapter IV. Thus, control trees in Chapter IV were renamed as “healthy trees” for Chapters V and VI. Additionally, we updated the designation for the trees growing in the declining zone for Chapters V and VI. Hence, trees growing in the declining zone with less than 10% defoliation but high rates of early stress markers were designed as “susceptible trees”. In the same way, trees with more than 10% defoliation and high rates of early stress markers were designed as “declining trees”. In addition, we also rename sites and zone from Chapter IV for dehesa and sites in chapters V and VI due to publication issues.

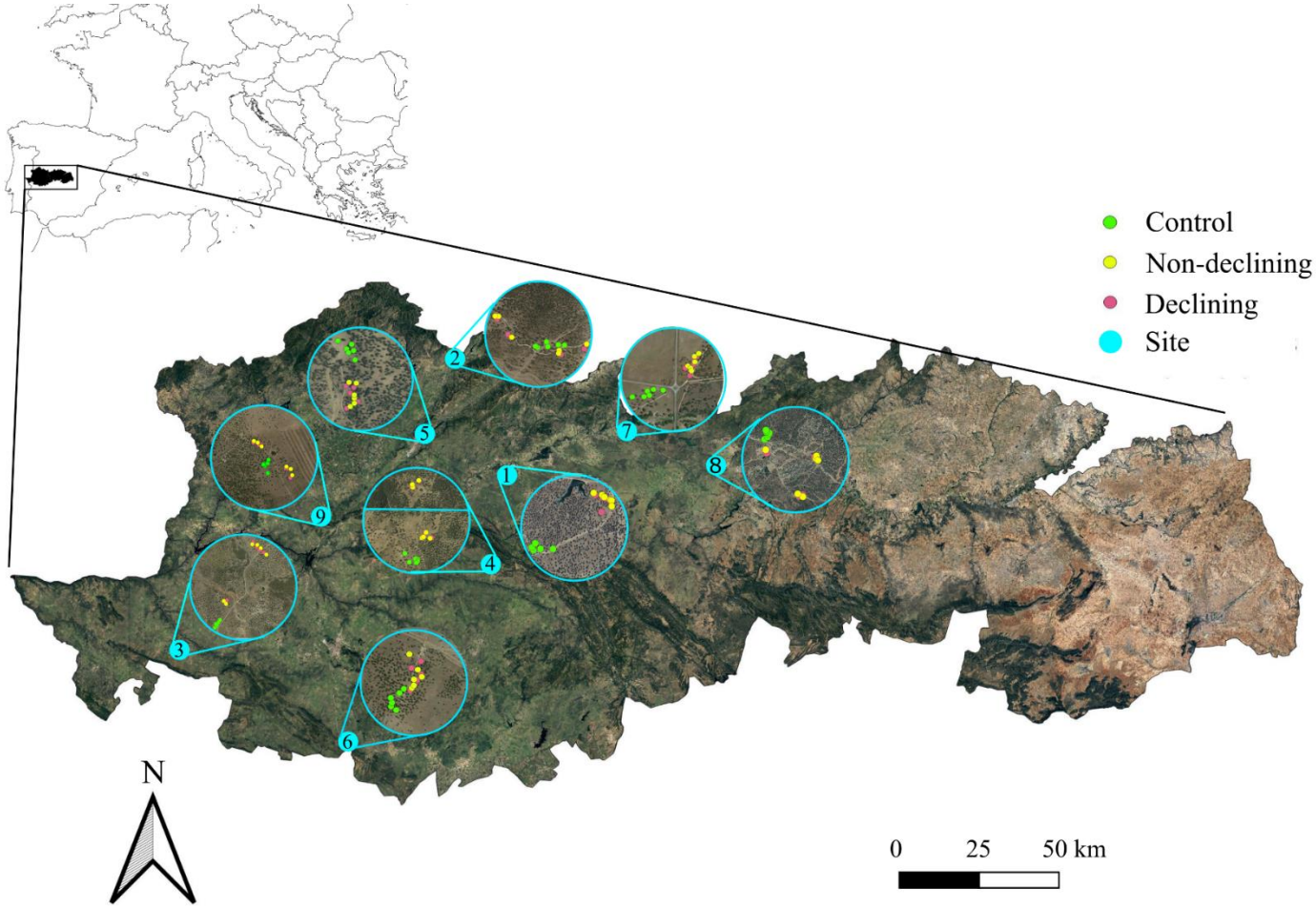

Figure 4. Location of the nine dehesa study sites (indicated with blue circles) within the central–western area of the Iberian Peninsula (the location within Europe is indicated in the upper map). The sampling design included 18 holm oak individuals per each study site: six control holm oak trees from healthy areas (marked with green points), six non-declining holm oak trees from declining areas (marked with yellow points) and six declining holm oak trees from declining areas (marked with red points). Google Earth Pro 7.3.3.7786 (July 21, 2020) Spain. 39◦ 40’ 44” N , 5◦ 25’40”W, Eye alt 419 km. Landsat/Copernicus. Google 2020. https://www.google.com/intl/es/earth/ [February 2020].

3.4. Sampling

To fulfill the general and specific objectives mentioned in Chapter II, we collected the following types of samples from each sampled tree in April and July 2019 (**Fig 5**):

- Four mature leaf samples from the four cardinal directions to measure photosynthetic pigments (i.e., carotenoids and chlorophylls) and the lipophilic antioxidants (i.e., tocopherols). These samples were conserved with silica gel following the method of (Esteban *et al.*, 2009a) (**Fig 5.**).In addition, another mature leaf was collected to analyse the chlorophyll *a* fluorescence induction (Fig. 5). These samples were immediately stored in hermetic bags with high relative humidity and measured after an "artificial predawn". More details in Chapter IV.
- The shallowest roots of each tree by digging (≈ 15 cm depth) until collecting a representative number of root fragments to conduct our analysis (i.e., non-structural carbohydrates for coarse and fine roots and fine root morphology and architecture).
- Bulk soil from the surrounding zone of the roots to perform chemical soil analysis (nitrate, nitrite, ammonia, phosphate, potassium, org. C, org. P, org. N, pH) and asses microbial soil functional genes involved in the biogeochemical cycles.

Additionally, and during the sampling process, we recorded information regarding each holm oak tree: i) the identification of each dehesa (i.e., number), ii) the date of the sampling, iii) the sampling zone (i.e., healthy or declining), iv) the identification of the tree, v) the health status of the tree (i.e., control, non-declining and declining) and vi) the diameter at breast height (i.e., DBH). Additionally, we took pictures of the trees from different angles (i.e., frontal and underneath the tree canopy) and from the soil pits. We used these images to characterize the height of the tree, its level of defoliation and the soil depth (where the soil was collected). More detailed information on the methodology employed and the characteristics we extracted from the images may be found in chapters IV and V.

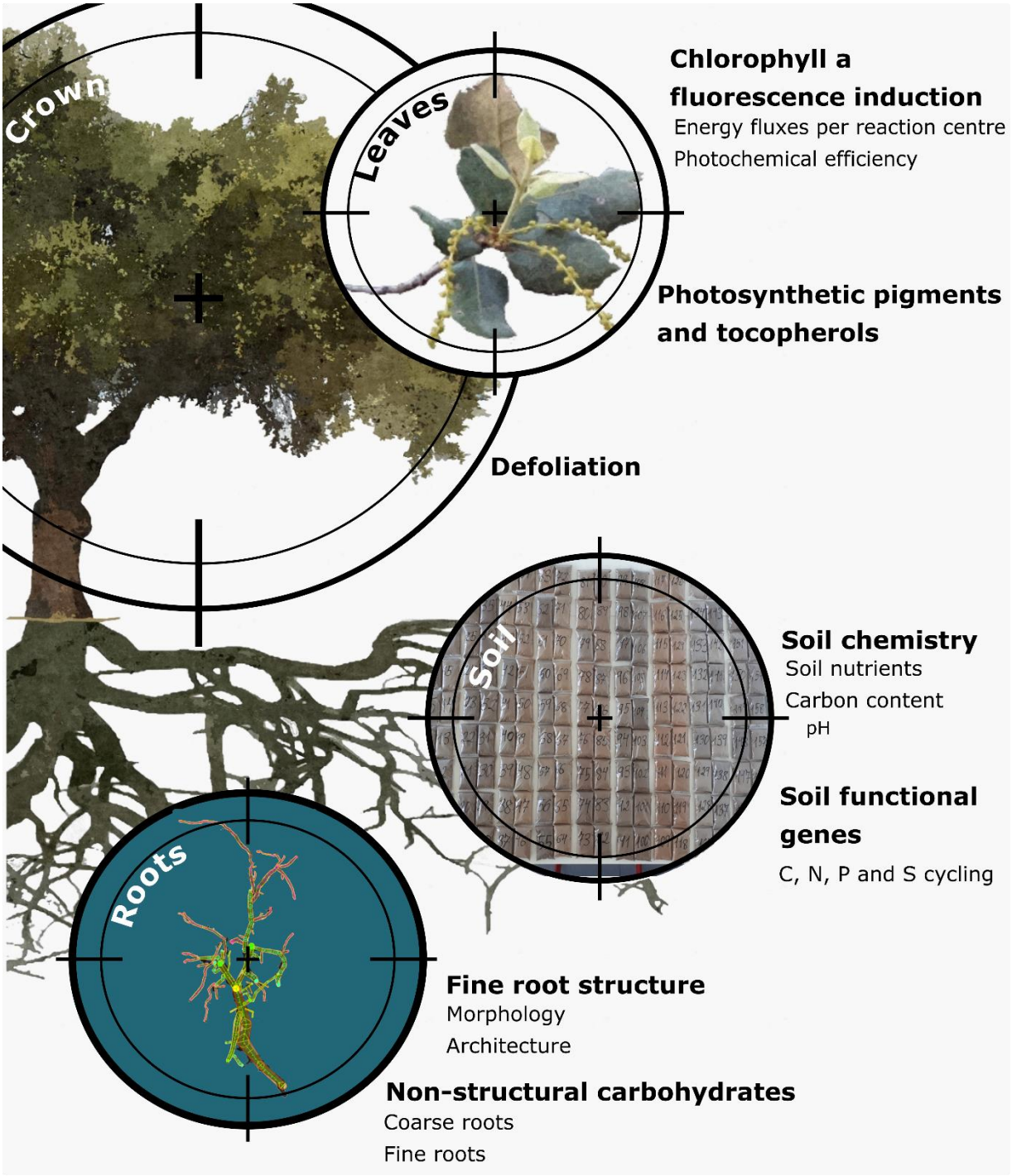

Figure 5. Depiction of the collected samples and the measured variables in this thesis.

3.5. General physiological and analytical techniques

In this section, we briefly describe the techniques we used to assess:

3.5.1. Defoliation

Tree defoliation is critical to assess holm oak decline. In this thesis, we used frontal pictures of the trees to quantify the degree of defoliation. For that, we considered a standardised criterion to accurately assess the loss of foliage. We consider branches without leaves highlighted in the sky-defoliated areas of the crown. By calculating the total defoliated areas relative to the crown area we assessed defoliation. This analysis was made with the Java-based image processing program ImageJ (more details in Chapter IV).

3.5.2. Chlorophyll *a* fluorescence induction

When photosynthetic machinery is not functioning optimally due to a particular stress, the absorbed energy may be dissipated as heat or fluorescence (Maxwell & Johnson, 2000). By exposing a leaf to light of a defined wavelength and quantifying the light re-emitted this technique may provide several parameters related to photosynthesis efficiency and the energy flow through the photosystems (Strasser *et al.*, 2000, 2004). The association of these measurements with the environmental conditions may be used to identify potential stresses that reduce photosynthetic efficiency. The parameters and the definition used in this thesis may be found in Chapter IV and supplementary material. More details in Chapter IV.

3.5.3. Quantification of pigments and tocopherols

The quantification of pigments and tocopherols was performed using ultra-Hight-Performance Liquid Chromatography (uHPLC). This technique is based on the fact that pigments and tocopherols present: i) differential solubility in the mobile phase (i.e., a mixture of solvents) and ii) interact differently with the stationary phase (i.e., column). In uHPLC, the extracts are injected into a mixture of solvents (mobile phase). When the mobile phase passes at high pressure through the stationary phase, the distinct compounds are separated at varying rates based on their respective chemical properties. The compounds are detected by a detector that measures the absorbance of each molecule at a specific wavelength and generates a chromatogram that shows the amount of each pigment in the sample. The photodiode detector was then used to detect pigments, while the tocopherols were detected by fluorescence. More detailed information on this technique is provided in Chapter IV.

3.5.4. Soil chemistry

Organic carbon (org. C): The principle behind the dichromate oxidation method for the estimation of organic carbon content in soil is based on the reaction between acidified dichromate and the organic carbon present in the soil sample. The organic carbon is oxidized and the unreacted dichromate is then estimated by titration using an indicator (N-phenylanthranilic acid) (Walkley & Black, 1934; Yeomans & Bremner, 1988). More details in Chapters V and VI.

Total N and P. The determination of these soil components is based on the conversion of nitrogen compounds (most of them organic) to NH_3-N by the addition of sulphuric acid with a catalizator (Cu, Se and KSO_4). Total N is determined by the Skalar autoanalyzer (spectrophotometer). The final result is the sum of organic N and NH_3 presented in the sample, albeit the inorganic part in this determination (NH_3) is considered insignificant (Radojevic *et al.*, 1999).

Ammonium. The determination of ammonia is based on the modified Berthelot reaction. This involves the chlorination of ammonia to monochloramine followed by the reaction with salicylate to produce 5-aminosalicylate. The oxidized product generates a green-colored complex, whose absorbance is measured at 630 nm to quantify the ammonia content in the sample (Krom, 1980; Searle, 1984).

Nitrate and nitrite. The principle behind this determination is based on the reduction of nitrate by a copper-cadmium complex to nitrite. The nitrite is determined by diazotizing with sulphanilamide and coupling with N (1-naphthyl) ethylenediamine dihydrochloride to produce a colored azo complex that can be measured at 540 nm (Navone, 1964; Walinga *et al.*, 1989).

Phosphate: The determination of phosphate involves the reaction of heptamolibdate and potassium antimony (III) oxide tartrate in acidic medium with a diluted solution of phosphate to form the antimony-phospho-molybdate complex. This complex is reduced by ascorbic acid to a blue-coloured complex. This complex is measured at 880 nm (Boltz & Mellon, 1948).

Potassium: To determine the concentration of potassium in a sample, the sample is aspirated into a flame, which atomizes the potassium of the sample. The atomized potassium absorbs light at a specific wavelength of 776 nm, and the amount of light absorbed is proportional to the concentration of potassium in the sample (Richards, 1954).

pH: The saturated soil paste method to determine the pH is based on the exchange between the H+ ions of the soil and the water solution. The pH of the sample is the result of the concentration of H+ ions in the water solution (Kalra, 1995).

3.5.5. Non-structural carbohydrates quantification

The detection of soluble carbohydrates (i.e., glucose, fructose and sucrose) was performed using an ion chromatography system (Mariem *et al.*, 2020). This technique is based on the chromatographic principle described above. The difference lies in the fact that the stationary phase separates the compounds (i.e., glucose, fructose and sucrose) according to their charges and affinity for the stationary phase. After the separation, the ions are detected and quantified.

3.5.6. Root structure

The characterization of the root architecture (i.e., root branching) and its association with the root uptake strategies requires identifying the position of the root components that constitute the root system (Beidler *et al.*, 2015). Since root sampling involved the collection of non-intact root fragments (modified and broken by the digging and harvesting process in the dry soil, the characterization of the root architecture was based on: i) a root diameter-based classification to determine the hierarchy and position of the sampled root components within the root system (Eissenstat *et al.*, 2015) and ii) the analogy of the root branching with the morphometric characterization of the watersheds (Altaf *et al.*, 2013; Chen *et al.*, 2016). This approach allowed us to reorganize artificially the root component positions and calculate the branching ratio of the fine roots (Chen *et al.*, 2016).

The characterization of the fine root morphology (i.e., diameter, length and insertion angle) was determined using the image analysis software Smartroot (**Fig. 6**, Lobet *et al.*, 2011). Further information on the fine root architecture and morphology may be found in Chapter V).

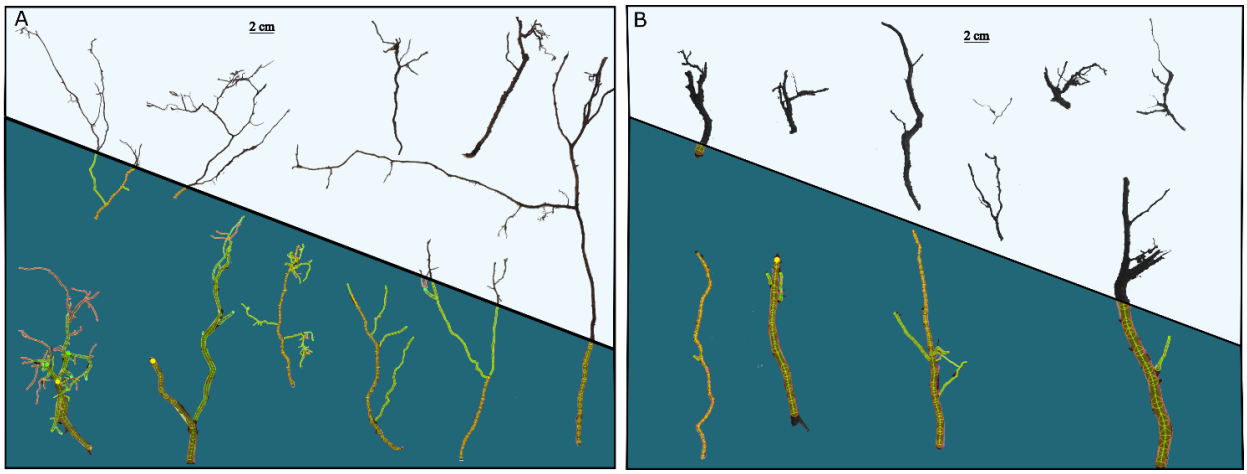

Figure 6. Root fragments from two different sampled trees. The top half of the panels show the natural aspect that the root presented after being collected, whereas the bottom half of the panels show the roots processed by the Smartroot software. Note that the thinner root components are in pink colour while the thicker root components are in red colour. The root system in the panel A presented: fine roots, 100 (%); fine root branching, 4.5; insertion angle 53º, fine root length, 0.8 (cm), fine root diameter, 0.03 (cm). The root system in panel B presented: fine roots, 48 (%); fine root branching, 0.7; insertion angle, 47 º; fine root length, 2.4 (cm); fine root diameter 0.1 (cm).

3.5.7. Soil functional genes

The quantification of the microbial element cycling (QMEC) was performed using qPCR high-throughput. This technique is based on PCR real-time, which targets a fragment of nucleic acid by using specific primers that flank the region of interest. This fragment is then amplified using a polymerase, and the amplification is detected in real-time by using a fluorochrome. Finally, the amount of amplified DNA is quantified by measuring the fluorescence level emitted by the amplification product when it reaches a threshold.

Specifically, the high-throughput quantitative PCR was performed by applying the nanofluidic qPCR BioMarkTM HD system developed by the Fluidigm Corporation (https://www.fluidigm.com/). This system operates by performing qPCR reactions in a Dynamic Array (IFC) that contains thousands of interconnected channels, controlled by valves. The nucleic acid of the sample and reagents are automatically mixed in a matrix within the device. The use of this system. allows to perform 9 216 qPCR reactions, using the g a 96.96 chip format (96 samples × 96 assays) in a single qPCR run (https://www.fluidigm.com/). This technique allows to assess and quantify the genetic potential of microbiota to use and transform soil organic matter and to release C, N, P and S (Zheng *et al.*, 2018) across the gradient of tree health. More detailed information of these techniques is provided in Chapter VI.

3.6. Statistical analysis of this thesis

In this section, we describe the most common statistical tools used in this thesis.

3.6.1. Spearman's rank correlation coefficient

This analysis is a non-parametric statistical method that evaluates the strength and direction of the association between two variables. It is used in case one of the variable is not normally distributed or in case a variable presents outliers. The analysis converts the values of each variable into ranks (ordered values) and replaces the value by their respective orders, after that, the correlation is computed (Dalgaard, 2008). The resulting coefficient ranges from -1 to 1. Values close to 1 indicate a strong positive correlation; values close to -1 indicate a strong negative correlation and values close to 0 indicate a weak correlation. In this thesis, we used this method to explore the relationship among variables. In Chapters IV and VI.

3.6.2. Linear mixed models

The linear mixed model is an extension of the linear model. However, it combines fixed and random effects to model the relationship between one or more independent variables, (i.e., explanatory variable) and a dependent variable (i.e., response variable) in data that are grouped according to a classification factor. Fixed effects refer to parameters associated with the entire population whereas the random effects are associated with the experimental unit (Pinheiro & Douglas, 2000). The general formula of linear mixed models is:

$$Y = X\beta + z\upsilon + \varepsilon$$

Were υ and ε are random vectors with normal distribution and a mean of 0. Xβ represents the fixed factor (explanatory variable), zυ the random factor (parameters involved in the modelization of the structure and the properties of the variables) and ε the vector of distribution errors.

To assess the significance of the terms in the fixed-effects (β≠0), ANOVA function is applied. We used different types of ANOVA (i.e., type II or III) depending on the number of observations and missing values of each variable (i.e., balanced or unbalanced design). Finally, these models are validated by checking the residuals. The residuals of the models need to fulfill normality and homoscedasticity assumptions. To evaluate the normality assumption, residual histograms and quantile-quantile plots were checked. In addition, the Kolmogorov-Smirnov test was also applied to the residuals to assess normality. To evaluate homoscedasticity, residual vs fitted and residuals vs explanatory variable plots were checked.

In this thesis, we considered these types of models due to the nature of the experimental design as data are groped in each of the nine dehesas. Additionally, we included the effect of the 9 dehesa at the site level (i.e., healthy and unhealthy) in the chapters V and VI. Overall these models were used in the following chapters (IV, V and V) to evaluate the effect of the tree health (either health status, defoliation or crown health) on the different leaf biochemical traits, root parameters and soil functional genes. Additionally, we also performed multiple linear regressions including interactions.

3.6.3. Structural equation models

A structural equation model (SEM) is a statistical technique based on the association of multiple linear regressions. They incorporate multiple explanatory and response variables into a causal network. SEM is commonly represented using path diagrams and uses arrows to indicate the direction of the causal-effect relationships (Toms & Lesperance, 2003; Lefcheck, 2016). A simple representation of these path diagrams is:

$Z \rightarrow X1 \rightarrow Y \leftarrow X2$

Where Y is the response variable that is affected by X1 and X2, and X1 is affected by Z. The equation of this SEM is the combination of these two models:

$Y \sim X1 + X2;$

$X1 \sim Z$

Thus, SEM allows to analyze of complex relationships between variables and test theoretical models. In this thesis, we used SEM to test hypothesized processes to predict holm oak defoliation and decline. In this sense, in Chapter IV we tested a mechanistic process that precedes defoliation by analyzing the relationship between the downregulation of the PSII (PiAbs), the increase in VAZ and the upregulation of antioxidant compounds (tocopherols). In chapter VI we tested the hypothesized effect of the crown health on the soil microbial functional genes, the effect of the soil microbial functional genes on soil chemistry and finally the impact of soil chemistry on the crown health.

3.6.4. Multivariate ordination techniques

PCA is a multivariate technique that transforms a set of correlated variables into a smaller number of uncorrelated variables, called, principal components, axes or gradients. The main purpose of this analysis is to simplify and reduce the dimensionality of the data while

retaining as much variability of the data as possible (i.e., capturing the most important information of all the variables in a few axes). The first principal component is the linear combination of variables that retain more variance (retain more information) followed by the second, third and so successively (Zur *et al.*, 2016).

In this thesis, we used this technique to obtain principal components or new variables that defined soil nutrients (Chapter V), crown health and fine root system (Chapter VI).

Redundancy analysis is an extension of the PCA analysis, however, one or several explanatory variables are included in the analysis to determine the effect of the explanatory variable on the linear combination of the response variables. Hence the axes of the RDA are not only linear combination of the response variable but also on the explanatory variable (Zur *et al.*, 2016) .

In this thesis, we used this technique to depict the stress level of the leaves in the three different health statuses (i.e., healthy, susceptible and declining) in Chapter V.

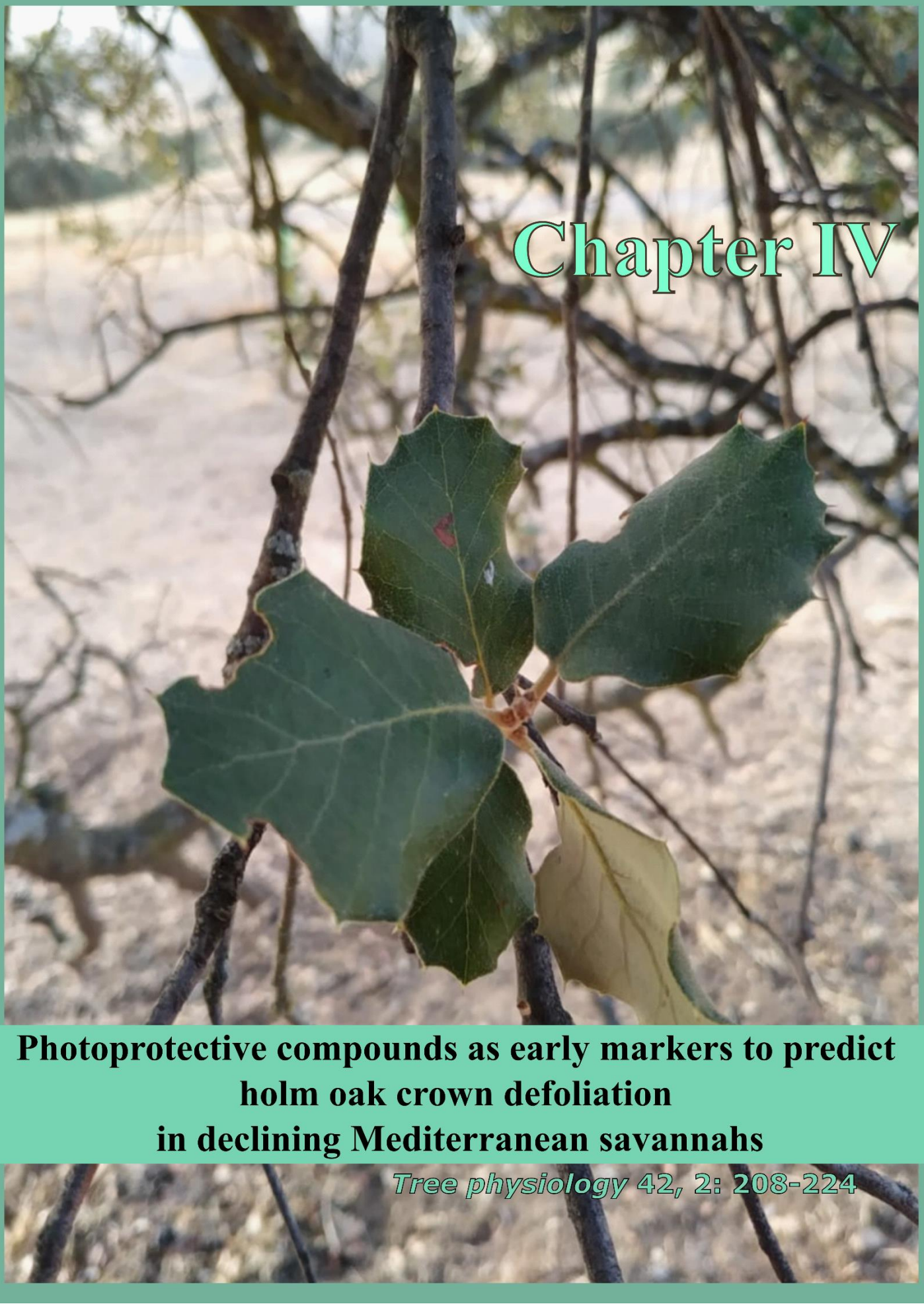

Chapter IV

Photoprotective compounds as early markers to predict holm oak crown defoliation in declining Mediterranean savannahs

Tree physiology 42, 2: 208-224

Photoprotective compounds as early markers to predict holm oak crown defoliation in declining Mediterranean savannah

Manuel Encinas-Valero[1],†, Raquel Esteban [2,6]†, Ana-Maria Heres [1,3], José María Becerril[2], José Ignacio García-Plazaola [2], Unai Artexe[2], María Vivas[4], Alejandro Solla [4], Gerardo Moreno[4] and Jorge Curiel Yuste[1,5]

Tree physiology: doi:10.1093/treephys/tpab006

[1] BC3-Basque Centre for Climate Change, Scientific Campus of the University of the Basque Country, 48940 Leioa, Bizkaia, Spain;
[2] Department of Plant Biology and Ecology, University of Basque Country (UPV/EHU), Barrio Sarriena s/n, 48940 Leioa, Bizkaia, Spain;
[3] Department of Forest Sciences, Transilvania University of Brasov, Sirul Beethoven-1, 500123 Brasov, Romania; 4Faculty of Forestry, Institute for Dehesa Research (INDEHESA), University of Extremadura, Avenida Virgen del Puerto 2,
10600 Plasencia, Spain;
[5] IKERBASQUE, Basque Foundation for Science, Plaza Euskadi 548009 Bilbao, Bizkaia, Spain;

Corresponding author (raquel.esteban@ehu.eus)
† These authors contributed equally to this work

Abstract

Dehesas, human-shaped savannah-like ecosystems, where the overstorey is mainly dominated by the evergreen holm oak (*Quercus ilex* L. subsp. *ballota* (Desf.) Samp.), are classified as a global conservation priority. Despite being *Q. ilex* a species adapted to the harsh Mediterranean environmental conditions, recent decades have witnessed worrisome trends of climate-change-induced holm oak mortality. Holm oak decline is evidenced by tree vigour loss, gradual defoliation and ultimately, death. However, before losing leaves, trees undergo leaf-level physiological adjustments in response to stress that may represent a promising field to develop biochemical early markers of holm oak decline. This study explored holm oak photoprotective responses (pigments, tocopherols and photosynthetic performance) in 144 mature holm oak trees with different health statuses (i.e., crown defoliation percentages) from healthy to first-stage declining individuals. Our results indicate differential photochemical performance and photoprotective compounds concentration depending on the trees' health status. Declining trees showed higher energy dissipation yield, lower photochemical efficiency and enhanced photoprotective compounds. In the case of total violaxanthin cycle pigments (VAZ) and tocopherols, shifts in leaf contents were significant at very early stages of crown defoliation, even before visual symptoms of decline were evident, supporting the value of these biochemical compounds as early stress markers. Linear mixed-effects models results showed an acute response, both in the photosynthesis performance index and in the concentration of foliar tocopherols, during the onset of tree decline, whereas VAZ showed a more gradual response along the defoliation gradient of the crown. These results collectively demonstrate that once a certain threshold of leaf physiological damage is surpassed, that leaf cannot counteract oxidative stress and progressive loss of leaves occurs. Therefore, the use of both photosynthesis performance indexes and the leaf tocopherols concentration as early diagnostic tools might predict declining trends, facilitating the implementation of preventive measures to counteract crown defoliation.

4.1. Introduction

An increasing number of reports highlight that climate change-induced tree decline and mortality events represent a worldwide phenomenon of global importance (Allen *et al.*, 2010; Hartmann *et al.*, 2018). Potential consequences of tree decline and subsequent mortality on ecosystem functioning (Curiel Yuste *et al.*, 2019; Rodríguez *et al.*, 2019; García-Angulo *et al.*, 2020), land-atmosphere interactions (Anderegg *et al.*, 2013; Bonan, 2016) and ecosystem services (Breshears *et al.*, 2011; Xiong *et al.*, 2011) are large and difficult to disentangle. Therefore, it is of utmost importance to identify the early events and physiological causes of tree decline, aiming to improve and develop predictive tools for early diagnosis.

The Mediterranean basin, a biodiversity hotspot of global conservation priority (Matesanz & Valladares, 2014; Bellard *et al.*, 2014), is one of the regions of the world where the number of climate-change-induced tree decline and mortality events has increased the most during the last decades (Carnicer *et al.*, 2011; Martínez-Vilalta *et al.*, 2012; Natalini *et al.*, 2016; Gazol *et al.*, 2020). Within the Mediterranean region, the dehesas (Spain) or montados (Portugal), which are human-shaped savannah-like ecosystems, are among the most threatened ecosystems (Pulido *et al.*, 2001; Herguido-Sevillano *et al.*, 2017). The causes that underlie the phenomenon of tree decline are complex, varying from purely climatic ones (Natalini et al. 2016, Hereş et al. 2018, García-Angulo et al. 2020) to the occurrence of soil-borne pathogen outbreaks, mainly of *Phytophthora* spp. (Brasier, 1996; Solla *et al.*, 2009; Martín-García *et al.*, 2015). However, in most cases, the interactions of different factors explain better the declining trend than a single stressor (Thomas, 2008; Camilo-Alves *et al.*, 2013; Ruíz-Gómez *et al.*, 2019a).

The dominant tree species in dehesas ecosystems are evergreen broadleaf species from the *Quercus* genus, especially the holm oak (*Quercus ilex* L. subsp. *ballota* (Desf.) Samp.) and the cork oak (*Quercus suber* L.) (Pulido *et al.*, 2001; Moreno & Pulido, 2009). Holm oak is a tree species that is well-adapted to the harsh conditions of the Mediterranean continental climate, and it thrives well in hot and dry summers and cold winters (Canadell *et al.*, 1992; Ramírez-Valiente *et al.*, 2020). During the last decades, holm oak has started to show a worrisome symptomatic declining trend (i.e., root rot, carbon starvation, hydraulic failure, leaves wilting, stem mortality, defoliation reduced carbon gain potential) followed by high mortality rates (Pollastrini *et al.*, 2019; Ogaya *et al.*, 2020). The oomycete *Phytophthora cinnamomi* Rands has been considered as the main factor responsible for the loss of its vigour,

decline and mortality in Southern Europe (Brasier, 1996; Sánchez *et al.*, 2002) and especially in the western part of the Iberian Peninsula. Pathogen-induced symptoms resemble those of drought (Camilo-Alves *et al.*, 2013) and occur primarily due to a loss of fine roots and ectomycorrhizal root tips (Corcobado *et al.*, 2014c). The immediate consequence is a loss in tree water uptake ability (hydraulic failure) in combination with a reduction in non-structural carbohydrates that lead to carbon starvation (Ogaya et al. 2020), which results in a rapid wilting of leaves of one part of the canopy and/or in a gradual loss of foliage (crown defoliation), followed by tree death after one or two growing seasons (Brasier, 1996; Gallego *et al.*, 1999; Corcobado *et al.*, 2013c). Besides, *Q. ilex* species showed higher stem mortality than other Mediterranean species (Ogaya *et al.*, 2020), which leads to ecosystem composition alteration. Therefore, crown defoliation in holm oaks, which is the consequence of the physiological loss of tree vigour, is generally attributed to the activity of this soil-borne pathogen (i.e., *Phytophthora* spp.), drought stress or, more realistically, to the interaction of both factors (Gómez-Aparicio et al. 2012, Poyatos et al. 2013, Esteban et al. 2014a).

Before crown defoliation occurs, a set of fine-tuning biochemical adjustments are triggered at leaf level (Fernández-Marín *et al.*, 2017), reflecting profound modifications of the photosynthetic apparatus (Esteban et al. 2015a). These adjustments involve a variety of photoprotective mechanisms, mainly regu- lated by specialized metabolites, which may include: pigment concentration adjustments, the activation of xanthophyll cycles (both violaxanthin, VAZ and lutein epoxide-lutein, LxL; Esteban and García-Plazaola 2014) and the antioxidant network (Fernández-Marín *et al.*, 2017), such as the tocopherols that act as scavengers of reactive oxygen species (Munné-Bosch, 2005; Nogués *et al.*, 2014). Enhancement of these metabolites, trig- gered under moderate stress, may be good predictors of plant fitness (Fernández-Marín *et al.*, 2017). For this reason, metabolites are widely employed as early stress markers to evaluate and predict plant physiological status (García-Plazaola & Becerril, 2001; Tausz *et al.*, 2004; Munné-Bosch & Lalueza, 2007; Esteban *et al.*, 2009a; Fenollosa & Munné-Bosch, 2018). In the case of *Quercus* spp., the photosynthetic efficiency (Bussotti, 2004; Holland *et al.*, 2014) and the pigment (i.e., chlorophylls and carotenoids; Nogués *et al.*, 2014; Ramírez-Valiente *et al.*, 2015) or tocopherols content (Camarero *et al.*, 2012) have been employed to evaluate photoprotective responses under a wide variety of environmental conditions. However, unlike the huge body of knowledge currently available on early markers (Bussotti 2004, Camarero et al. 2012, Holland et al. 2014, Nogués et al. 2014, Ramírez-Valiente et al. 2015), their use as a crown defoliation warning

indicator under Mediterranean forest decline scenarios has been poorly studied (García-Plazaola & Becerril, 2001).

As stated above, the functioning of the antioxidant and photoprotection mechanisms in holm oaks have been relatively well studied and described. This knowledge could therefore be used to develop biochemical markers of environmental stress in native holm oak trees, which would be of paramount importance for the early diagnosis of tree decline. Therefore, the aims of the present study were (i) to identify plant performance markers that precede crown defoliation in holm oak trees with contrasting health status using chlorophyll a fluorescence induction, pigments and tocopherols, and (ii) to link these plant performance markers with tree defoliation, using a wide range of tree defoliation rates, to identify the physiological thresholds that may be used to predict tree decline. We hypothesized that before holm oak defoliation occurs, leaves undergo different physiological adjustments of their photoprotective compounds in line with the photochemical efficiency loss determined by an external mild perturbation. The stress markers proposed in this study may be considered as tools of high capacity for the diagnosis of early vigour losses at the plant and even ecosystem level. The results from this study therefore represent a data and theoretical baseline for the future applicability of tools able to predict in advance potential tree mortality events that may occur locally and even globally

4.2. Materials and methods

4.2.1. Study sites

We considered eight holm oak dehesa sites, i.e., ecosystems characterized by a low density of trees (Pulido et al. 2001), as independent study sites. All these study sites were located in the central–western part of the Iberian Peninsula, at 430 ± 6 m above sea level. The plant community of these sites is defined as *Pyro bourgaeanae-Querceto rotundifoliae sigmentum* Rivas Mart. (Rivas-Martínez, 1987). Here, scattered holm oak trees, with a low canopy cover (10–25%), grow in native permanent pastures dominated by annual species such *as Agrostis pourretii* Wild., *Xolantha guttata* (L.) Raf., *Plantago lagopus* L., *Vulpia myuros* (L.) C.C.Gmel., *Trifolium subterraneum* L., *Hordeum leporinum* Link, etc. Most of these dehesas have been traditionally used for livestock rearing and grazing, their average livestock being estimated at 0.4 units ha−1 year−1 . The pH of the soil varies from 4 to 7.7. The climate is Mediterranean, is characterized by hot and dry summers and mild winters. The mean monthly temperatures and rainfall in January and August 2019 were 6.96 ◦C, 29.88 mm, and 25 ◦C and 10.48 mm, respectively (CRU TS v.4; Harris et al. 2020; 2019 reference period).

The selection of sites was performed based on a previous study (Corcobado et al. 2013a), in which a combination of drought and P. cinnamomi were identified as the main tree decline causes. Specifically, for the final selection, we followed these criteria: (i) representative forests of the southwestern part of Spain, where dehesas abound; (ii) sites with trees at different stages of decline, from healthy to symptomatic (0 to 40% defoliation, respectively); (iii) sites were selected to define two distinctive situations, including plots with trees prominently healthy and plots in which healthy and affected trees coexisted; and (iv) sites with permission to conduct research and sampling (most of them are private properties).

4.2.2. Experimental design

Within each of the eight study sites, we identified and considered two areas of study, as in Corcobado-Sánchez (2013a): one 'healthy' area, where the whole population of holm oak trees showed no evident signs of crown defoliation; and one 'declining' area, where both healthy and declining (i.e., defoliated) holm oak trees coexisted. From each of the healthy areas, we selected six healthy holm oak trees (hereinafter referred to as control trees). From each of the declining area, we selected 12 holm oak trees, as it follows: 6 healthy holm oak trees (asymptomatic with no signs of defoliation, hereinafter referred to as non-declining trees) and 6 holm oak trees with signs of defoliation and evidenced in higher crown transparency than asymptomatic trees and/or sparser foliage in small branches (Corcobado, 2013b) (hereinafter referred to as declining trees). Accordingly, within each study site, we selected 18 holm oak trees, with the total number of holm oak trees selected for the eight sites being 144 individuals. In each individual, crown-condition assessment, chlorophyll a fluorescence induction, and sampling for pigments and tocopherols determinations were performed during July 2019.

4.2.3. Crown assessment

In the field, we categorized individuals in healthy and declining holm oak trees based on their crown condition, as explained above. A posteriori, the quantitative crown condition was estimated using two independent methods: crown transparency (i.e., hereinafter referred to as crown defoliation), and relative irradiance at the floor level (i.e., the quantity of solar radiation below each selected holm oak tree). To estimate the crown defoliation, we took photographs of each selected holm oak tree (i.e., 144). These photographs were always taken south facing at a distance of 20 m from the holm oaks' trunks and at 1.65 m above ground using a digital camera in automatic mode (Canon Eos 1200D, Amstelveen, The Netherlands). Then, we developed a metric to quantify the crown condition processing images by estimating the

total tree crown area and the defoliated areas within the crowns (i.e., branches with no leaves). Final crown defoliation was represented by the percentage of the total area occupied by the defoliated branches relative to the total crown area of the tree. This analysis was made with the Java-based image processing program ImageJ (1.52p; Ferreira and Rasband 2019, http://rsbweb.nih.gov/ij/).. To estimate the relative irradiance at the floor level, we took hemispheric photographs below each selected holm oak tree. These photographs were always taken at a distance of 50 cm from the trunks of the trees and 2 m above ground using a Nikon Coolpix 4500 digital camera, mounted on a tripod and equipped with a Nikon Fisheye Converter. Photographs were then analyzed using the Gap Light Analyser (GLA; version 2.0; Frazer et al. 1999), which transforms the colours of the photographs into black and white to estimate their pixels and separated into the sky or non-sky classes to determine canopy openness. Final relative irradiance values were expressed in percentages (Esteban *et al.*, 2007).

4.2.4. Chlorophyll a fluorescence induction analyses

In July 2019, from each selected healthy and declining holm oak tree, we sampled branches with 2 to 3 years-old fully-expanded mature leaves. This was a criterion to uniform and standardize the response because holm oaks may retain their leaves up to three years (Montserrat-Martí et al. 2009), and photosynthetic capacity is strongly affected by leaf age (Niinemets *et al.*, 2005). We analysed their photochemical efficiency and chlorophyll *a* fluorescence induction (OJIP). Specifically, four branches were sampled from the four cardinal directions, at approx. 3 m height and one fully-expanded leaf from was randomly collected. They were immediately stored in hermetic plastic bags, where relative humidity and temperatures were maintained constant, and kept in darkness for 6 hours. This "artificial predawn" (Tausz *et al.*, 2003; Esteban *et al.*, 2007) allowed the complete relaxation of the photosynthetic reaction centers and provide comparable conditions (due to logistics, more details in photosynthetic pigments and tocopherols analysis), a process needed to correctly determine the minimum level of fluorescence (F_o). Measurements were then performed in darkness, at room temperature (20°C), using a fluorimeter (FluorPen FP 100; Photon Systems Instruments, Drasov, Czech Republic). This technique estimates the flow of energy through the photosystem II (PSII), being a highly sensitive signature of the linear electron transport flow and the photosynthetic efficiency (for detailed reviews see Strasser et al. 2000, Stirbet and Govindjee 2011). Excitation via blue light-emitting diodes (455 nm), optically filtered to provide a light intensity of 3000 μmol photons $m^{-2}s^{-1}$, allow to record fluorescence transients during 2s at a frequency of 10μs, 100 μs, 1ms, and 10ms for time intervals of 10–600 μs, 0.6–

14 ms, 14–100 ms, and 0.1–2s, respectively. The fluorescence values at 40 μs (F_o, step O, all reaction centers of the PSII are open), 100 μs (F_{100}), 300 μs (F_{300}), 2ms (step J), 30 ms (step I), and maximal (maximum level of fluorescence, F_m, step P, closure of all reaction centers), were taken into consideration for further analyses. We further calculate the chlorophyll *a* fluorescence induction parameters (energy fluctuations and yields; more details below) from F_o and F_m and the fluorescence intensities selected at 40 μs, 100 μs, 300 μs, 2m, and 30 ms. These parameters were: *i*) the relative variable chlorophyll fluorescence derived from steps I and J (i.e., V_j and V_i); ii) specific energy fluxes per primary quinone acceptor reducing PSII centre (i.e., ABS/RC, DI_o/RC, TR_o/RC, ET_o/RC). In detail, ABS refers to the photon flux absorbed by the chlorophyll antenna pigments of the PSII. Part of this energy is dissipated, mainly as heat (DI_o). Another part of this absorbed energy is funnelled to the Reaction Center (RC), as trapping flux (TR_o). In the reaction centre, the excitation energy is converted into redox energy by reducing the electron acceptor QA to QA^-, which is then reoxidised to QA, creating an electron transport (ET_o; Strasser et al. 2000, Hermans et al. 2003). iii) quantum yields and efficiencies (i.e., φ_{Po}, Ψ_o, φ_{Eo}, φ_{Do}, and φ_{Pav}). These yields are directly related to the energetic fluctuations obtained from the specific fluxes per RC (Strasser *et al.*, 2000; Hermans *et al.*, 2003). In detail, φ_{Po}, the maximum quantum yield of primary photochemistry: represents the probability that an absorbed photon is trapped by the RC and used for primary photochemistry (it is calculated as TR_o/ABS); Ψ_o, the efficiency which a trapped exciton can move an electron into the electron transport chain further than QA (it is calculated as ET_o/TR_o). φ_{Eo}, the quantum yield of electron transport: represents the probability that an absorbed photon moves an electron into the electron transport chain (it is calculated as ET_o/ABS); φ_{Do}, the quantum yield for energy dissipation. Finally, we calculated the *iv*) performance index (Pi_{Abs}) which allows *in vivo* evaluation of plant performance (in terms of biophysical parameters that quantify photosynthetic energy conservation; Strasser et al. 2000). This parameter summarizes three important events i) the light trapping, ii) the quantum efficiency of reduction of QA and iii) the efficiency of electron transport from quinone to the intersystem carriers of the electron chain (Hermans *et al.*, 2003). Thus, this index is a useful tool to screen photosynthetic performance and characterize plant vitality under stress conditions as is sensitive to changes in antenna properties, light trapping efficiency and electron transport (Strasser *et al.*, 2000; Hermans *et al.*, 2003). The formulas used to calculate the above parameters plus more detailed information are provided in **Table S4.1** available as Supplementary data at the online version. **Fig. 2** also illustrates a highly simplified model of the energy fluxes and yields. The formulas used to calculate the above parameters plus more detailed information are provided in **Table**

S4.1 available as Supplementary data at Tree Physiology Online.

4.2.5. Photosynthetic pigments and tocopherols analyses

In July 2019, from each of the 144 holm oak trees, we also sampled branches with 2 to 3-year-old fully expanded mature leaves, from the four cardinal directions, and at approx. 3 m height. These samples were used to quantify the photosynthetic pigments (carotenoids and chlorophylls) and the lipophilic antioxidants (tocopherols). Due to logistics (i.e., the eight selected dehesas were spread over a large area and were thus sampled in different days and at different hours) and to the fact that these compounds (i.e., pigments and tocopherols) exhibit a high degree of environment modulation (Esteban et al. 2015b), the sampled branches were kept at constant temperature and in darkness for 6 h. This pre-treatment avoided circadian effects, facilitating the comparison among different sampling study sites and dates (Fernández-Marín *et al.*, 2019). To obtain homogenized samples at the tree level, all the leaves collected from each holm oak were pooled. Then, from each leaf, we cut four discs (hereinafter referred to as plant material for simplicity), each of them having a diameter of 3 mm. This plant material was further stored in plastic bags filled with silica gel (<10% RH; Esteban *et al.*, 2009a). This is a standardized methodology, specifically designed to collect and preserve plant material, that will be used for biochemical (pigment and antioxidant) analyses from remote locations where there is no close access to liquid nitrogen or to a −80 ◦C freezer (Esteban et al. 2009a).

Once in the laboratory (UPV/EHU laboratory, Basque Country, Spain), we used the plant material to extract pigments and tocopherols following the protocol described by Fernández-Marín et al. (2018).. Specifically, the extractions were made using 95% acetone and the resulting liquid was homogenized (Tissue Tearor model 965670) and then centrifuged at 16,100 g and 4 ◦C. Further on, the pellet was then resuspended in pure acetone, mixed in a vortex, and centrifuged again. Both supernatants were pooled and syringe filtered through a 0.22-µm PTFE filter (Whatman, Maidstone, UK). The extractions were performed under cold conditions (4 ◦C) and protecting the samples against direct light. The final quantification of the pigments and tocopherols was made using the ultra-rapid uHPLC method (Lacalle *et al.*, 2020). For this, the extracted samples were injected into the system Acquity^{TM} uHPLC H-Class (Waters ®, Milford, MA, USA) using a reversed-phase column (Acquity UPLC® HSS C18 SB, 100Å, 1.8 µm, 2.1 mm X 100 mm) and a Vanguard^{TM} pre-column (Acquity UPLC HSS C18 SB, 1.8µm). The photodiode detector (Acquity PDA uHPLC; Waters) was then used to detect pigments, while the tocopherols were detected by fluorescence (FLR; uHPLC Acquity

Waters). The retention times and conversion factors for carotenoids were the same as those described by (Lacalle *et al.*, 2020).

This study was focused on compounds that indicate the level of photoprotection in holm oak leaves (Esteban *et al.*, 2015a). For this reason, in figures and tables, the following compounds are shown: the total chlorophyll pool expressed on leaf area basis (Chl a + b, μmol m^{-2}) and the a to b chlorophyll ratio (Chl a/b, mol mol^{-1}). Additionally, the rest of the compounds were expressed on a chlorophyll basis (mmol mol−1 Chl): lutein (L); lutein epoxide (Lx); β-carotene (β-Car); total xanthophyll pool (VAZ = V + A + Z); total carotenoids (t-Car = neoxanthin + V + Lx + A + L + Z + α-carotene + β- Car); and total tocopherols (t-Toc, the sum of the tocopherols isomers, i.e., β - γ + α).

4.2.6. Statistical analyses

To analyze how the crown condition of the trees (i.e., crown defoliation and relative irradiance) and the chlorophyll a fluorescence induction (V_i, V_j, φ_{Po}, Ψ_o, φ_{Eo}, φ_{Do}, φ_{Pav}, Pi_{Abs}, ABS/RC, TR_o/RC, DI_o/RC, ET_oRC), pigments (Chl a + b, Chl a/b, VAZ, Lx, L, β-Car) and tocopherols (t-Toc), measured on their leaves, differed between the three health statuses (i.e., control, non-declining and declining holm oaks), we performed linear mixed-effects models (LMEs). Prior to LMEs, we checked the normality (Kolmogorov–Smirnoff test) and the homoscedasticity (Levene's test) of all response variables. When these assumptions were not met, we logarithmically transformed them. We performed individual LMEs for each response variable using the 'lme' function from the 'nlme' R package (Pinheiro *et al.*, 2020b). The fixed part of the LMEs included one of the above-mentioned response variables and the crown condition of the trees. 'Sites' were introduced as random effects. We then performed ANOVAs of either type II (when dealing with a balanced design; i.e., crown defoliation, relative irradiance, pigments, and tocopherols) or type III (when dealing with an unbalanced design; i.e., chlorophyll a fluorescence induction parameters) using the 'car' R package (Fox and Weisberg 2019). To further look for differences between the three health statuses, we used the 'emmeans' R package (Lenth, 2020) using the Tukey correction. The residuals of the models fulfilled the normality assumption. The final coefficients of the models were estimated using the restricted maximum likelihood method (REML).

For the radar plot, we calculated the average values of the chlorophyll *a* fluorescence induction parameters for each health status and we standardized them using the control group, for which we used a value of 1, as a reference. We then plotted these values using the

'radarchart' function from the 'fmsb' R package (Nakazawa, 2019). Deviations from the 1 value denote an effect in each of the chlorophyll a fluorescence induction parameter due to health status.

We performed Spearman correlations matrix to see how crown defoliation and relative irradiance correlated with the parameters more affected by environmental modulation, φ_{Po}, Pi_{Abs}, Chl a+b, Chl a/b, VAZ, L, β-Car, t-Car, and t-Toc, using the 'rcorr' function from the 'Hmisc' R package (Harrell 2019). The results of these preliminary analyses showed that crown defoliation was the variable that best correlated with most of the considered variables (i.e., φ_{Po}, Pi_{Abs}, VAZ, t-Car and t-Toc).

Based on the above-mentioned Spearman correlation results, we conducted LMEs considering Pi_{Abs}, VAZ and t-Toc as a function of crown defoliation. Note that no LMEs were run considering φ_{Po} since this parameter strongly covariates with PiAbs, the latter being a more integrative parameter of the photosynthetic performance (Strasser *et al.*, 2000). Likewise, the t-Car parameter was not considered either to conduct LMEs as its relationship with crown defoliation was weak comparing with the correlation between crown defoliation and VAZ. Prior to analyses, we log transformed the Pi_{Abs}, VAZ and t-Toc variables as they did not meet the normality assumption. The fixed part of the LMEs included Pi_{Abs}, VAZ or t-Toc and crown defoliation, while the random part of the LMEs accounted for 'sites'. For each response variable (i.e., Pi_{Abs}, VAZ and t-Toc), we run three different LMEs: lineal, logarithmic and polynomial. We did so in order to see which of these three functions better explained the fit of the Pi_{Abs}, VAZ and t-Toc variables as a function of crown defoliation. We selected the best models (i.e., lineal, logarithmic or polynomial) based on the Akaike Information Criterion (AIC) and Bayesian Information Criterion (BIC). When we failed to choose the best models based on either AIC or BIC (i.e., due to no significant differences), the most parsimonious model was selected. We quantified the fit of the final selected LMEs with a pseudo-R2 (R2 p; Nakagawa et al. 2017), whose values represent the coefficient of determination based on the likelihood-ratio test ('r.squaredLR' function from the 'MuMIn' R package; Barton 2020). The residuals of the models fulfilled the normality assumption. The final coefficients of the models were estimated using the REML.

Based on the results of the previous described LMEs, we looked for break-point values that may be used to estimate thresholds (i.e., values that mark a significant trend change; Toms and Lesperance 2003, Vito 2008) for the fit of Pi_{Abs}, VAZ and t-Toc as a function of crown

defoliation. For this, we run segmented regressions using the 'segmented' function from the 'segmented' R package (Vito, 2008). Break points were calculated using the 'confint.segmented' function from the 'segmented' R package (Vito 2008). As we did not find significant break-points for the Pi_{Abs} and VAZ variables, we only show the results corresponding to the t-Toc variable.

Finally, we also run a Structural Equation Model (SEM) based on the results of the Pi_{Abs}, VAZ and t-Toc LMEs. For this, we used the 'psem' function ('piecewiseSEM' R package; Lefcheck 2016), which allowed us to introduce random effects (i.e., in order to have a similar structure as the one used for LMEs). We run SEM to look for all possible causal-effect relationships between Pi_{Abs}, VAZ, t-Toc and crown defoliation. Prior to analyses, we log transformed the Pi_{Abs}, VAZ and t-Toc variables as they did not meet the normality assumption. We checked the goodness of fit of the SEM based on Fisher's C statistic, which follows a chi-squared distribution and tests if the model fits the data (P-value >0.05) or not ($P < 0.05$).

All statistical analyses were performed in R (v. 4.0.0, 2020, R Development Core Team 2020). Statistical relationships were considered significant at $P < 0.05$.

4.3. Results

4.3.1. Defining crown defoliation and relative irradiance to the categorized trees

Crown defoliation was found to be significantly higher for declining trees than for non-declining and control trees ($P < 0.05$) (**Fig 1A**). As for the relative irradiance, this variable varied significantly between all health status groups ($P < 0.05$), the declining trees having again the highest values, while the control trees showing the lowest values (**Fig 1B**). According to these results, the control holm oaks were the least affected by leaf loss (i.e., crown defoliation estimated to vary around $4.3 \pm 0.5\%$; relative irradiance estimated to vary around $24.0 \pm 1.0\%$),

while the declining trees were the most affected by leaf loss (i.e., crown defoliation estimated to vary around 18.8 ± 1.7%; relative irradiance estimated to vary around 35.6 ± 1.5%).

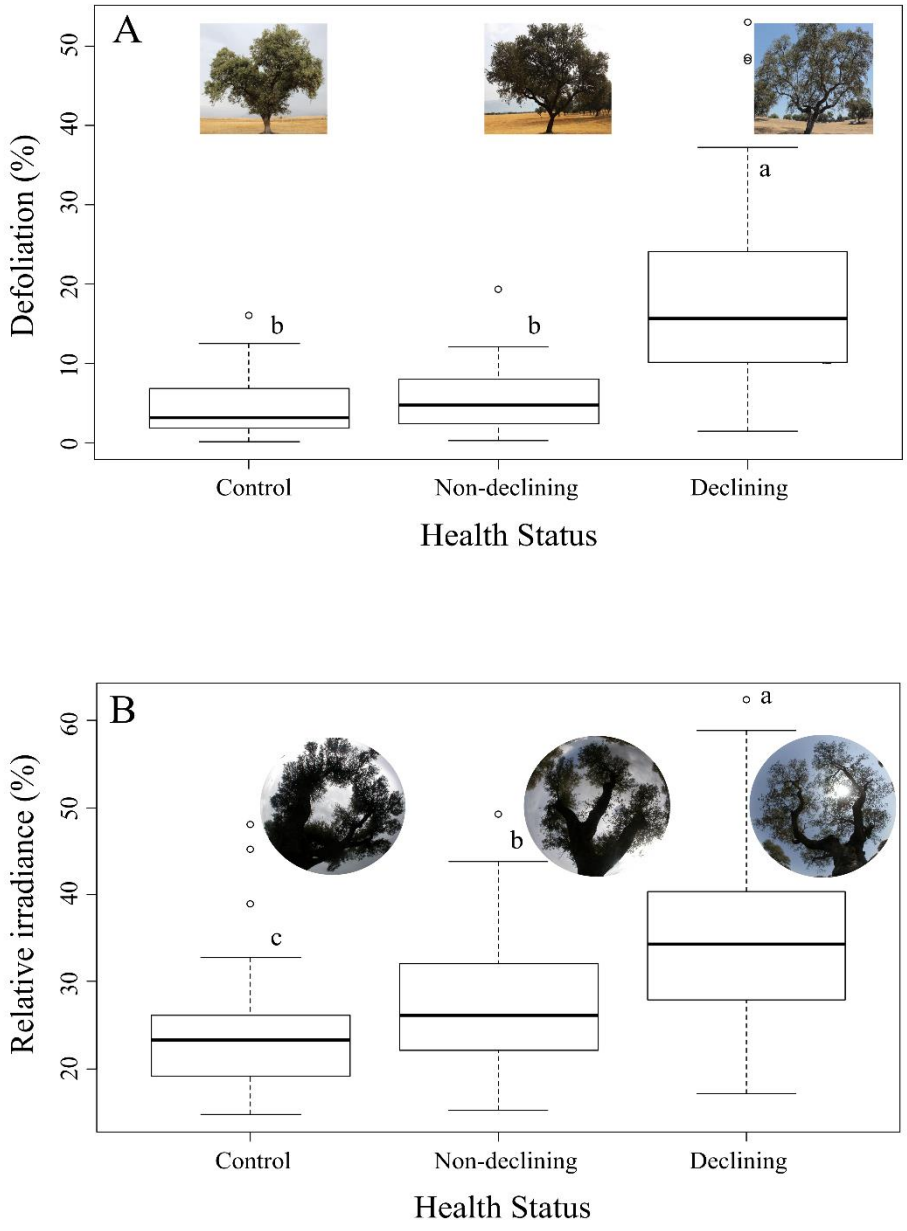

Figure 1. Boxplots showing crown defoliation (%; A) and relative irradiance (%; B) for each health status: control holm oak trees from healthy areas, non-declining holm oak trees from diseased areas, and declining holm oak trees from diseased areas. Each box represents 50% of data (n = 48 trees per each health status) distribution between the first and the third quartile; the central line represents the median; the upper and below whiskers cover the 1.5 interquartile range; empty circles represent outliers. Different letters indicate significant differences ($P < 0.05$) among control, non-declining and declining holm oak trees based on a Tukey multiple pairwise comparisons test.

4.3.2. Comparing chlorophyll *a* fluorescence induction response between health status

Declining holm oak trees differed significantly from the control holm oak trees in i) the specific energy flux related with the energy dissipation (DI_o/RC), ii) in the following quantum yields: φ_{Po}, φ_{Eo}, and φ_{Do} and iii) in the Pi_{Abs} (i.e., chlorophyll *a* fluorescence induction parameters; **Fig. 2**, **Table 1**). No such significant differences were found between control trees and non-declining trees, or between non-declining trees and declining trees (**Fig 2**, **Table 1**). No significant differences were found between the control, non-declining and declining holm oak trees regarding the rest of the chlorophyll a fluorescence induction parameters (**Fig 2, Table 1**). Overall, this indicates that the most affected processes affected in declining trees were the excitation energy dissipation (DI_o/RC and φ_{Do}), the maximum quantum yield of primary photochemistry (φ_{Po}), the probability that an absorbed photon moves an electron into the electron transport chain (φ_{Eo}), and the integrative parameter Pi_{Abs} that indicates that declining trees showed lower energy conservation from photons absorbed to the reduction of intersystem electron acceptors.

4.3.3. Pigments and tocopherols responses as a function of health status

The content of chlorophylls, carotenoids and tocopherols were analyzed in the three health status categories (**Table 1**). Declining trees showed a lower total chlorophyll content than the control trees, while the non-declining trees showed intermediate values for this variable. The decrease in the total chlorophyll content registered by the declining trees was not reflected by the changes in the antenna size, since no significant differences regarding the Chl a/b were found between the health statuses. As regarding the xanthophylls implicated in the LxL cycle (Lx and L), declining trees showed a significantly higher content of L and a significantly lower content of Lx than control trees. However, the overall Lx + L pool did not differ significantly between health statuses (data not shown). The content of total xanthophylls from the VAZ cycle differed significantly between the trees from the diseased areas (i.e., declining and non- declining) and the trees from the healthy areas (i.e., control), with lower values in the latter group. The content of t-Toc was significantly higher for the trees from the diseased areas (i.e., declining and non-declining) than for the trees from the healthy areas (i.e., control).

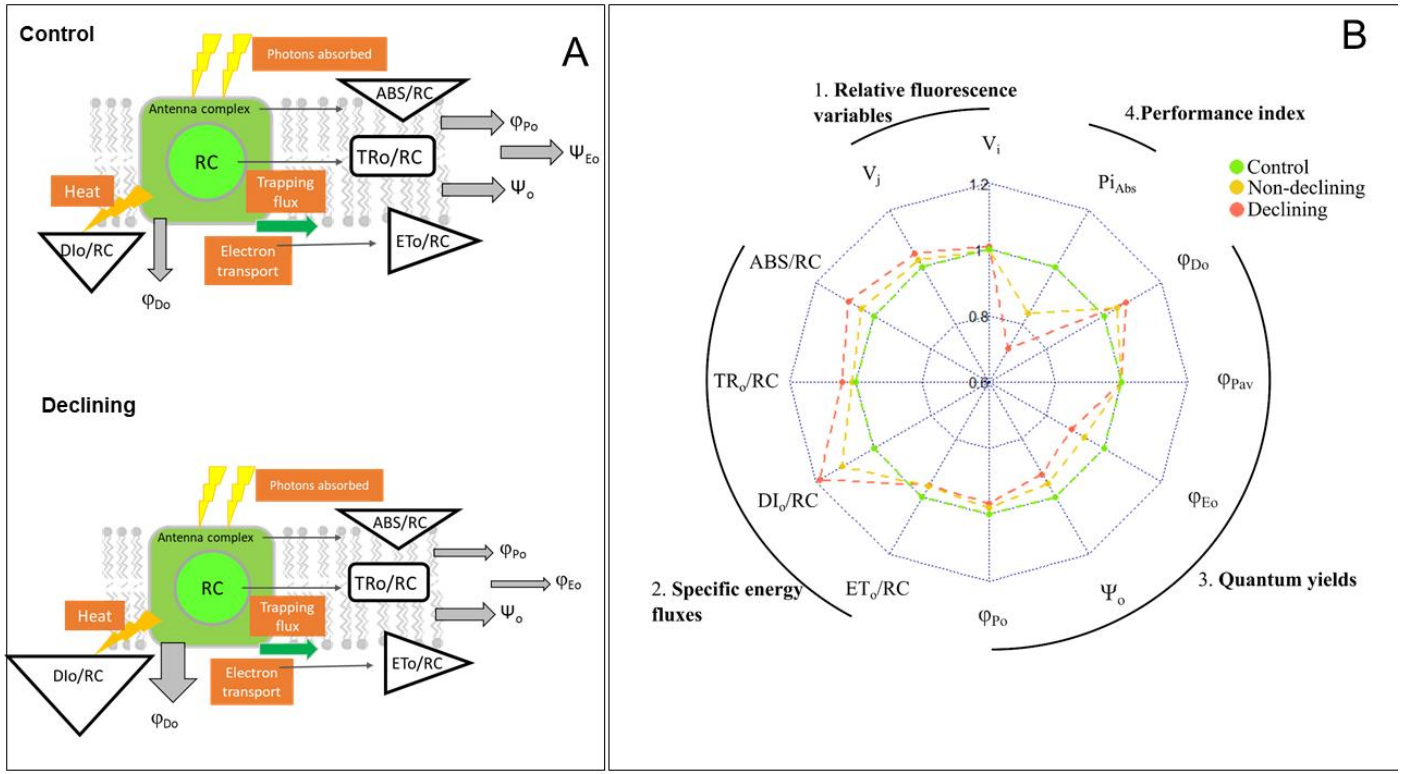

Figure 2. A) Schematically simplified representation of the model of energy transfer from solar light to photosynthetic electron transport in the photosynthetic apparatus (adapted from (Strasser *et al.*, 2000; Hermans *et al.*, 2003) for control and declining trees. ABS refers to the flux of photons absorbed by the antenna complex. Part of this excitation energy is dissipated, mainly as heat (DI_o), and another part is canalized as trapping flux (TR) to the reaction centre (RC) and converted to redox energy and creating an electron transport (ET_o). The size of the triangles and arrows are directly proportional to the change. We only depicted significant changes based on Table 1. B) Radar plot depicting the main chlorophyll *a* fluorescence induction parameters derived from the OJIP test (n = 41-47): control holm oak trees from healthy areas (marked in green), non-declining holm oak trees from diseased areas (marked in yellow), and declining holm oak trees from diseased areas (marked in red). Where, (i) Relative variable chlorophyll fluorescence as Vj and Vi; (ii) specific energy fluxes per primary quinone acceptor reducing PSII centres as ABS/RC, TR_o/RC, ET_o/RC and DI_o/RC, (iii) quantum yields as φ_{Po}, Ψ_o, φ_{Eo}, φ_{Do} and φ_{Pav}; and (iv) potential performance index for energy conservation (Pi_{Abs}). Note that standard error is not shown on the figure for clarity, but the coefficient of data variation was <0.7 in all cases. For further details on how the radar plot was built, refer to the Materials and Methods section (cf. *Statistical analyses*).. Definitions and formulae for all variables are given in the Materials and methods, and Table S4.1 available as Supplementary data at Tree Physiology Online

Table 1. Physiological variables for each health status: control holm oak trees from healthy areas, non-declining holm oak trees from diseased areas, and declining holm oak trees from diseased areas: i) chlorophyll a fluorescence induction parameters derived from the OJIP test (n = 42 – 47 ± SE): relative variable chlorophyll fluorescence (V_j and V_i); quantum yields (φ_{Po}, Ψ_o, φ_{Eo} and φ_{Do}, and φ_{Pav}); specific energy fluxes per primary quinone acceptor reducing PSII centres (ABS/RC, TR_o/RC, ET_o/RC and DI_o/RC); potential performance index for energy conservation (Pi_{Abs}); ii) Pigments and tocopherols (n = 48 ± SE): total chlorophyll pool (Chl a + b, μmol m^{-2}), a to b chlorophyll ratio (Chl a/b, mol mol^{-1}), lutein epoxide (Lx, mmol mol^{-1}Chl), β-carotene (β-Car, mmol mol^{-1}Chl), total xanthophyll cycle pool (VAZ, mmol mol^{-1} Chl), and total tocopherols (t-Toc, mmol mol^{-1} Chl). Asterisks (*p < 0.05; **p < 0.01; ***p < 0.001) represent statistically significant differences according to the linear mixed-effects models (LMEs) results. Different letters indicate significant differences (p < 0.05) between the three health status based on the post-hoc estimated marginal means test using the Tukey correction.

	Health Status			p-value
Variables	Control	Non-declining	Declining	
Chlorophyll *a* fluorescence induction parameters				
V_i	0.76±0.01	0.76±0.01	0.77±0.01	0.869
V_j	0.63±0.01	0.65±0.01	0.66±0.01	0.113
ABS/RC	1.43±0.03	1.40±0.06	1.55±0.05	0.089
TR_o/RC	0.98±0.02	0.99±0.02	1.02±0.02	0.304
DI_o/RC	0.45±0.02^{a}	0.5±0.04^{ab}	0.53±0.03^{b}	0.032*
ET_o/RC	0.36±0.01	0.34±0.01	0.34±0.01	0.453
φ_{Po}	0.69±0.01^{a}	0.68±0.01^{ab}	0.67±0.01^{b}	0.048*
Ψ_o	0.37±0.01	0.35±0.01	0.34±0.01	0.113
φ_{Eo}	0.25±0.01^{a}	0.24±0.01^{ab}	0.23±0.01^{b}	0.038*
φ_{Pav}	958.54±1.65	957.22±1.6	958.36±1.59	0.663
φ_{Do}	0.31±0.01^{a}	0.32±0.01^{ab}	0.33±0.01^{b}	0.021*
Pi_{Abs}	1.08±0.11^{a}	0.91±0.09^{ab}	0.78±0.07^{b}	0.023*
Pigments and tocopherols				
Chl a+b	692.28±28.35^{a}	626.89±19.29^{ab}	604.21±23.43^{b}	0.005**
Chl a/b	2.52±0.03	2.5±0.03	2.46±0.04	0.190
VAZ	25.33±1.18^{a}	29.1±1.41^{b}	32.22±1.94^{b}	< 0.001***
Lx	1.57±0.22^{a}	0.81±0.11^{b}	0.74±0.10^{b}	< 0.001***
L	132.89±2.23^{a}	137.47±1.54^{ab}	139.06±2.13^{b}	0.035*
β-Car	89.46±1.79	92.47±1.8	94.44±1.93	0.073
t-Car	292.85±4.31^{a}	304.18±3.09^{b}	310.73±4.11^{b}	< 0.001***
t-Toc	185.74±15.8^{a}	298.41±22.16^{b}	357.25±24.67^{b}	< 0.001***

*Definitions and formulae for chlorophyll a fluorescence induction parameters are shown in the Materials and Methods section and Table S4.1.

4.3.4. The performance index, total xanthophylls and tocopherols as a function of crown defoliation

Crown defoliation showed a more significant relationship with the chlorophyll *a* fluorescence induction parameters, the pigments and the tocopherols than the relative irradiance (**Fig 3**). In detail, crown defoliation was negatively correlated with φ_{Po} ($r = -0.18$; $P < 0.05$) and Pi_{Abs} ($r = -0.17$; $P < 0.05$) and positively correlated with relative irradiance ($r = 0.22$; $P < 0.01$), t-Car ($r = 0.24$; $P < 0.01$), total VAZ ($r = 0.31$; $P < 0.001$) and t-Toc ($r = 0.35$; $P < 0.001$) (Fig 3). As for the relative irradiance, it was only positively correlated with Pi_{Abs} ($r = 0.24$; $P < 0.05$) (**Fig 3**). Furthermore, negative correlations were also found between Pi_{Abs} and VAZ ($r = -0.24$; $P < 0.05$), and between Pi_{Abs} and t-Toc ($r = -0.19$; $P < 0.005$).

The results of the LMEs (i.e., where Pi_{Abs}, VAZ and t-Toc were modelled as a function of crown defoliation based on the Spearman correlations' results) showed that the model that best fitted the response of Pi_{Abs} to crown defoliation, was the logarithmic model (**Fig 4A, Table 2**). Specifically, we found higher Pi_{Abs} values for the holm oaks that showed a lower than 10% crown defoliation (i.e., mainly control trees) than for the holm oaks that showed a higher than 10% crown defoliation (i.e., mainly declining trees) (**Fig 4A**). The model that best fitted the response of VAZ (expressed on chlorophyll bases) to crown defoliation, was the linear one. Accordingly, VAZ increased gradually along with crown defoliation (**Fig 4B, Table 2**). In the case of the t-Toc variable (**Fig 4C, Table 2**), the model that best fitted its response to crown defoliation was the polynomial model. Furthermore, the predicted values of the segmented regression model (**Fig 4C**, blue line) indicated that t-Toc increased at the first defoliation phases (<8.9% crown defoliation). At this crown defoliation stage, t-Toc reached its maximum value (i.e., 344.4 mmol mol^{-1} Chl). Accordingly, we established this value as a threshold.

According to the results of the SEM (**Fig 5**), the decrease of Pi_{Abs} would affect the increase in VAZ and t-Toc levels due to the negative effect of Pi_{Abs} on the photoprotective compounds. The antioxidant t-Toc had a positive effect on defoliation. Simultaneously, VAZ increased t-Toc. Eventually, these three variables (Pi_{Abs}, VAZ and t-Toc) were predictive of crown defoliation.

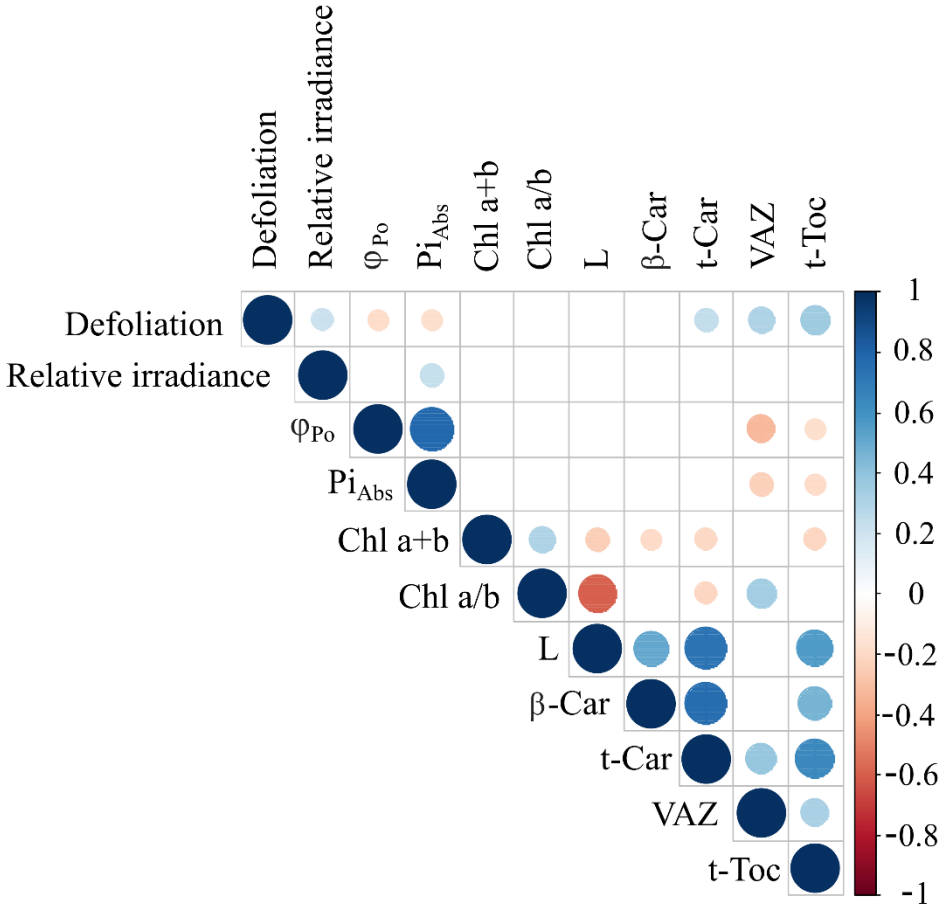

Figure 3. Spearman's rank correlation matrix plot showing the relationship between: (i) crown assessment variables (defoliation (%) and relative irradiance (%)); (ii) chlorophyll a fluorescence induction parameters derived from the OJIP test (photochemical efficiency (ϕ_{Po}) and potential), a to b chlorophyll ratio (Chl a/b, mol mol^{-1} performance index for energy conservation (Pi_{Abs}); (iii) pigments (total chlorophyll pool (Chl a + b, µmol m^{-2}), lutein (L, mmol mol^{-1} Chl), β-carotene (β-Car, mmol mol^{-1} Chl), total xanthophyll pool (VAZ, mmol mol^{-1})

Table 2. Results of the Linear mixed-effects models (LMEs) (i.e., the ANOVA table) in which Pi_{Abs}, VAZ, and t-Toc were fitted as a function of crown defoliation. Asterisks (*p < 0.05; **p < 0.01; ***p < 0.001) indicate statistically significant relationships. Pseudo-R^2 values represent the coefficient of determination based on the likelihood-ratio test. Where, degrees of freedom, Df; standard error, SE; potential performance index for energy conservation, Pi_{Abs}; total xanthophyll cycle pool, VAZ; total tocopherols, t-Toc.

Fixed effects	Df (numerator)	Df (denominator)	Estimate	SE	F	p-value	Pseudo-R^2
Pi_{Abs} as function of defoliation							0.168
Intercept	1	121	-0.112	0.122	5.51	0.025*	
Log (defoliation)	1	121	-0.077	0.038	3.98	0.048*	
VAZ as function of defoliation							0.439
Intercept	1	135	3.225	0.094	1277.25	< 0.001***	
Defoliation	1	135	0.007	0.002	12.72	< 0.001***	
t-Toc as function of defoliation							0.206
Intercept	1	134	4.659	0.209	2909.13	< 0.001***	
Defoliation	1	134	-0.052	0.018	4.47	0.036*	
√Defoliation	1	134	0.464	0.126	13.56	< 0.001***	

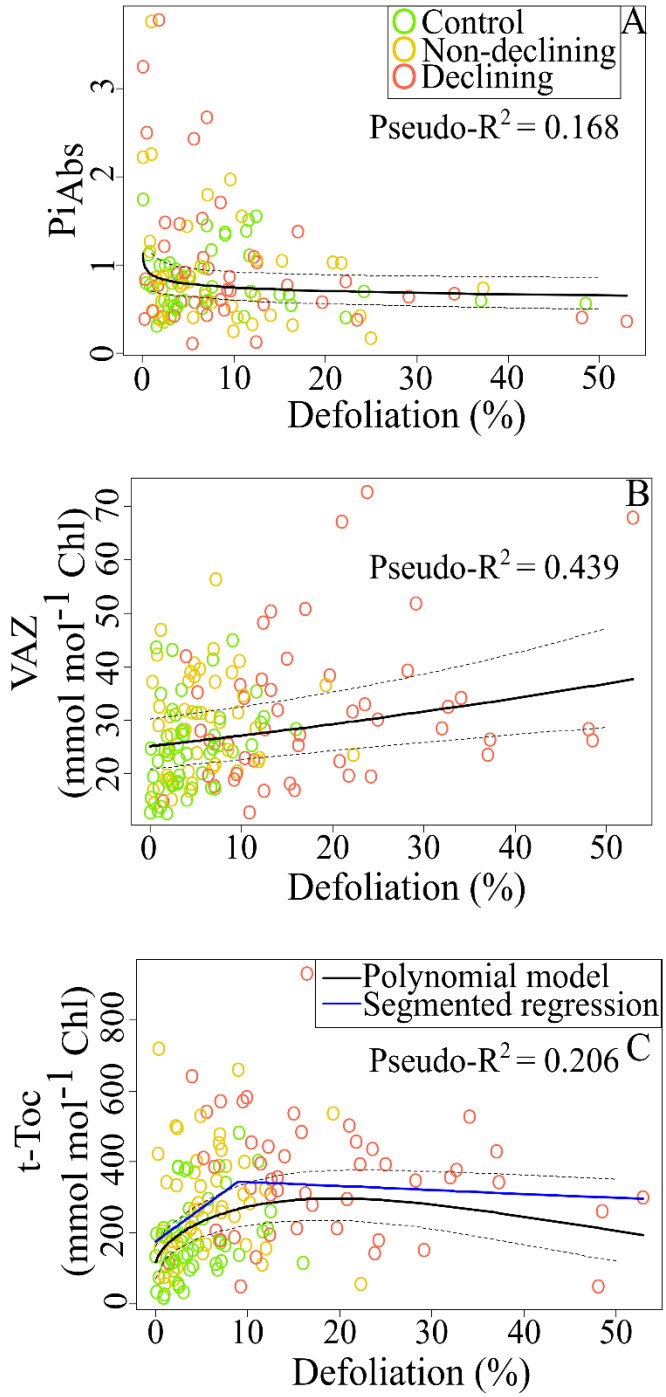

Figure 4. LME results showing Pi_{Abs} (i.e., potential performance index for energy conservation; A), VAZ (total xanthophyll pool expressed on total chlorophyll, mmol mol^{-1} Chl; B) and t-Toc (total tocopherols expressed on total chlorophyll, mmol mol^{-1} Chl; C) fits as a function of crown defoliation. Solid black lines represent fitted data, while dotted upper and lower lines represent the 95% confidence interval. In the case of t- Toc (C), the 'A-shaped' segmented regression is also represented with a blue bold line, on which the highest point represents the break point. This break point value depicts the maximum level reached by t-Toc (i.e., its threshold value) and its trend change along with crown defoliation (see Table 2 for statistics parameters). Empty circles in each plot represent the different health status: control holm oak trees from healthy areas (marked in green), non-declining holm oak trees from diseased areas (marked in yellow) and declining holm oak trees from diseased areas (marked in red). For each variable, we show the R^2_p; measuring the fraction of variation explained by the model (Nakagawa et al. 2017)

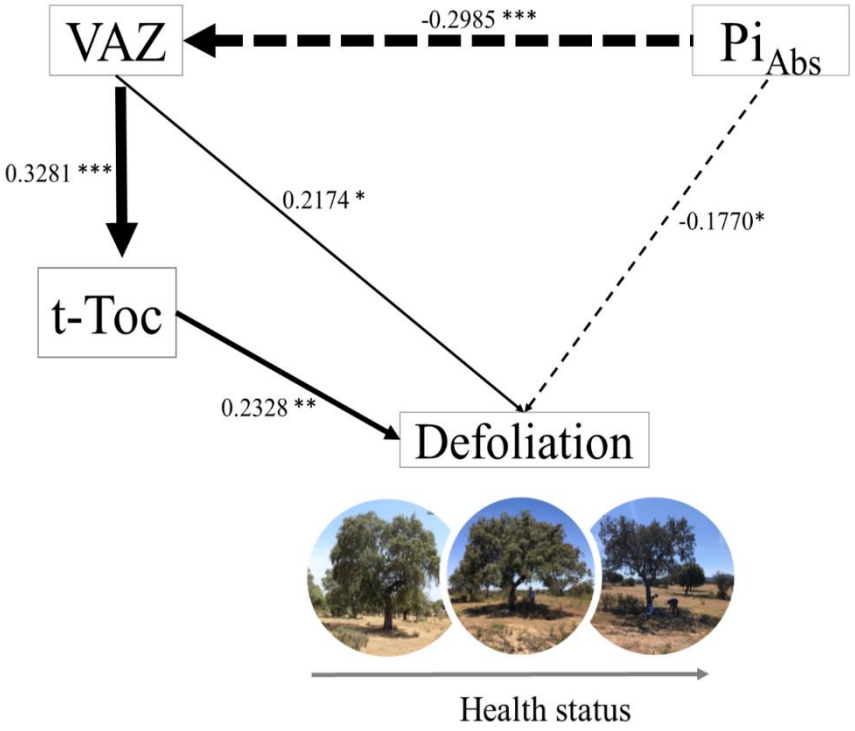

Figure 5. SEM results. Path diagram representing hypothesized causal- effect relationships between crown defoliation, photoprotective com- pounds (i.e., total xanthophyll pool, VAZ, mmol mol^{-1} Chl; and total tocopherols, t-Toc, mmol mol^{-1} Chl) and potential performance index for energy conservation (i.e., Pi_{Abs}, formula available in Table S4.1 available as Supplementary data at Tree Physiology Online). Note that all variables were logarithmically transformed prior to analyses. Causal-effect relationships are indicated by arrows as follows: positive and negative effects are indicated by solid and dashed lines, respectively, and the line thickness represents the weakness or strength of the relationship. Numbers indicate the standardized estimated regression weights. All the relationships represented are significant. Asterisks represent statistically significant differences (∗P<0.05; ∗∗P <0.01; ∗∗∗P <0.001).

4.4. Discussion

4.4.1. Early crown defoliation biochemical markers

Drought and pathogen infection elicit a cascade of physiological mechanisms, beginning with the oxidative stress-related signalling followed by an acclimation process or modification of a plant phenotype (decreasing the number of leaves; Ogaya and Peñuelas 2006), finally ending in crown defoliation and plant death (Vranova *et al.*, 2002; Baier & Dietz, 2005; Niinemets, 2010). Crown defoliation represents just a snapshot of a decline process(Camilo-Alves *et al.*, 2013). When *P. cinnamomi* infects non-declining holm oak, trees decline relatively fast (i.e., in a few years; Camilo-Alves et al. 2013), not only because this species is highly susceptible to the oomycete, but also because root rot and drought damage

may act in a synergistic way. This study showed that holm oak vigour losses resulting from the stress caused by drought and/or *P. cinnamomi* root rot damage was associated with chlorophyll *a* fluorescence induction parameters (i.e., higher energy dissipation yield, φ_{Do}, DI_o/RC; lower photochemical efficiency, φ_{Po}; and lower electron transport yield, φ_{Eo}; **Fig.3, Table 1**). This specific regulation of the photosynthetic apparatus function is in line with the specific adjustments showed by leaf-associated photoprotection compounds (i.e., Chl a + b, VAZ, Lx, L, t- Toc; **Table 1**). Similar upregulations in lipophilic photoprotective defences, such as the xanthophyll pool pigments (VAZ and LxL) (Hormaetxe *et al.*, 2007; Peguero-Pina *et al.*, 2008b; Esteban *et al.*, 2015a) and the tocopherols (Munné-Bosch & Alegre, 2000; Hormaetxe *et al.*, 2007; García-Plazaola *et al.*, 2008; Fernández-Marín *et al.*, 2017), have been previously reported for Mediterranean evergreen species. Our results thus reinforce the idea that such reactions at the leaf level are common acclimation responses to the harsh summer cocktail of unfavourable conditions that characterize the Mediterranean regions by thylakoid stabilization (Havaux *et al.*, 2005), energy dissipation (indicated by φ_{Do}) by the operation of VAZ and LxL cycles (Demmig-Adams *et al.*, 1999; Li *et al.*, 2009; Esteban *et al.*, 2015a), and/or antioxidant activity (Havaux et al. 2005, Dall'osto et al. 2006, Havaux. and García-Plazaola 2014)

A stress marker may be any variable that correlates with plant stress (Fenollosa & Munné-Bosch, 2018). Accordingly, any of the biochemical compounds implicated in the holm oak leaf- level reactions explained above fit within the definition of stress markers, which could indicate deeper damages in the plant physiological performance that may lead to irreversible defoliation processes and ultimately to the death of the individual. According to our results, the parameters that correlated well with crown defoliation could be considered as markers (i.e., mainly VAZ and t-Toc) of early decline since their response, triggered by drought stress, preceded crown defoliation. In this sense, the visually non-declining holm oaks from the diseased areas may give us important clues regarding tolerance strategies and may further serve to define early stress biomarkers. In this regard, at the early stages of tree vigour losses, when rates of defoliation are low (≈10%; **Fig 1**), we found significant differences in the VAZ and t-Toc pools (expressed on a chlorophyll basis; **Table 1**) between the holm oak trees from the diseased areas (with no differences between declining and non-declining trees) and the holm oak trees from the healthy areas (i.e., control trees). These findings suggest that the compounds induced in the leaves of the non-declining trees (i.e., both VAZ and t-Toc) could be assessed as early indicators of defoliation as they appear before the characteristic tipping points of crown defoliation that define the onset of holm oak decline and death.

4.4.2. The physiological threshold to predict plant performance

As both t-Toc and VAZ pigments are subjected to environmental modulation, we found a positive correlation between them (**Fig 3**), suggesting that both act synergistically to prevent damages at the leaf-level caused by stress factors. Changes of both pools of photoprotective compounds, under environmental stress, seem to usually display a highly synchronized mode (Garcia-Plazaola *et al.*, 2004; Munné-Bosch, 2005; Havaux. & García-Plazaola, 2014). This synchrony indicates a synergistic and complementary function as controllers of membrane fluidity photoprotection (Havaux et al. 2005, Esteban et al. 2009b). However, when modelling t-Toc and VAZ as a function of crown defoliation, we found a continuous rise of VAZ content and a non-linear saturated curve for t-Toc (**Fig 4**). These reactions respond to their differential role in the biochemical adjustments that the photosynthetic apparatus undergoes (Anderson et al. 2008, Esteban et al. 2015a). Explicitly, in the case of the xanthophylls (VAZ pigments), and considering the PSII antenna proteins constricted composition, the linear fit as a function of crown defoliation (Fig 4) supports the presence of a free pool of VAZ xanthophylls in the thylakoid membranes (Havaux and García-Plazaola 2014, Esteban et al. 2015a) and/or indicates that this extra pool of VAZ pigments is bound to stress proteins such as early light-induced proteins that are upregulated in response to unfavourable conditions (Alamillo & Bartels, 2001; Zarter *et al.*, 2006). Conversely, at the onset of the crown defoliation process, a quick rise in t-Toc occurred, reaching its maximum threshold level when declining symptoms (crown defoliation) were already evident (8.9% defoliation) and descending afterword along with the increase of crown defoliation. Most of this newly formed t-Toc pool is probably sequestered in plastoglobules (Vidi *et al.*, 2006), dynamically exchanging with the thylakoid t-Toc pool. This 'A-shaped' curve resulted from an initial activation phase to counteract the damage, followed by a decreasing second phase when the oxidative stress was too severe and t-Toc degradation exceeded the rate of recycling and synthesis *de novo* (Munné-Bosch, 2005; Havaux. & García-Plazaola, 2014). Similar trends of tocopherols have been reported in previous studies (Juvany *et al.*, 2012, 2013). Stress-tolerant plants only exhibit the initial t-Toc phase, similar to that observed for our control holm oak trees (**Fig 4C**, green circles). Stress-sensitive plants instead exhibit the decreasing collapse phase (Munné-Bosch 2005), similar to the observed in the declining holm oak trees included in our study (**Fig 4C**, red circles). This indicates that a senescence non-reversible process (probably related to signalling role and remobilization phase) may be occurring in declining holm oak trees. Hence, our segmented regression model, which linked early markers with a tree health status gradient (based on crown

defoliation; **Fig 4C**), provided us with the opportunity to find a threshold t-Toc value (i.e., 344.4 mmol mol−1 Chl) that marks the onset of the non-reversible declining phase.

4.4.3. The mechanistic model

We propose a mechanistic process that may predict crown defoliation based on the causal-effect relationships that we found between Pi_{Abs} and the photoprotective compounds (VAZ and t-Toc), especially at the early stages of tree defoliation (**Fig 5**). Specifically, at low crown defoliation levels (<10%), we observed a down-regulation of the photochemical efficiency ($\varphi_{Po} \approx 0.7$) associated with defoliation, since in declining trees, φ_{Po} and Pi_{Abs} were significantly lower than in the control holm oak trees from the healthy areas. Down-regulation of the photochemical efficiency could be associated with a decrease in carbon assimilation (Gratani & Bombelli, 2000) as, during the summertime, the diffusion of CO2 from the atmosphere to the carboxylation sites in leaves may experience greater resistance due to stomata closure (Nogués *et al.*, 2014).. However, the lower values of photosynthetic efficiency found for the declining trees ($\varphi_{Po} < 0.68$) could be explained by a lower electron transport rate (Strasser et al. 2000, indicated by the parameter φ_{Eo}) possibly leading to the activation of photoprotective responses (Bussotti *et al.*, 2011) triggered by the increase in leaf concentration of LxL, VAZ and t-Toc (**Table 1, Fig 4**).

The question that now arises is whether the reactions of these compounds (VAZ and t-Toc) are induced at the onset of the tree decline process (‘damage response’) or are a part of the photoacclimation process (‘tolerance response’) in response to water stress. Based on our results (i.e., **Fig 4** and **5**) these reactions may be interpreted more as a photoacclimation process (‘tolerance response’) rather than as a ‘damage response’ (García-Plazaola et al. 2008). This photoacclimation process agrees with literature that reports holm oak photoprotective responses to drought stress (Camarero *et al.*, 2012), which seems to be part of a conservative resource-use strategy of this species (i.e., low responsiveness to changes in environmental conditions and scarce use of available resources). Similar pat- terns have been found for other evergreen woody species and seem to allow them to adapt and tolerate the harsh Mediterranean conditions and avoid the use of deficient resources once conditions reach stressful levels (Valladares *et al.*, 2000a). Moreover, photoprotective responses acquired during stressful conditions may confer them more tolerance and resistance to face subsequent stressful factors and conditions not only at the tree-level but also at within-population level(Matesanz & Valladares, 2014). Nevertheless, based on our results, we may also take into consideration the

presence of a photooxidative damage in trees at advanced defoliation stages ('damage response') where the t-Toc trend dropped down (Munné-Bosch, 2005). This decrease may be attributed to the deficiency of t-Toc recycling by ascorbate due to the possible lack of carbohydrates for its synthesis (Tausz *et al.*, 2004; García-Plazaola *et al.*, 2008). As biochemical and diffusion limitations of photosynthesis-related with leaf age have been described for *Q. ilex* (Niinemets *et al.*, 2005), the declining process observed in this study could be related to age-associated increased biochemical limitation (Niinemets et al. 2005). Overall, the reduction of leaf longevity, simulating premature aging, would imply a decreasing number of leaves (Ogaya & Peñuelas, 2006) and shifts in branching and shoot length (as has been described for conifers; Niinemets & Lukjanova, 2003), causing shorter current-year shoots (Ogaya and Peñuelas 2006) that may counteract for the overall canopy depletion in declining holm oaks. Overall, further research will be needed to confirm to what extent the observed leaf-level physiological adjustments preceding defoliation could be a consequence of damage or of acclimation and tolerance. Disentangling shoot bifurcation rates (Niinemets and Lukjanova 2003) and canopy dynamics could provide insights into the defoliation process at the whole-plant level. Hence, controlled experiments in which trees' health status and their physiological responses to drought are monitored over time are thus needed to address these complex questions.

4.4.4. Final remarks and conclusions

Early photoprotective responses to stress, reflected in the variations of the photoprotective compounds (mainly VAZ and t- Toc), represent a conservative resource-use strategy that allows holm oak to survive in the harsh Mediterranean conditions. These responses preceded crown defoliation, the most radical response to stress and a tipping point of no recovery for holm oak. We identified early markers of stress that may be used as a useful diagnostic tool given that drought and pathogen incidence are expected to enhance holm oak decline (Brasier, 1996; Resco De Dios *et al.*, 2007; Lindner *et al.*, 2010; Natalini *et al.*, 2016). Accordingly, the results presented in this study may provide basic knowledge to elaborate preventive measures and adaptive strategies (Pollastrini *et al.*, 2016) intended to prevent both the appearance and the propagation of declining foci in the dehesa ecosystems. The early stress markers implemented here could be more easily estimated by remote sensing techniques (i.e., hyperspectral and thermal images), currently used to diag- nose the health status of trees at a landscape level (Gamon *et al.*, 2016; Zarco-Tejada *et al.*, 2018; Ensminger, 2020). Indeed, the Earth Explorer Fluorescence Explorer mission that will map fluorescence vegetation (our site

1 will be included) will greatly expand the potential of these early markers in the near future to track forest decline incidence (Hernández-Clemente *et al.*, 2019) and to facilitate the adoption of preventive measures that may counterbalance the effects of drought and pathogens on trees

Chapter V

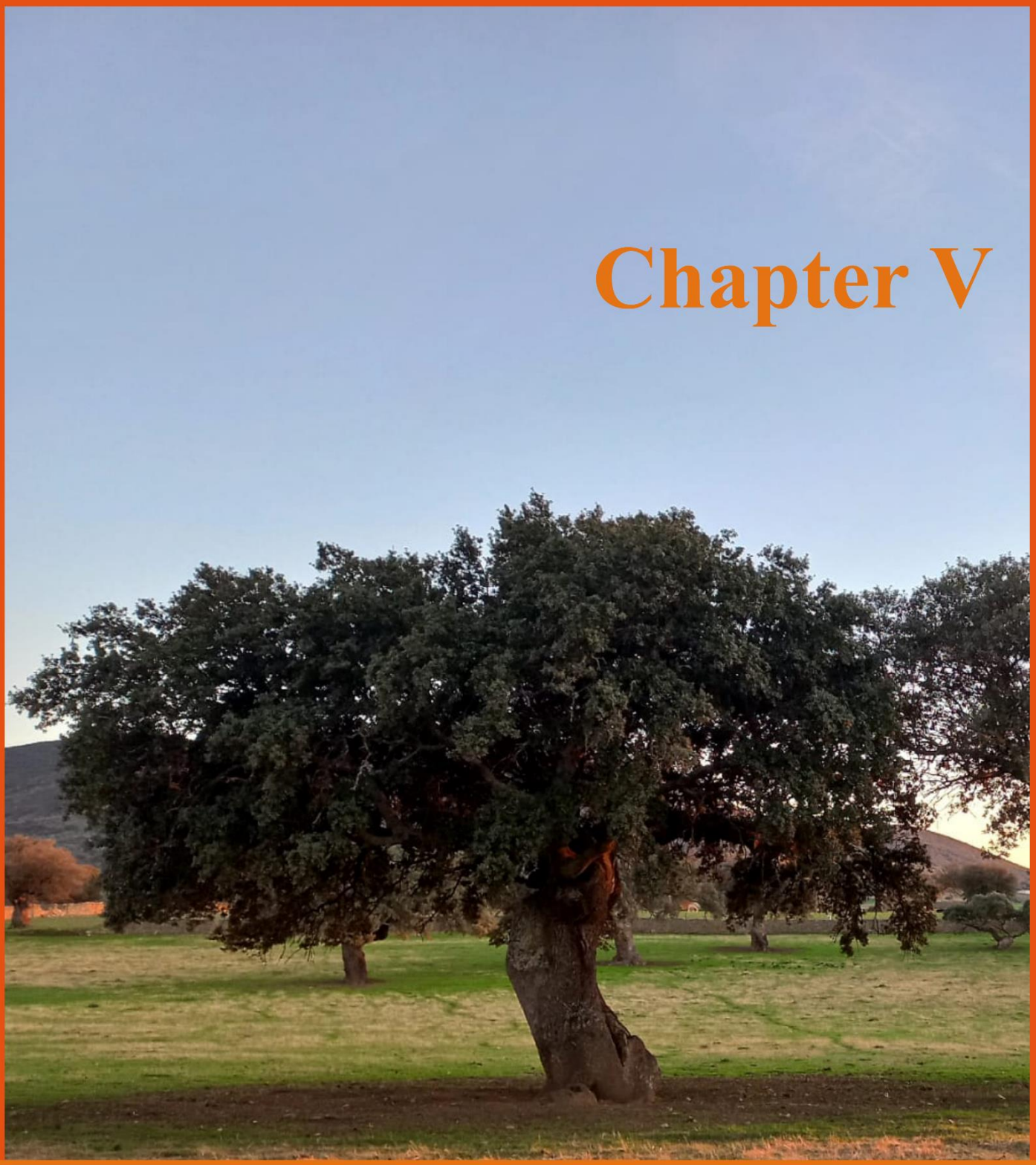

Holm oak decline is determined by shifts in fine root phenotypic plasticity in response to bellowground stress

New Phytologist 235, 6: 2237-2251

Holm oak decline is determined by shifts in fine root phenotypic plasticity in response to belowground stress

Manuel Encinas-Valero[1], Raquel Esteban[2], Ana-Maria Hereş[1,3], María Vivas[4], Dorra Fakhet[5], Iker Aranjuelo[5], Alejandro Solla[4], Gerardo Moreno[4], Jorge Curiel Yuste[1,6]

New Phytologist (2022) doi: 10.1111/nph.18182

[1] BC3-Basque Centre for Climate Change, Scientific Campus of the University of the Basque Country, B/ Sarriena s/n 48940 Leioa, Bizkaia, Spain
[2] Department of Plant Biology and Ecology, University of Basque Country (UPV/EHU), B/Sarriena s/n, 48940 Leioa, Bizkaia, Spain
[3] Department of Forest Sciences, Transilvania University of Braşov, Sirul Beethoven-1, 500123 Braşov, Romania
[4] Faculty of Forestry, Institute for Dehesa Research (INDEHESA), Universidad de Extremadura, Avenida Virgen del Puerto 2, 10600 Plasencia, Cáceres, Spain.
[5] Instituto de Agrobiotecnología (IdAB), Consejo Superior de Investigaciones Científicas (CSIC)-Gobierno de Navarra; Avenida Pamplona 123, 31192, Mutilva, Spain
[6] IKERBASQUE. Basque Foundation for Science, Plaza Euskadi 5, E-48009 Bilbao, Bizkaia, Spain

Corresponding author (encinasvaleromanuel@gmail.com)

Abstract

- Climate change and pathogen outbreaks are the two major causes of decline in Mediterranean holm oak trees (*Quercus ilex* L. subsp. *ballota* [Desf.] Samp.). Crown-level changes in response to these stressful conditions have been widely documented but the responses of the root systems remain unexplored. The effects of environmental stress over roots and its potential role during the declining process need to be evaluated.
- Here, we aimed to study how key morphological and architectural root parameters and non-structural carbohydrates of roots are affected along a holm oak health gradient (i.e., healthy, susceptible and declining).
- Holm oaks with different health statuses had different soil resource-uptake strategies. While healthy and susceptible trees showed a conservative resource-uptake strategy independently of soil nutrient availability, declining trees optimized soil resource acquisition by increasing the phenotypic plasticity of their fine root system.
- This increase in fine root phenotypic plasticity in declining holm oaks represents an energy-consuming strategy promoted to cope with the stress and at the expense of foliage maintenance. Hence, our study describes a potential feedback loop resulting from strong unprecedented belowground stress that ultimately may lead to poor adaptation and tree death in the Spanish dehesa.

Key words: defoliation, holm oak, nonstructural carbohydrates, phenotypic plasticity, root architecture, soil nutrient availability, trade-off

5.1. Introduction

The tree root systems are key components maintaining the functioning and services of the forests (Faucon *et al.*, 2017; Freschet & Roumet, 2017). On the one hand, they play an important role in biogeochemical cycling by providing biomass input and mineral nutrients to the soil, through root tissues turnover (Ruess *et al.*, 2003; Brunner & Godbold, 2007; McCormack *et al.*, 2012), and by determining soil structure and stability (Bardgett *et al.*, 2014). On the other hand, roots are also essential for plant fitness and functioning as they are responsible for foraging and transporting water and nutrients (Poorter & Ryser, 2015), providing physical support and storing carbohydrates (Freschet *et al.*, 2021b). However, biotic and abiotic factors determine how roots influence plants' and ecosystems' functioning (Langley *et al.*, 2006; Berendsen *et al.*, 2012; Bardgett *et al.*, 2014). Investigating the potential risks to which the tree root systems are subjected is thus fundamental for understanding the overall ecosystem functioning and stability. In this regard, associations between root traits and environmental factors make it possible to link root characteristics to a particular process, determine the function of the trait and evaluate the impact of climate change over plants' and ecosystems' functioning (Beidler *et al.*, 2015; Faucon *et al.*, 2017; Marañón *et al.*, 2020).

Many biotic factors determine root functioning and functional traits. For instance, mycorrhizal fungi or pathogens infection may affect root structure (i.e., morphology, architecture) and different aspects of plant physiology (i.e., resource uptake kinetic change, accumulation of phenolic compounds, exudates; Ruíz-Gómez *et al.*, 2015; Freschet *et al.*, 2021a) while plant-plant competition for soil resources may also modify root characteristics (Gea-Izquierdo *et al.*, 2009; Gazol *et al.*, 2021). Also, the soil matrix may strongly affect root functional traits. Contrasting physicochemical soil properties such as texture, water availability, nutrients and/or other factors may modify the architecture, morphology and physiology of the roots (Makita *et al.*, 2011; Alameda & Villar, 2012; Trubat *et al.*, 2012). These modifications represent strategies to optimize the acquisition of resources when soil environmental conditions become challenging (Bardgett *et al.*, 2014). For instance, root branching may increase in response to soil nutrient hotspots (Mou *et al.*, 2013; Eissenstat *et al.*, 2015; Freschet *et al.*, 2021b), or root diameter and/or length may be altered by soil compaction (Alameda & Villar, 2012) and water availability (Cubera *et al.*, 2012; Brunner *et al.*, 2015). Thus, in response to the spatio-temporal soil heterogeneity, roots may exhibit phenotypical plasticity (i.e., different phenotypes) by reflecting differences in their morphology, architecture and/or physiological traits, which result from the interaction between

the genotype and the environment (Arnold *et al.*, 2019). This phenotypical plasticity allows roots to maintain efficiently their functioning (i.e., resource acquisition) under challenging environmental conditions. Given the fact that soils are characterized by high spatial heterogeneity, the characterization of the soil properties is critical to capture the variability of intraspecific root functional traits and their link to root functioning (Kumordzi *et al.*, 2019). Although an increasing number of studies have recently been focused on root ecophysiology (i.e., root functional traits, roots physiology and soil interaction; Łakomy *et al.*, 2019; Suseela *et al.*, 2020; Freschet *et al.*, 2021b) many gaps remain in our understanding of root functioning under field conditions.

The effects of the climate on the functioning of the root systems may have strong implications for plant fitness and ecosystem functioning (Brunner *et al.*, 2015; Freschet *et al.*, 2021b). During recent decades, large forested regions around the globe have undergone drought and heatwave-associated decline and mortality (Allen *et al.*, 2010; Hartmann *et al.*, 2018; Hammond *et al.*, 2022). In this regard, in the Mediterranean basin, even well adapted to the Mediterranean conditions, tree species as holm oak (*Quercus ilex* L. subsp. *ballota* [Desf.] Samp.), have suffered such increased decline (i.e., canopy defoliation; Brasier, 1996; Peñuelas *et al.*, 2001; Carnicer *et al.*, 2011) and mortality since the 80s. Holm oak decline is characterized by sudden tree death or a gradual loss of foliage that affects the hole crown or just some branches (Camilo-Alves *et al.*, 2013). Furthermore, holm oak decline has been associated with alterations in the physiological (i.e., non-structural carbohydrates) and structural traits of roots (Villar-Salvador *et al.*, 2004; León *et al.*, 2017). Identifying root functional traits related with tree decline is crucial to define risk factors of tree mortality and understanding the underlying mechanisms of the tree decline and death processes (Hartmann *et al.*, 2018).

Warmer and drier conditions are climate change-related factors with potential effects on the root functional traits (Brunner *et al.*, 2015). Additionally, the presence of soil-borne pathogens such as *Phytophthora cinammonni* Rands. exacerbate the impact of drought events (Ruíz-Gómez *et al.*, 2019b). This pathogen is present worldwide (Scott *et al.*, 2013) and is responsible for fine root rot in holm oak (Corcobado *et al.*, 2013b,c, 2017; Ruíz-Gómez *et al.*, 2015) and thus, for diminishing the capacity of the trees to uptake and transport water and essential nutrients to the crown (Jönsson, 2006; Ruíz-Gómez *et al.*, 2019b). Once tree physiological damage surpasses a threshold, tree death occurs (Anderegg & Anderegg, 2013). However, before physiological damage is irreversible, trees trigger different strategies, simultaneously (i.e., anatomical, physiological, chemical, biochemical and molecular), to

mitigate such environmental belowground stress. Those adjustments occur at the expense of changes in carbon (C) allocation to belowground compartments (i.e., by increasing the root-to-shoot ratio; Brunner & Godbold, 2007; Moser *et al.*, 2015) and by extending the taproots to the deep water level (Barbeta & Peñuelas, 2017), mechanisms that will further affect the morphology and physiology in the fine root system (Zadworny *et al.*, 2021). Such responses occur at the expense of different metabolic substrates such as carbohydrates (Ritchie & Dunlap, 1980; Camisón *et al.*, 2020). Nonetheless, water deprivation may lead to photosynthesis limitation and predispose the tree to carbon depletion and deficiency (McDowell *et al.*, 2008; Gessler *et al.*, 2018) affecting the availability of carbohydrates and consequently, leaf flush (Freschet *et al.*, 2021b), root growth (Ritchie & Dunlap, 1980; Willaume & Pagès, 2006, 2011) and restricting the use of carbohydrates to respiration and osmoregulation processes (Hartmann *et al.*, 2013). Additionally, the availability of carbohydrates, critical for the development of the roots systems, does not depend solely on environmental conditions (i.e., drought) but also on phenological events (i.e., the developmental stage of the tree tissues; leaf flush, flowering or root growth;Willaume & Pagès, 2006; Angay *et al.*, 2014). The alternation between root and shoot development has been observed for different *Quercus* species (Reich *et al.*, 1980; Willaume & Pagès, 2006; Angay *et al.*, 2014), where maximum leaf expansion usually coincides with minimum root growth and *vice versa* (Reich *et al.*, 1980; Willaume & Pagès, 2006, 2011). In this context, it is essential to better understand the energy costs associated with increased phenotypic plasticity of the tree root system under high-stress conditions and its implications for defoliation.

In this study, we focused on holm oak trees growing in Spanish dehesas. The dehesas are human-shaped savannah-like ecosystems, considered to be among the most threatened ecosystems in Spain (Pulido *et al.*, 2001; Herguido-Sevillano *et al.*, 2017) as a consequence of the interaction between pathogen outbreaks (i.e., *Phytophthora* spp., Brasier, 1996; Solla *et al.*, 2009; Martín-García *et al.*, 2015; Corcobado *et al.*, 2017), climate change-related extreme events (i.e., drought and high temperatures; Allen *et al.*, 2015) and an intensive human management in recent decades due to the abandonment of traditional uses of the dehesa. Specifically, our study focused on investigating the fine root phenotypical plasticity and the potential trade-offs that may occur between the aboveground (i.e., tree defoliation) and the belowground (i.e., roots) compartments of holm oaks. The morphology and architecture of roots are determined by genetic factors, soil physicochemical properties (Alameda & Villar, 2012; Giehl & von Wirén, 2014), biotic interactions (Chen *et al.*, 2016) and the availability and distribution patterns of carbohydrates (Ritchie & Dunlap, 1980). The hypotheses of this study

are: **(1)** stress caused by summer drought and *Phytophthora* on the belowground tree compartment leads to potential changes in the resource uptake strategy of fine roots in holm oak trees through alterations in their morphology and architecture, and **(2)** changes in the resource-uptake capacity of fine roots imply shifts in non-structural carbohydrates resource allocation (i.e., NSC). In other words, the improvement of soil resource acquisition may be at the expense of maintaining the photosynthetic capacity of the tree and may lead to crown defoliation.

5.2. Materials and Methods

5.2.1. Study sites and experimental design

The study was performed in nine dehesas, characterized by a low tree canopy cover (10–25%). These dehesas are situated in the south west of Spain and were selected based on a previous study (Corcobado, 2013a) in which the interaction between drought and *Phytophthora cinnamomi* Rands. was identified as the main cause of holm oak decline. Further details on the criteria that were used to select the dehesas may be found in Encinas-Valero *et al.*, (2022). The selected dehesas are traditionally used for livestock rearing and grazing, the estimated density of cattle being of 0.4 units ha^{-1} $year^{-1}$. The pH of the soil varies from 4 to 7.7. The climate is Mediterranean, being characterized by hot and dry summers and mild winters. Mean monthly temperatures vary from 6.9±0.6º C (January) to 25.0±0.6º C (August), while mean monthly precipitation varies from 29.8±1.2 mm (January) to 10.4±2.1 mm (August)(CRU TS v.4; Harris *et al.*, 2020, reference period 2019).

In the nine dehesas, we selected 162 holm oak trees with a mean diameter at breast height of 51.3±1.0 cm and a mean height of 8.4±0.1 m, located in two sampling sites close to each other: *i*) a healthy site, where only healthy (i.e., with no apparent crown defoliation) holm oak trees (n=6 per dehesa) were present; and *ii*) an unhealthy site, where non-defoliated (n=6) and defoliated (n=6) trees were present (Chapter III, **Fig. 1**). These sampling sites respond to the natural pattern of the holm oak decline in dehesas where healthy and unhealthy sites are spatially separated (Brasier, 1992). The *a priori* visual classification of the health status was later examined by using a three-step protocol. **Step 1**, crown defoliation of each holm oak was estimated considering the percentage of the total area occupied by the defoliated branches (without leaves) relative to the total crown area of the tree. We used images taken at 20 m away from the trunks and 1.65 m above the ground that were then analysed using the ImageJ software

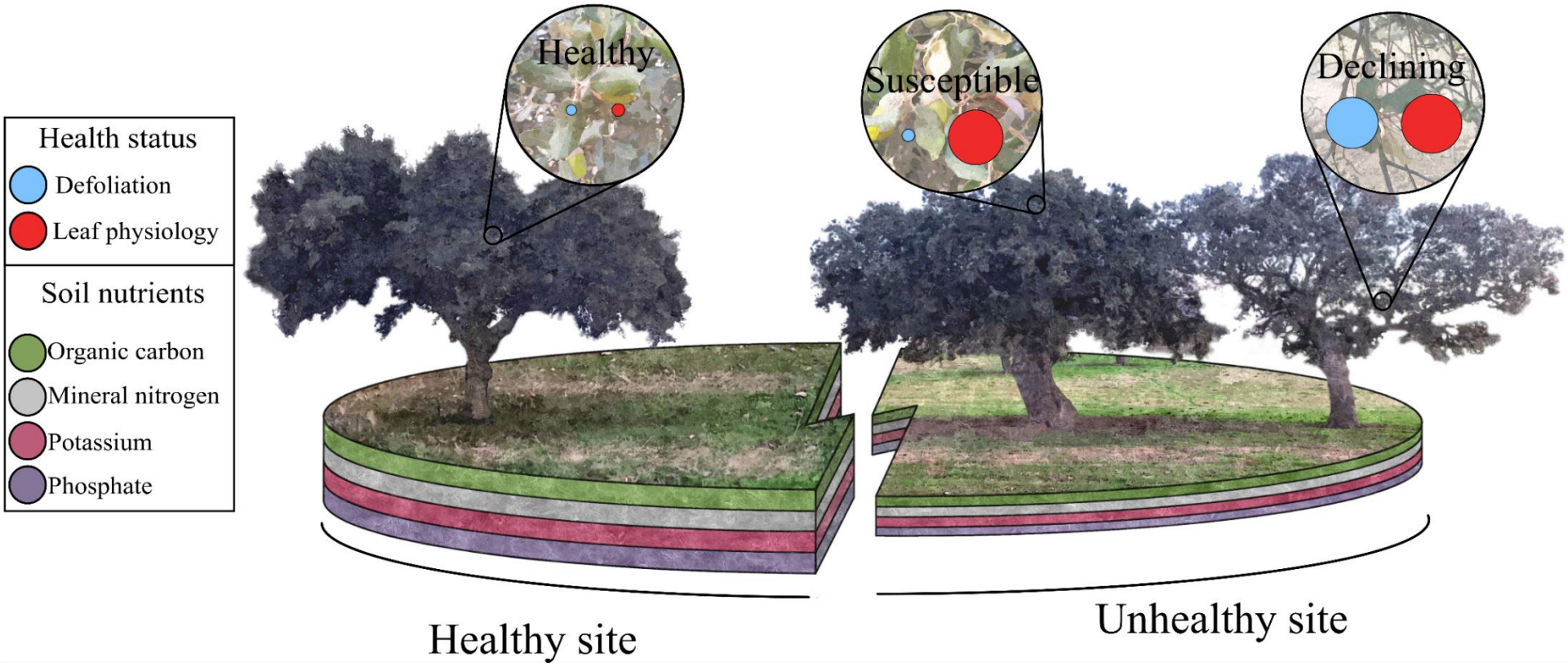

Figure 1. Depiction of the health statuses of the holm oak trees and soil nutrient content in each site (i.e., healthy and unhealthy). In detail, the health status is represented by the crown defoliation (blue circle) and the leaf physiology (red circles) (obtained by RDA1, Fig. **S5.1a**) of the trees. The size of each circle is proportional to the mean crown defoliation and the physiological stress of leaves (group centroid position in RDA1). The soil nutrient content is represented by horizons, in accordance with the Table **1**, and a thicker soil horizon indicates higher nutrient content.

(1.52p; Ferreira & Rasband, 2019, http://rsbweb.nih.gov/ij/). **Step 2**, to further characterize the health status of each holm oak, we measured chlorophyll *a* fluorescence induction, pigments and photoprotective compounds (i.e., chlorophylls, carotenoids and tocopherols, up to now 'leaf traits') on fully expanded leaves randomly collected at approximately 3 m height. The leaf traits used are early stress markers (Esteban *et al.*, 2015a; Fenollosa & Munné-Bosch, 2018) that indicate damage at the leaf physiological level and precede the defoliation process. Further details on step 2 may be found in Encinas-Valero *et al.*, (2022). **Step 3**, redundancy analyses (RDA; **Fig. S5.1a**) using the leaf traits from step 2 were run. Based on RDA of leaf stress markers, we classified the selected holm oak trees into the three health statuses (**Fig. 1**): *i*) healthy, non-defoliated holm oak trees growing in healthy sites and that were characterized by a lower rate of early stress markers in their leaf traits in comparison to the trees from the unhealthy sites (i.e., both non-defoliated and defoliated); *ii*) susceptible, holm oak trees growing in the unhealthy sites characterized by low defoliation rates (less than 10% of crown defoliation) and a higher rate of early stress markers in comparison to healthy trees, and *iii*) declining, holm oak trees growing in unhealthy sites characterized by more than 10% of crown defoliation and a higher rate of early stress markers in comparison to healthy trees.

Root and soil sampling

Our target was to collect the shallowest roots of each of the 162 holm oaks. We found a high variability regarding the depth where we could actually collect the roots. This is because the roots of the holm oaks in dehesas are found below the roots of the herbaceous compartment, which reach very variable depths (Moreno *et al.*, 2005). We hence defined a sampling protocol that consisted in digging until we were able to collect a representative number of roots enough to conduct all our proposed analyses (including non-destructive and destructive analyses, such as NSC). The average sampling depth was 15 cm not generally exceeding 30 cm depth (most holm oak fine roots, responsible for nutrient uptake, are found in the first 30 cm; Canadell *et al.*, 1992). No significant differences in sample collection depth were found among the health statuses ($p=0.7$, data not shown). To account for the spatial heterogeneity, the roots were sampled from three random points around the trunks and at a distance of 1 m from them. The three subsamples were then pooled into a single composite sample per each holm oak tree. Soil samples from the vicinity of the sampled roots were collected following the same protocol. Both roots and soil samples were immediately stored in a portable fridge and maintained at 4°C until they were transported to the laboratory. In the laboratory, soil and root samples were separated into different subsamples to perform different analyses. Soil samples were dried at room temperature (~20ºC), sieved using a 2 mm mesh size and stored in darkness for further

analyses. Root samples were gently washed using deionized water to remove the attached residual soil particles and dried, using filter paper. Five to fifteen sampled root fragments from each holm oak were then photographed, at a constant distance of 30 cm using a DSLR camera in automatic mode (Canon Eos 1200D, Amstelveen, Netherlands), to further characterize their morphology and architecture. Finally, we separated these roots into fine (< 2 mm) and coarse (≥ 2 mm), using a digital caliper. Then, we oven-dried all these roots at 60°C for 48h and subsequently ground them, using a ball mill (MM400, Retsch, Düsseldorf, Germany), until we obtained a fine powder. To avoid re-hydration, all ground samples were stored at low humidity conditions (i.e., with silica gel in hermetic bags) until further analyses.

5.2.2. Soil nutrient variables assessment

The soil organic carbon (i.e., org. C) content was determined using the dichromate oxidation method described by Walkley and Black (1934) and modified by Yeomans and Bremner (1988). The nitrogen (i.e., tot. N) and phosphorus (i.e., tot. P) content were determined based on the Kjeldahl digestion method (Radojevic *et al.*, 1999). Results were expressed as mg of org. C, tot. N or tot. P per 100 mg of soil (%). The ammonium determination was performed based on the modified Berthelot reaction (Krom, 1980; Searle, 1984), while the nitrate and nitrite contents were determined following the cadmium reduction method (Navone, 1964; Walinga *et al.*, 1989). The phosphate soil content was determined following the ammonium-heptamolybdate and potassium antimony oxide tartrate reaction in an acidic medium, using a phosphate solution to form the antimony-phospho-molybdate complex (Boltz & Mellon, 1948), while the potassium soil content was determined at 776 nm by aspirating the sample into a flame (Richards, 1954). Ammonium, nitrate, nitrite, phosphate and potassium results were expressed as μg per g of soil. Finally, the pH of the soil samples was measured through the saturated soil paste method (Kalra, 1995).

5.2.3. Fine root morphological and architectural assessment.

All root images were analysed using the image analysis software SmartRoot (Lobet *et al.*, 2015), a freeware based on ImageJ (Ferreira & Rasband, 2019). Specifically, each sampled root fragment was measured using the semi-automatic mode of the SmartRoot software. The length, surface, volume, diameter and insertion angle of every single component of the sampled root fragments were measured. In total, 11,757 root components were measured. These roots were categorized using the following diameter-based classification: fine roots, including roots < 0.5 mm in diameter (class 1), roots 0.5 – 1 mm in diameter (class 2), roots 1 – 1.5 mm in diameter (class 3), and roots 1.5 – 2 mm in diameter (class 4); and coarse roots (≥2 mm in

diameter). To finally assess the root morphology and architecture of each of the 162 holm oak trees, five parameters were obtained: *i*) fine root percentage (FR, %), calculated as the sum of the lengths of the first four classes relative to the sum of the lengths of all the root components (including fine and coarse roots) from the same sample; *ii*) fine root branching ratio (FRB), calculated as the average of the sum of the ratios between consecutive diameter classes; class 1:class 2 (*ratio I*) + class 2: class 3 (*ratio II*)+ class 3: class 4 (*ratio III*) (Chen *et al.*, 2016). This allowed us to estimate the abundance of fine root components relative to thicker fine root components. As our purpose was to obtain a value that summarises as much as possible the structure of the fine roots, we averaged the three ratios explained above as in Altaf *et al.* (2013); *iii*) insertion angle (IA, degrees), calculated as the mean insertion angle of each of the root components; *iv*) fine root diameter (FRD, cm) (López *et al.*, 2001), calculated as the mean diameter of the first four diameter classes; and *v*) fine root length (FRL, cm), quantified as the mean length of the first four diameter classes.

5.2.4. Non-structural carbohydrate measurements

For all fine (< 2 mm) and coarse (≥ 2 mm) sampled roots, non-structural carbohydrate pools (i.e., glucose, fructose, sucrose and starch) were quantified as described in Mariem *et al.*, (2020). Briefly, 25 mg of ground root samples were treated with 0.5 ml of 100% ethanol and 0.5 ml of 80% ethanol. These samples were heated in a thermomixer (70°C, 90 min, 1,100 rpm) and then centrifuged. The resulting supernatant fractions were used to determine soluble sugars (i.e., sucrose, glucose, fructose), using Ion Chromatography System (ICS-3000, Thermo Scientific Dionex, USA), after previous sample dilution with water. The starch content was determined in the pellet by adding KOH (0.2 N) and adjusting the pH with acetic acid. The extractions were performed by using a kit that contained amyloglucosidase (R-Biopharm, AG; Darmstadt, Germany). The absorbance was measured at 340 nm using a spectrophotometer. The different NSC forms were expressed as mg g^{-1} per dry weight (DW).

5.2.5. Data processing and statistical analyses

To obtain an integrated view of the soil conditions, we performed RDA analyses using a matrix data of soil variables including: org. C, tot. N, tot. P, ammonium, nitrate, nitrite, phosphate, potassium and pH (**Fig. S5.2**). This matrix was used as the response variable, while the health status of the holm oak (i.e., healthy, susceptible and declining) and the "dehesa" (condition) were used as explanatory variables. For these analyses, we used the "rda" function from the vegan R package (Oksanen *et al.*, 2020).

To define a single variable, we performed Principal Component Analyses (PCA) using all the analysed soil variables logarithmically transformed. For this, we used the "prcomp" function available in the R base learning functions. Based on the obtained results (**Fig. 2**), axis 1 accounted for 48.4% of the variance and was thus used in further analyses as the soil nutrient availability variable.

To test our two hypotheses, we performed two different sets of linear mixed-effects models (LMEs) using the "lme" function available from the "nlme" R package (Pinheiro *et al.*, 2020): *i)* LMEs, which included the health status (explanatory variable), and *ii*) LMEs which included an interaction between a continuous variable and the health status (explanatory variables). The fixed effects of the two sets of LMEs included the response and the explanatory variables, while for the random effect, we used "site" (i.e., healthy and unhealthy) nested within "dehesa" to overcome the experimental design limitation of the two separated sites. To calculate the coefficients of the two sets of LMEs and thus to estimate the effects of each of the explanatory variables, we run an ANOVA type III test (available from the "car" R package; Fox & Weisberg, 2019) to deal with the unbalanced design. When significant differences among health statuses of trees were found, we run least-square means test based on Tukey HSD, using the 'emmeans' R package (Lenth, 2020). All reported LMEs coefficients were estimated based on the restricted maximum likelihood method (REML). The residuals of the two sets of LMEs were checked for normality using the quantile-quantile plot and the Kolmogorov–Smirnof test. The overall fit of the LMEs was estimated using the pseudo-R^2 (R^2_p; Nakagawa *et al.*, 2017) whose values represent the coefficient of determination based on the likelihood-ratio test ('r.squaredLR' function from the 'MuMIn' R package; Barton, 2020).

For our first hypothesis we used the first set of LMEs to look for differences between the health statuses of trees in soil variables (i.e., org. C, tot. N, tot. P, ammonium, nitrate, nitrite, phosphate, potassium and pH, Table **1**) and in the morphology and architecture of roots (i.e., FR, FRB, IA, FRD, FRL). Additionally, a second set of LMEs was used to test for the effects of soil nutrient availability (i.e., axis 1 of the PCA), health status and their interaction with roots morphology and architecture (**Table 2**, **Fig. 3**). For each of the morphological and architectural root parameters that responded significantly to the interaction, a phenotypic plasticity index that ranged from zero to one was calculated (**Fig. 3**). Specifically, we extracted the regression coefficients of the models (Arnold *et al.*, 2019) and used them to predict values at both ends of the soil nutrient availability gradient (n = 1000). For that, we considered the confidence intervals calculated by the LME to predict minimum and maximum values. We finally determined this phenotypic plasticity index by calculating the difference between the

minimum and maximum values and dividing the obtained result by the maximum value (Valladares *et al.*, 2006). We then performed one-way ANOVA analyses (i.e., using the "t1way" function from de "WRS2" package; Mair & Wilcox, 2018), using the trimmed means, to test for significant differences in terms of phenotypic plasticity index among health statuses. When we found significant differences between health statuses, we performed post-hoc tests using the "lincon" function from the WRS2 package (Mair & Wilcox, 2018). Finally, to represent them graphically, we calculated a mean phenotypic plasticity index for each health status.

For our second hypothesis, a first set of LMEs was used to look for differences in NSC fractions among the health statuses (**Fig. 4**). Additionally, a second set of LMEs was used to test for the effect of the NSC fractions (i.e., NSC, starch and soluble sugars), health status and their interaction with the parameters of root morphology and architecture (**Table S1**, **Fig. 5**). Finally, to evaluate a possible above-belowground trade-off, the tree foliage (the inverse of tree defoliation, see section 2.1) was divided by FRB, FRD and FRL, separately. We performed LMEs using the three different foliage:root parameter ratios (response variable) and soil nutrient availability, health status and its interaction (explanatory variables) (**Table S2**, **Fig. 6**), and LMEs using the foliage:root parameter ratios (response variable) and health status (explanatory variable) (**Fig. 6b**, **f**).

All statistical analyses were performed in R (v. 4.0.0, 2020, R Core Team, 2020).

5.3. Results

5.3.1. Are root parameters affected by soil nutrient availability and the health status of the holm oak trees?

Soil nutrients (i.e., nitrate, ammonium, phosphate, potassium) and organic carbon content were affected by health status (**Table 1)**. In healthy sites, the soil under healthy trees showed significantly higher values of nitrate ($p < 0.01$), ammonium ($p < 0.01$), phosphate ($p < 0.001$), potassium ($p < 0.001$) and org. C content ($p < 0.05$) compared to the soil under susceptible and declining trees (**Table 1**, **Fig. 1**). The results of this analysis were complemented by those

Table 1. Results of the linear mixed-effects models (LMES) that tested our first hypothesis: soil pH, nutrients and stoichiometry as a function of the health status (i.e., healthy, susceptible and declining) of holm oak trees.

	Health status			p-value
Variables	Healthy	Susceptible	Declining	
Soil pH	5.56±0.09a	5.53±0.06a	5,49±0.07a	n.s.
Soil nutrient (units)				
Nitrate (μg g^{-1})	6.11±1.33**a**	1.81±0.30**b**	1.62±0.25**b**	**
Nitrite (μg g^{-1})	0.12±0.04a	0.06±0.01a	0.05±0.01a	n.s.
Ammonium (μg g^{-1})	3.97±0.81**a**	2.09±0.20**b**	2.11±0.23**b**	**
Phosphate (μg g^{-1})	5.92±1.2**a**	3.15±0.72**b**	2.69±0.60**b**	***
Potassium (μg g^{-1})	84.36±9.31**a**	57.45±7.65**b**	52.27±4.38**b**	***
org. C (%)	2.60±0.16**a**	2.13±0.16**b**	2.36±0.16**b**	*
tot. N (%)	0.16±0.01a	0.13±0.01a	0.14±0.01a	n.s.
tot. P (%)	0.05±0.004a	0.05±0.007a	0.05±0.005a	n.s.
Soil stoichiometry				
org. C.: tot. N	16.51±0.66a	16.92±0.61a	16.81±0.69a	n.s.
org. C.: tot. P	65.12±5.02a	59.96±3.68a	60.71±4.84a	n.s.
tot. N: tot. P	3.95±0.22a	3.51±0.19a	3.58±0.22a	n.s.

Mean ± standard error (SE) values (n = 49-59) are given for each analysed soil variable. Different letters indicate statistically significant differences (i.e., least-square means based on Tukey HSD tests) between the different health status (healthy, susceptible and declining) of the holm oak trees. Asterisks indicate statistically significant differences as it follows: *, for $p < 0.05$; ** for $p < 0.01$; and *** for $p < 0.001$. Bold letters indicate significant differences among the health statuses. Abbreviations stand for roots functional parameters [org. C (%), soil organic carbon; tot. N, total nitrogen; tot. P, total phosphorus]. n.s. stands for non-significant relationships

obtained from RDA which showed a significant effect of the health status of the trees (R^2 = 0.03; $p < 0.001$) on the linear combination of the soil variables (i.e., org. C, tot. N, tot. P, nitrite, nitrate, ammonium, potassium, phosphate and pH). The 'dehesa' and 'health status' explanatory variables explained 40% and 4% of the total variation, respectively. On the axis 1, nitrate had the highest loading factor (-0.67). On the axis 2, nitrate and potassium explained most of the variation, these two variables had the highest (0.11) and the lowest (-0.16) loading factors on this axis, respectively (**Fig. S5.2**).

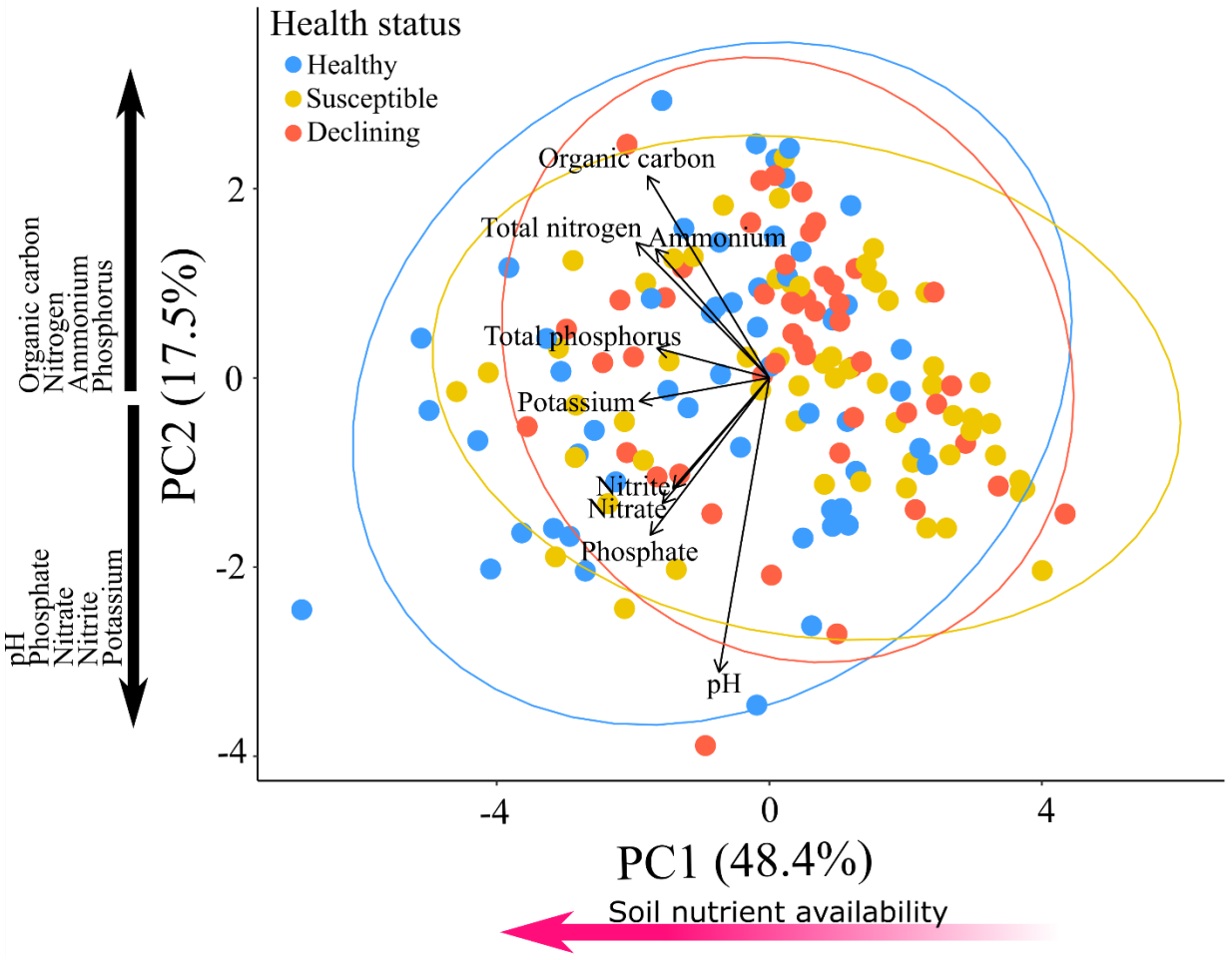

Figure 2. Results of the principal component analyses (PCA) run to reduce the number of soil variables and define a single variable, i.e., soil nutrient availability. The soil variables considered were org. C, tot. N., tot. P, ammonium, nitrate, nitrite, phosphate, potassium and pH. Holm oak trees are marked in blue (healthy trees), yellow (susceptible trees) and red (declining trees). The arrows indicate the contribution of the soil variables on each axis.

On axis 1 of the PCA, created to integrate soil nutrient availability (i.e., the defined soil nutrient availability variable), tot. N was the variable that had the highest loading factor (-0.39) (**Fig. 2**). On the axis 2, org. C (loading factor = 0.43) and pH (loading factor = -0.63) were the two soil variables that contributed most. Hence, we used this axis to test our first hypothesis (i.e., effects of soil nutrient availability and the health status on the root parameters). The results of the LME that tested our first hypothesis, indicated that the interaction between soil nutrient availability and health status affected the morphology and architecture of the fine roots (i.e., FRB, FRD, FRL) of holm oak trees (Table **2**, **Fig. 3b, e, g**). Specifically, declining trees showed lower FRB values at low soil nutrient availability and higher FRB values at high soil nutrient availability than susceptible and healthy trees (**Fig. 3b**). Regarding FRD, declining trees showed higher FRD values under conditions of lower soil nutrient availability and lower FRD values under conditions of higher soil nutrient availability in comparison to susceptible and healthy trees (**Fig. 3e**). Finally, regarding FRL, declining trees presented longer fine roots under conditions of low soil nutrient availability and shorter fine roots under conditions of high soil nutrient availability than susceptible and healthy trees (**Fig. 3g**). Additionally, FRB, FRD and FRL showed a higher phenotypic plasticity in declining than in susceptible and healthy ones (**Fig. 3c, f, h**).

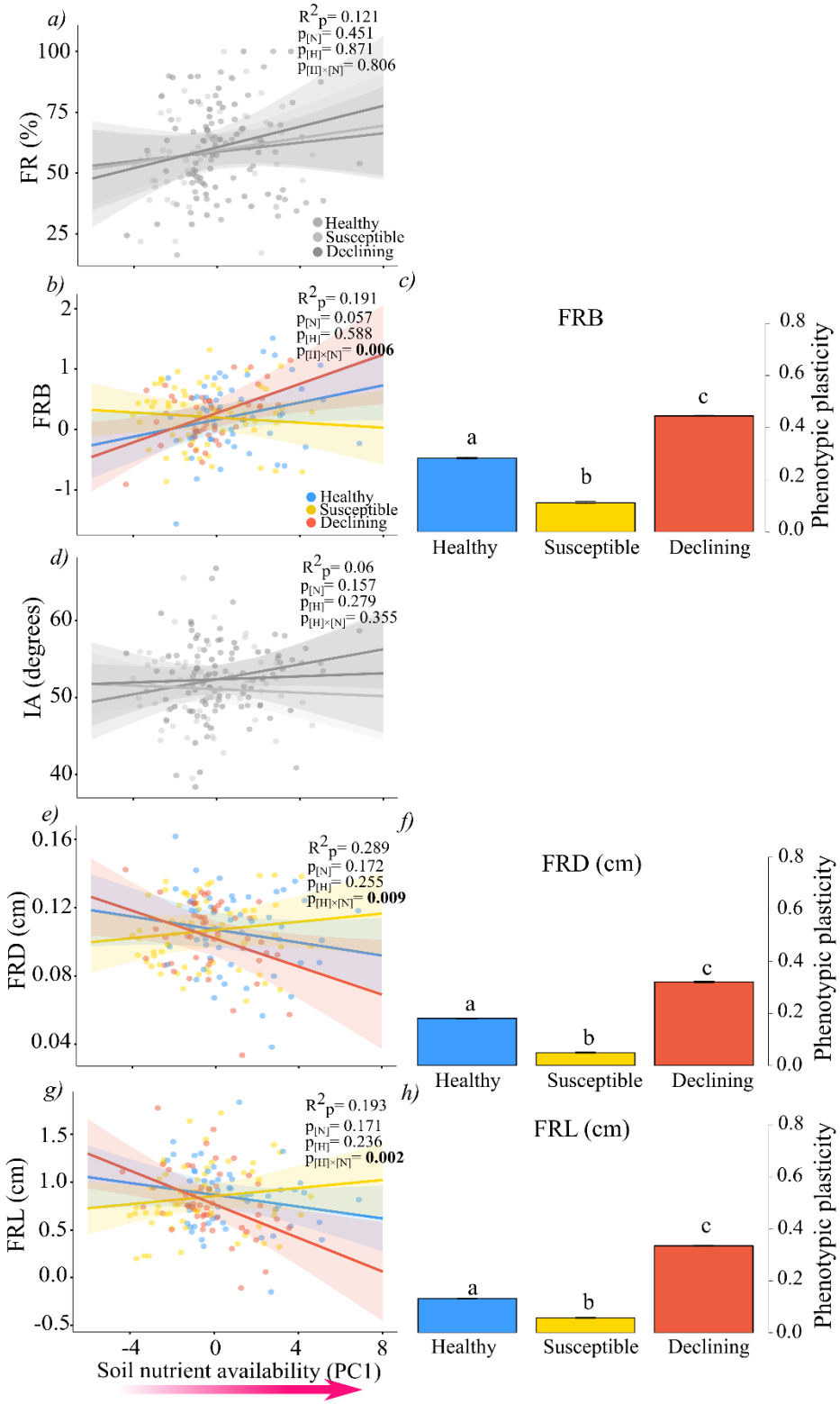

Figure 3. Results of linear mixed-effects models showing, on the one hand, how the fine root parameters of the holm oak trees respond as a function of soil nutrient availability, health status and their interaction (a, b, d, e, g panels) and, on the other hand, how the phenotypic plasticity index varies across health statuses (i.e., when significant effects of the health status are found) (c, f, h panels). Abbreviations stand for: FR (%), fine root percentage; FRB, fine root branching; IA (degrees), insertion angle; FRD (cm), fine root diameter; FRL (cm), fine root length. The soil nutrient availability variable was derived from the axis 1 of the Principal Component Analyses (PCA, **Fig. 2**). This component was multiplied by -1 to facilitate comprehension. Solid lines represent the trends of each root parameter along the gradient of soil nutrient availability (i.e., fitted LME values) as a function of health status. The shaded areas represent the 95% confidence intervals. The R^2_p or fraction of variation explained by the model was calculated according to Nakagawa *et al.* (2017). The phenotypic plasticity, calculated for each health status as described in section 2.6., is represented by bar plots (mean ± SE). Different letters indicate significant differences ($p < 0.05$) according to the multiple pairwise comparisons test. Colourless figures (a, b) show non-significant LME results.

Table 2. Effects of the soil nutrient availability, health status (healthy, susceptible and declining) and their interaction on the morphology and architecture of the parameters of the holm oak root.

	FR (%)			FRB			IA (degrees)			FRD (cm)			FRL (cm)		
Source of variation	Df	$\chi2$	p-value	Df	$\chi2$	p-value	Df	$\chi2$	p-value	Df	$\chi2$	p-value	Df	$\chi2$	p-value
Intercept	1	248.7	**0.000**	1	1.991	0.158	1	3316	**0.000**	1	423.8	**0.000**	1	153.9	**0.000**
Soil nutrient availability	1	0.565	0.451	1	3.618	0.057	1	2.002	0.157	1	1.862	0.172	1	1.868	0.171
Health status	2	0.276	0.871	2	1.061	0.588	2	2.548	0.279	2	2.725	0.255	2	2.882	0.236
Soil nutrient availability × Health status	2	0.430	0.806	2	10.27	**0.006**	2	2.067	0.355	2	9.218	**0.009**	2	12.41	**0.002**

Abbreviations stand for roots functional parameters [FR (%), fine root percentage; FRB, fine root branching; IA (degrees), insertion angle; FRD (cm), fine root diameter; FRL (cm), fine root length]; Df, degrees of freedom; $\chi2$, chi-square statistic. Values in bold indicate significant relationships based on the ANOVA type III tests performed along with the linear mixed-effects models (LMEs).

5.3.2. Does fine root branching (FRB) response to tree resources allocation depend on the trees health status?

NSC fractions did not differ as a function of health status, neither for fine nor for coarse roots (**Fig. 4a, c, d, e**) except for fine root starch and coarse root fructose contents (**Fig. 4b, f**). Specifically, susceptible trees showed marginally higher fine root starch values (28.4 ± 2.2) than declining trees (21.2 ± 1.7) ($p < 0.1$). Coarse roots showed a significantly higher ($p<0.001$) fructose content in healthy (11.4 ± 2.0) and declining (11.5 ± 1.7) holm oaks than in susceptible ones (5.3 ± 0.6) (**Fig. 4f**). These differences were also reflected in the total soluble sugars content of the coarse roots, which was significantly higher ($p < 0.001$) in healthy (21.6 ± 2.6) and declining (20.4 ± 2.0) holm oaks than in susceptible ones (13.9 ± 0.9) (**Fig. 4f**).

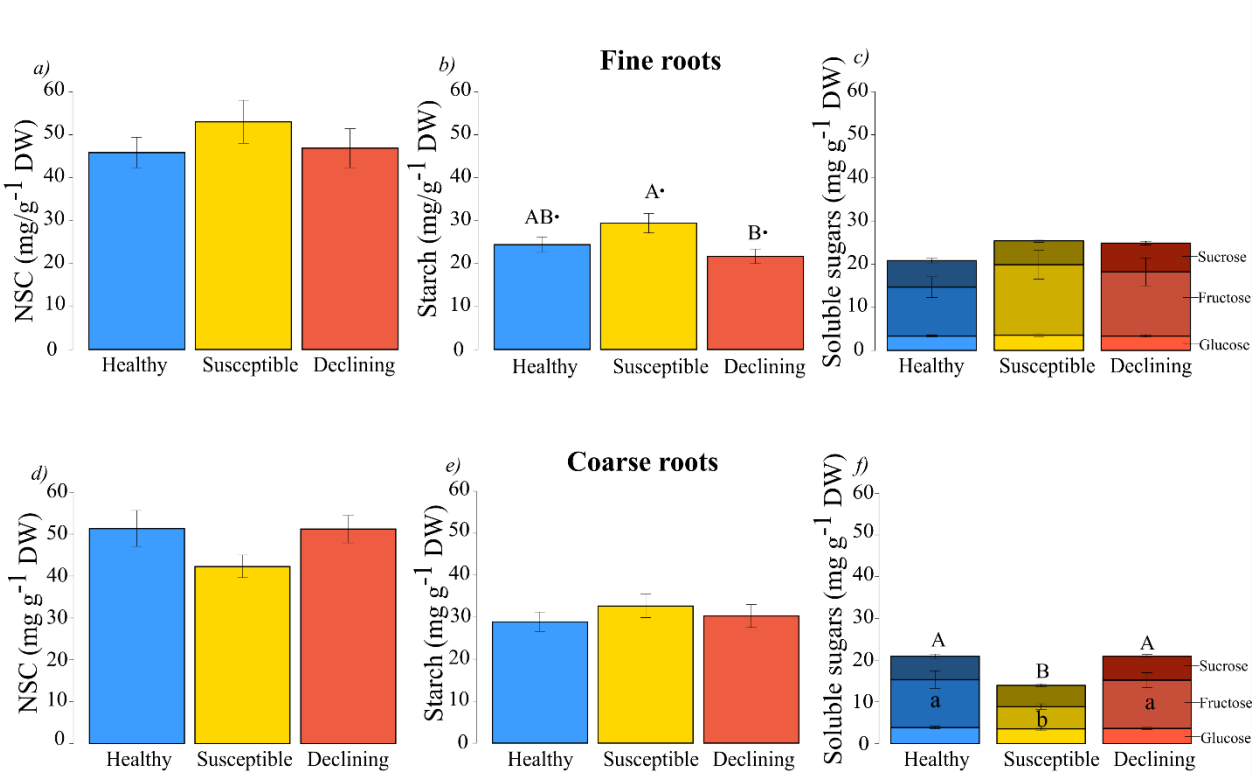

Figure 4. Total non structural carbohydrates (NSC), starch and soluble sugars for fine and coarse roots as a function of health status (healthy, susceptible and declining holm oak trees): i.e., total NSC (sum of starch and soluble sugars; panels a and d), starch (panels b and e) and soluble sugars (sum of sucrose, fructose and glucose, marked from darker to brighter colours; panels c and f). Each bar indicates the mean ± standard error of each health status (healthy, n=54-33; susceptible, n=59-38; declining n=49-26). Different uppercase letters indicate statistically significant differences between health statuses of the holm oaks, while different lowercase letters indicate statistically significant differences between the different fractions of the soluble sugars (least-square means based on Tukey HSD tests). Close points beside the letters indicate marginally significant differences.

The results of the LMEs that tested our second hypothesis showed that FRB responded significantly to the interaction between NSC, starch or soluble sugars and health status (**Fig. 5**; **Table S5.1.**). Specifically, we found that, at higher content of NSC and soluble sugars, FRB in declining trees tended to increase in contrast to healthy trees (**Fig. 5a, c**). Additionally, we also found that, at higher content of starch, FRB of trees from the healthy site tended to decrease in contrast to the trees from the unhealthy site (**Fig. 5b**).

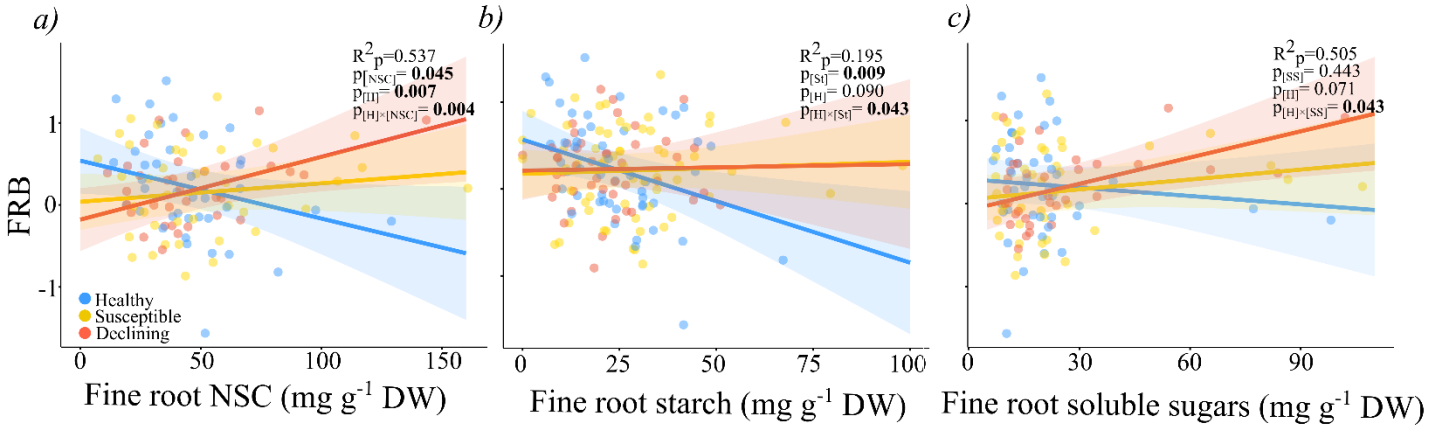

Figure 5. Linear mixed-effects models of the fine root branching ratio (FRB) as a function of non-structural carbohydrates fractions, health status and their interaction. The FRB was logarithmically transformed to account for normality as a function of fine roots NSC (panel a; mg g^{-1} DW), fine roots starch (panel b; mg g^{-1} DW) and fine roots soluble sugars (panel c; mg g^{-1} DW). Different colours indicate different health statuses of the holm oak trees, i.e., blue (healthy trees), yellow (susceptible trees) and red (declining trees). Shaded areas represent the 95% confidence interval. The pseudo-R^2 (R^2_p; i.e., the fraction of variation explained by the model) was calculated according to Nakagawa *et al.*, (2017)

5.3.3. Is there a trade-off in terms of foliage:root ratio considering soil nutrient availability gradient and health status?

The foliage:FRB and foliage:FRL ratios responded significantly to the interaction between health status and soil nutrient availability, while the foliage:FRD ratio showed no response in this regard (**Fig. 6**, **Table S5.2.**). Specifically, the foliage:FRB ratio decreased significantly, along the soil nutrient availability gradient, in declining holm oaks compared with healthy ones. Also, susceptible holm oaks exhibited no response at all to the soil nutrient availability gradient (**Fig. 6a**). Contrary to the foliage:FRB ratio, the foliage:FRL ratio showed lower values at low soil nutrient availability and higher values at high soil nutrient availability in declining trees (Fig. **6d**). Finally, regarding the response of the foliage:FRB and foliage:FRL ratios to health status, we found that declining holm oak trees showed significantly lower values than healthy and susceptible holm oak trees ($p<0.05$, **Fig. 6b, f**).

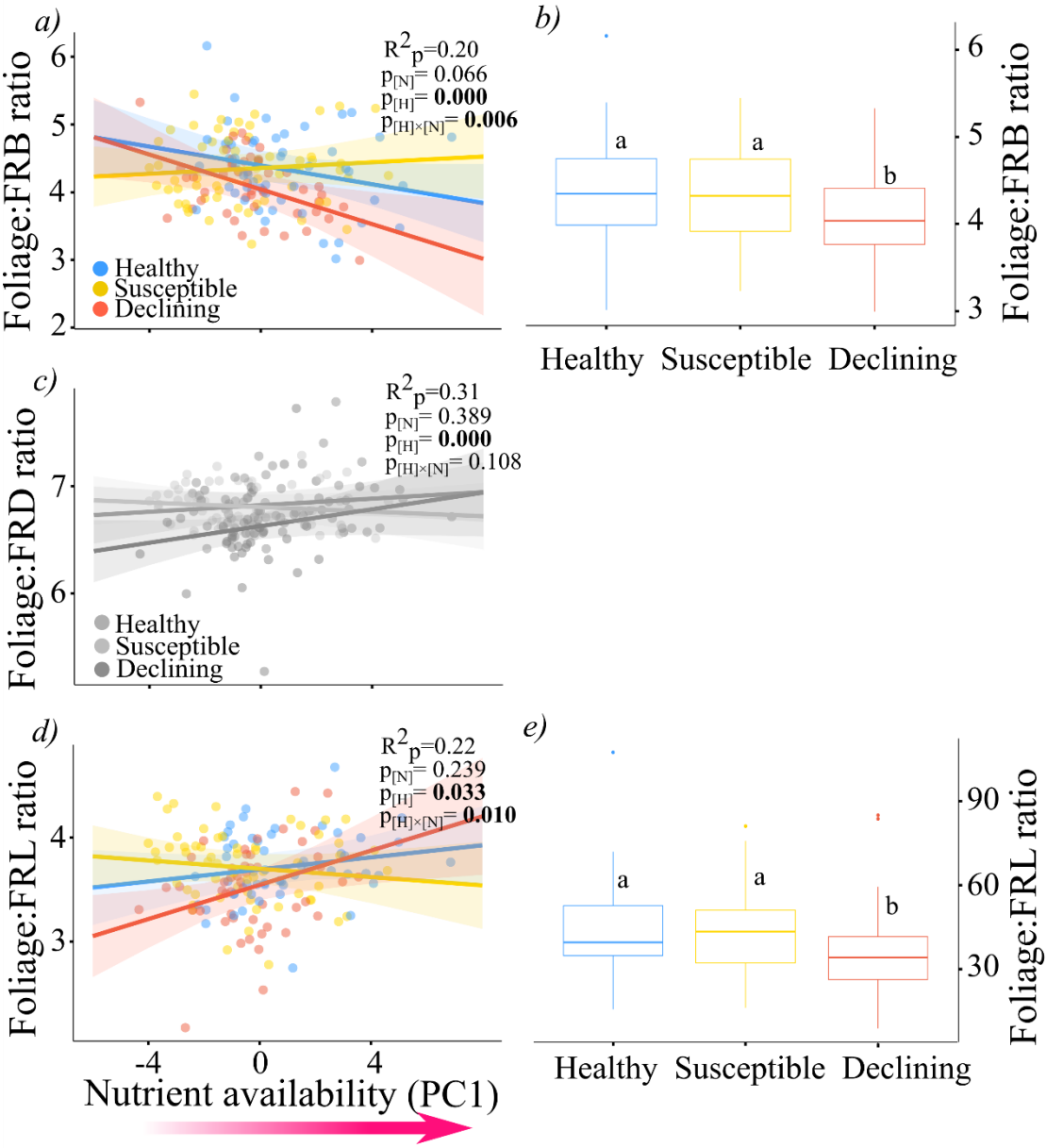

Figure 6. Linear mixed-effects models of the foliage-fine root parameter ratio as a function of nutrient availability, health status and its interaction. The fine root parameters represented are fine root branching ratio (FRB, panel a), fine root diameter (FRD, panel b) and fine root length (FRL, panel c). Ratios were logarithmically transformed to fulfil assumptions. Soil nutrient availability is derived from the principal component analysis (PC1; Fig. **2**) and multiplied by -1to facilitate comprehension. The health status of the holm oak trees is marked in blue (healthy), yellow (susceptible) and red (declining) colours. Solid lines represent the trend of each health status along soil nutrient gradient (fitted values). The shaded area represents the 95% confidence interval. R^2_p (fraction of variation explained by the model) was calculated according to Nakagawa *et al.* (2017). The colourless interaction model represents non-significant interaction. Note that the foliage:root parameter ratio are also represented by boxplots (panels b and f; only for significant interactions). Box represents 50% of data (n = 43-53 trees per health status) distribution between the first and the third quartile; the central line represents the median; the upper and below whiskers cover the 1.5 interquartile range. Different letters indicate significant differences ($p < 0.05$) between the different health statuses on a Tukey multiple pairwise comparisons test.

5.4. Discussion

5.4.1. Declining holm oak trees showed higher phenotypic plasticity to soil nutrient availability in fine roots parameters than susceptible and healthy trees

The results support our first hypothesis that the stress level of the tree (i.e., health status) determined soil resource uptake strategies (**Fig. 3**) reflected in root morphological and architectural changes. The mild response or absence of response in morphological and architectural fine root parameters from healthy and susceptible holm oak trees along the soil nutrient availability indicated a constant conservative resource uptake strategy. By contrast, when soil nutrient availability was high, declining holm oaks presented more branched fine roots (FRB, **Fig. 3b**) and consequently a higher number of fine root tips along with thinner (FRD, **Fig. 3e**) and shorter fine roots (FRL, **Fig. 3g**) in comparison to healthy and susceptible holm oaks. The responses observed in declining trees may represent an acquisitive strategy (Jia *et al.*, 2013) that would enhance the effective absorbing local root surface and favour soil resource acquisition (Pregitzer, 2008; Beidler *et al.*, 2015; Liese *et al.*, 2017; Yahara *et al.*, 2019; Wambsganss *et al.*, 2021) to counteract the potentially negative effects of drought, defoliation (Gessler *et al.*, 2017) and other indirect factors that reduce soil nutrient uptake, like the loss of ectomycorrhizal fungi in declining trees (Corcobado *et al.*, 2015). By contrast, under low soil resource availability, few roots branches and the presence of thicker and longer fine roots (**Fig. 3b, e, g**) may favour the exploration of a large volume of soil when resources are limited in declining trees (Belsky, 1994; Beidler *et al.*, 2015; Eissenstat *et al.*, 2015; Montagnoli *et al.*, 2018). These characteristics are associated with a more conservative resource uptake strategy (Liese *et al.*, 2017; Li *et al.*, 2020).

Overall, three out of the five morphological and architectural fine root parameters analysed here (i.e., FRB, FRD and FRL) were found to be significantly affected by the interaction between soil nutrient availability gradient and the health status of the trees. The large changes in the fine root architecture and morphology in declining trees along the soil nutrient availability revealed a higher fine root phenotypic plasticity in comparison to susceptible and healthy trees (**Fig. 3c, f, h**). This high phenotypic plasticity suggests that declining holm oaks develop their root systems to cope with the stress to which they are subjected (i.e., drought and root-rot by pathogens such as *Phytophthora*; Corcobado *et al.*, 2010, 2013a; Ruiz-Gómez *et al.*, 2019). However, Mediterranean evergreen holm oaks have been reported to exhibit low phenotypic plasticity (Valladares *et al.*, 2000b, 2007; Baquedano

et al., 2008). Thus, we speculate that the phenotypic plasticity associated with declining trees may not constitute an adaptive advantage (Stotz *et al.*, 2021) or an increase in fitness (Bonser, 2021) in the context of the Spanish dehesas. While holm oak trees are well adapted to the harsh environmental conditions where they have evolved (Moreno & Cubera, 2008; García-Angulo *et al.*, 2020) Spanish dehesas are susceptible to experience a sequence of different stochastic disturbances, including unusually or extreme long drought, clearing, ploughing, grazing and other anthropic land use-related disturbances that expose holm oak to unpredictable changes in water and nutrient availability (Plieninger, 2006). All these factors may favour lower phenotypic plasticity and thus a conservative resource-use strategy, like the one we observed in healthy and susceptible holm oak trees (**Fig. 3c, f, h**), even when the resources are temporary abundant, to avoid the development of plant structures too costly to maintain once conditions deteriorate (Baquedano *et al.*, 2008). In addition, conservative root growth in oaks has been reported to be more resilient to pathogen infections and subsequent to drought, than a more acquisitive and extensive root system (Biocca *et al.*, 1993; Haavik *et al.*, 2015).

5.4.2. Changes in the resource acquisition strategy of the fine roots of declining trees imply a carbon cost

Our results indicated no carbon depletion during the onset of holm oak decline, i.e., no changes in the overall NSC content as a function of health status (**Fig. 4a, d;**). This implies that carbon availability was not affected by the health status of the holm oak trees and fine roots were not subjected to potential carbon deprivation from photosynthesis limitation (Sanz-Pérez *et al.*, 2009; Zang *et al.*, 2014) and/or from the belowground stressful conditions imposed by the interaction between the root rot pathogen *P. cinnamomi* and drought (Corcobado *et al.*, 2013a). Nonetheless, the higher values that we found regarding the fructose content in the coarse roots of the declining trees in comparison to susceptible trees (**Fig. 4f**), may indicate an osmotic response to enhance water uptake (Dietze *et al.*, 2014; Brunner *et al.*, 2015) or higher respiratory demands (Hartmann & Trumbore, 2016). This is because NSC are involved in a wide variety of functions such as energy metabolism, growth, osmoregulation, transport, storage, defenses and symbiotic interactions (Hartmann & Trumbore, 2016). In addition, the marginally significant decrease of the starch content in the fine roots of the declining holm oak trees in comparison with the fine roots of the susceptible ones (**Fig. 4b**), may be caused by the decrease of canopy carbon uptake, which in turn may be caused by a decrease in foliage cover and hence in the capacity of the trees to properly photosynthesize (Willaume & Pagès, 2006, 2011; Peguero-Pina *et al.*, 2018).

Analysing the FRB responses to the total NSC, starch and soluble sugars content (**Fig. 5**), we found that the total NSC and soluble sugars content may play an important role in increasing the acquisitive capacity of the fine roots of the declining holm oak trees, which partially confirms our second hypothesis. Specifically, we found a positive relationship between FRB and total NSC and between FRB and the soluble sugars content in declining holm oak trees in contrast to healthy and susceptible ones (**Fig. 5a, c**). These results highlight the importance of both overall NSC and soluble sugars in the development of the fine roots under stress conditions (Ritchie & Dunlap, 1980). This suggests that under scenarios of high drought stress induced by a pathogen, root branching (FRB) in declining trees may come at the expense of a high energetic demand (overall NSC and soluble sugars) (Ritchie & Dunlap, 1980; Zadworny *et al.*, 2021) to optimize resource acquisition (Dewar *et al.*, 1994; Montagnoli *et al.*, 2018). We, however, cannot rule out the possibility that this positive relation between FRB and overall NSC or soluble sugars may also be explained by the increase in carbon cost associated with the mechanisms of defense against *Phytophthora* (Jönsson, 2006). It has been reported that the severity of *Phytophthora* may increase at high soil nutrient availability (mainly organic matter and nitrate; Broadbent & Baker, 1974; Jönsson, 2006; Corcobado *et al.*, 2013c). Interestingly, high values of overall NSC and soluble sugars in growing secondary fine roots as a result of an acquisitive strategy (declining trees, **Fig. 5**) have been associated with the success of *Phytophthora* spp. infection in oak roots (Angay *et al.*, 2014).

5.4.3. Trade-offs between foliage maintenance and root exploration strategies as drivers of health status

It has been reported that the maintenance costs of leaves and roots increase under soil stressful conditions (Laureano *et al.*, 2013, 2016). Under these adverse environmental conditions, we observed that declining trees presented a high percentage of crown defoliation (Fig. **1**, Encinas-Valero *et al.*, 2022). The observed trade-off between NSC investment in fine root branching associated with defoliation (**Fig. 6**) further confirms our second hypothesis. Hence, we speculate that in such a demanding environment, where roots are affected by drought and pathogen infection, a shift in holm oak allocation of carbohydrates takes place to maintain a root system architecture and morphology that enhance tree resource acquisition capacity. These changes occur at the expense of maintaining foliage, which further results in tree defoliation (**Fig. 6a**, **d**). While our results are more qualitative than quantitative (neither fine root nor leaf biomass wer measured), they are consistent with previous studies which showed that a greater root investment at the expense of leaf biomass takes place under drought

conditions (Dewar *et al.*, 1994; Jacobs *et al.*, 2009; Moser *et al.*, 2015; Ruíz-Gómez *et al.*, 2018b), during dry seasons (Montagnoli *et al.*, 2018) and when an infestation of soil-borne pathogens occurs (León *et al.*, 2017; Łakomy *et al.*, 2019; Vivas *et al.*, 2021). Hence, an alternative to phenotypic plasticity explanation could be a potential feedback loop ultimately resulting in tree death that may consist of shifts in the tree carbohydrates allocation towards maintaining root functioning at the expense of foliage to cope with stressful conditions (i.e., drought and root rot pathogens). This response is expressed in declining trees, whereas healthy and susceptible trees, not affected by root pathogens (i.e., absent or less virulent), might not suffer sufficient stress to trigger this root response and negative feedback loop. This would alternatively explain why they exhibit lower phenotypic plasticity.

5.4.4. Final remarks and conclusions

Our study provides new insights on the mechanisms that underlie the decline in holm oak trees growing under conditions of drought and root rot. Our findings suggest that belowground stress and the subsequent substantial reduction in the ability of trees to access soil resources determine the architecture and morphology of their root system). In order to cope with these stressful conditions, a shift in tree NSC allocation is expected to occur to enhance the ability of the radical system to acquire key soil resources at the expense of foliage maintenance, which ultimately leads to tree death. Hence, climate change, land use, soil resource variability and root rot by pathogens in Spanish dehesas revealed the lack of adaptation of holm oaks in these representative ecosystems of southern Europe. The study further points to the roots as essential elements to define holm oak health, and how roots adaptation to a changing and harsh environment, or their lack of adaptation, will determine holm oak survival these representative Mediterranean systems. Since dehesas represent a sustainable model of extensive livestock farming, further and urgent research is needed with a focus on how unpredictable environmental conditions can elicit adaptive responses in holm oak roots. A long-term monitoring study that assesses survival rates of trees (i.e., mainly trees with the highest and lowest root phenotypic plasticity) may elucidate whether roots responses increase survival chances or leads to tree death. The identification of the resilient phenotypes may lead to the implementation of local breeding programs to propagate those individuals capable of coping with the current climatic and biotic environmental challenges faced by dehesa ecosystems. Furthermore, a parallel quantitative assessment of the differences in microbial community structure and functions associated with tree health may help to

understand which plant-soil interaction mechanisms are involved in the resistance/vulnerability of holm oak to the environmental stressors under study.

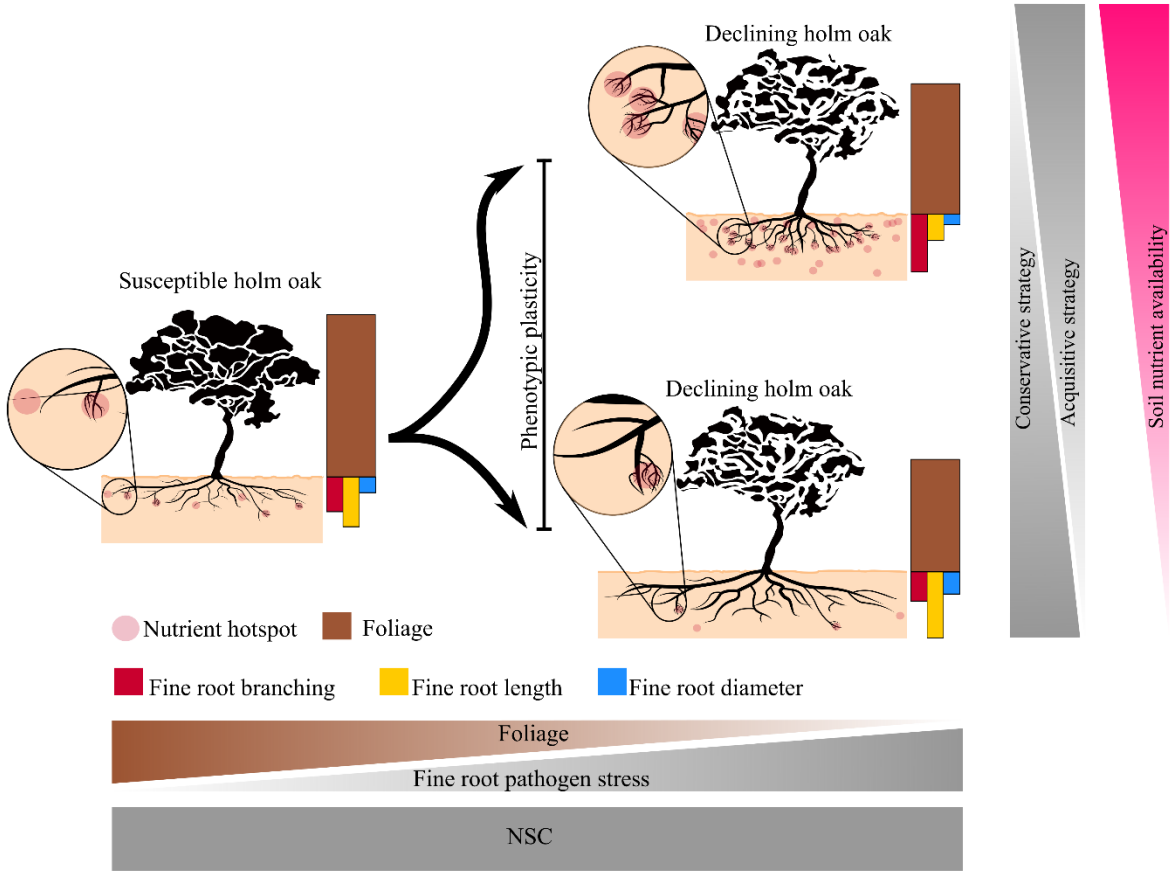

Figure 7. Depiction of the main results obtained in this chapter. Whereas the fine root system of susceptible trees did not respond to the soil nutrient availability, declining trees presented an acquisitive strategy when soil nutrient availability was high and a conservative strategy when soil nutrient availability was low. Above-beolowground trade off in declining trees is represented in the right side of the tree icon. Therepresentation of the defoliation, fine root branching, fine root length and fine root diameter are proportional to the results obtained in this study. Icon tree and roots were redrawn from: Hey Rabbit Ilustrator and Guilhem Ilustrator, accessed through (https://thenounproject.com/)

Chapter VI

Alteration of the tree-soil-microbial system triggers a feedback looop that boosts holm oak decline

Submitted to *Functional Ecology*

Alteration of the tree-soil-microbial system triggers a feedback loop that boosts holm oak decline

Manuel Encinas-Valero[1], Raquel Esteban[2], Ana-Maria Hereş[1,3], María Vivas[4], Alejandro Solla[4], Gerardo Moreno[4], Tamara Corcobado[5], Iñaki Odriozola[6], Carlos Garbisu[7], Lur Epelde[7], Jorge Curiel Yuste[1,8]

Submitted to *Functional Ecology*

[1] BC3-Basque Centre for Climate Change, Scientific Campus of the University of the Basque Country, B/ Sarriena s/n 48940 Leioa, Bizkaia, Spain
[2]Department of Plant Biology and Ecology, University of Basque Country (UPV/EHU), B/Sarriena s/n, 48940 Leioa, Bizkaia, Spain
[3]Faculty of Silviculture and Forest Engineering, Transilvania University of Braşov, Sirul Beethoven-1, 500123 Braşov, Romania
[4] Faculty of Forestry, Institute for Dehesa Research (INDEHESA), Universidad de Extremadura, Avenida Virgen del Puerto 2, 10600 Plasencia, Spain.
[5] Mendel University in Brno, Faculty of Forestry and Wood Technology, Department of Forest Protection and Wildlife Management, Phytophthora Research Centre, 613 00 Brno, Czech Republic.
[6] Institute of Microbiology of the Czech Academy of Sciences, Vídeňská 1083, 14220 Prague, Czech Republic.
[7]Department of Conservation of Natural Resources, NEIKER-Basque Institute for Agricultural Research and Development, Basque Research and Technology Alliance (BRTA) Parque Científico y Tecnológico de Bizkaia, P812, 48160 Derio, Spain
[8] IKERBASQUE. Basque Foundation for Science, Plaza Euskadi 5, E-48009 Bilbao, Bizkaia, Spain

Abstract

1. In anthropic savannah ecosystems from the Iberian Peninsula (i.e., dehesa), complex interactions between climate change, pathogen outbreaks and human land use are presumed to be behind the increase in holm oak decline. These environmental disturbances alter the plant-soil microbial continuum, which can greatly destabilize the ecological balance that sustains the health of trees. Yet, little is known about the underlying mechanisms and particularly the directions and nature of the causal-effect relations between plants and soil microbial communities.

2. In this study, we aimed to determine the role of plant-soil microbiome relationships in the holm oak declining process by reconstructing key soil biogeochemical cycles in a gradient of holm oak heath (characterized by indicators below- and aboveground). We employed quantitative microbial element cycling (QMEC), a functional gene-array-based high-throughput technique to assess microbial functional potential in carbon (C), nitrogen (N), phosphorous (P), and sulfur (S) cycling.

3. Results showed a significant relationship between the crown health and changes in the relative abundances of key soil microbial functional genes responsible for the loss of forms of N and P, essentials for plant metabolism and crown health.

4. Hence, we propose a potential tree-soil feedback loop, in which the decline of holm oak promotes changes in the soil environment that triggers changes in key microbial-mediated metabolic pathways related to the net loss of soil N and P mineral forms. The shortage of essential nutrients, in turn, affects the ability of the trees to withstand the environmental stressors to which they are exposed. Identifying the factors that promote this feedback, would be the next step to prevent further holm oak decline processes.

6.1. Introduction

The plant-soil microbial community interactions constitute a system, whose correct functioning marked life on the planet, as we know it. Overall, the binomial plant-soil microbial community constitutes a feedback relationships: i) On the one hand, plants supply carbohydrates that boost microbial functioning and nutrient cycling (Curiel Yuste *et al.*, 2007) and induce changes in soil by modifying both physicochemical properties and biotic activity (Ehrenfeld et al., 2005) ii) On the other hand, soil microbial communities are key to maintain plant health. They are responsible for plant nutrient availability and uptake as they underpin biogeochemical cycles. In addition, they support the plant immune system and provide suppressive properties to the soil (Berendsen *et al.*, 2012). Thus, the plant-soil microbial systems provide important regulating and supporting services to the ecosystem such as carbon sequestration and climate regulation (Smith *et al.*, 2015). Disentangling the mechanisms involved in these plant-soil microbial feedback processes may allow us to improve our understanding of ecosystem responses to natural and anthropogenic disturbances associated with climate change (van der Putten *et al.*, 2016).

Soil microbial communities play a pivotal role in plant-soil feedback through biogeochemical cycles. In these processes, carbon (C), nitrogen (N), phosphorus (P) and sulfur (S) forms are transformed through a series of redox reactions that change the properties and the availability of the essential soil nutrients for plants (Willey *et al.*, 2008). The contribution of the soil microbial communities to nutrient cycling lies on their metabolic diversity and their capacity to use different molecules as energy sources and electron acceptors for microbial respiration to maintain their metabolism and growth. This aspect makes them particularly versatile in terms of the energy (Nealson & Stahl, 2018). Thus, important soil biogeochemical cycles, such as the one of C and N are driven by the balance between the fixation of a gas form (CO_2, N_2), their incorporation into organic matter and their mineralization and respiration (Levy-Booth *et al.*, 2014; Kuypers *et al.*, 2018; Singh *et al.*, 2020). By contrast, phosphorus cycling has no gas phase and its assimilation into biological processes exclusively derives from weathering of the phosphate-containing rocks, the action of phosphate-solubilizing microorganisms, or the mineralization and recycling of the organic phosphorus. This fact makes phosphorus a limiting factor for plant growing in many ecosystems (Sardans *et al.*, 2004; Moreno *et al.*, 2007). Furthermore, climate change-related events may affect biogeochemical cycles, (Deng *et al.*, 2021). Drought and high temperatures increase microbial physiological stress by reducing water availability and enzymatic activity, affecting the different biogeochemical processes. For

example, drought increases microbial CO_2 emissions and reduces the soil organic carbon content and the mineralization rate of nitrogen (Deng *et al.*, 2021) and phosphorus (Margalef *et al.*, 2017). Understanding how the microbial community metabolism shapes soil biogeochemical cycles is of paramount importance to assess the quality of the soil, its state of degradation (Harris & Bedfordshire, 2003; Tu *et al.*, 2014) and its relationship with plant vulnerability to environmental perturbations (Scarlett *et al.*, 2020). Overall, these biogeochemical cycles consist of numerous steps, each mediated by soil microbial functional genes (Tu *et al.*, 2014; Zheng *et al.*, 2018). For instance, key functional genes involved in nitrogen cycling have been used to assess the potential use of nitrogen in different scenarios and include: *amoA, hao* and *narG* (for nitrification, Rotthauwe & Witzel, 1997; Francis *et al.*, 2005), *nirK/nirS* and *nosZ* (for denitrification, Henry *et al.*, 2006; Wei *et al.*, 2015) and *nifH* (for N fixation, Rösch & Bothe, 2005).

Trees greatly influence the functioning of soil microbial communities, not only by providing tree-derived carbohydrates (Tang *et al.*, 2005; Curiel Yuste *et al.*, 2007, 2010) but also by affecting the factors that govern soil processes and microbial communities. For example, the tree layer counteracts the negative effects of climate change on the microbial community by buffering extreme temperatures and regulating hydrological conditions under its influence (Prescott, 2002). This may favour the resilience of the microbial community to warming and drought scenarios (Avila *et al.*, 2019; San-Emeterio *et al.*, 2023). However, drought and heatwave-induced tree decline events may affect physicochemical soil properties and microbial communities, modifying their metabolism and survival rates (Schlesinger *et al.*, 2016; Avila *et al.*, 2019; García-Angulo *et al.*, 2020; Deng *et al.*, 2021). Microbial communities respond to these disturbances through changes in the population at functional and taxonomic levels. For instance, changes in the abundance of microbial nitrifiers have been related to changes in the canopy cover (Shvaleva *et al.*, 2015; Ibañez *et al.*, 2021) and tree girdling (Rasche et al., 2011). Soil microbial community changes driven by tree decline may result in a net loss of soil nutrients (García-Angulo, 2020; Avila *et al.*, 2021). Hence, although some studies have described the influence of the canopy cover on soil microclimatic conditions, soil microbiome (at functional and taxonomic level; Shvaleva et al., 2015; García-Angulo et al., 2020) and nutrient cycling (Ibañez et al., 2021) few studies have assessed the influence of tree crown health on biogeochemical soil functional genes and *vice versa* (Scarlett *et al.*, 2020). A comprehensive functional examination of the microbial community is key to assess biogeochemical cycling and its role in tree-soil feedback in response to climate change (Graham *et al.*, 2016; Deng *et al.*, 2021).

This study focuses on the Spanish dehesa, a savannah-like woodland of agrosilvopastoral use presents in the Iberian Peninsula, where trees, generally Mediterranean holm oak (*Quercus ilex* L. subsp. *ballota* (Desf.) Samp.), are sparsely distributed. Dehesas are among the most endangered ecosystems in the Mediterranean basin (Pulido *et al.*, 2001) due to drought and heatwave-induced tree decline (Allen *et al.*, 2015), pathogen outbreaks such as *Phytophthora cinnamomi* Rands (Solla *et al.*, 2009; Corcobado *et al.*, 2017; Frisullo *et al.*, 2018) and inappropriate human management (Moreno & Pulido, 2009). Previous works contributed to the early detection of holm oak decline (Encinas-Valero *et al.*, 2022a) demonstrating that increased foliar content of photoprotective compounds (i.e., carotenoids and tocopherols) is associated with tree decline. Further the decline was also determined by an increase in the fine root phenotypic plasticity (Encinas-Valero *et al.*, 2022b). However, it remains unclear which is the role of the soil microbial community. The present study aimed at investigating whether and to which extent tree-soil microbial relations may determine holm oak health. The study is based on the fact that tree health is subjected to a bidirectional process, from the plant to the microbial community and *vice versa*. However, much remains to be discerned, as the control mechanisms that determine these bidirectional processes is unclear. This study particularly focuses on how microbial-mediated biogeochemical cycling, customized into soil functional genes encoding enzymes responsible for key steps of microbial metabolism interacts with tree crown health. We hypothesized that crown health is strongly linked to soil microbial functioning and subsequent changes in microbial-mediated nutrient cycling, particularly: (*i*) the loss of crown health (i.e., declining process) would affect the relative abundance of soil microbial functional genes and hence the functioning of soil microbial communities; and (*ii*) the alteration in the relative abundance of these soil microbial functional genes would regulate the availability of key soil nutrients that will further impact on the holm oak crown health.

6.2. Materials and Methods

6.2.1. Sites description and experimental design

Nine holm oak dehesas, located in the central-west Iberian Peninsula, were considered for this research. All these dehesas were selected based on a previous study (Corcobado *et al.*, 2013a) where the interaction between drought and *P. cinnamomi* was identified as the main cause of holm oak decline. Their mean monthly temperature and total monthly rainfall ranged from 6.9ºC and 29.8 mm in January, to 25ºC and 10.4 mm in August 2019 (CRU TS v.4; Harris *et al.*, 2020, reference period 2019). The pH of the soil ranged from 4.0 to 7.7. The tree layer,

characterized by a low density of the tree canopy cover, was dominated by holm oak whereas the understorey vegetation was dominated by grazing pastures.

Within each of the nine dehesas, two different sites were considered: a healthy site (i.e., characterized by the presence of only healthy holm oaks) and an unhealthy site (i.e., characterized by the coexistence of susceptible and declining holm oaks. The health status of the trees (i.e., healthy, susceptible and declining) was assigned after integrating the results obtained on a previous studies (Encinas-Valero et al., 2022a, b). Briefly, healthy trees (n=54) were defined as being those growing in the healthy sites, susceptible trees (n=59) were defined as being those that had less than 10% of defoliation but high rates of early stress markers (i.e., photoprotective compounds) and declining trees (n=49) were defined as being those that had more than 10% of defoliation and high rates of early stress markers. Thus a total of 162 holm oak trees were thus considered for this study.

6.2.2. Crown health and root system determination.

To define a numerical variable that define the health of each trees, we combined the results of previous studies (above and belowground tree compartments; Encinas-Valero *et al*., 2022a, b) into a Principal Components Analysis (PCA). Specifically, for the aboveground tree components that characterized the crown health (Encinas-Valero *et al*., 2022a), we considered: i) the photosynthetic performance index (PiAbs), as a proxy of the photosynthetic energy conservation (Strasser *et al.*, 2000), *ii*) chlorophylls (Chl a + b, μmol m^{-2}), as a proxy of light harvesting regulation and plant acclimation (Esteban *et al.*, 2015a), *iii*) the violaxanthin cycle pigment pool (VAZ, violaxanthin + zeaxanthin + antheraxanthin, mmol mol Chl^{-1}), as proxy photoprotective compounds through thermal dissipation (García-Plazaola *et al.*, 2017), *iv*) total tocopherols (mmol mol Chl^{-1}), as a proxy of antioxidant compounds (Juvany *et al.*, 2013); and *v*) the defoliation (%). As for the characterization of the belowground compartment, the following variables were considered: fine root branching, fine root length (cm) and fine root diameter (cm) as proxies of the resource-uptake strategies of holm oak roots (Encinas-Valero *et al.*, 2022b).The results of the PCA showed that the first two axes (**Fig. 1**) explained 50.1% of the variance and segregated the belowground (PC1) and the aboveground (PC2) tree compartments. The first axis (PC1; hereinafter, fine root system) accounted for 27.5% of the variance and was defined by the root functional traits: the fine root diameter accounted for the highest loading factor (0.61), while the fine root branching accounted for the lowest loading factor (-0.59). This axis was represented in a gradient colour from brown to yellow, i.e., from high fine root branching to high fine root diameter and fine root length. The second axis (PC2;

hereinafter, crown health) accounted for 22.6% of the variance and was defined by the level of crown defoliation in combination with the leaf functional traits. The photosynthetic performance index (i.e., PiAbs) had the highest loading factor (0.41) and was positively correlated with the chlorophylls, while the total tocopherol pool had the lowest loading factor (-0.46) and was positively correlated with the defoliation and violaxanthin cycle pigment pool (i.e., VAZ). The PC2 axis segregated the sampled holm oaks in a continuous gradient depending on the holm oak crown health (**Fig. 1**). The holm oak crown health was represented using a colour gradient from red (i.e., high total tocopherols pool, VAZ and defoliation, characteristics that defined declining holm oaks) to blue (i.e., high chlorophylls and PiAbs, characteristics that defined the healthy holm oaks) (**Fig. 1**).

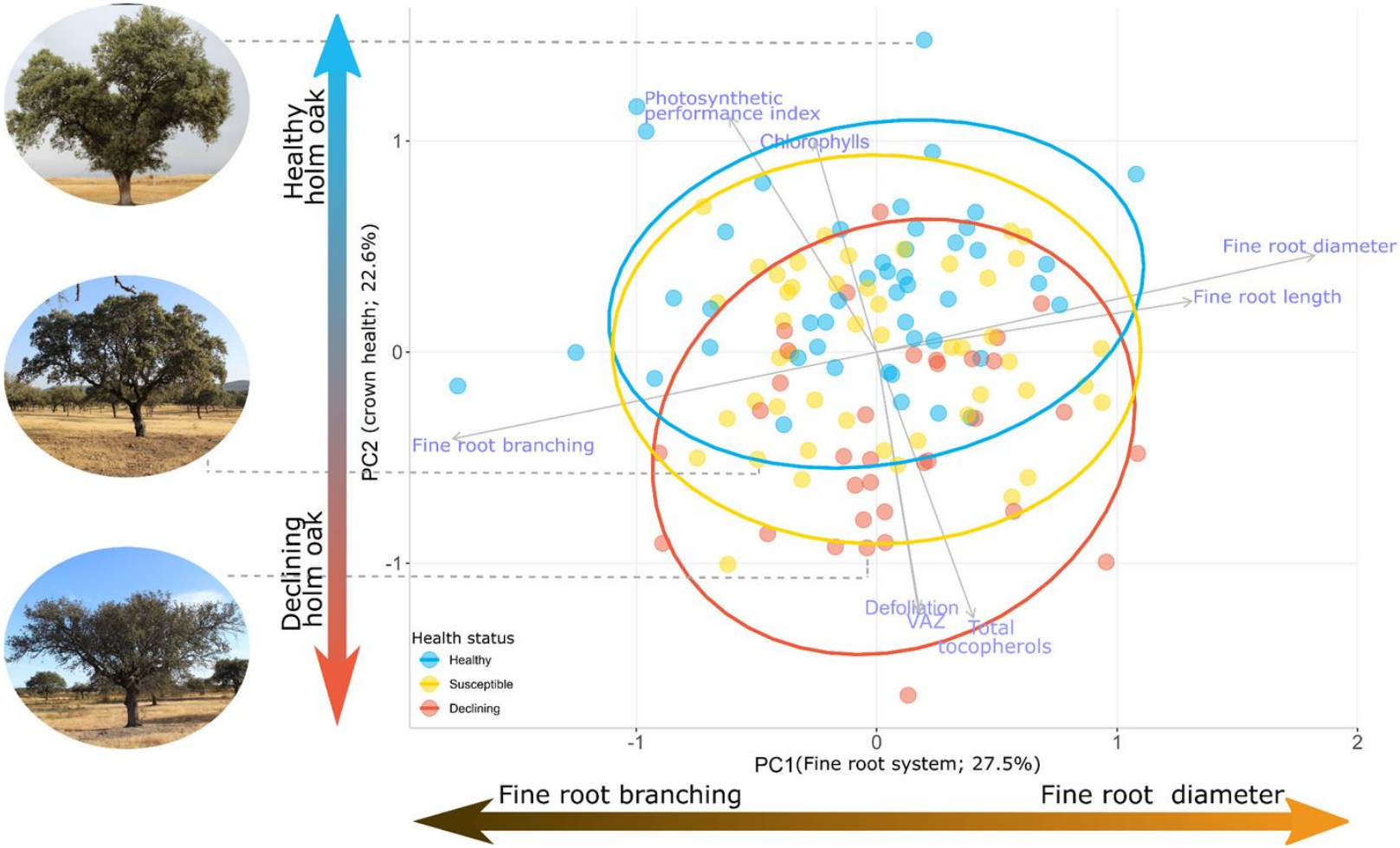

Figure 1 Biplot of the PCA showing the first two axes that represent the belowground (root system) and the aboveground (crown health) tree compartments. The considered belowground variables were: fine root branching, fine root length (cm) and fine root diameter (cm). The considered aboveground variables were: the photosynthetic performance index, chlorophylls (μmol m^{-2}), the violaxanthin cycle pigment pool (i.e., VAZ mmol mol^{-1}Chl), the total tocopherol pool (mmol mol^{-1}Chl) and the defoliation (%). Healthy (n=47), susceptible (n=48) and declining (n=34) holm oak trees are represented in blue, yellow and red respectively. Due to technical problems, some samples were not included in this analysis. Grey arrows indicated the contribution of the analysed variables. The linear combination of the analysed variables (PC1 and PC2) is represented in a colour gradient; from brown to yellow (PC1) and from red to blue (PC2).

6.2.3. Soil sampling

To account for the soil spatial heterogeneity, three different soil samples were collected below each of the 162 holm oak trees at a distance of 1 m from each trunk and at mean depths of 15 cm. Then, the three soil samples were pooled in one single composite sample that was stored at 4°C until arrival to the laboratory. These soil samples were then used to do soil chemical analyses and to quantify soil microbial functional genes. Specifically, for the soil chemical analyses, the 162 soil samples were dried at room temperature (~20ºC), sieved using a 2 mm mesh size and stored in darkness. As for the analyses of the soil microbial functional genes, aliquots from the 162 soil samples were frozen and stored in darkness (cf. section 2.5.).

6.2.4. Soil chemical analyses

Total organic carbon content (organic C) was determined using the dichromate oxidation method described by Yeomans & Bremner, (1988). Total organic nitrogen (organic N) and phosphorus (organic P) contents were determined based on the Kjeldahl digestion method (Radojevic *et al.*, 1999). The final results of organic P and N are the sum of organic and inorganic forms although the inorganic part in this determination is considered insignificant compared to the organic part of the soil. All the results were expressed as mg of organic C, N or P per 100 mg of soil (%). The ammonium determination was performed based on the modified Berthelot reaction (Krom, 1980; Searle, 1984), while the nitrate (NO_2^-) and nitrite (NO_3^-) contents were determined following the cadmium reduction method (Navone, 1964; Walinga *et al.*, 1989). The mineral N was calculated as the sum of ammonium, nitrite and nitrate. The phosphate soil content was determined following the ammonium-heptamolybdate and potassium antimony oxide tartrate reaction in an acidic medium, using a phosphate solution to form the antimony-phospho-molybdate complex (Boltz & Mellon, 1948), while the potassium soil content was determined at 776 nm by aspirating the sample into a flame (Richards, 1954). The ammonium, nitrate, nitrite, phosphate and potassium results were expressed as ppm, μg per g of soil. The pH of the soil samples was measured through the saturated soil paste method (Kalra, 1995). Further details on the soil chemical analyses and the results obtained may be found in Encinas-Valero *et al*., 2022b.

Briefly, mineral N, nitrate, ammonium, phosphate, potassium and organic C were found to be significantly lower (48%, 65%, 35%, 56%, 37% and 17% respectively) in susceptible and declining trees than in healthy trees (**Fig. S6.1**).

6.2.5. Soil microbial functional genes characterization

Soil DNA was extracted from each frozen soil aliquot (250 mg) using the DNAeasy PowerSoil Pro Kit (QIAGEN, Germany) and following the manufacturer's guidelines. Before the extraction, samples were washed twice in 120 mM of K_2PO_4 (pH=8.0) to remove extracellular DNA (Kowalchuk *et al.*, 2002). The amount of DNA was quantified on a ND-1000 spectrophotometer (Thermo-Scientific, Wilmington, DE).

The abundance, relative to 16S, of the soil microbial functional, involved in the C, N, P and S cycles, were quantified through high-throughput quantitative PCR (HT-qPCR) by applying the nanofluidic qPCR BioMarkTM HD system developed by the Fluidigm Corporation (https://www.fluidigm.com/). This system performs qPCR reactions in a Dynamic Array IFC of integrated fluidic circuits and it was applied to the 162 soil DNA samples that corresponded to the 162 studied holm oak trees. A total of 71 validated primer sets (Zheng *et al.*, 2018) were used: 18 targeting C hydrolysis genes (i.e., genes involved in starch, hemicellulose, cellulose, chitin, pectin and lignin degradation); 13 for the C fixation genes; 4 for the methane metabolism (i.e., methane oxidation); 22 for the N cycling (i.e., genes involved in N fixation, nitrification, denitrification, ammonification, anaerobic ammonium oxidation, assimilatory and dissimilatory N reduction and organic N mineralization); 9 for the P cycling genes (i.e., mineralization, solubilization, biosynthesis and hydrolysis of P); and 5 for the S cycling (i.e., S reduction and oxidation). The primer pairs and the encoded enzymes of the analyzed soil microbial functional genes may be found in the electronic supplementary material published by Zheng *et al.*, (2018) and in **Table S6.1**. All the samples were pre-amplified through specific Target Amplification STA-reactions with a pool of primers (250 nM) at 14 PCR cycles using the 12.12 FLEXSix Dynamic Arrays IFC and exonuclease I (Thermo Scientific, Cat N. EN0582). These reactions were performed using the GE FLEXSix PCR + Melt v2 protocol. For the amplification, the 1:10 diluted STA reactions were loaded onto the 96.96 Dynamic Array IFC along with the Master Mix SsoFastTM EvaGreen® Supermix with Low ROX (Bio-Rad Laboratories, Redmond, WA), with a final primer concentration, both forward and reverse, of 250 nM. For the thermocycling, an initial denaturation at 95°C was considered for 1 minute. Then, this process was followed by 30 cycles of 5s at 96°C and 20s at 60°C followed by a melting curve (from 60°C to 95°C). Three technical replicates per sample were added. The Fluidigm Real-Time PCR Analysis Software (v. 4.1.3.) was used to quantify the Cycle Threshold (Cts) of the replicates. The Ct cut-off (i.e., detection limit) was established at 29 considering the highest Ct of the technical replicate samples and a standard deviation

between replicates below 0.25. The detection of a specific gene in a sample was considered positive when two out of three replicates were positive and below the Ct cut-off. The relative abundance of the genes was expressed as a copy number relative to 16S (Looft *et al.*, 2012; Zheng *et al.*, 2018):

$$GR = 10^{(29-Ct)/(10/3)}$$

$$GR_{per\ 16S} = \frac{GR_{target\ gene}}{GR_{16S}}$$

where 29 was the detection limit and Ct was the qPCR threshold cycle. Hence, the relative abundance assessed the presence and proportion of specific genes in the microbial community that increased or decreased (Zheng *et al.*, 2018). From the 71 studied genes, 14 were not detected (**Fig. S6.2**). The relative abundance of a non-detected gene in a sample was considered as being 0.

All the soil microbial functional genes analyses were conducted at the Gene Expression Unit of SGIker (University of the Basque Country UPV/EHU, Spain).

6.2.6. Statistical analyses

To estimate the effect of the tree health status (i.e., healthy, susceptible and declining) on the relative abundance of the soil microbial functional genes, a first set of linear mixed effect models (LMEs) were run. The soil microbial functional genes data were logarithm or square-root transformed before analyses to meet the normality and homoscedasticity assumptions or to reduce the influence of outliers. The fixed part of the model included the health status while for the random part of the model, the site (i.e., healthy and unhealthy) was nested within dehesa to account for the among-sampling site variation. All final reported coefficients were estimated based on the restricted maximum likelihood method (REML) and ANOVA Type III (car R package; Fox & Weisberg, 2019) to deal with unbalanced design. Finally, conditional coefficients of determination (i.e., variance explained by the entire model, R^2_c) were calculated using the r.squaredGLMM function (package MuMIn; Barton, 2020). When significant differences in the health status were found, least-square means tests based on Tukey HSD were run (package *emmeans*; Lenth, 2020). Finally, normality and homoscedasticity assumptions of the residuals were checked using the Kolmogorov–Smirnov test, histogram and quantile-quantile plots. To represent the change in the relative abundance of the analysed soil microbial functional genes of the susceptible and declining holm oak trees relative to the healthy holm oak trees (**Table S6.2**), the estimated category means and p-values were extracted from the post-hoc tests (i.e., least-square means test based on Tukey HSD). Hence, change relative to healthy trees (CR_H) was calculated as follows:

$$CR_H = \frac{EM_D - EM_H}{EM_H}$$

where EM_D and EM_H were the estimated relative abundances of the analysed genes for the susceptible/declining (EM_D) and healthy (EM_H) trees, respectively (**Fig. 2**).

To analyse the relationship between between the soil chemical analyses and the different soil microbial functional genes involved in the biogeochemical cycles (, a Spearman correlation matrix was performed (**Fig. 3**) using the 'rcorr' function from the 'Hmisc' R package (Harrell, 2019).

The multidimensionality of the crown defoliation assessment and the leaf and root functional traits was explored by computing principal component analysis (PCA). For this, the *rda* function from the *vegan* package was used (Oksanen *et al.*, 2020). Based on the obtained results (**Fig. 1**) the principal components 1 (PC1; fine root system) and 2 (PC2; crown health) were used for further analyses. PC1 and PC2 axis were represented using a colour gradient (**Fig. 1**) that went from yellow to brown in the case of PC1 (from more root diameter or positive PC1 values to more root branching or negative PC1 values). In the case of PC2, the colour gradient went from blue to red gradient (from healthier holm oaks or positive PC2 values to more declining holm oaks or negative PC2 values).

In order to analyze the influence of the belowground (PC1; fine root system) and the aboveground (PC2; crown health) tree compartments on the soil microbial functional genes (i.e., our first hypothesis), a second set of linear mixed effect models (LMEs) were run. A similar structure with the one explained above was applied but this time using the soil microbial functional genes (i.e., response variable) and PC1/PC2 (i.e., explanatory variable) as fixed factor in the LMEs. The influence of the PC1/PC2 on the analyzed soil microbial functional genes (**Table S6.3**) is represented in **Fig. 4**. Specifically, the PC1 (fine root system) and PC2 (crown health), increased or decreased the relative abundance of the analysed soil microbial functional genes. These tendencies were represented using the same colour gradient that was used for the PC1 and PC2 (**Fig. 1**) in the cycle step where the gene was involved (**Fig. 4**). Hence, an increase in the relative abundance of a specific gene explained by the fine root branching (i.e., negative values of the PC1 represented from yellow to brown gradient) was represented using the same colour gradient (yellow to brown). Instead, an increase in the relative abundance of a functional gene explained by the loss of crown health (i.e., negative values of the PC2 represented from blue to red gradient) was represented using the same colour gradient (blue to red) (**Fig. 4**).

Finally, a structural equation model (SEM) was run to test the potential causal-effect

relationships between the loss of crown health (i.e., PC2), the soil microbial functional genes involved in the soil biogeochemical cycles and the soil chemical variables (**Fig. 5**). Briefly, our second hypothesis expected a potential tree-soil feedback through the soil microbial functional genes and chemistry. Specifically, SEM was built based on: *i*) the influence of the soil chemistry on the crown health (i.e., PC2); *ii*) the influence of the microbial functional genes involved in the inorganic phosphate solubilization, organic P transformation and phosphate transport mechanisms (i.e., *gcd, pqqC, ppk, ppx, phnk, phoD, phoX*) on the soil chemistry that affected the crown health (i.e., phosphate and organic P); *iii*) the hypothesis that postulates that phosphorus mineralizing enzymes as phosphatases are directly dependent on mineral nitrogen, defined in the literature (Margalef et al., 2017; Chen et al., 2020) and *iv*) the results obtained from our first hypothesis that showed the effect of the crown health (PC2) on the soil microbial functional genes (**Fig. 4**, **Table S6.3**). Thus, in order to meet the first two points (i.e., *i* and *ii*) multiple regression models were first performed (i.e., using LMEs and the same random effects explained before). Variables were logarithm or square-root transformed to meet the normality and homoscedasticity assumptions or to reduce the influence of outliers. The best models were selected based on the stepwise AIC (Akaike Information Criterion) method by using the *stepAIC* function from the package *Mass* (Venables & Ripley, 2002). To do so, the candidate models were adjusted by the Maximum Likelihood method (ML). Finally, the results of the best multiple regressions were adjusted by the Restricted Maximum Likelihood method (REML) and the selected explanatory variables were retained for use in SEM. SEM analyses were performed by using the *psem* function available from the *piecewiseSEM* package (Lefcheck, 2016). Several SEMs were run and the best was selected based on Fisher's C statistic (chi-squared test greater than the 0.05 threshold value; Lefcheck, 2016).

All statistical analyses were performed in R (v.4.1.1; R Core Team, 2021).

6.3. Results

6.3.1. Soil microbial functional gene differences among holm oak health status.

The relative abundance of the genes involved in the carbon hydrolysis (iso-pullulanase, *iso-plu* and lignin peroxidase, *lig*) were significantly higher in declining than in healthy trees (an increase of 98% and 128% respectively, **Fig. 2**, **Table S6.2**). The relative gene abundance for carbon fixation (i.e., ribulose-bisphosphate carboxylase, *rbcL* and S-malate-CoA transferase, *smtA*) was higher at the declining sites than at the healthy sites (i.e., an increase of

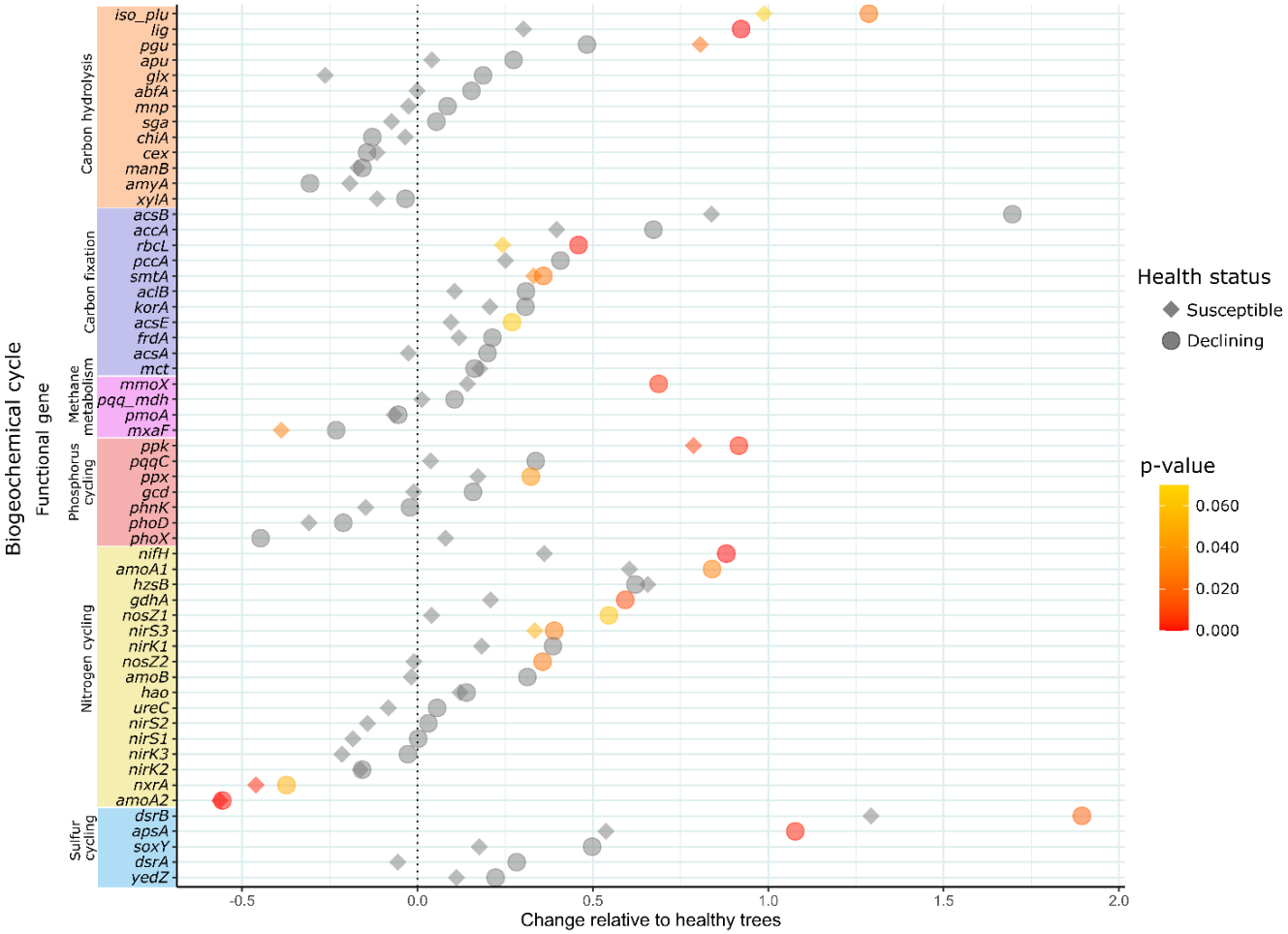

Figure 2 Scatter plot showing the changes (relative to the healthy holm oak trees, n=54) in the analysed soil microbial functional genes of the susceptible (n=59) and declining (n=48) holm oak trees Table S4.2. Due to technical problems, one sample was not included in this analysis The analysed microbial functional genes are arranged by their increase relative to healthy trees and by their role in the different biogeochemical cycles: carbon cycling (carbon hydrolysis, carbon fixation and methane metabolism), phosphorus cycling, nitrogen cycling and sulfur cycling. Change relative to healthy trees was calculated using the estimated mean of post-hoc tests from the LMEs for each health status. P-values, extracted from the pairwise differences in health status, are indicated from red (p-value=0) to yellow (p-value≤0.07).

24% and 33% in susceptible trees and 45 and 35% in declining trees for *rbcL* and *smtA* respectively, **Fig. 2**, **Table S6.2**). The relative abundances of methane monooxygenase component A α chain, *mmoX*; polyphosphate kinase, *ppk* and exopolyphosphatase, *ppx* genes were higher in declining than in healthy trees (68%, 91% and 32% respectively, **Fig. 2**, **Table S6.2**). In addition, the relative abundance of alkaline phosphatase/Pho regulon, *phoX* was marginally higher in susceptible (44%) than in declining trees (**Table S6.2**). Genes involved in the nitrogen cycle, ammonia monooxygenase α subunit for archaea (*amoA1)* was significantly higher at the declining sites (i.e., both 60 % and 84 % higher in susceptible and declining trees respectively) than at the healthy sites (**Fig. 2**, **Table S6.2**). In contrast, ammonia monooxygenase α subunit for bacteria (*amoA2)* was significantly higher (55%) at the healthy sites than at the declining sites. Nitrogenase iron protein (*nifH);* glutamate dehydrogenase *(gdhA),* nitrous-oxide reductase *(nosZ1/2) and* nitrite reductase *(nirS3)* were significantly more abundant in declining (88%, 59%, 56%, 35%, and 39% respectively) than in healthy trees (**Fig. 2**, **Table S6.2**). Finally, nitrite oxidoreductase α subunit (*nxrA)* was significantly higher in the healthy trees than in susceptible and declining trees (46% and 37%) (**Fig 2, Table S6.2**). Genes involved in the sulfur cycle (sulfite reductase β subunit, *dsrB* and adenosine-5'-phosphosulfate reductase α subunit, *apsA*) were significantly higher in declining (189% and 107% respectively) than in healthy trees.

6.3.2. Relationship between soil microbial functional genes and soil chemical analysis

The genes that showed a higher relative abundance in the unhealthy than in the healthy sites (*iso-plu, pgu, lig, rbcL, smtA, mmoX, ppk, ppx, nifH, amoA1, gdhA, nirS3, nosZ1, nosZ2, dsrB* and *apsA*) were negatively related with the soil chemical analysis (**Fig. 3**). In contrast, the genes that showed a higher relative abundance in the healthy than in the unhealthy sites (*nxrA, amoA2* and *mxaF*) were positively correlated with the soil chemical analysis (**Fig. 3**).

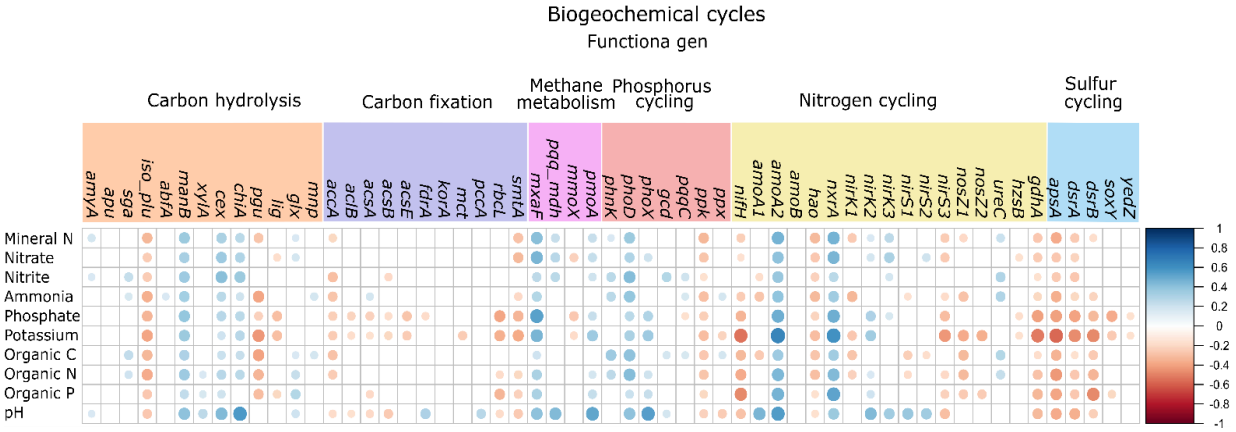

Figure 3. Spearman's rank correlation matrix plot showing the relationship between *i*) soil chemical analysis: mineral N, nitrate, nitrite, ammonia, phosphate, potassium, organic C, organic N and organic P. and *ii*) the different microbial functional genes involved in the biogeochemical cycles: carbon cycling (carbon hydrolysis, carbon fixation, methane metabolism), phosphorus cycling, nitrogen cycling and sulfur cycling. Negative and positive correlations are indicated in red and blue, respectively. The strength of the correlation is indicated by dot size and colour.

6.3.3. Influence of the belowground and aboveground tree compartments on the microbial community.

Figure 4 depicted how the different analyzed soil microbial functional genes (relative abundance) significantly increased as a function of the fine root system (PC1) and crown health (PC2) (**Fig. 4**) in each of the biogeochemical steps where they are involved. This was assessed by the second sets of LMEs (**Table S6.3**, **Fig. 4**). A decrease in PC1 led to an increase of the genes involved in mannan and cellulose hydrolysis (β- mannanase, *manB* and exoglucanase, *cex*, **Table S6.3**, Fig 4a), as well as, fumarate reductase flavoprotein subunit, *frdA* (**Fig. 4**b). Similarly, PC1 decrease significantly increased the methane/ammonia monooxygenase subunit A, *pmoA*, gene involved in the methane oxidation (**Table S6.3**, **Fig. 4**c).

Regarding the influence of the crown health (PC2) on the soil microbial functional genes (**Table S6.3**, **Fig. 4**), the genes involved in lignin (*lig*) and starch hydrolysis (*iso-plu*) significantly increased while decrease PC2 (crown health), (**Table S6.3, Fig 4a**). *FrdA*, ATP-citrate lyase β subunit (*aclB*), the acetylpropionyl-CoA carboxylase (*pccA*) and the methane monoxygenase (*mmoX*) also increased while decrease PC2 (**Table S6.3**, **Fig. 4**b, c). In addition, the genes that were involved in the denitrification were also affected by the loss of crown health (PC2). Specifically, copper and haem-containing nitrite reductase, (*nirK1* and *nirS3* respectively) significantly increased while decreased PC2 (**Table S6.3, Fig. 4**e). In the same way, the genes that were involved in the reduction of the nitrous oxide to nitrogen gas, were

found to marginally increase while decrease PC2 (*nosZ2*, p-value = 0.064). The gene involved in the nitrogen fixation (*nifH*) significantly increased while decreased PC2. With regard to the phosphorus cycling, the genes that codified the pyrroloquinoline-quinone synthase (*pqqC*) and the exopolyphosphatase (*ppx*) significantly increase while decreased PC2 (**Table S6.3**, **Fig. 4**d). Finally, the genes involved in sulfur oxidation, sulfur-oxidizing protein (*soxY*), sulfur oxidase (*yedZ*) and sulfite reductase β subunit (*dsrB*) were found to significantly increase while decrease PC2, (**Table S6.3**, **Fig. 4**f).

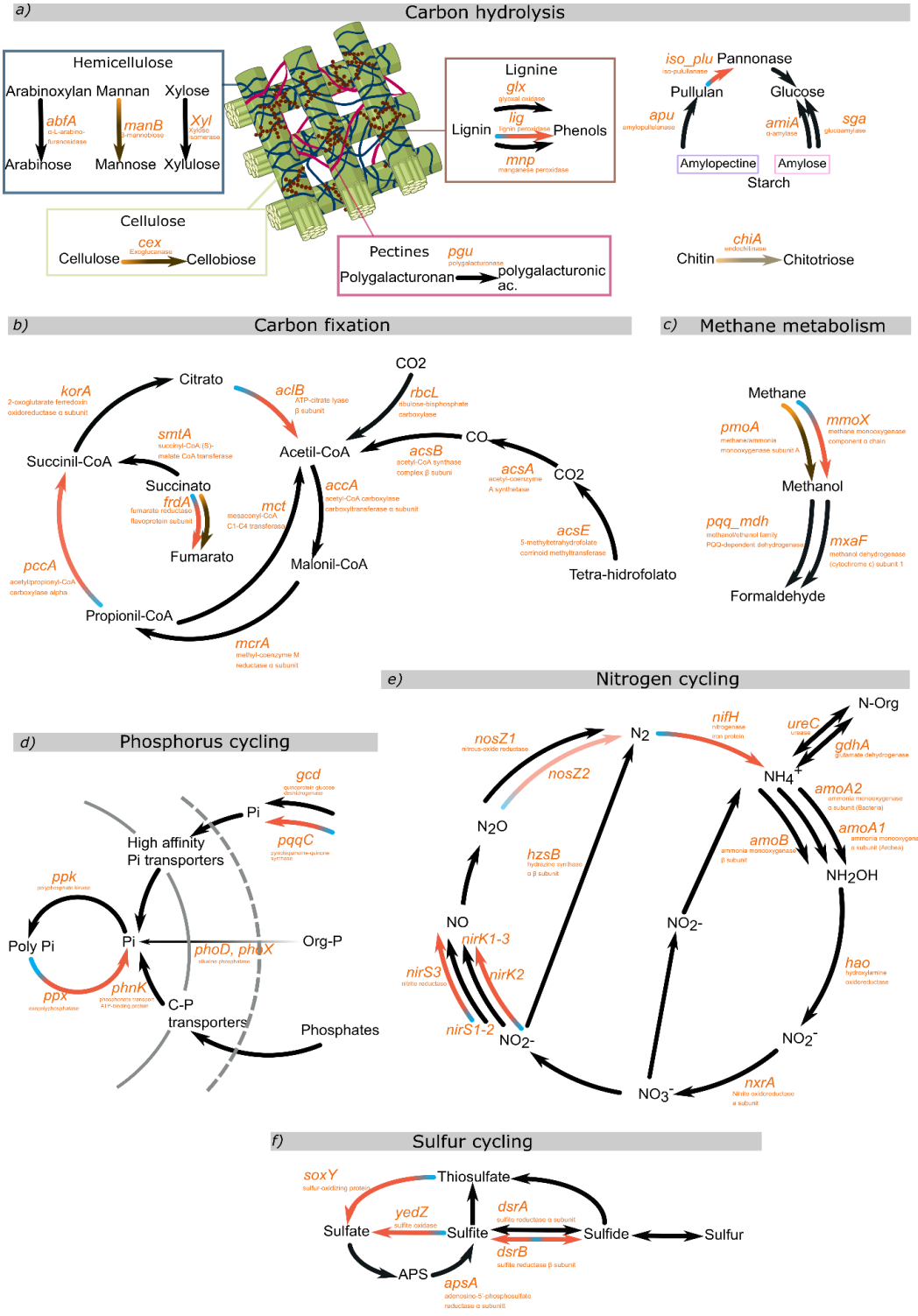

Figure 4. Depiction of the second set of LMEs (Table S6.3). This figure shows how the different soil microbial functional genes, significantly increased ($p < 0.05$) as a function of the belowground (fine root system) and aboveground (crown health) tree compartments (**Fig. 1**) in each of the biogeochemical steps where they are involved. This relationship is indicated by the used gradient colour that represents PC1/PC2 in **Fig. 1**. Mild-coloured arrows indicated a marginally significant effect of the principal component (PC1/PC2) on the soil microbial functional genes ($p \leq 0.07$). Instead, the black arrows indicated non-significant effects of the principal components on the analysed soil microbial functional genes. The non-detected genes are not shown. The representation of the biogeochemical cycles is based on the figures published in Zheng *et al.*, (2018).

6.3.4. Holm oak decline triggered a feedback loop

Figure 5 represented a sequential effects of the components involved in the feedback and triggered by holm oak decline and how the alteration in the relative abundance of soil microbial functional genes would regulate the availability of key soil nutrients that will further impact on the holm oak crown health (hypothesis 2). Particularly, **Fig. 5** described how: *i*) the loss of crown health increased the soil functional genes involved in nitrogen and phosphorus cycling (*nirS3, ppx* and *pqqC*, represented with a red circle), *ii*) these soil functional genes affected mineral N, phosphate and organic P, *iii*) these soil nutrients in turn affected the crown health and *iv*) mineral N affected *phoD* and *phoX*-harboring comumunities. The proposed SEM provided a good fit as indicated by the Fisher's C statistic and p-value ($\chi 2 = 32.26$, p-value = 0.73). According to the results of this analysis (**Fig. 5**), the phosphorus cycling was proposed to be the key biogeochemical cycle that determined the leaf health of the studied holm oak trees. This influence was mainly based on the negative and positive effects of organic P and phosphate on PC2 (the crown health), respectively (**Fig. 5**). The soil microbial functional genes involved in the phosphorus cycling (*pqqC* and *ppx*, positively affected by PC2) had a negative effect on the organic P and phosphate concentration. In addition, a plausible relationship between nitrogen and phosphorus cycling through genes that codified alkaline phosphatases (*phoX* and *phoD*) and the negative effect of the denitrier community (*nirS3*, positively affected by PC2) on the mineral N pool is shown (**Fig. 5**).

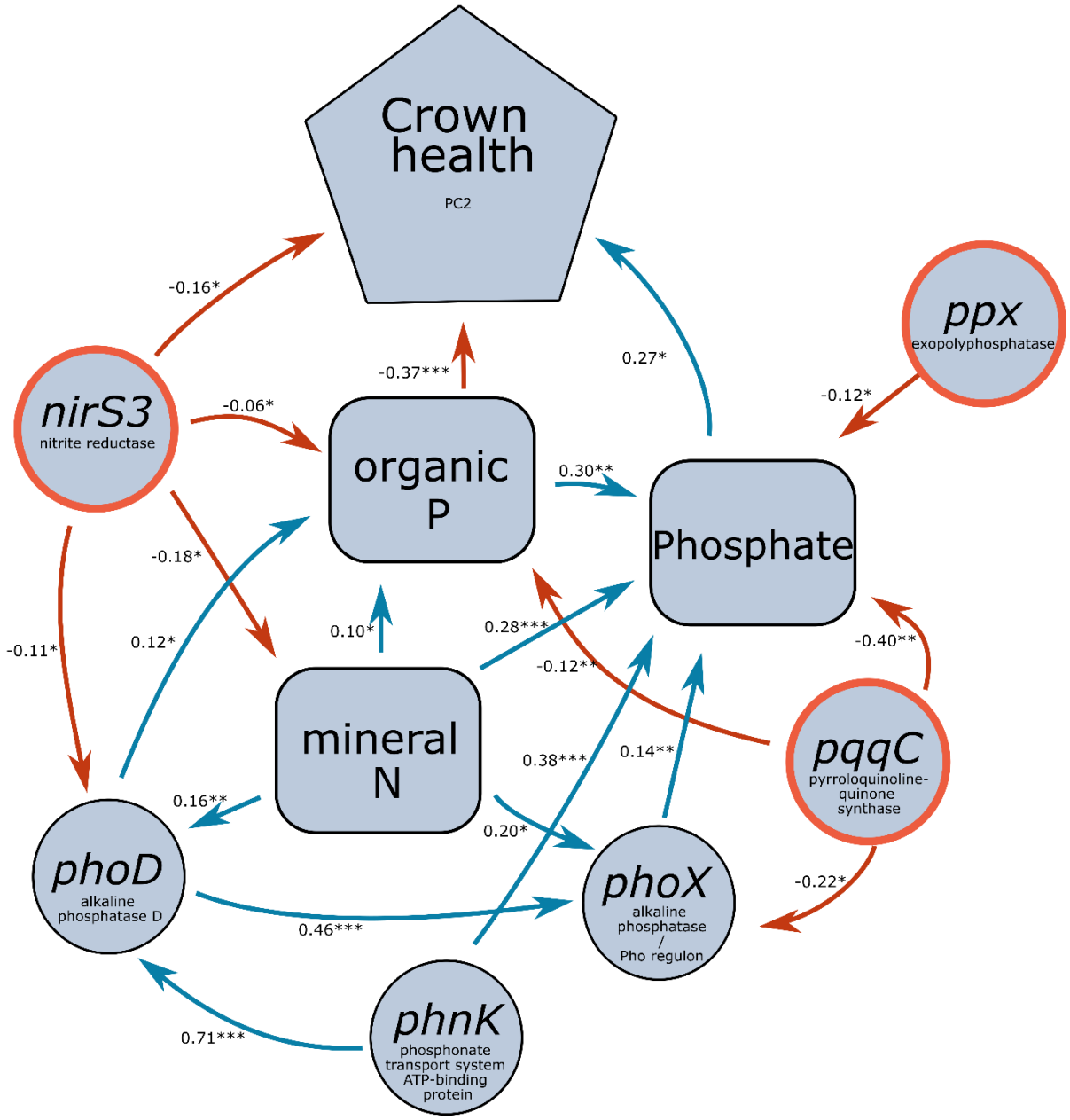

Figure 5. Structural equation modelling (SEM) results. The path diagram shows a putative causal-effect relationship among soil functional genes involved in the nitrogen (*nirS3*) and phosphorus cycling (*phoX*, *phoD*, *pqqC*, *ppx*, *phnk*), the mineral N (sum of ammonia, nitrite and nitrate, μg g^{-1}), phosphate (μg g^{-1}), organic P (%) and crown health (PC2). Arrows indicate causal relationships, numbers indicate the standardized estimated regressions' weights and asterisks represent significant relationships (*, $p < 0.05$; **, $p < 0.01$; ***, $p < 0.001$). Blue arrows indicate positive relationships while red arrows indicate negative relationships

6.4. Discussion

The obtained results point out that changes in soil microbial functioning and its influence on soil nutrient cycling were rather related to the crown health (PC2) than fine root system (PC1, **Fig. 4**). This result provides novel insight on the adjustments that the crown-soil microbiome system undergoes in response to climate change-related events, opening up opportunities not only for holm oak decline detection (Cavender-Bares & Logan, 2022) but also for early detection of changes in soil nutrient cycling dynamics under the influence of climate change. Overall, this study describes a feedback loop in which the effect of holm oak on soil generated a cascade of soil responses that affected holm oak crown health and boosted the declining process. In this feedback loop, the loss of crown health and the subsequent decline was positively related with an increase in the relative abundance of soil microbial functional genes involved in downregulating mineral N and ultimately phosphate (*nirS3*, *pqqC* and *ppx*, **Fig. 5**). Since both nitrogen and phosphorus are essential limiting factors for tree growth in dehesas, their scarcity was, in turn, responsible for limiting holm oak ability to recover. Therefore, bidirectionality is described in the causal-effect relationships in which the effect of the loss of crown health on the soil (i.e., functional genes and chemistry) caused a reciprocating effect of soil on crown health. Below we describe the two directions of causation and the mechanisms involved.

6.4.1. The loss of crown health affects the relative abundance of the soil microbial functional genes

Tree decline affects the soil abiotic and biotic environments under its influence (Rodríguez et al., 2016; Flores-Rentería et al., 2018; Curiel-Yuste et al., 2019; García-Angulo et al., 2020) having both direct (Solla *et al.*, 2021; Encinas-Valero *et al.*, 2022b) and indirect (Rodríguez *et al.*, 2016, 2023 *in press*) effects on the soil properties. The overall biological functioning of the soil system is affected (Curiel Yuste *et al.*, 2019). In agreement with our first hypothesis, our results suggest that certain biogeochemical steps, like denitrification, lignin and starch degradation, carbon fixation, inorganic phosphorus solubilisation and sulfite oxidation may be potentially affected by holm oak decline (**Fig. 4**, **Table S6.3**). As observed here, changes in the soil abiotic environment, due to shifts in the tree cover, have been directly associated with alterations in the abundance of nitrogen-transforming microorganisms (Shvaleva *et al.*, 2015; García-Angulo *et al.*, 2020; Scarlett *et al.*, 2020). Particularly, denitrifiers (*nirS3, nirK1* and *nosZ2*) and nitrogen fixation communities (*nifH*) were enhanced by the loss of crown health that resulted from holm oak defoliation and decline (**Table S6.3**,

Fig 4). This contrasting result may be partly explained by the polyphyletic distribution of denitrifying genes and their co-occurrence with nitrogen-fixation genes in many strains (Levy-Booth *et al.*, 2014). In addition, *nirS3* and *nirK1*-harboring communities (denitrifier genes) were negatively correlated with the availability of nitrogen mineral forms (mineral N, nitrate and ammonia, **Fig. 3**). This suggests that these communities may be implicated in the loss of mineral nitrogen through denitrification. This phenomenon constitutes a net potential source of nitric oxide (NO) that may partially explain the depletion of mineral N under declining trees. In addition, full denitrification (i.e., N_2O reduction to N_2 by *nosZ*-harbouring communities) may also occur due to the loss of tree cover (Shvaleva *et al.*, 2015; Ibañez *et al.*, 2021). In this sense, previous studies attributed the enhancement of *nirS* and *nosZ*-harboring communities to the increase in water content (Rasche *et al.*, 2011). These conditions may result from the reduction of evapotranspiration and the loss of tree foliage (Corcobado et al 2013c). Hence, we speculate that soil microclimatic changes associated with the loss of crown health and tree decline have the potential to favour certain microbial communities over others (denitrifiers over nitrifiers), resulting in major changes in the pool of available nutrients essential for crown health. Concerning the rest of the affected biogeochemical cycles, this study also reports the presence of higher values of starch and lignin-degrading genes (*iso-plu* and *lig*, **Fig. 4**, **Table S6.3**) associated with the loss of crown health and decline. This may be explained by an increasing presence of saprotrophs, wood degraders and/or tree pathogens, probably involved in the loss and degradation of necrotic fine roots in declining trees (Pinho *et al.*, 2020; Solís-García *et al.*, 2021). Also, the increase of *soxY*, *yedZ* and *dsrB*-harboring communities (**Fig. 4**, **Table S6.3**) indicated the presence of sulfur-oxidizing bacteria. Some of these bacteria have also the capacity to use oxidized nitrogen forms as terminal electron acceptors, resulting in denitrification under anaerobic conditions (Willey *et al.*, 2008). Moreover, the increase in genes involved in the reverse tricarboxylic acid cycle (*aclB* and *frdA*, Campbell et al., 2003) in conjunction with 3-hydroxypropionate cycle (*pccA*) indicate an increase in carbon fixation potential. The reduction in soil carbon turnover due to holm oak decline (García-Angulo et al., 2020) may slightly favour microbial carbon fixation as an homeostatic response to the progressive soil carbon depletion (Xiao *et al.*, 2022). In addition, the higher relative abundance of *pqqC* and *ppx*-harboring communities also indicated the potential for inorganic-P solubilization (Meng *et al.*, 2022).

6.4.2. Microbial-induced changes in nutrient cycling regulate tree health

The obtained results reported potential changes in the soil microbial functional genes that may be directly related to changes in soil nutrient cycling, ultimately affecting the availability of soil nutrients (**Fig. 3**), essential for crown health. Soil microbial communities are responsible for soil carbon and nutrient cycling (Smith *et al.*, 2015) and may support or constrain tree performance under stress through the modulation of soil nutrients. In this sense, *nirS3*-harboring communities were enhanced by the loss of crown health and had a negative effect on mineral N (**Fig. 5**). Thus, it is likely that *nirS*-harboring communities may partly consume nitrogen mineral forms, resulting in nitrogen loss through gas emissions under declining holm oaks in the Spanish dehesa. This will further reduce nitrogen availability for plants and other bacterial communities (Lennon & Houlton, 2017). The unavailability of nitrogen has been described to be responsible for the downregulation of phosphorus cycling rates, in the short term (Chen *et al.*, 2020). This is because, under phosphorus limitation, phosphorus mineralizing enzymes as phosphatases are N-rich enzymes directly dependent on mineral nitrogen (Margalef et al., 2017; Chen et al., 2020), and its absence promotes the accumulation of organic P and the decrease in phosphates, becoming the limiting factor for holm oak growth (Avila *et al.*, 2016). In agreement with this idea, SEM (**Fig. 5**) describes how both mineral N shaped *phoD* and *phoX*-harboring communities, responsible for hydrolyzing carbon-phosphorus ester bonds to phosphate under phosphorus shortage (Ragot *et al.*, 2017). Hence, the shortage of mineral N might be responsible, at least partially, for the phosphate depletion observed under declining trees and for the further effect on early stress markers associated with the loss of crown health and tree decline (indicated by PC2, **Fig. 5**). As in previous studies, the obtained results highlighted the role of organic P and phosphate in holm oak health (Sardans *et al.*, 2004; Avila *et al.*, 2016) and indicated that the unavailability of phosphate may increase early stress markers associated with the loss crown health (i.e. PC2; Encinas-Valero *et al.*, 2022a). In this regard, phosphorus limitation has been reported to reduce holm oak biomass (Sardans *et al.*, 2004) and water use efficiency, resulting in faster senescence (El-Madany *et al.*, 2021). In contrast, organic P abundance showed a negative effect on PC2 (**Fig. 5**) in agreement with a previous study that reported a negative effect in the physiology of leaves in *P. cinnamomi*-infected holm oak when an organic fertilizer at high dose was applied (López-Sánchez *et al.*, 2022).

The results of the SEM further illustrated alternative metabolic paths involving the use and dynamics of inorganic forms of phosphorus directly regulated by microbial communities

(i.e., *pqqC* and *ppx*, **Fig. 5**). In the case of *pqqC* and *ppx*-harboring communities, responsible for inorganic-P mobilization (Bi *et al.*, 2019; Wu *et al.*, 2022), they both increased while decrease crown health (PC2) in (**Fig. 4**, **5**, **Table S6.3**). While *ppx* genes encode enzymes involved in bacterial intracellular polyphosphate degradation, *pqqC*-harboring communities promote the solubilization of the recalcitrant phosphorus-metal complex by producing organic acids (Hwangbo *et al.*, 2003; Wu *et al.*, 2022). Although it might be presumed that these communities increase the phosphorus availability for the trees (Wu *et al.*, 2022), we observed a negative relationship with the soil phosphate concentrations. In this sense, studies under controlled and field conditions have shown inconsistent effects concerning plant performance and inorganic phosphorus solubilisation by microorganisms (Meyer *et al.*, 2019). This is because soil characteristics (i.e., phosphorus, organic C, nitrogen shortage, pH, and soil texture) may affect the functioning and effectiveness of the *pqqC* and *ppx*-habouring communities to solubilize available phosphorus for tree uptake (Raymond *et al.*, 2020). Thus, we suggest that these communities might be potential competitors for the available phosphate with the tree (Raymond *et al.*, 2020), since inorganic P solubilization is an energy-demanding metabolic path rather unlikely to increase under the low organic C availability of these soils and at intense competence with other microorganisms (Meyer *et al.*, 2019). In any case, the results of this study point out *pqqC* and *ppx*-harboring communities as potential key regulators of the phosphorus cycle in dehesa ecosystems.

6.4.3. Final remarks and conclusions

Our study provides new insight into the Spanish dehesa functioning and the tree-soil feedback stablished between crown health, soil functional genes and soil chemistry. In agreement with our hypotheses, this study shows a potential plant-soil feedback loop in which soil microbiome plays a central role determining tree health. The significant adjustments in the functioning of the soil microbial communities at the early stages of tree decline promoted metabolic paths responsible for losing key soil nutrients for tree consumption. This may further result in a loss of dominance of holm oaks in declining areas (Gómez-Aparicio *et al.*, 2017). Although numerous studies focus on the unidirectionality of this process (either plant affecting soil or *vice versa*), we here describe the bi-directionality of the causal-effect plant-soil relations as a more plausible way to explain the observed trends of holm oak decline. Factors that affect one compartment (plant or soil) will inexorably affect the other and will potentially boost holm oak decline. Identifying the factors that promote this positive feedback loop, like climate

change events, land use and/or agricultural management, would be of paramount importance in order to prevent holm oak decline.

Chapter VII

General Discussion

The increasing number of observed events of drought- and heatwave-induced tree decline and mortality highlights the stress to which forests around the world are being subjected due to climate change (Hammond *et al.*, 2022; Hartmann *et al.*, 2022). The increment in holm oak decline observed in the Iberian dehesa ecosystems during the last decades (López-Ballesteros *et al.*, i*n press*) is just another example of this phenomenon. The dehesa is a very traditional use given to the holm oak in this part of the peninsula, closely linked to the local economy and culture, so its decline may have severe consequences not only at ecological, but also at the social and economic levels (Plieninger *et al.*, 2021). We here propose that a mechanistic understanding of the physiological and ecological processes underlying the phases that precedes and follows early stages of defoliation as well as a, more holistic view of this phenomenon (from the leaf biochemistry and crown structure to the root physiology and the microbial community involved in nutrient mineralization) is required to predict, prevent or mitigate tree decline and its impacts on ecosystem functioning. To address these challenges, in this thesis, we bridged gaps between different scales of analysis (i.e., from the leaf to the tree-soil system level), different organs (from the leaf to the fine root system), and different levels of complexity (from leaf biochemistry to complex plant-soil ecological interactions). Specifically, we integrated biochemical leaf adjustments (Chapter IV) along with key structural root parameters to understand the responses at the tree level. In addition, we evaluated the complex relationships and interactions that holm oak established with the soil chemistry (Chapter V) and the microbial communities involved in soil biogeochemical cycling (Chapter VI) during the process of holm oak decline (**Fig. 1**). Overall, in the following lines, it is highlighted and discussed the need for a holistic approach to understand the physiological and ecological responses of plants and the plant-soil system to the environmental challenges to which these anthropic oak savannahs are currently being subjected.

7.1. Application of a holistic approach to improve the understanding of the process of tree decline

This thesis puts into perspective the importance of applying a very holistic approach to study tree decline, i.e. the study of key physiological processes from the leaf to the root, and the role of the ecological interactions of the plant with its environment, especially with the soil system. This thesis begins by analysing the responses that occur at the leaf biochemical level. The study of leaf photoprotective compounds (chapter IV: mainly VAZ and tocopherol) provided some insight into the biochemical adjustments that the holm oak sets in the photosynthetic organs before defoliation. We observed downregulation of the photosystem II presumably mediated by the enhancements of de-epoxidated xanthophylls (i.e., A, Z and L) as well as an upregulation of tocopherol. These results suggested an acclimation response triggered at the leaf level to protect the photosystems in the thylakoid membranes. Nevertheless, once the tocopherol threshold is reached (at <9% of defoliation) we discussed (chapter IV) the potential impact that photo-oxidative damage may have on the thylakoid membranes of the chloroplast, cell death (Guadagno *et al.*, 2017; Morales *et al.*, 2021) leaf senescence and loss and finally the defoliation of the tree. These responses at the biochemical level are just a consequence of the stresses that the photosystems are subjected to due to the negative impact that drought/*Phytophthora* spp imposes at the tree level (Ruiz-Gómez et al., 2019). At this point, in a scenario of high belowground stress, especially associated with a limited capacity of the tree to obtain soil resources (due to drought and *Phtytophtora* spp), adjustments in the carbohydrates plant allocation take place to develop a root system able to uptake soil resources more efficiently. This is done at the expense of maintaining foliage. This allowed us to determine how adjustments at the organ and tissue level were affecting the functioning of the whole tree (Chapter V). However, the connexion between hydraulic and biochemical traits of the roots, stems, leaves and allometric parameters is needed to reinforce and fulfil this knowledge gap (Trugman, 2022). Thus, tree health depends on the uptake of soil nutrients which are controlled by the development of the root system but also by the ecological relationships that the plant establishes with the soil microbiota, responsible for the cycling and mineralization of essential plant nutrients (Willey *et al.*, 2008). Particularly important is to understand the intensity and the direction of the functional relations between the tree and the soil microbial community. We observed a complex feedback between the crown structure and biochemistry and the soil microbial communities, reflected in the relation between crown health and the abundance of the genes responsible for the cycling of essential plant nutrients

such as nitrogen (N) and phosphorous (P). Hence, from an applied perspective, observable changes of the crown structure (i.e., defoliation) in combination with photosystem II efficiency and photoprotection reflects not only the aboveground physiological functioning of the tree but also adjustments at the tree level on resource allocation to the belowground organs (fine roots) and changes in the relationship of the tree with the soil. In this regard, during the process of holm oak decline, the changes at the leaf biochemical level that induced defoliation at the tree level exerted an alteration in the soil environmental conditions. This triggered the upregulation of certain microbial communities (as denitrifiers, P solubilizers) that induced the loss of mineral forms of N and available forms of P essential for tree growth and survival. Hence, we here described how tree decline boosts a plant-soil feedback loop that promoted the loss of nutrients and result in more decline. This represents a mechanistic pathway to model tree decline and hence the ecosystem functioning disruptions that arise from this process (Guadagno *et al.*, 2017; Gómez-Sagasti *et al.*, 2023), opening up opportunities to evaluate not only the health of the tree but also the functioning of the ecosystem, in this case, changes in soil nutrient cycling dynamics under the influence of climate change.

In the following sections, each piece of the "puzzle" of the tree decline phenomenon is analysed. Finally, we put together the pieces of the puzzle to propose a holistic view of the declining process.

7.2. Modifications in the photosynthetic apparatus are triggered before declining symptoms are evident

Holm oak decline is a slow process that may be initiated years or even decades before tree mortality occurs (Gea-Izquierdo et al., 2021). Throughout the declining process, and to survive, the tree triggers an array of structural, physiological, and molecular mechanisms to adapt to the new conditions of stress. These responses are initiated when water deficit (triggered by the combination of drought and *Phytophthora* spp), reflected in low leaf water potentials (Corcobado et al., 2013b; Ruíz-Gómez et al., 2018b), induces stomatal closure. In holm oaks, these responses are associated with an increase in abscisic acid and a reduction in mesophyll conductance that lead to a reduction in carboxylation and net CO_2 assimilation (Peguero-Pina et al., 2018). At this point, excited chlorophyll cannot drive photochemistry, and excess energy needs to be dissipated to avoid photooxidative damage (García-Plazaola *et al.*, 2017). In these conditions, photoprotection mechanisms play an essential role in the survival of Mediterranean plant species (Fernández-Marín *et al.*, 2017). ***With the aim to identify early-onset indicators***

of holm oak decline, we investigated the performance of different photoprotective compounds in different initial stages of the declining process (chapter IV). We observed that holm oak trees from the declining area (i.e., both non-declining and declining) exhibited an increased foliar expression of photoprotective compounds (mainly VAZ-cycle pigments and total tocopherols) in comparison to control trees from the healthy area (Chapter IV, **Table 1**). The increase in concentration of these compounds before trees exhibit declining symptoms led us to consider them as early stress markers for holm oak decline. Hence, we proposed these pre-settings as critical indicators for forecasting holm oak susceptibility in the context of the dehesa. Secondly, ***aiming to identify a physiological threshold that indicates the tree´s inability to cope with the current stressful conditions, we modelled VAZ and tocopherol content along a defoliation gradient***. Interestingly, we obtained different behaviour in response to the loss of tree vigour and defoliation. Whereas VAZ exhibited a continuous rise along the defoliation gradient, the tocopherol response was saturated at ≈9% of defoliation (Chapter IV, **Fig. 4**). Both the non-saturated response of the VAZ-pigments along defoliation and the rise of tocopherol content up to ≈9% of defoliation was interpreted as part of the acclimation process in response to drought stress and more xeric conditions (Tausz *et al.*, 2004; Camarero *et al.*, 2012). Nevertheless, when tocopherol trends dropped after ≈9% of defoliation, we recognized photooxidative damage. This supports the idea that stress-tolerant trees exhibit the initial tocopherol phase, whereas stress-sensitive trees exhibit the decreasing collapse phase (Munné-Bosch, 2005; Juvany et al., 2012, 2013). Lower photoprotective capacity in plants may promote the accumulation of ROS, causing irreversible damage at the cellular level and leading to plant death (Morales *et al.*, 2021).

7.3. Lipophilic photoprotective compounds serve as an effective tool to assess the level of vulnerability of holm oaks (Chapter IV)

Overall, the results in chapter IV reinforced the idea that VAZ and tocopherols present high responsiveness not only to factors such as high light intensity, drought or high temperature (Camarero et al., 2012; Wujeska et al., 2013; Esteban et al., 2015a; Fernández-Marín et al., 2017; Fenollosa & Munné-Bosch, 2018) but also to the progressive process of vigour losses, defoliation and decline. The discovery is ground-breaking as it reveals that increased photoprotection may not necessarily indicate improved vigour (Morales *et al.*, 2021), but rather declining vigour resulting from decreased stress resistance. The monitorization of the forest

has been traditionally evaluated by the degree of defoliation (Forest Europe, 2020; Michel *et al.*, 2020). The assessment of these biochemical parameters may complement and provide a more accurate determination of the level of stress. However, a crucial question that raised from this study was the extent to which the use of these early warnings in the dehesa may be applied to other forest systems (Cavender-Bares & Logan, 2022). The implementation of these insights requires first a comprehensive understanding of the factors that contribute to tree decline and ultimately to the physiological mechanism that is affected. This depends on the host species, the specific pathogen and environmental conditions (Schmied *et al.*, 2023). For example, the pathogen responsible for the oak decline in North America may not necessarily induce the upregulation of photoprotective compounds (Cavender-Bares & Logan, 2022). Further investigation is required to explore this line of investigation and identify new mechanisms triggered before the onset of decline and adapt them to each particular case. In recent years, we have witnessed the development of highly precise tools to assess plant fitness. For example, the use of sensors and biosensors provides continuous and precise long-term sensing of physiological and biochemical parameters such as carbohydrates, ROS, phytohormones and other plant signalling compounds induced during the stress (Wang *et al.*, 2021; Giraldo & Kruss, 2023; Lo Presti *et al.*, 2023).

Key I: we characterized the health of the trees, determine those photoprotective compounds induced before defoliation and identified a biochemical threshold beyond which damage at the leaf level and defoliation occurs. The use of these compounds may allow the detection of the biochemical alterations induced before the decline and ***forecast future declining hotspots***.

7.4. Above and belowground adjustments in declining holm oaks

The "health status" categories were upgraded according to the level of the defoliation and the amount of the photoprotective compounds. Susceptible trees were those trees that had not reached 10% of defoliation but exhibited high rate of photoprotective compounds, whereas declining trees were those trees with more than 10% of defoliation and high rates of photoprotective compounds. These trees are in the collapse phase of the tocopherol (Chapter V, **Fig. 4c**). The point to which tocopherol reached a threshold marked the inability of the holm oak to cope with the environmental stress to which it was subjected (**chapter IV**). ***At this point, we hypothesized an additional response in the declining trees once tocopherol reached this threshold to prevent further damage.*** The observed photooxidative damage is presumably induced by water stress (i.e., drought but especially by the action of *Phytophthora* spp root rot).

Nevertheless, plants may also trigger mechanisms to minimize the effect of the existing stress, for example by allocating more resources to belowground organs, to develop a more efficient root system (Moser *et al.*, 2015; Montagnoli *et al.*, 2018; Ruíz-Gómez *et al.*, 2018b; Fromm, 2019; Vivas *et al.*, 2021). We, therefore, investigated how different key fine-root functional parameters, associated with soil resource acquisition varied along a gradient of soil nutrient availability and health status. (Chapter V). We found that the soil nutrient availability revealed a high fine root phenotypic plasticity in the most stressed trees (i.e., declining holm oaks) (Chapter V, **Fig. 3**). This indicated that trees experiencing higher levels of stress (i.e., declining holm oaks) were able to adjust their root features in response to the soil nutrient variability. Under nutrient-rich soils stressed trees developed short, thin, and highly branched fine roots while under nutrient-poor conditions trees develop a more "exploratory" fine root system, consisting of thicker and longer but poorly branched fine root system.

These adjustments may be explained as an adaptive response to maintain root functioning under the generally changing Mediterranean environmental conditions at which this species have evolved (Makita *et al.*, 2011; Mou *et al.*, 2013; Fromm, 2019; Suseela *et al.*, 2020; Suz *et al.*, 2021). As a response to localized resource-rich patches, a high number of root tips and branches (Liese *et al.*, 2017) enhance the effective absorbing local root surface and favour soil resource acquisition (Pregitzer, 2008; Beidler *et al.*, 2015; Yahara *et al.*, 2019; Wambsganss *et al.*, 2021). These characteristics accelerate water and nutrient uptake. Conversely, longer and non-branched roots are presumed to be effective for exploring a large volume of soil when resources are limited (Belsky, 1994; Beidler *et al.*, 2015; Eissenstat *et al.*, 2015; Montagnoli *et al.*, 2018; Freschet *et al.*, 2021b). These morphological and architectural changes along soil nutrient availability in declining trees revealed high phenotypic plasticity that presumably allows them to cope with the stress to which they are subjected (i.e. drought and root-rot by pathogens such as *Phytophthora*; Corcobado et al., 2013; Ruiz-Gómez et al., 2019). Thus, ***this work concluded that even after surpassing a certain level of physiological damage, holm oaks still could adjust the structure of their fine root system to the local conditions of soil nutrient availability, thereby optimizing belowground resource acquisition (i.e., fine root phenotypic plasticity).*** Nevertheless, the particular conditions in the Spanish dehesa, subjected to long summer droughts and anthropic disturbances, expose holm oaks to unpredictable changes in soil resources (Plieninger, 2006). Hence, "low phenotypic plasticity" strategy, as observed in susceptible and healthy trees, may be more favoured than a "high

phenotypic plasticity" as it avoids the development of plant structures too costly to maintain, in terms of investments in NSC (Baquedano *et al.*, 2008).

Previous studies have reported that increasing the roots' ability to uptake soil nutrients is an energy-consuming process (Lynch et al., 2011) because it requires a significant investment in NSC to grow and develop branches (Ritchie & Dunlap, 1980; Willaume & Pagès, 2011; Hartmann & Trumbore, 2016; Wang et al., 2018). With this idea in mind***, we explored the carbon costs of these root uptake strategies in different health statuses***. We observed a positive relationship between the NSC pool (including the soluble sugars) and the state of fine root branching development in declining trees. Given the role of carbohydrates in promoting root branching (Thaler & Pagès, 1998), we proposed that the soluble sugars may be potentially involved in promoting fine root branching to optimize resource acquisition (Dewar *et al.*, 1994; Montagnoli *et al.*, 2018). Hence, a shift in patterns of holm oak allocation of carbohydrates took place at the tree level to maintain a root system architecture and morphology that optimize tree resource acquisition capacity. Therefore, a potential above-belowground adjustment (i.e., trade-off) at the tree level is discussed in this work (Chapter V). The preferential allocation of carbohydrates in fine roots to increase soil resource acquisition did further occur at the expense of maintaining foliage, resulting in defoliation (Chapter V, **Fig 5**). In conclusion, with the study in Chapter V**,** we highlighted the capacity of the tree to adjust to the challenging environmental conditions by shifting allocation patterns of non-structural carbohydrates in order to maintain a root system that, in the Spanish dehesa, it plays a critical role to cope with the stress conditions to which holm oaks are subjected (David *et al.*, 2004). However, some questions emerge from this study. As the root system in declining trees exhibited a high level of phenotypic plasticity in response to soil nutrient availability we wonder how long the root system in declining holm oaks will continue to respond to the stressors. Since defoliated trees had much less ability to photosynthesize and synthesize carbohydrates to maintain a plastic root system adapted to stress conditions, it is expected a non-reversible collapse of the tree. In addition, it is still unclear the mechanistic link between these above-belowground adjustments to acquire key soil resources and the mechanisms that allow trees to avoid mortality and survive (i.e., preventing cavitation, repairing damaged tissues or minimizing the impact on the meristematic tissues; Mantova et al., 2022; Martín-Sánchez et al., 2022). Understanding the impact of the soil nutrients on tree health and the processes that regulate soil nutrient availability is crucial to further determine the responses of the root system and the tree itself. In this sense, we addressed this last idea in Chapter VI.

Key II: we identified a belowground-level physiological adjustment of the fine root system in response to stress. This presumably allows to optimize the uptake of soil resources under stressful conditions and survive. Identifying those soil resources that promote holm oak health and resilience is key to mitigate and delay this process to a certain extent.

7.5. How tree decline may affect the plant-soil continuum and the interaction of the plant with the soil microbial community (chapter VI)

In the previous sections, we synthesized the sequential responses that holm oak, as an organism, triggered from the leaf to the root, at the onset and during the declining process. The identification of these responses opened up new opportunities to characterize holm oak health in its two above-belowground compartments: i) by combining the degree of defoliation with the biochemical adjustments that we observed at the leaf level (Chapter IV) and ii) by including the root parameters that characterized the stage of decline (Chapter V). These advances allowed us to further explore the role of plant-soil relationships on tree health, which introduce another level of complexity to the study. Among other services, microbial communities are crucial for maintaining the health of trees as they exhibit certain resilience against potential plant pathogens (Ginnan *et al.*, 2020) and provide trees with the mineral nutrients essential for their growth and development (Berendsen *et al.*, 2012). For instance, through key steps in soil cycling, such as nitrogen mineralization, nitrification, and phosphorus solubilization, microbial communities are responsible for making nitrogen and phosphorus available for tree uptake (Willey *et al.*, 2008). On the other hand, trees are the major suppliers of energy in the form of carbohydrates, which are needed for the functioning of the soil microbial communities (Curiel Yuste *et al.*, 2007). Moreover, as trees modify the microclimatic environment (temperature and moisture) at which microbial communities grow they also affect rates of microbial metabolic activity (Cubera & Moreno, 2007a; Curiel Yuste *et al.*, 2007, 2010). During the development of this thesis, many questions have arisen, but one of the questions is key for the scientific community. **What comes first, holm oak decline or changes in the soil microbial community.** Some investigations point out about the difficulty to unravel cause and effect relations in field studies regarding tree decline (Corcobado *et al.*, 2014c; Sapsford *et al.*, 2017). Nevertheless, other studies highlight the effect of the microbial community on tree decline (Scarlett *et al.*, 2020) or *vice versa* (García-Angulo *et al.*, 2020; Gómez-Aparicio *et al.*, 2022).

Our experimental set up, focusing on the early stages of tree decline, was explicitly designed to circumvent these potential shortcomings associated with field observations. Observing and monitoring changes in the physiological state of the plant in these three early stages of defoliation and its relationship with the functioning of the microbial community through genes associated with nutrient cycling allowed us, through the use of advanced statistical techniques (structural equation modelling, SEM) to delve into the causal relationships established between the soil and plant communities in this gradient of health. To give a response to this issue, we integrated these two perspectives of the declining process (i.e., the reciprocating effect of the tree decline on soil microbial community and *vice versa*), using the tree responses we described in Chapters IV and V and characterized the role of the soil microbial communities involved in the soil cycling of nutrients. Using a high-throughput quantitative-PCR-based chip, we detected and quantified the genetic potential of the microbial communities to use and transform C, N, P and S in soil (Zheng *et al.*, 2018). Our results suggested that microbial communities customized into microbial soil functional genes were more associated with the crown health of the tree than with the morphology and architecture of the fine root system. More in detail, we observed how the loss of crown health and the subsequent holm oak decline affected certain biogeochemical steps, like denitrification, lignin and starch degradation, carbon fixation, inorganic phosphorus solubilisation and sulfite oxidation.

Particularly, denitrification genes (i.e., *nirS3*, *nirK1* and *nosZ2*) along with nitrification genes (*nifH*) were enhanced due to the loss of crown health and were negatively associated with nitrogen mineral forms (Chapter VI, **Fig 4**). These results provided evidences that the loss of mineral nitrogen during the process of holm oak decline is mediated by denitrifiers (Rasche *et al.*, 2011; Shvaleva *et al.*, 2015; Ibañez *et al.*, 2021). Furthermore, the analysis also revealed that the loss of crown health was associated with the upregulation of functional genes related to saprotrophs and wood-degraders (i.e., *lig*, and *iso-plu*-habouring communities) (Pinho *et al.*, 2020; Solís-García *et al.*, 2021), sulfur-oxidizing bacteria with the capacity to denitrify under anaerobic conditions (*soxY*, *yedZ* and *dsrB*-habouring communities; Willey *et al.*, 2008), carbon-fixation bacteria (*aclB*, *frdA*, *pccA*-habouring communities) and inorganic-P solubilizer bacteria (*pqqC* and *ppx*-harboring communities (Meng *et al.*, 2022). The reason for the increase of these communities is not clear, However, we suggested that changes in soil environmental conditions, and particularly microclimatic conditions (since several of the mentioned metabolic paths are strongly regulated by the redox soil potential, which depends on soil water) resulting from shifts in tree cover could be a plausible explanation for the upregulation of these

communities. For example, it is expected that the decline of holm oak and the subsequent defoliation would be associated with an increase in soil water content due to the reduction of tree evapotranspiration (Corcobado *et al.*, 2013a; Curiel Yuste *et al.*, 2019; Rodríguez *et al.*, 2023). These conditions, for instance, would favour *nirS* and *nosZ*-harboring communities (Rasche *et al.*, 2011). Moreover, the majority of the mentioned functional genes above were negatively related to carbon and soil nutrients (Chapter VI, **Fig. 3**). Hence, we proposed that the loss of crown health in holm oak increased the abundance of certain soil functional genes which downregulated mineral forms of essential soil limiting nutrients such as N and P. Thus, we here proposed a plant-soil feedback loop, established as a consequence of the loss of crown health. This is discussed in Chapter VI, where *nirS*-harboring communities, responsible for denitrification, consume part of the available nitrogen forms for plants and microbes (Lennon & Houlton, 2017) under the most declining trees. The unavailability of nitrogen would downregulate phosphorus cycling since phosphorus mineralizing enzymes, as phosphatases (i.e., *phoD* and *phoX*), are N-rich enzymes directly dependent on mineral nitrogen (Margalef *et al.*, 2017; Chen *et al.*, 2019). This would promote the accumulation of organic P and the unavailability of phosphate, reducing water use efficiency and accelerating leaf senescence in holm oak (Sardans & Peñuelas, 2004; El-Madany *et al.*, 2021). Additionally, microbial communities responsible for solubilizing inorganic phosphorus (*ppx* and *pqqC*-harboring communities) might be potential competitors for the phosphate with the tree in an environment limited in organic C (Raymond *et al.*, 2020). This is supported by the observed increase in *ppx* and *pqqC* under declining holm oaks, and it's negative relation with phosphate. This is thoroughly explained in the Chapter VI, **Fig 5**.

Overall, our results described a tree-soil feedback loop in which the loss of crown health promoted the upregulation of certain soil functional genes. This resulted in a net loss of soil nutrient availability (nitrogen and phosphate) which, in turn, negatively influences crown health. The observed decrease in defoliation during the last decades, especially in areas more prone to flooding with a shallower water table, may result in the net loss of important pools of nutrients (Prescott, 2002; López-Ballesteros *et al.*, 2023) as observed in the declining or unhealthy areas under study (Chapters IV and V). Our results, therefore, suggested that improving holm-oak health in declining areas, especially in those areas prone to favour anaerobic soil metabolic pathways may be achieved by preventing redox levels that favour nutrient losses. Management aimed at favouring more aerobic soil conditions, by, for example, creating of "shrubby islands" (Cubera & Moreno, 2007b) or avoiding excessive pruning

(Rodríguez-Calcerrada *et al.*, 2017), may increase evapotranspiration, enhance soil redox conditions and avoid nutrient losses.

Key III: we describe a potential feedback loop that enhances holm oak decline and the loss of soil nutrients in which certain bacterial communities are involved. We highlight the potential consequences that holm oak decline may have not only at the tree-soil system level but also at a stand and even regional level and ***the relationship between certain bacterial communities (i.e., amoA2, nxrA, phoX, phoD) and soil nutrient (i.e., phosphate) that promote holm oak health and resilience***.

7.6. Final remarks of the discussion

This thesis proposes to apply a holistic approach to improve our understanding of the decline process (**Fig. 1**). Comprehension of the declining phenomenon requires a deep understanding of the relationships that exist between the different organs of the tree (e.g. leaves and roots) as well as the relationship that the tree establishes with its biotic environment and especially with the soil biota, responsible for providing essential nutrients for its growth and survival. The tree may withstand stress through physiological adjustments in its different vital organs (leaves and roots). For example, in this thesis we showed that biochemical leaf adjustments are triggered before defoliation occurs. At a certain point, under continuous stress, holm oak redistributed energetic resources (i.e., NSC) to prioritize functions that are most impacted by the stress (acquisition of soil nutrients) over others (photosynthesis) with the consequent loss of leaves. Finally, our studies also demonstrated that during these adjustments, the relationship between the plant and soil microbial communities was altered, which also implied changes in the capacity of soil microbial communities to supply nutrients to the tree. All of this had an impact on the declining process, which resulted in a tree-soil feedback process in which the effects of stress at leaf level propagated to the root and microbial communities. In turn, alteration in their nutrient cycling capacity, ultimately affected affecting the tree health. Here are the questions we answered throughout this work:

i. Which individuals within a population are more susceptible to decline and why?

Trees with high levels of VAZ-cycle pigments and tocopherol contents without surpassing the tocopherol threshold (chapter IV) may be considered susceptible trees to initiate the declining process. Although we did not conduct long-term monitoring that confirmed the onset of holm oak decline in the subsequent years, the tocopherol threshold predicted if the declining symptoms (i.e., leaves loss) were about to appear and progress (Chapter IV).

ii) Which physiological threshold and traits may be used as early indicators to predict holm oak decline?

The increase of concentrations of both VAZ and mainly tocopherol were good proxies of declining risk in dehesas (chapter IV) and the use of their UV absorption or fluorescence properties in remote sensing opened up opportunities for holm oak stress detection (Hernández-Clemente et al., 2019; Hornero et al., 2021; Cavender-Bares & Logan, 2022). It is still unclear whether the declining patterns in the unhealthy site (i.e., where susceptible and declining holm oaks coexist) respond to the expression of a selective process against sensibility to drought/*Phytophthora* spp (Bréda et al., 2006) or on the other hand is a consequence of the presence of favourable microsite conditions that increase the resilience of the visually non-declining trees (i.e., susceptible trees) (Ruíz-Gómez et al., 2019b).

iii) Which soil conditions predispose holm oak to decline?

While Schmied *et al.*, (2023) did not identify soil microsites conditions as an essential factor determining tree drought symptoms ***we highlight the differences that microbial communities exhibited between these susceptible trees compared to declining trees*** (Chapter V). For example, *phoX* (i.e., phosphatase-harbouring communities, p-value=0.06) and *nosZ* (i.e., nitrous-oxide-reductase harbouring communities) were respectively higher and lower in susceptible trees, than in declining trees. In any case, the soil nutrients content responded to the patchy pattern that tree decline presents in dehesas (Brasier, 1992, 1996; Cardillo *et al.*, 2021), where declining/unhealthy zones presented lower nutrient content than healthy zones(chapters V and VI). ***Lower soil nutrient content (mainly phosphate) may presumably restrain photosynthesis and water use efficiency, resulting in faster senescence, defoliation and decline*** (Sardans & Peñuelas, 2004; El-Madany *et al.*, 2021).

iv) How could we apply this knowledge to prevent holm oak decline?

Our results, therefore, suggested that improving holm oak health in declining areas, especially in those areas prone to favour anaerobic soil metabolic pathways, may be achieved by avoiding redox levels that favour nutrient losses. Management aimed at favouring more aerobic soil conditions, by, for example, creating of "shrubby islands" (Cubera & Moreno, 2007b) or avoiding excessive pruning (Rodríguez-Calcerrada *et al.*, 2017), may prevent waterlogging, increase evapotranspiration, enhance soil redox conditions and avoid nutrient losses. By doing so, we can improve the nutritional status of the trees and enhance their physiological status, which can help to avoid the onset of decline in susceptible trees or delay

defoliation in declining trees. Such an approach may effectively prevent holm oak decline and preserve these important ecosystems for future generations.

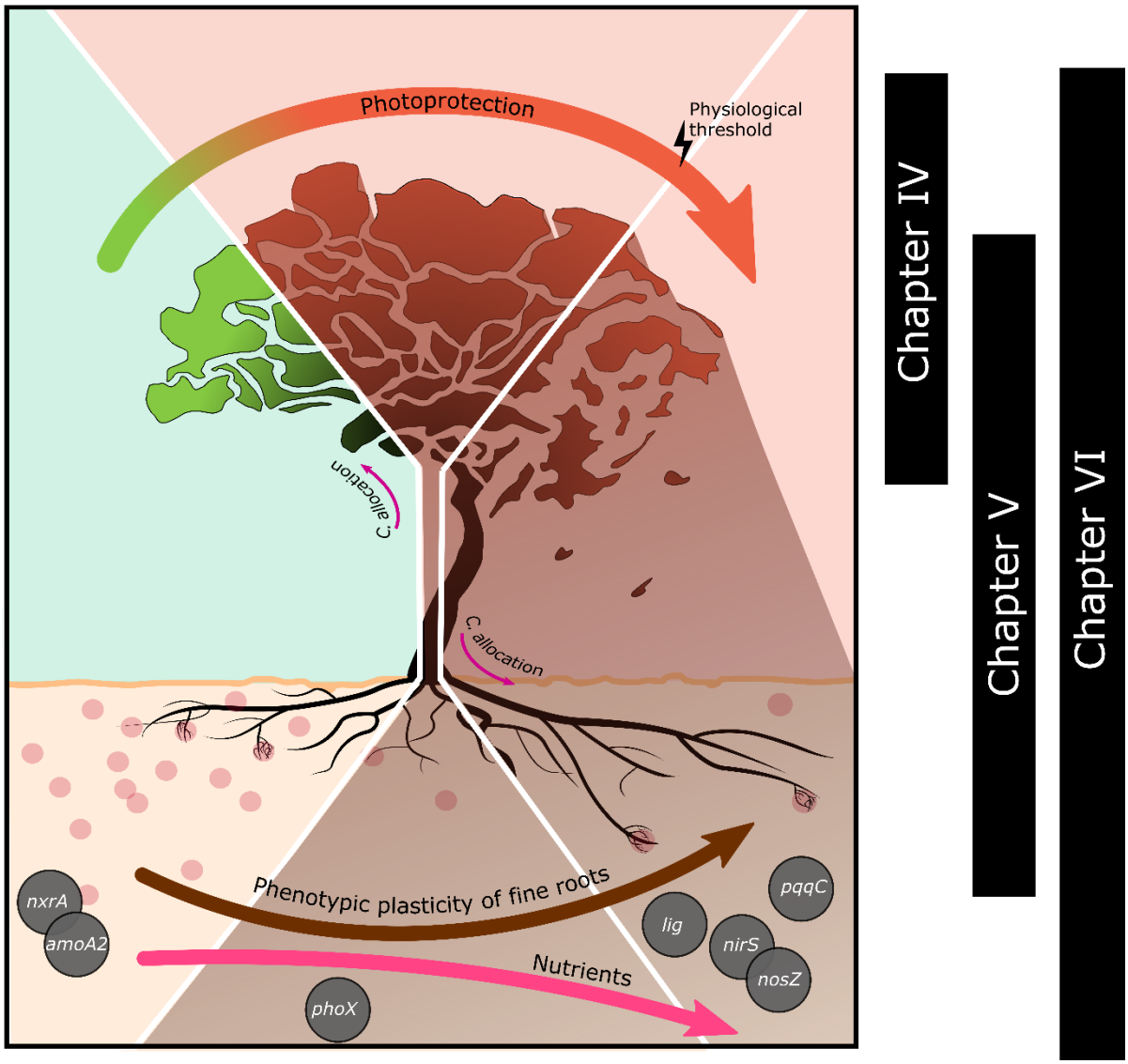

Figure 1. Representation of the declining mechanisms studied in this thesis. The shape of the arrows represents the evolution of a given mechanisms (e.g. photoprotection, fine root phenotypic plasticity and soil nutrient availability) along the declining process. Nutrient hotspots are represented in pink circles. Genes that were upregulated at each stage of tree health are represented in grey circles. Patterns of carbon allocation are also represented with pink arrows. Icon tree and roots were redrawn from: Hey Rabbit Ilustrator and Guilhem Ilustrator, accessed through (https://thenounproject.com/).

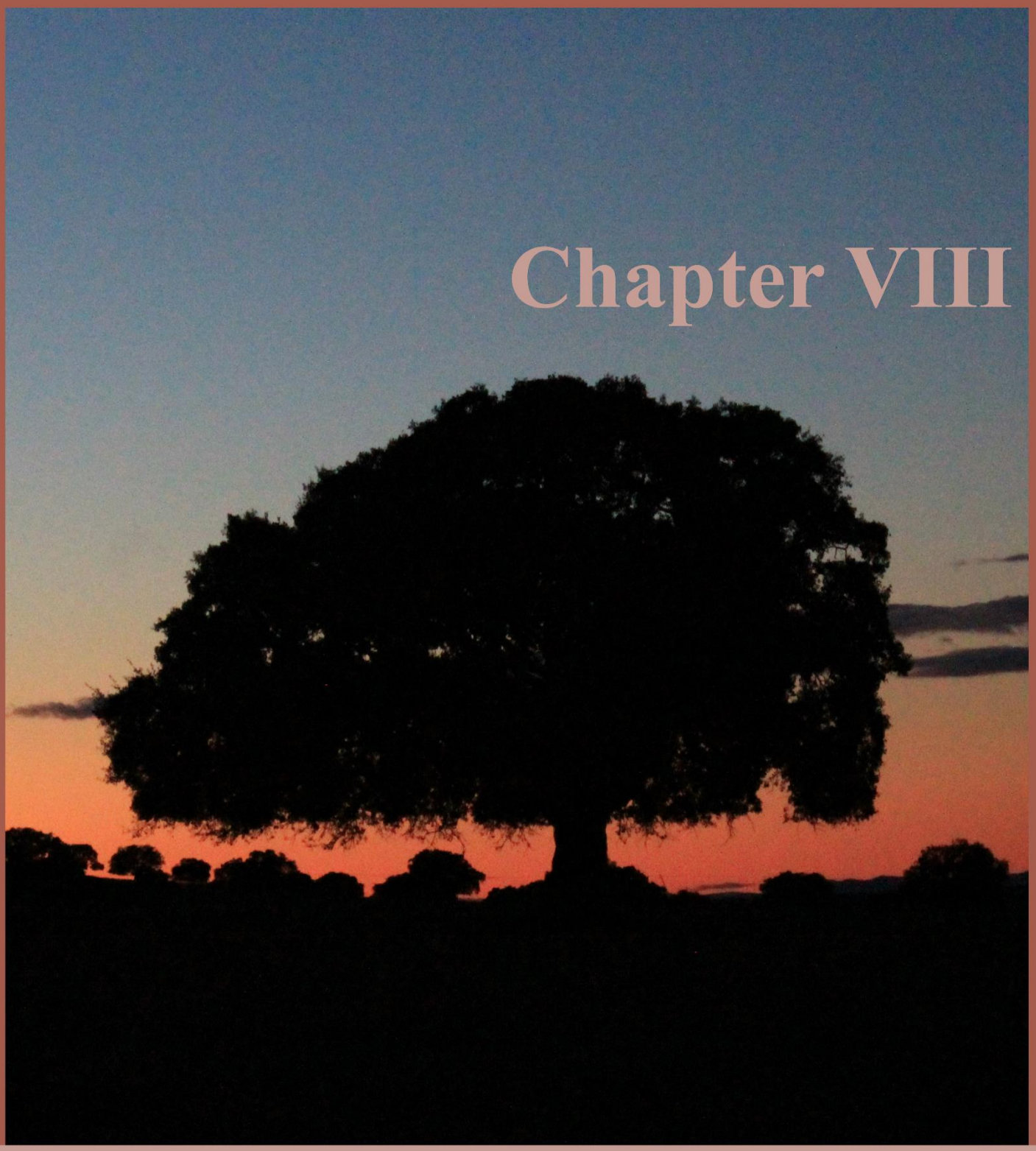

Chapter VIII

General conclusions

This thesis deeply describes the holm oak responses before and during the declining process as well as the role of the soil system in holm oak health in the dehesa. This research outlines the following conclusions:

1. The activation of VAZ-cycle pigments and total tocopherols allows holm oak to acclimatize to the stresses in the dehesa (i.e., drought and/or *Phytophthora*). However, tocopherols exhibited a threshold content (at ≈9% of defoliation), which represents the point at which the tree is unable to cope with stressful environmental conditions. Beyond this threshold, photoprotection is no longer sufficient to prevent photo-oxidative damage and defoliation occurs.

2. VAZ pigments and total tocopherols are suitable early stress markers because shifts in their content were found at early stages of crown defoliation, before visual symptoms of declining. The use of their UV absorption or fluorescence properties in remote sensing opened up opportunities for holm oak stress detection.

3. Once photoprotection mechanisms no longer prevent photooxidative damage, declining holm oaks adjust their soil resource acquisition strategy to the local availability of soil nutrients. It was observed a high level of fine root responsiveness to the availability of soil nutrients in trees that surpassed the tocopherol threshold (i.e., declining holm oaks). This reveals high fine-root phenotypic plasticity that presumably optimizes soil resource acquisition.

4. The adjustments toward a more root acquisitive capacity in declining trees imply a carbon cost that may come at the expense of allocating high energetic substrates (i.e. NSC) to other tissues and functions. This involves the preferential allocation of NSC to optimize a root structure at the expense of maintaining the foliage.

5. The process of tree decline alters the redox potential of soils favouring some metabolic paths (e.g. denitrification) over others, resulting in net losses of mineral forms of key nutrients. These losses, moreover, affect crown health resulting in a feedback loop characterized by the loss of crown health and the upregulation of certain microbial communities involved in the loss of soil nutrients.

6. The high relative abundance of certain functional genes (i.e., *amoA2*, *nxrA*, *phoX*) responsible for the aerobic mineralization of essential nutrients was associated with good soil nutritional status under healthy trees (i.e., high mineral N, nitrate, ammonium, phosphate, potassium and organic C). On the contrary, the high relative abundance of certain functional genes (i.e., *nirS, nosZ*) responsible for the reduction of nitrogen and the decrease in the soil capacity to mineralize P (i.e., *pqqC* and *ppx*) was associated with poor soil nutrient status under unhealthy and declining trees.

7. The loss of crown health is determined by the phosphate, organic phosphorus and mineral nitrogen content. Phosphate promotes crown health whereas organic phosphorus decreases crown health and the vigour of the canopy. Phosphatase-harboring communities (i.e., *phoX* and *phoD*) play an essential role in maintaining optimal phosphate levels for tree health.

8. A management strategy aimed at avoiding the changes in soil redox potentials (explained above) is proposed here. This plan could be focused on creating "shrubby islands" or planting more trees in areas, where the water table is closer to the surface, or on avoiding or minimizing pruning that reduces the evapotranspiration capacity of the crowns. This may help to maintain the redox conditions that optimize soil nutritional status. It may also serve to reduce the impact of *Phytophtora spp*, which is favoured under water-saturated soils.

Chapter IX

General references

Adams HD, Zeppel MJB, Anderegg WRL et al. 2017. A multi-species synthesis of physiological mechanisms in drought-induced tree mortality. *Nature Ecology and Evolution* **1**: 1285–1291.

Alameda D, Villar R. **2012**. Linking root traits to plant physiology and growth in Fraxinus angustifolia Vahl. seedlings under soil compaction conditions. *Environmental and Experimental Botany* **79**: 49–57.

Alamillo JM, Bartels D. **2001**. Effects of desiccation on photosynthesis pigments and the ELIP-like dsp 22 protein complexes in the resurrection plant *Craterostigma plantagineum*. *Plant Science* **160**: 1161–1170.

Allen CD, Breshears DD, McDowell NG. **2015**. On underestimation of global vulnerability to tree mortality and forest die-off from hotter drought in the Anthropocene. *Ecosphere* **6**: 1–55.

Allen CD, Macalady AK, Chenchouni H, Bachelet D, Mcdowell N, Vennetier M, Kitzberger T, Rigling A, Breshears DD, Hogg EH. **2010**. A global overview of drought and heat-induced tree mortality reveals emerging climate change risks for forests. *Forest Ecology and Management* **259**: 660–684.

Altaf F, Meraj G, Romshoo SA. **2013**. Morphometric analysis to infer hydrological behaviour of lidder watershed, Western Himalaya, India. *Geography Journal* **2013**: 178021.

Álvarez JRG. **2016**. The image of a tamed landscape: Dehesa through history in Spain. *Culture and History Digital Journal* **5**: 1–17.

Anderegg WRL, Anderegg LDL. **2013**. Hydraulic and carbohydrate changes in experimental drought-induced mortality of saplings in two conifer species. *Tree Physiology* **33**: 252–260.

Anderegg W, Kane JM, Anderegg L. **2013**. Consequences of widespread tree mortality triggered by drought and temperature stress. *Nature Climate Change* **3**: 30–36.

Anderson JM, Chow WS, De Las Rivas J. **2008**. Dynamic flexibility in the structure and function of photosystem II in higher plant thylakoid membranes: The grana enigma. *Photosynthesis Research* **98**: 575–587.

Angay O, Fleischmann F, Recht S, Herrmann S, Matyssek R, Oßwald W, Buscot F, Grams TEE. **2014**. Sweets for the foe – effects of nonstructural carbohydrates on the

susceptibility of *Quercus robur* against *Phytophthora quercina*. *New Phytologist* **203**: 1282–1290.

Arias Sánchez B. **2015**. Las dehesas del Campo de Montiel en la Edad Media. *Revista de Estudios del Campo de Montiel* **1213**: 171–188.

Arnold PA, Kruuk LEB, Nicotra AB. **2019**. How to analyse plant phenotypic plasticity in response to a changing climate. *New Phytologist* **222**: 1235–1241.

Augusta C, Helena P, Manuel M. **2010**. Analysis of spatial patterns of oak decline in cork oak woodlands in Mediterranean conditions. *Annals of forest science* **67**: 204.

Avila J, Gallardo A, Ibáñez B, Gómez-Aparicio L. **2016**. *Quercus suber* dieback alters soil respiration and nutrient availability in Mediterranean forests. *Journal of Ecology* **104**: 1441–1452.

Avila M, Gallardo A, Gómez-Aparicio L. **2019**. Pathogen-induced tree mortality interacts with predicted climate change to alter soil respiration and nutrient availability in Mediterranean systems. *Biogeochemistry* **3**: 53–71.

Avila JM, Gallardo A, Ibáñez B, Gómez-Aparicio L. **2021**. Pathogen-induced tree mortality modifies key components of the C and N cycles with no changes on microbial functional diversity. *Ecosystems* **24**: 451–466.

Baier M, Dietz KJ. **2005**. Chloroplasts as source and target of cellular redox regulation: a discussion on chloroplast redox signals in the context of plant physiology. *Journal of Experimental Botany* **56**: 1449–1462.

Baquedano FJ, Valladares F, Castillo FJ. **2008**. Phenotypic plasticity blurs ecotypic divergence in the response of *Quercus coccifera* and *Pinus halepensis* to water stress. *European Journal of Forest Research* **127**: 495–506.

Barbero M, Loisel R, Quezel P. **1992**. Biogeography, ecology and history of Mediterranean *Quercus ilex* ecosystems. In: Romane F, Terradas J, eds. *Quercus ilex* L. ecosystems: function, dynamics and management. Springer Science & Business Media, 1992, 99–100.

Barbeta A, Peñuelas J. **2017**. Increasing carbon discrimination rates and depth of water uptake favor the growth of Mediterranean evergreen trees in the ecotone with temperate deciduous forests. *Global Change Biology* **23**: 5054–5068.

Bardgett RD, Mommer L, De Vries FT. **2014**. Going underground: Root traits as drivers of ecosystem processes. *Trends in Ecology and Evolution* **29**: 692–699.

Barton K. **2020**. Package 'MuMIn' Title Multi-Model Inference. *R package version 1.43.17*.

Beidler K V., Taylor BN, Strand AE, Cooper ER, Schönholz M, Pritchard SG. **2015**. Changes in root architecture under elevated concentrations of CO2 and nitrogen reflect alternate soil exploration strategies. *New Phytologist* **205**: 1153–1163.

Bellard C, Leclerc C, Leroy B, Bakkenes M, Veloz S, Thuiller W, Courchamp F. **2014**. Vulnerability of biodiversity hotspots to global change. *Global Ecology and Biogeography* **23**: 1376–1386.

Belsky J. **1994**. Influences of trees on savanna productivity : Tests of shade , nutrients , and tree-grass competition. *Ecological society of America* **75**: 922–932.

Berendsen RL, Pieterse CMJ, Bakker PAHM. **2012**. The rhizosphere microbiome and plant health. *Trends in Plant Science* **17**: 478–486.

Bi Q, Li K, Zheng B, Liu X, Li H. **2019**. Partial replacement of inorganic phosphorus (P) by organic manure reshapes phosphate mobilizing bacterial community and promotes P bioavailability in a paddy soil. *Science of the Total Environment* **703**.

Biocca FH, Tainter DA, Starkey SW, Oak, Williams JG. **1993**. The persistence of oak decline in the western north Carolina Nantahala. *Southern Appalachian Botanical Society* **58**: 178–184.

Boltz DF, Mellon MG. **1948**. Spectrophotometric determination of phosphorus as molybdiphosphoric acid. *Analytical Chemistry* **20**: 749–751.

Bonan G. **2016**. Forests, Climate, and Public Policy: A 500-Year Interdisciplinary Odyssey. *Annual Review of Ecology, Evolution, and Systematics* **47**: 97–121.

Bonser SP. **2021**. Misinterpreting the adaptive value of phenotypic plasticity in studies on plant adaptation to new and variable environments. *Plant Biology* **23**: 683–685.

Brasier CM. **1992**. Oak tree mortality in Iberia. *Nature* **360**: 539.

Brasier CM. **1996**. *Phytophthora cinnamomi* and oak decline in southern Europe. Environmental constraints including climate change. *Annales des Sciences Forestieres* **53**: 346–358.

Bréda N, Huc R, Granier A, Dreyer E. **2006**. Temperate forest trees and stands under severe drought: a review of ecophysiological responses, adaptation processes and long-term consequences. *Annals of Forest Science* **28**: 625–644.

Breshears DD, López-Hoffman L, Graumlich LJ. **2011**. When ecosystem services crash: Preparing for big, fast, patchy climate change. *Ambio* **40**: 256–263.

Broadbent P, Baker KF. **1974**. Behaviour of *Phytophthora cinnamomi* in soils suppressive and conducive to root rot. *Australian Journal of Agricultural Research* **25**: 121–137.

Brunner I, Godbold DL. **2007**. Tree roots in a changing world. *Journal of Forest Research* **12**: 78–82.

Brunner I, Herzog C, Dawes M, Arend M, Sperisen C. **2015**. How tree roots respond to drought. *Frontiers in Plant Science* **6**: 1–16.

Bugalho MN, Caldeira MC, Pereira JS, Aronson J, Pausas JG. **2011**. Mediterranean cork oak savannas require human use to sustain biodiversity and ecosystem services. *Frontiers in Ecology and the Environment* **9**: 278–286.

Bugalho M, Pinto-Correia T, Pulido F. **2018**. Human use of natural capital generates cultural and other ecosystem services in montado and dehesa oak woodlands. In: Paracchini ML, Zingari P, Blasi C, eds. Reconnecting natural and cultural capital. Contribution from science and policy. Luxembourg: Publications Office of the European Union.

Bussotti F. **2004**. Assessment of stress conditions in *Quercus ilex* L. leaves by O-J-I-P chlorophyll a fluorescence analysis. *Plant Biosystems* **138**: 101–109.

Bussotti F, Desotgiu R, Cascio C, Pollastrini M, Gravano E, Gerosa G, Marzuoli R, Nali C, Lorenzini G, Salvatori E, *et al.* 2011. Ozone stress in woody plants assessed with chlorophyll a fluorescence. A critical reassessment of existing data. *Environmental and Experimental Botany* **73**: 19–30.

Cahill DM, Rookes JE, Wilson BA, Gibson L, McDougall KL. **2008**. *Phytophthora cinnamomi* and Australia's biodiversity: Impacts, predictions and progress towards control. *Australian Journal of Botany* **56**: 279–310.

Cailleret M, Dakos V, Jansen S, Robert EMR, Aakala T, Amoroso MM, Antos JA, Bigler C, Bugmann H, Caccianaga M, *et al.* 2019. Early-warning signals of individual tree mortality based on annual radial growth. *Frontiers in Plant Science* **9**: 1–14.

Camarero JJ, Olano JM, Jackeline S, Alfaro A, Fernández-Marín B, Becerril JM, García-Plazaola I. **2012**. Photoprotection mechanisms in *Quercus ilex* under contrasting climatic conditions. *Flora* **207**: 557– 564.

Camilo-Alves CS, da Clara M, de Almeida Ribeiro N. **2013**. Decline of Mediterranean oak trees and its association with *Phytophthora cinnamomi*: A review. *European Journal of Forest Research* **132**: 411–432.

Camisón Á, Ángela Martín M, Dorado FJ, Moreno G, Solla A. **2020**. Changes in carbohydrates induced by drought and waterlogging in *Castanea sativa*. *Trees* **34**: 579–591.

Campbell BJ, Stein JL, Cary SC. **2003**. Evidence of chemolithoautotrophy in the bacterial community associated with *Alvinella pompejana* , a Hydrothermal Vent Polychaete. *Applied and Environmental Microbiology* **69**: 5070–5078.

Canadell J, Djema A, López B, Lloret F, Sabate S, Siscart D, Gracia C, 4.1. **1992**. Structure and dynamics of the root system. In: Roda F, Retana J, Gracia C A, Bellot J (Eds.) Ecology of Mediterranean Evergreen Oak Forest. Berlin Heidelberg 1999: Springer-Verlag, 1689–1699.

Cardillo E, Abad E, Meyer S. **2021**. Spatio-temporal analysis at landscape scale of the Iberian oak decline epidemic caused by *Phytophthora cinnamomi*. *Forest Pathology* **51**.

Carnicer J, Coll M, Ninyerola M, Pons X, Sánchez G, Peñuelas J. **2011**. Widespread crown condition decline, food web disruption, and amplified tree mortality with increased climate change-type drought. *Proceedings of the National Academy of Sciences of the United States of America* **108**: 1474–1478.

Cavender-Bares J, Logan B. **2022**. Novel insights on the linkage between enhanced photoprotection and oak decline. *Tree Physiology* **42**: 203–207.

Chao L, Liu Y, Zhang W, Wang Q, Guan X, Yang Q, Chen L, Zhang J, Hu B, Zhanfeng L, *et al.* 2021. Root functional traits, but not biomass, determine the magnitude of the rhizosphere priming effect among eight tree species.

Chen J, Groenigen K van, Hungate BA, Terrer C, Groenigen J van, Maestre F, Ying SC, Luo Y, Jørgensen U, Sinsabaugh RL, *et al.* 2020. Long-term nitrogen loading alleviates phosphorus limitation in terrestrial ecosystems. *Global Change Biology* **26**.

Chen X, Jiang N, Condron LM, Dun KE, Chen Z, Wang J, Chen L. **2019**. Soil alkaline

phosphatase activity and bacterial phoD gene abundance and diversity under long-term nitrogen and manure inputs. *Geoderma* **349**: 36–44.

Chen W, Koide RT, Adams TS, De Forest JL, Cheng L, Eissenstat DM. **2016**. Root morphology and mycorrhizal symbioses together shape nutrient foraging strategies of temperate trees. *Proceedings of the National Academy of Sciences of the United States of America* **113**: 8741–8746.

Corcobado T, Cubera E, Pérez-Sierra A, Jung T, Solla A. **2010**. First report of *Phytophthora gonapodyides* involved in the decline of *Quercus ilex* in xeric conditions in Spain. *New Disease Reports* **22**: 33.

Corcobado T. **2013a**. Influencia de *Phytophthora cinnamomi* Rands en el decaimiento de *Quercus ilex* L. y su relación con las propiedades del suelo y las ectomicorrizas. *(Doctoral dissertation, Universidad de Extremadura).*

Corcobado T, Cubera E, Moreno G, Solla A. **2013b**. *Quercus ilex* forests are influenced by annual variations in water table, soil water deficit and fine root loss caused by *Phytophthora cinnamom*i. *Agricultural and Forest Meteorology* **169**: 92–99.

Corcobado T, Solla A, Madeira MA, Moreno G. **2013c**. Combined effects of soil properties and *Phytophthora cinnamomi* infections on *Quercus ilex* decline. *Plant and Soil* **373**: 403–413.

Corcobado T, Cubera E, Juárez E, Moreno G, Solla A. **2014a**. Drought events determine performance of *Quercus ilex* seedlings and increase their susceptibility to *Phytophthora cinnamomi*. *Agricultural and Forest Meteorology* **192**–**193**: 1–8.

Corcobado T, Vivas M, Moreno G, Solla A. **2014b**. Ectomycorrhizal symbiosis in declining and non-declining *Quercus ilex* trees infected with or free of *Phytophthora cinnamomi*. *Forest Ecology and Management* **324**: 72–80.

Corcobado T, Miranda-Torres JJ, Martín-García J, Jung T, Solla A. **2017**. Early survival of *Quercus ilex* subspecies from different populations after infections and co-infections by multiple *Phytophthora* species. *Plant Pathology* **66**: 792–804.

Corcobado T, Moreno G, Azul AM, Solla A. **2015**. Seasonal variations of ectomycorrhizal communities in declining *Quercus ilex* forests: Interactions with topography, tree health status and *Phytophthora cinnamomi* infections. *Forestry* **88**: 257–266.

Cramer W, Guiot J, Fader M, Garrabou J, Gattuso JP, Iglesias A, Lange MA, Lionello P, Llasat MC, Paz S, *et al.* 2018. Climate change and interconnected risks to sustainable development in the Mediterranean. *Nature Climate Change* **8**: 972–980.

Cubera E, Moreno G. **2007a**. Effect of single *Quercus ilex* trees upon spatial and seasonal changes in soil water content in dehesas of central western Spain. *Annals of Forest Science* **64**: 355–364.

Cubera E, Moreno G. **2007b**. Effect of land-use on soil water dynamic in dehesas of Central-Western Spain. *Catena* **71**: 298–308.

Curiel Yuste J, Baldocchi D, Gershenson A, Goldstein A, Misson L, Wong S. **2007**. Microbial soil respiration and its dependency on carbon inputs , soil temperature and moisture. *Global Change Biology* **13**: 2018–2035.

Curiel Yuste J, Ma S, Baldocchi DD. **2010**. Plant-soil interactions and acclimation to temperature of microbial-mediated soil respiration may affect predictions of soil CO2 efflux. *Biogeochemistry* **98**: 127–138.

Curiel Yuste J, Flores-Rentería D, García-Angulo D, Hereş A-M, Bragă C, Petritan A-M, Petritan IC. **2019**. Cascading effects associated with climate-change-induced conifer mortality in mountain temperate forests result in hot-spots of soil CO2 emissions. *Soil Biology and Biochemistry* **133**: 50–59.

Dalgaard P. **2008**. *Introductory Statistics with R*. New York: Springer.

Dall'osto L, Lico C, Alric J, Giuliano G, Havaux M, Bassi R. **2006**. Lutein is needed for efficient chlorophyll triplet quenching in the major LHCII antenna complex of higher plants and effective photoprotection in vivo under strong light. *BMC Plant Biology* **6**: 32.

David TS, Ferreira MI, Cohen S, Pereira JS, David JS. **2004**. Constraints on transpiration from an evergreen oak tree in southern Portugal. *Agricultural and Forest Meteorology* **122**: 193–205.

Demmig-Adams B, Adams WW, Ebbert V, Logan BA. **1999**. Ecophysiology of the Xanthophyll Cycle. In: Frank HA, Young AJ, Britton G, Cogdell RJ (eds) The photochemistry of carotenoids. Kluwer Academic Publishers, 245–269.

Deng L, Peng C, Kim D, Li J, Liu Y, Hai X, Liu Q, Huang C, Shangguan Z, Kuzyakov Y. **2021**. Drought effects on soil carbon and nitrogen dynamics in global natural ecosystems.

Earth-Science Reviews **214**: 103501.

Denman S, Doonan J, Ransom-Jones E, Broberg M, Plummer S, Kirk S, Scarlett K, Griffiths AR, Kaczmarek M, Forster J, *et al.* 2018. Microbiome and infectivity studies reveal complex polyspecies tree disease in Acute Oak Decline. *ISME Journal* **12**: 386–399.

Dewar RC, Ludlow AR, Dougherty PM, Ludlow R, Dewar C, Dougherty PM, Guio S. **1994**. Environmental influences on carbon allocation in pines. *Ecological Bulletins*: 92–101.

Díaz M, Pulido F. **1997**. The Spanish dehesas: A diversity in land-use and wildlife. In: Pain D, Pienkowsky M, eds. Farming and birds in Europe: The common Agricultural Policy and its implications for bird conservation. Academic Press, London, 178–209.

Dietze MC, Sala A, Carbone MS, Czimczik CI, Mantooth JA, Richardson AD, Vargas R. **2014**. Nonstructural carbon in woody plants. *Annual Review of Plant Biology* **65**: 667–687.

Dyson K, Ziter C, Fuentes TL, Patterson MS. **2019**. Conducting urban ecology research on private property: advice for new urban ecologists. *Journal of Urban Ecology* **5**: 1–10.

Ehrenfeld JG, Ravit B, Elgersma K. **2005**. Feedback in the plant-soil system. *Annual Review of Environment and Resources* **30**: 75–115.

Eissenstat DM, Kucharski JM, Zadworny M, Adams TS, Koide RT. **2015**. Linking root traits to nutrient foraging in arbuscular mycorrhizal trees in a temperate forest. *New Phytologist* **208**: 114–124.

El-Madany TS, Reichstein M, Carrara A, Martín MP, Moreno G, Gonzalez-Cascon R, Peñuelas J, Ellsworth DS, Burchard-Levine V, Hammer TW, *et al.* 2021. How nitrogen and phosphorus availability change water use efficiency in a Mediterranean savanna ecosystem. *Journal of Geophysical Research: Biogeosciences* **126**: 1–21.

Encinas-Valero M, Esteban R, Hereş A-M, Becerril JM, García-Plazaola JI, Artexe U, Vivas M, Solla A, Moreno G, Curiel Yuste J. **2022a**. Photoprotective compounds as early markers to predict holm oak crown defoliation in declining Mediterranean savannahs. *Tree Physiology* **42**: 208–224.

Encinas-Valero M, Esteban R, Heres A-M, Vivas M, Fakhet D, Aranjuelo I, Solla A, Moreno G, Curiel-Yuste J. **2022b**. Holm oak decline is determined by shifts in fine root phenotypic plasticity in response to belowground stress. *New Phytologist* **235**: 2237–2251.

Ensminger I. **2020**. Fast track diagnostics: hyperspectral reflectance differentiates disease from drought stress in trees. *Tree physiology* **40**: 1143–1146.

Esteban R, Jiménez E, Jiménez MS, Morales D, Hormaetxe K, Becerril JM, García-Plazaola JI. **2007**. Dynamics of violaxanthin and lutein epoxide xanthophyll cycles in Lauraceae tree species under field conditions. *Tree Physiology* **27**: 1407–1414.

Esteban R, Balaguer L, Manrique E, Rubio de Casas R, Ochoa-Hueso R, Fleck I, Pintó-Marijuan M, Casals I, Morales D, Jiménez MS, *et al.* 2009a. Alternative methods for sampling and preservation of photosynthetic pigments and tocopherols in plant material from remote locations. *Photosynthesis Research* **101**: 77–88.

Esteban R, Olano J, Castresana J, Fernández-Marín B, Hernández A, Becerril J, García-Plazaola JI. **2009b**. Distribution and evolutionary trends of photoprotective isoprenoids (xanthophylls and tocopherols) within the plant kingdom. *Physiologia Plantarum* **135**: 379–389.

Esteban R, Fernández-Marín B, Olano JM, Becerril JM, García-Plazaola JI. **2014a**. Does plant colour matter? Wax accumulation as an indicator of decline in Juniperus thurifera. *Tree Physiology* **34**: 267–274.

Esteban R, García-Plazaola JI. **2014b**. Involvement of a second xanthophyll cycle in non-photochemical quenching of chlorophyll fluorescence: The lutein epoxide story. In: B. Demmig-Adams, G. Garab, W. Adams, Govindjee (eds.), Non-Photochemical quenching and energy dissipation in plants, algae and cyanobacteria, advances in photosynthesis and respiration. Springer Dordrecht 2014, 277–295.

Esteban R, Barrutia O, Artetxe U, Fernández-Marín B, Hernández A, García-Plazaola JI. **2015a**. Internal and external factors affecting photosynthetic pigment composition in plants: A meta-analytical approach. *New Phytologist* **206**: 268–280.

Esteban R, Moran JF, Becerril JM, García-Plazaola JI. **2015b**. Versatility of carotenoids: An integrated view on diversity, evolution, functional roles and environmental interactions. *Environmental and Experimental Botany* **119**: 63–75.

Faucon MP, Houben D, Lambers H. **2017**. Plant functional traits: Soil and ecosystem services. *Trends in Plant Science* **22**: 385–394.

Fenollosa E, Munné-Bosch S. **2018**. Photoprotection and photo-oxidative stress markers as

useful tools to unravel plant invasion success. In: Sánchez-Moreiras AM, Reigosa MJ, eds. Advances in Plant Ecophysiology Techniques. Springer International Publishing, 153–175.

Fernández-González AJ, Cardoni M, Gómez-Lama Cabanás C, Valverde-Corredor A, Villadas PJ, Fernández-López M, Mercado-Blanco J. **2020**. Linking belowground microbial network changes to different tolerance level towards *Verticillium* wilt of olive. *Microbiome* **8**: 1–19.

Fernández-Marín B, Gago J, Clemente-Moreno MJ, Flexas J, Gulías J, García-Plazaola JI. **2019**. Plant pigment cycles in the high-Arctic Spitsbergen. *Polar Biology* **42**: 675–684.

Fernández-Marín B, García-Plazaola JI, Hernández A, Esteban R. **2018**. Plant photosynthetic pigments: Methods and tricks for correct quantification and identification. In: A. M. Sánchez-Moreiras, M. J. Reigosa (eds.), Advances in Plant Ecophysiology Techniques. Springer International Publishing AG, part of Springer Nature 2018, 29–50.

Fernández-Marín B, Hernández A, Garcia-Plazaola JI, Esteban R, Míguez F, Artetxe U, Gómez-Sagasti MT. **2017**. Photoprotective strategies of Mediterranean plants in relation to morphological traits and natural environmental pressure: A meta-analytical approach. *Frontiers in Plant Science* **8**: 1051.

Ferreira T, Rasband W. **2019**. ImageJ User Guide ImageJ User Guide IJ 1.46r.

Ferrer-Galego PP, Sáez L. **2019**. Type designation of the oaks *Quercus ballota* and *Q. rotundifolia* (Fagaceae). *Nordic Journal of Botany* **37**: 1–8.

Flores-Rentería D, Rincón A, Morán-López T, Hereş A-M, Pérez-Izquierdo L, Valladares F, Curiel Yuste J. **2018**. Habitat fragmentation is linked to cascading effects on soil functioning and CO 2 emissions in Mediterranean holm-oak-forests . *PeerJ* **6**: e5857.

Forest Europe. **2020**. State of Europe's Forests 2020.

Fox J, Weisberg S. **2019**. An R companion to applied regression. *Third edition. Sage, Thousand Oaks CA*.

Francis CA, Roberts KJ, Beman JM, Santoro AE, Oakley BB. **2005**. Ubiquity and diversity of ammonia-oxidizing archaea in water columns and sediments of the ocean. *PNAS* **102**: 14683–14688.

Frazer GW, Canham CD, Lertzman KP. **1999**. Gap Light Analyzer (GLA): Imaging

software to extract canopy structure and gap light transmission indices from true-colour fisheye photographs, users manual and program documentation. Copyright © 1999. *Simon Fraser University, Burnaby, British Columbia, and the Institute of Ecosystem Studies, Millbrook, New York.*

Freschet GT, Roumet C. **2017**. Sampling roots to capture plant and soil functions (K Treseder, Ed.). *Functional Ecology* **31**: 1506–1518.

Freschet GT, Pagès L, Iversen CM, Comas LH, Rewald B, Roumet C, Klimešová J, Zadworny M, Poorter H, Postma JA, *et al.* 2021a. A starting guide to root ecology: strengthening ecological concepts and standardising root classification, sampling, processing and trait measurements. *New Phytologist* **232**: 973–1122.

Freschet GT, Roumet C, Comas LH, Weemstra M, Bengough G, Rewald B, Bardgett RD, Deyn GB De, Johnson D, Klime J, *et al.* 2021b. Root traits as drivers of plant and ecosystem functioning: current understanding, pitfalls and future research needs. *New Phytologist* **232**: 1123–1158.

Frisullo S, Lima G, Magnano G, Camele I, Melissano L, Puglisi I, Pane A, Agosteo GE, Prudente L, Cacciola SO. **2018**. *Phytophthora cinnamomi* involved in the decline of holm oak (*Quercus ilex*) stands in southern Italy. *Forest Science* **64**: 290–298.

Fromm H. **2019**. Root plasticity in the pursuit of water. *Plants* **8**.

Gallego FJ, Perez De Algaba A, Fernandez-Escobar R. **1999**. Etiology of oak decline in Spain. *European Journal of Forest Pathology* **29**: 17–27.

Gamon JA, Huemmrich KF, Wong CYS, Ensminger I, Garrity S, Hollinger DY, Noormets A, Peñuelas J. **2016**. A remotely sensed pigment index reveals photosynthetic phenology in evergreen conifers. *Proceedings of the National Academy of Sciences* **113**: 13087–13092.

García-Angulo D. **2020**. Efectos del decaimiento del encinar Mediterráneo inducido por sequía y del papel modulador del manejo histórico sobre los ciclos biogeoquímicos y las comunidades microbianas del suelo.

García-Angulo D, Hereş AM, Fernández-López M, Flores O, Sanz MJ, Rey A, Valladares F, Curiel Yuste J. **2020**. Holm oak decline and mortality exacerbates drought effects on soil biogeochemical cycling and soil microbial communities across a climatic

gradient. *Soil Biology and Biochemistry* **149**.

García-Plazaola JI, Becerril JM. **2001**. Seasonal changes in photosynthetic pigments and antioxidants in beech (*Fagus sylvatica*) in a Mediterranean climate: Implications for tree decline diagnosis. *Australian Journal of Plant Physiology* **28**: 225–232.

Garcia-Plazaola JI, Becerril JM, Hernandez A, Niinemets U, Kollist H. **2004**. Acclimation of antioxidant pools to the light environment in a natural forest canopy. *New Phytologist* **163**: 87–97.

García-Plazaola JI, Esteban R, Hormaetxe K, Fernández-Marín B, Becerril JM. **2008**. Photoprotective responses of Mediterranean and Atlantic trees to the extreme heat-wave of summer 2003 in Southwestern Europe. *Trees* **22**: 385–392.

García-Plazaola JI, Hernández A, Fernández-Marín B, Esteban R, Cavender-Bares, José Peguero-Pina JJ, Verhoeven A, Cavender-Bares J. **2017**. Photoprotective mechanisms in the genus *Quercus* in response to winter cold and summer drought. In: Gil-Pelegrín E, Peguero-Pina JJ, Sancho-Knapik D, eds. Oaks Physiological Ecology. Exploring the Functional Diversity of Genus *Quercus* L. Cham: Springer International Publishing, 361–393.

Gazol A, Camarero JJ, Vicente-Serrano SM, Sánchez-Salguero R, Gutiérrez E, de Luis M, Sangüesa-Barreda G, Novak K, Rozas V, Tíscar PA, *et al.* 2018. Forest resilience to drought varies across biomes Antonio. *Global Change Biology* **24**: 2143–2158.

Gazol A, Sangüesa-Barreda G, Camarero JJ. **2020**. Forecasting forest vulnerability to drought in Pyrenean silver fir forests showing dieback. *Frontiers in Forests and Global Change* **3**: 1–13.

Gazol A, Hereş AM, Curiel Yuste J. **2021**. Land-use practices (coppices and dehesas) and management intensity modulate responses of Holm oak growth to drought. *Agricultural and Forest Meteorology* **297**.

Gea-Izquierdo G, Montero G, Cañellas I. **2009**. Changes in limiting resources determine spatio-temporal variability in tree-grass interactions. *Agroforestry Systems* **76**: 375–387.

Gea-Izquierdo G, Natalini F, Cardillo E. **2021**. Holm oak death is accelerated but not sudden and expresses drought legacies. *Science of the Total Environment* **754**: 141793.

Gentilesca T, Camarero JJ, Colangelo M, Nolè A, Ripullone F. **2017**. Drought-induced

oak decline in the western mediterranean region: An overview on current evidences, mechanisms and management options to improve forest resilience. *IForest* **10**: 796–806.

Gessler A, Schaub M, McDowell NG. **2017**. The role of nutrients in drought-induced tree mortality and recovery. *New Phytologist* **214**: 513–520.

Gessler A, Cailleret M, Joseph J, Schönbeck L, Schaub M, Lehmann M, Treydte K, Rigling A, Timofeeva G, Saurer M. **2018**. Drought induced tree mortality – a tree-ring isotope based conceptual model to assess mechanisms and predispositions. *New Phytologist* **219**: 485–490.

Giehl RFH, von Wirén N. **2014**. Root nutrient foraging. *Plant Physiology* **166**: 509–517.

Ginnan NA, Dang T, Bodaghi S, Ruegger PM, Mccollum G, England G, Vidalakis G, Borneman J, Rolshausen PE, Roper MC. **2020**. Disease-induced microbial shifts in *Citrus indicate* microbiome-derived responses to huanglongbing across the disease severity spectrum. *Pytobiomes journal* **4**: 375–387.

Giraldo JP, Kruss S. **2023**. Nanosensors for monitoring plant health. *Nature Nanotechnology* **18**: 107–108.

Gómez-Aparicio L, Ibáñez B, Serrano MS, De Vita P, Ávila JM, Pérez-Ramos IM, García L V., Esperanza Sánchez M, Marañón T. **2012**. Spatial patterns of soil pathogens in declining Mediterranean forests: Implications for tree species regeneration. *New Phytologist* **194**: 1014–1024.

Gómez-Aparicio L, Domínguez-Begines J, Kardol P, Ávila JM, Gomez-aparicio L, Dominguez-begines J, Kardol P, Avila JM, Ibänez B, Garcia L V. **2017**. Plant-soil feedbacks in declining forests : implications for species coexistence. *Ecology* **98**: 1908–1921.

Gómez-Aparicio L, Domínguez-Begines J, Villa-Sanabria E, García L, Muñoz-Pajares J. **2022**. Tree decline and mortality following pathogen invasion alters the diversity , composition and network structure of the soil microbiome. *Soil Biology and Biochemistry* **166**: 108560.

Gómez-Sagasti MT, López-Pozo M, Artetxe U, Becerril JM, Hernández A, García-Plazaola JI, Esteban R. **2023**. Carotenoids and their derivatives: A “Swiss Army knife-like” multifunctional tool for fine-tuning plant-environment interactions. *Environmental and Experimental Botany* **207**.

Graham EB, Knelman JE, Schindlbacher A, Siciliano S, Breulmann M, Yannarell A, Beman JM, Abell G, Philippot L, Prosser J, *et al.* 2016. Microbes as engines of ecosystem function: When does community structure enhance predictions of ecosystem processes? *Frontiers in Microbiology* **7**: 1–10.

Grant OM, Tronina Ł, Ramalho JC, Kurz Besson C, Lobo-Do-Vale R, Santos Pereira J, Jones HG, Chaves MM. **2010**. The impact of drought on leaf physiology of *Quercus suber* L. trees: Comparison of an extreme drought event with chronic rainfall reduction. *Journal of Experimental Botany* **61**: 4361–4371.

Gratani L, Bombelli A. **2000**. Correlation between leaf age and other leaf traits in three Mediterranean maquis shrub species: *Quercus ilex, Phillyrea latifolia* and *Cistus incanus. Environmental and Experimental Botany* **43**: 141–153.

Guadagno CR, Ewers BE, Speckman HN, Aston TL, Huhn BJ, Devore SB, Ladwig JT, Strawn RN, Weinig C. **2017**. Dead or alive? using membrane failure and chlorophyll a fluorescence to predict plant mortality from drought. *Plant Physiology* **175**: 223–234.

Haavik LJ, Billings SA, Guldin JM, Stephen FM. **2015**. Emergent insects, pathogens and drought shape changing patterns in oak decline in North America and Europe. *Forest Ecology and Management* **354**: 190–205.

Hammond WM, Williams AP, López R, Sáenz-romero C, Allen CD, Adams HD, Klein T, Breshears DD. **2022**. Global field observations of tree die-off reveal hotter-drought fingerprint for Earth's forests. *Nature Communications* **13**: 1761.

Hardham AR, Blackman LM. **2018**. *Phytophthora cinnamomi*. *Molecular Plant Pathology* **19**: 260–285.

Harrell F. **2019**. Hmisc: Harrell Miscellaneous. *R package version 4.3-0*.

Harris J, Bedfordshire MK. **2003**. Measurements of the soil microbial community for estimating the success of restoration. *European Journal of Soil Science* **54**: 801–808.

Harris I, Osborn TJ, Jones P, Lister D. **2020**. Version 4 of the CRU TS monthly high-resolution gridded multivariate climate dataset. *Scientific Data* **7**: 1–18.

Hartmann H. **2015**. Carbon starvation during drought-induced tree mortality – are we chasing a myth? *Journal of Plant Hydraulics* **2**:

Hartmann H, Trumbore S. **2016**. Understanding the roles of nonstructural carbohydrates in forest trees - from what we can measure to what we want to know. *The New phytologist* **211**: 386–403.

Hartmann H, Moura CF, Anderegg WRL, Ruehr NK, Salmon Y, Allen CD, Arndt SK, Breshears DD, Davi H, Galbraith D, *et al.* 2018. Research frontiers for improving our understanding of drought-induced tree and forest mortality. *New Phytologist* **218**: 15–28.

Hartmann H, Bastos A, Das AJ, Esquivel-Muelbert A, Hammond WM, Martínez-Vilalta J, Mcdowell NG, Powers JS, Pugh TAM, Ruthrof KX, *et al.* 2022. Climate Change risks to global forest health: Emergence of unexpected events of elevated tree mortality worldwide. *Annual Review of Plant Biology* **73**: 673–702.

Hartmann H, Ziegler W, Trumbore S. **2013**. Lethal drought leads to reduction in nonstructural carbohydrates in Norway spruce tree roots but not in the canopy. *Functional Ecology* **27**: 413–427.

Havaux M. **1998**. Carotenoids as membrane stabilizers in chloroplasts. *Trends in Plant Science* **3**: 147–151.

Havaux M, Eymery F, Porfirova S, Rey P, Dörmann P. **2005**. Vitamin E protects against photoinhibition and photooxidative stress in Arabidopsis thaliana. *Plant Cell* **17**: 3451–3469.

Havaux M. **2013**. Carotenoid oxidation products as stress signals in plants. *Plant Journal* **79**: 597–606.

Havaux. M, García-Plazaola J i. **2014**. Beyond non-photochemical fluorescence quenching: The overlapping antioxidant functions of zeaxanthin and tocopherols. In: Demmig-Adams B, Garab G, Adams W, Govindjee, eds. Non-Photochemical Quenching and Energy Dissipation in Plants,

Henry S, Bru D, Stres B, Hallet S, Philippot L, Al HET. **2006**. Quantitative detection of the nosZ gene , encoding nitrous oxide reductase , and comparison of the abundances of 16S rRNA , narG , nirK , and nosZ genes in soils. *Applied and Environmental Microbiology* **72**: 5181–5189.

Hereş AM, Kaye MW, Granda E, Benavides R, Lázaro-Nogal A, Rubio-Casal AE, Valladares F, Curiel Yuste J. **2018**. Tree vigour influences secondary growth but not responsiveness to climatic variability in Holm oak. *Dendrochronologia* **49**: 68–76.

Herguido-Sevillano E, Pulido M, Lavado J, Schnabel S. **2017**. Spatial patterns of lost and remaining trees in the Iberian wooded rangelands. *Applied Geography* **87**: 170–183.

Hermans C, Smeyers M, Maldonado Rodriguez R, Eyletters M, Strasser RJ, Delhaye JP. **2003**. Quality assessment of urban trees: A comparative study of physiological characterisation, airborne imaging and on site fluorescence monitoring by the OJIP-test. *Journal of Plant Physiology* **160**: 81–90.

Hernández-Clemente R, Hornero A, Mottus M, Penuelas J, González-Dugo V, Jiménez JC, Suárez L, Alonso L, Zarco-Tejada PJ. **2019**. Early Diagnosis of Vegetation Health From High-Resolution Hyperspectral and Thermal Imagery: Lessons Learned From Empirical Relationships and Radiative Transfer Modelling. *Current Forestry Reports* **5**: 169–183.

Holland V, Koller S, Brüggemann W. **2014**. Insight into the photosynthetic apparatus in evergreen and deciduous European oaks during autumn senescence using OJIP fluorescence transient analysis. *Plant Biology* **16**: 801–808.

Hormaetxe K, Becerril JM, Hernández A, Esteban R, García-Plazaola JI. **2007**. Plasticity of photoprotective mechanisms of *Buxus sempervirens* L. leaves in response to extreme temperatures. *Plant Biology* **9**: 59–68.

Hornero A, Zarco-Tejada PJ, Quero JL, North PRJ, Ruiz-Gómez FJ, Sánchez-Cuesta R, Hernandez-Clemente R. **2021**. Modelling hyperspectral- and thermal-based plant traits for the early detection of *Phytophthora*-induced symptoms in oak decline. *Remote Sensing of Environment* **263**: 1–33.

Huntsinger L, Oviedo JL. **2014**. Ecosystem services are social-ecological services in a traditional pastoral system: The case of California's mediterranean rangelands. *Ecology and Society* **19**.

Hwangbo H, Park RD, Kim YW, Rim YS, Park KH, Kim TH, Suh JS, Kim KY. **2003**. 2-Ketogluconic acid production and phosphate solubilization by Enterobacter intermedium. *Current microbiology* **47**: 87–92.

Ibañez M, Chocarro C, Aljazairi S, Ribas À, Sebasti M. **2021**. Tree-open grassland structure and composition drive greenhouse gas exchange in holm oak meadows of the Iberian peninsula. *Agronomy* **11**: 1–16.

IPCC. **2014**. Impacts, Adaptation, and Vulnerability Part A: Global and Sectoral Aspects: Cambridge University Press.

Jacobs DF, Salifu KF, Davis AS. **2009**. Drought susceptibility and recovery of transplanted *Quercus rubra* seedlings in relation to root system morphology. *Annals of Forest Science* **66**: 1–12.

Jia S, McLaughlin NB, Gu J, Li X, Wang Z. **2013**. Relationships between root respiration rate and root morphology, chemistry and anatomy in Larix gmelinii and Fraxinus mandshurica. *Tree Physiology* **33**: 579–589.

Jönsson U. **2006**. A conceptual model for the development of *Phytophthora* disease in *Quercus robur*. *New Phytologist* **171**: 55–68.

Jules ES, Carroll AL, Garcia AM, Steenbock CM, Kauffman MJ. **2014**. Host heterogeneity influences the impact of a non-native disease invasion on populations of a foundation tree species. *Ecosphere* **5**: 1–17.

Juvany M, Müller M, Munné-Bosch S. **2012**. Leaves of field-grown mastic trees suffer oxidative stress at the two extremes of their lifespan. *Journal of Integrative Plant Biology* **54**: 584–594.

Juvany M, Müller M, S M-B. **2013**. Photo-oxidative stress in emerging and senescing leaves: a mirror image? *Journal of Experimental Botany* **64**: 3087–3098.

Kalra YP. **1995**. Determination of pH of soils by different methods: Collaborative study. *Journal of AOAC International* **78**: 310–324.

Kowalchuk GA, Buma DS, Boer W De, Klinkhamer PGL, Veen JA Van. **2002**. Effects of above-ground plant species composition and diversity on the diversity of soil-borne microorganisms. *Antonie van Leeuwenhoek* **81**: 509–520.

Krom MD. **1980**. Spectrophotometric determination of ammonia: A study of a modified berthelot reaction using salicylate and dichloroisocyanurate. *The Analyst* **105**: 305–316.

Kumordzi BB, Aubin I, Cardou F, Shipley B, Violle C, Johnstone J, Anand M, Arsenault A, Bell FW, Bergeron Y, *et al.* 2019. Geographic scale and disturbance influence intraspecific trait variability in leaves and roots of North American understorey plants. *Functional Ecology* **33**: 1771–1784.

Kuypers MMM, Marchant HK, Kartal B. **2018**. The microbial nitrogen-cycling network. *Nature Reviews Microbiology* **16**: 263–276.

Lacalle RG, Aparicio JD, Artetxe U, Urionabarrenetxea E, Polti MA, Soto M, Garbisu C, Becerril JM. **2020**. Gentle remediation options for soil with mixed chromium (VI) and lindane pollution: biostimulation, bioaugmentation, phytoremediation and vermiremediation. *Heliyon* **6**: e04550.

Łakomy P, Kuźmiński R, Mucha J, Zadworny M. **2019**. Effects of oak root pruning in forest nurseries on potential pathogen infections. *Forest Pathology* **49**: 1–11.

Langley A, Chapman SK, Hungate BA. **2006**. Ectomycorrhizal colonization slows root decomposition: The post-mortem fungal legacy. *Ecology Letters* **9**: 955–959.

Laureano RG, García-Nogales A, Seco JI, Rodríguez JGP, Linares JC, Martínez F, Merino J. **2013**. Growth and maintenance costs of leaves and roots in two populations of *Quercus ilex* native to distinct substrates. *Plant and Soil* **363**: 87–99.

Laureano RG, García-Nogales A, Seco JI, Linares JC, Martínez F, Merino J. **2016**. Plant maintenance and environmental stress. Summarising the effects of contrasting elevation, soil, and latitude on *Quercus ilex* respiration rates. *Plant and Soil* **409**: 389–403.

Lefcheck JS. **2016**. piecewiseSEM: Piecewise structural equation modelling in r for ecology, evolution, and systematics. *Methods in Ecology and Evolution* **7**: 573–579.

Lennon EFE, Houlton BZ. **2017**. Coupled molecular and isotopic evidence for denitrifier controls over terrestrial nitrogen availability. *ISME Journal* **11**: 727–740.

Lenth R. **2020**. emmeans: Estimated marginal means, aka least-squares means. R package. *R package version 1.4.6*.

León I, García JJ, Fernández M, Vázquez-Piqué J, Tapias R. **2017**. Differences in root growth of *Quercus ilex* and *Quercus suber* seedlings infected with *Phytophthora cinnamomi*. *Silva Fennica* **51**: 1–12.

Levy-Booth DJ, Prescott CE, Grayston SJ. **2014**. Microbial functional genes involved in nitrogen fixation, nitrification and denitrification in forest ecosystems. *Soil Biology and Biochemistry* **75**: 11–25.

Li Z, Ahn TK, Avenson TJ, Ballottari M, Cruz JA, Kramer DM, Bassi R, Fleming GR,

Keasling JD, Niyogi KK. **2009**. Lutein accumulation in the absence of zeaxanthin restores nonphotochemical quenching in the arabidopsis thaliana npq1 mutant. *Plant Cell* **21**: 1798–1812.

Li J, Attaullah K, Wang J, Yu D, Yang Y, Yang L, Lu Z. **2020**. Root traits determine variation in nonstructural carbohydrates (NSCs) under different drought intensities and soil substrates in three temperate tree species. *Forests* **11**.

Liese R, Alings K, Meier IC. **2017**. Root branching is a leading root trait of the plant economics spectrum in temperate trees. *Frontiers in Plant Science* **8**: 315.

Lindner M, Maroschek M, Netherer S, Kremer A, Barbati A, Garcia-Gonzalo J, Seidl R, Delzon S, Corona P, Kolström M, *et al.* 2010. Climate change impacts, adaptive capacity, and vulnerability of European forest ecosystems. *Forest Ecology and Management* **259**: 698–709.

Lionello P, Malanotte-rizzoli P, Boscolo R, Alpert P, Artale V, Li L, Luterbacher J, May W, Trigo R, Tsimplis M, *et al.* 2006. The Mediterranean Climate: An overview of the main characteristics and issues. *Developments in earth and environmental sciences* **4**: 1–26.

Lobet G, Pound MP, Diener J, Pradal C, Draye X, Godin C, Javaux M, Leitner D, Meunier F, Nacry P, *et al.* 2015. Root system markup language: Toward a unified root Architecture description language. *Plant Physiology* **167**: 617–627.

Lobet G, Pagès L, Draye X. **2011**. A novel image-analysis toolbox enabling quantitative analysis of root system architecture. *Plant Physiology* **157**: 29–39.

Looft T, Johnson TA, Allen HK, Bayles DO, Alt DP, Stedtfeld RD, Sul WJ, Stedtfeld TM, Chai B, Cole JR, *et al.* 2012. In-feed antibiotic effects on the swine intestinal microbiome. *Proceedings of the National Academy of Sciences of the United States of America* **109**: 1691–1696.

López-Ballesteros A, Rodríguez-Caballero E, Moreno G, Escribano P, Curiel-Yuste J. ***in press***. Topography modulates climate sensitivity of multidecadal trends of holm oak decline. : 1–27.

López-Sánchez A, Dirzo R, Roig S. **2018**. Changes in livestock footprint and tree layer coverage in Mediterranean dehesas: a six-decade study based on remote sensing. *International Journal of Remote Sensing* **39**: 4727–4743.

López-Sánchez A, Capó M, Rodríguez-Calcerrada J, Solla A, Martín JA, Perea R. **2022**. Exploring the use of solid biofertilisers to mitigate the effects of exploring the use of solid biofertilisers to mitigate the effects of *Phytophthora* oak root disease. *Forests* **13**.

López B, Sabaté S, Gracia CA. **2001**. Vertical distribution of fine root density, length density, area index and mean diameter in a *Quercus ilex* forest. *Tree Physiology* **21**: 555–560.

Mahamedi AE, Phillips AJL, Lopes A, Djellid Y, Arkam M, Eichmeier A, Zitouni A, Alves A, Berraf-Tebbal A. **2020**. Diversity, distribution and host association of Botryosphaeriaceae species causing oak decline across different forest ecosystems in Algeria. *European Journal of Plant Pathology* **158**: 745–765.

Mair P, Wilcox R. **2018**. Robust statistical methods using WRS2. *Behavior Research Methods*.

Makita N, Hirano Y, Mizoguchi T, Kominami Y, Dannoura M, Ishii H, Finér L, Kanazawa Y. **2011**. Very fine roots respond to soil depth: Biomass allocation, morphology, and physiology in a broad-leaved temperate forest. *Ecological Research* **26**: 95–104.

Manion PD. **1981**. *Tree disease concepts*. Prentice-Hall, Inc.

Marañón T, Navarro-Fernández CM, Gil-Martínez M, Domínguez MT, Madejón P, Villar R. **2020**. Variation in morphological and chemical traits of Mediterranean tree roots: linkage with leaf traits and soil conditions. *Plant and Soil* **449**: 389–403.

Margalef O, Sardans J, Janssens IA. **2017**. Global patterns of phosphatase activity in natural soils. *Scientific Reports* **7**: 1–13.

Mariem S Ben, Gámez AL, Larraya L, Fuertes-Mendizabal T, Cañameras N, Araus JL, McGrath SP, Hawkesford MJ, Murua CG, Gaudeul M, *et al.* 2020. Assessing the evolution of wheat grain traits during the last 166 years using archived samples. *Scientific Reports* **10**: 1–13.

Marklein AR, Houlton BZ. **2012**. Nitrogen inputs accelerate phosphorus cycling rates across a wide variety of terrestrial ecosystems. *New Phytologist* **193**: 696–704.

Martín-García J, Solla A, Corcobado T, Siasou E, Woodward S. **2015**. Influence of temperature on germination of *Quercus ilex* in *Phytophthora cinnamomi* , *P. gonapodyides*, *P. quercina* and *P. psychrophila* infested soils (L Belbahri, Ed.). *Forest Pathology* **45**: 215–223.

Martínez-Vilalta J, Lloret F, Breshears DD. **2012**. Drought-induced forest decline: causes, scope and implications. *Biology Letters* **8**: 689–691.

Matesanz S, Valladares F. **2014**. Ecological and evolutionary responses of Mediterranean plants to global change. *Environmental and Experimental botany* **103**: 53–67.

Maxwell K, Johnson G. **2000**. Chlorophyll fluorescence-a practical guide. *Journal of Experimental Botany* **51**: 659–668.

McCormack LM, Adams TS, Smithwick EAH, Eissenstat DM. **2012**. Predicting fine root lifespan from plant functional traits in temperate trees. *New Phytologist* **195**: 823–831.

McDowell N, Pockman WT, Allen CD, Breshears DD, Cobb N, Kolb T, Plaut J, Sperry J, West A, Williams DG, *et al.* 2008. Mechanisms of plant survival and mortality during drought: why do some plants survive while others succumb to drought? *New Phytologist* **178**: 719–739.

Meng S, Peng T, Liu X, Wang H, Huang T, Gu J, Hu Z. **2022**. Ecological role of bacteria involved in the biogeochemical cycles of mangroves based on functional genes detected through GeoChip 5.0. *American Society for Microbiology* **7**.

Meyer G, Maurhofer M, Frossard E, Gamper HA, Mäder P, Mészáros É, Schönholzer-Mauclaire L, Symanczik S, Oberson A. **2019**. *Pseudomonas protegens* CHA0 does not increase phosphorus uptake from 33P labeled synthetic hydroxyapatite by wheat grown on calcareous soil. *Soil Biology and Biochemistry* **131**: 217–228.

Michel A, Prescher A-K, Schwärzel K, editors (**2020**) Forest Condition in Europe: The 2020 Assessment. ICP Forests Technical Report under the UNECE Convention on Long-range Transboundary Air Pollution (Air Convention). Eberswalde: Thünen Institute. https://doi.org/10.3220/ICPTR1606916913000

Moles AT, Laffan SW, Keighery M, Dalrymple RL, Tindall ML, Chen SC. **2020**. A hairy situation: Plant species in warm, sunny places are more likely to have pubescent leaves. *Journal of Biogeography* **47**: 1934–1944.

Montagnoli A, Kasten Dumroese R, Terzaghi M, Onelli E, Scippa GS, Chiatante D. **2018**. Seasonality of fine root dynamics and activity of root and shoot vascular cambium in a *Quercus ilex* L. forest (Italy). *Forest Ecology and Management* **431**: 26–34.

Montserrat-Martí G, Camarero JJ, Palacio S, Pérez-Rontomé C, Milla R, Albuixech J,

Maestro M. **2009**. Summer-drought constrains the phenology and growth of two coexisting Mediterranean oaks with contrasting leaf habit: Implications for their persistence and reproduction. *Trees* **23**: 787–799.

Mora-Sala B, Berbegal M, Abad-Campos P. **2018**. The use of qPCR reveals a high frequency of *Phytophthora quercina* in Two Spanish holm oak areas. *Forests* **9**.

Mora-Sala B, Abad-Campos P, Berbegal M. **2019**. Response of *Quercus ilex* seedlings to *Phytophthora* spp. root infection in a soil infestation test. *European Journal of Plant Pathology* **154**: 215–225.

Morales M, Roach DA, Quarles BM, Cotado A, Salguero-Gómez R, Dwyer J, Munné-Bosch S. **2021**. Validity of photo-oxidative stress markers and stress-related phytohormones as predictive proxies of mortality risk in the perennial herb Plantago lanceolata. *Environmental and Experimental Botany* **191**.

Moreno-Fernández D, Ledo A, Martín-Benito D, Cañellas I, Gea-Izquierdo G. **2019**. Negative synergistic effects of land-use legacies and climate drive widespread oak decline in evergreen Mediterranean open woodlands. *Forest Ecology and Management* **432**: 884–894.

Moreno G, Obrador JJ, Cubera E, Dupraz C. **2005**. Fine root distribution in dehesas of Central-Western Spain. *Plant and Soil* **277**: 153–162.

Moreno G, Obrador J, García E, Cubera E, Montero MJ, Pulido F, Dupraz C. **2007**. Driving competitive and facilitative interactions in oak dehesas through management practices. *Agroforestry in Europe* **70**: 25–40.

Moreno G, Cubera E. **2008**. Impact of stand density on water status and leaf gas exchange in *Quercus ilex*. *Forest Ecology and Management* **254**: 74–84.

Moreno G, Pulido F. **2009**. The functioning, management and persistence of dehesas. In: Rigueiro-Rodríguez A, McAdam J M-LM, ed. Agroforestry in Europe. 127–160.

Moreno G, Gonzalez-Bornay G, Pulido F, Lopez-Diaz ML, Bertomeu M, Juárez E, Diaz M. **2016**. Exploring the causes of high biodiversity of Iberian dehesas: the importance of wood pastures and marginal habitats. *Agroforestry Systems* **90**: 87–105.

Moser B, Kipfer T, Richter S, Egli S, Wohlgemuth T. **2015**. Drought resistance of *Pinus sylvestris* seedlings conferred by plastic root architecture rather than ectomycorrhizal colonisation. *Annals of Forest Science* **72**: 303–309.

Mou P, Jones RH, Tan Z, Bao Z, Chen H. **2013**. Morphological and physiological plasticity of plant roots when nutrients are both spatially and temporally heterogeneous. *Plant Soil* **364**: 373–384.

Munné-Bosch S, Alegre L. **2000**. Changes in carotenoids, tocopherols and diterpenes during drought and recovery, and the biological significance of chlorophyll loss in *Rosmarinus officinalis* plants. *Planta* **210**: 925–931.

Munné-Bosch S. **2005**. The role of α-tocopherol in plant stress tolerance. *Journal of Plant Physiology* **162**: 743–748.

Munné-Bosch S. **2007**. α-Tocopherol: A Multifaceted Molecule in Plants. *Vitamins and Hormones* **76**: 375–392.

Munné-Bosch S, Lalueza P. **2007**. Age-related changes in oxidative stress markers and abscisic acid levels in a drought-tolerant shrub, Cistus clusii grown under Mediterranean Weld conditions. *Planta* **225**: 1039–1049.

Nakagawa S, Johnson PCD, Schielzeth H. **2017**. The coefficient of determination R2 and intra-class correlation coefficient from generalized linear mixed-effects models revisited and expanded. *Journal of the Royal Society Interface* **14**.

Nakazawa M. **2019**. fmsb: Functions for Medical Statistics Book with some Demographic Data. *R package version 0.7.0.*

Natalini F, Alejano R, Vázquez-Piqué J, Cañellas I. **2016**. The role of climate change in the widespread mortality of Holm oak in open woodlands of Southwestern Spain. *Dendrochronologia* **38**: 51–60.

Navakoudis E, Stergiannakos T, Daskalakis V. **2022**. A perspective on the major light-harvesting complex dynamics under the effect of pH, salts, and the photoprotective PsbS protein. *Photosynthesis Research* **156**: 163–177.

Navone R. **1964**. Proposed method for nitrate in potable waters. *Journal - American Water Works Association* **56**: 781–783.

Nealson KH, Stahl DA. **2018**. Microorganisms and biogeochemical cycles: What can we learn from layered microbial communities? In *Geomicrobiology* (pp. 5-34). De Gruyter.

Niinemets Ü, Lukjanova A. **2003**. Total foliar area and average leaf age may be more

strongly associated with branching frequency than with leaf longevity in temperate conifers. *New Phytologist* **158**: 75–89.

Niinemets Ü, Cescatti A, Rodeghiero M, Tosens T. **2005**. Leaf internal diffusion conductance limits photosynthesis more strongly in older leaves of Mediterranean evergreen broad-leaved species. *Plant, Cell and Environment* **28**: 1552–1566.

Niinemets Ü. **2010**. Responses of forest trees to single and multiple environmental stresses from seedlings to mature plants: Past stress history, stress interactions, tolerance and acclimation. *Forest Ecology and Management* **260**: 1623–1639.

Nogués I, Llusià J, Ogaya R, Munné-Bosch S, Sardans J, Peñuelas J, Loreto F. **2014**. Physiological and antioxidant responses of *Quercus ilex* to drought in two different seasons. *Plant Biosystems* **148**: 268–278.

O'Brien MJ, Engelbrecht BMJ, Joswig J, Pereyra G, Schuldt B, Jansen S, Kattge J, Landhäusser SM, Levick SR, Preisler Y, *et al.* 2017. A synthesis of tree functional traits related to drought-induced mortality in forests across climatic zones. *Journal of Applied Ecology* **54**: 1669–1686.

Ogaya R, Peñuelas J. **2006**. Contrasting foliar responses to drought in *Quercus ilex* and *Phillyrea latifolia*. *Biologia Plantarum* **50**: 373–382.

Ogaya R, Liu D, Barbeta A, Peñuelas J. **2020**. Stem mortality and forest dieback in a 20-Years experimental drought in a Mediterranean holm oak forest. *Frontiers in Forests and Global Change* **2**.

Oksanen J, Blanchet FG, Friendly M, Kindt R, Legendre P, Mcglinn D, Minchin PR, O'hara RB, Simpson GL, Solymos P, *et al.* 2020. vegan: Community Ecology Package. *R package version 2.5-7*.

Paoletti E, Nourrisson G, Garrec JP, Raschi A. **1998**. Modifications of the leaf surface structures of *Quercus ilex* L. in open, naturally CO2-enriched environments. *Plant, Cell and Environment* **21**: 1071–1075.

Pasquini D, Gori A, Pollastrini M, Alderotti F, Centritto M, Ferrini F, Brunetti C. **2023**. Effects of drought-induced holm oak dieback on BVOCs emissions in a Mediterranean forest. *Science of the Total Environment* **857**: 159635.

Peguero-Pina JJ, Mendoza-Herrer Ó, Gil-Pelegrín E, Sancho-Knapik D. **2018**.

Cavitation limits the recovery of gas exchange after severe drought stress in Holm Oak (*Quercus ilex* L.). *Forests* **9**.

Peguero-Pina JJ, Morales F, Flexas J, Gil-Pelegrín E, Moya I. **2008a**. Photochemistry, remotely sensed physiological reflectance index and de-epoxidation state of the xanthophyll cycle in *Quercus coccifera* under intense drought. *Oecologia* **156**: 1–11.

Peguero-Pina JJ, Morales F, Flexas J, Gil-Pelegrín E, Moya I. **2008b**. Photochemistry, remotely sensed physiological reflectance index and de-epoxidation state of the xanthophyll cycle in *Quercus coccifera* under intense drought. *Oecologia* **156**: 1–11.

Peguero-Pina JJ, Sancho-Knapik D, Morales F, Flexas J, Gil-Pelegrín E. **2009**. Differentiall photosynthetic performance and photoprotection mechanisms of three Mediterranean evergreen oaks under severe drought stress. *Functional Plant Biology* **36**: 453–462.

Peñuelas J, Lloret F, Montoya R. **2001**. Severe drought effects on Mediterranean woody flora in Spain. *Forest Science* **47**: 2001.

Pernek M, Kovač M, Jukić A, Dubravac T, Lacković N, Brady C. **2022**. Acute oak decline (AOD) new complex disese on holm oak (*Quercus ilex* L.) and possibilities of spread on other oak species in Croatia. *Šumarski list* **146**: 439–445.

Pinheiro J, Douglas B. **2000**. *Mixed-effects models in S and S-plus* (J Chambers, W Eddy, W Hardle, S Sheather, and L Tierney, Eds.). New York: Springer.

Pinheiro J, Bates D, DebRoy S, Sarkar D, Team RC. **2020**. nlme: Linear and nonlinear mixed effects models. *R package version 3.1-148*.

Pinho D, Barroso C, Froufe H, Brown N, Vanguelova E, Denman S. **2020**. Linking tree health , rhizosphere physicochemical properties , and microbiome in acute oak decline. *Forests* **11**.

Plieninger T. **2006**. Habitat loss, fragmentation, and alteration. Quantifying the impact of land-use changes on a Spanish dehesa landscape by use of aerial photography and GIS. *Landscape Ecology* **21**: 91–105.

Plieninger T, Flinzberger L, Hetman M, Horstmannshoff I, Reinhard-Kolempas M, Topp E, Moreno G, Huntsinger L. **2021**. Dehesas as high nature value farming systems: A social-ecological synthesis of drivers, pressures, state, impacts, and responses. *Ecology and*

Society **26**.

Pollastrini M, Feducci M, Bonal D, Fotelli M, Gessler A, Grossiord C, Guyot V, Jactel H, Nguyen D, Radoglou K, *et al.* 2016. Physiological significance of forest tree defoliation: Results from a survey in a mixed forest in Tuscany (central Italy). *Forest Ecology and Management* **361**: 170–178.

Pollastrini M, Puletti N, Selvi F, Iacopetti G, Bussotti F. **2019**. Widespread crown defoliation after a drought and heat wave in the forests of Tuscany (central Italy) and their recovery. A case study from summer 2017. *Frontiers in Forests and Global Change* **2**: 74.

Poorter H, Ryser P. **2015**. The limits to leaf and root plasticity: what is so special about specific root length? *New Phytologist* **206**: 1188–1190.

Poyatos R, Aguadé D, Galiano L, Mencuccini M, Martínez-Vilalta J. **2013**. Drought-induced defoliation and long periods of near-zero gas exchange play a key role in accentuating metabolic decline of Scots pine. *New Phytologist* **200**: 388–401.

Pregitzer KS. **2008**. Tree root architecture – form and function. *New Phytologist* **180**: 552–564.

Preisler Y, Tatarinov F, Grünzweig JM, Yakir D. **2021**. Seeking the "point of no return" in the sequence of events leading to mortality of mature trees. *Plant Cell and Environment* **44**: 1315–1328.

Prescott CE. **2002**. The influence of the forest canopy on nutrient cycling. *Tree Physiology* **22**: 1193–1200.

Lo Presti D, Di Tocco J, Massaroni C, Cimini S, De Gara L, Singh S, Raucci A, Manganiello G, Woo SL, Schena E, *et al.* 2023. Current understanding, challenges and perspective on portable systems applied to plant monitoring and precision agriculture. *Biosensors and Bioelectronics* **222**: 115005.

Pulido FJ, Díaz M. **2005**. Regeneration of a Mediterranean oak: A whole-cycle approach. *Ecoscience* **12**: 92–102.

Pulido F, Díaz M, Sebastian J. **2001**. Size structure and regeneration of Spanish holm oak *Quercus ilex* forests and dehesas: effects of agroforestry use on their long-term sustainability. *Forest Ecology and Management* **146**: 1–13.

van der Putten WH, Bradford MA, Pernilla Brinkman E, van de Voorde TFJ, Veen GF. **2016**. Where, when and how plant–soil feedback matters in a changing world. *Functional Ecology* **30**: 1109–1121.

Quero JL, Villar R, Marañón T, Murillo A, Zamora R. **2008**. Respuesta plástica a la luz y al agua en cuatro especies mediterráneas del género *Quercus* (Fagaceae). *Revista Chilena de Historia Natural* **81**: 373–385.

R Core Team. **2020**. R (v. 4.0.0, 2020): A language and environment for statistical computing. R Foundation for Statistical Computing, Vienna, Austria.

Radojevic M, Bashkin V, Bashkin V. **1999**. *Practical environmental analysis*. Royal Society of Chemistry.

Ragot S, Kertesz M, Meszaros E, Frossard E, Else Bunemann. **2017**. Soil phoD and phoX alkaline phosphatase gene. *FEMS Microbiology Ecology* **93**: 1–15.

Ramírez-Valiente JA, Koehler K, Cavender-Bares J. **2015**. Climatic origins predict variation in photoprotective leaf pigments in response to drought and low temperatures in live oaks (*Quercu*s series Virentes). *Tree Physiology* **35**: 521–534.

Ramírez-Valiente JA, Aranda I, Sanchéz-Gómez D, Rodríguez-Calcerrada J, Valladares F, Robson TM. **2018**. Increased root investment can explain the higher survival of seedlings of 'mesic' *Quercus suber* than 'xeric' *Quercus ilex* in sandy soils during a summer drought. *Tree Physiology* **39**: 64–75.

Ramírez-Valiente A, Opez RL, Hipp AL, Aranda I. **2020**. Correlated evolution of morphology, gas exchange, growth rates and hydraulics as a response to precipitation and temperature regimes in oaks (*Quercus*). *New Phytologist* **227**: 794–809.

Rasche F, Knapp D, Kaiser C, Koranda M, Kitzler B, Zechmeister-boltenstern S, Richter A, Sessitsch A. **2011**. Seasonality and resource availability control bacterial and archaeal communities in soils of a temperate beech forest. *The ISME Journal* **5**: 389–402.

Raymond NS, Raymond NS, Beatriz G, Nybroe O, Jensen LS, Dorette SM, Richardson AE. **2020**. Phosphate-solubilising microorganisms for improved crop productivity : a critical assessment. *New Phytologist* **229**: 1268–1277.

Redondo MÁ, Pérez-Sierra A, Abad-Campos P, Torres L, Solla A, Reig-Armiñana J, García-Breijo F. **2015**. Histology of *Quercus ilex* roots during infection by *Phytophthora*

cinnamomi. *Trees - Structure and Function* **29**: 1943–1957.

Reich PB, Teskey R, Johnson PS, Hinckley TM. **1980**. Periodic root and shoot growth in oak. *Forest Science* **26**: 590–598.

Resco De Dios V, Fischer C, Colinas C. **2007**. Climate change effects on mediterranean forests and preventive measures. *New Forests* **33**: 29–40.

Richards LA. **1954**. Diagnosis and Improvement of saline and alkali soils. Handbook.

De Rigo D, Caudullo G. **2016**. *Quercus Ilex* in Europe : Distribution , Habitat , Usage and Threats. In: San-Miguel-Ayanz J, de Rigo D, Caudullo G, Houston T, Mauri A, eds. European Atlas of Forest Tree Species. 152–153.

Ritchie G, Dunlap J. **1980**. Root growth potential : Its development and expression in forest tree seedlings. *New Zealand Journal of Forestry Science* **10**: 218–248.

Rivas-Martínez S. **1987**. Mapa de series de vegetacion de España: 1: 400 000. Instituto nacional para la conservacion de la naturaleza. *Icona*.

Rodríguez-Calcerrada J, Sancho-Knapik D, Martin-StPaul NK, Limousin J-M, McDowell NG, Gil-Pelegrín E. **2017**. Drought-induced oak decline-factors involved, physiological dysfunctions and potential attenuation by forestry practises. In: Gil-Pelegrín E, Peguero-Pina J, Sancho-Knapik D, eds. Oaks physiological ecology. Exploring the functional diversity of Genus *Quercu*s. Cham, Switzerland.

Rodríguez-Serrano C. **2011**. De las puertos de León a las dehesas de Extremadura: siete siglos por un camino de ida y vuelta. In: IV Encuentro de estudios comarcales: Vegas Altas, La Serena y La Siberia. Badajoz: Imprenta de la Diputación de Badajoz.

Rodríguez A, Curiel Yuste J, Rey A, Durán J, García-Camacho R, Gallardo A, Valladares F. **2016**. Holm oak decline triggers changes in plant succession and microbial communities, with implications for ecosystem C and N cycling. *Plant and Soil 2016 414:1* **414**: 247–263.

Rodríguez A, Durán J, Rey A, Boudouris I, Valladares F, Gallardo A, Yuste JC. **2019**. Interactive effects of forest die-off and drying-rewetting cycles on C and N mineralization. *Geoderma* **333**: 81–89.

Rodríguez A, Durán J, Curiel Yuste J, Valladares F, Rey A. **2023**. The effect of tree

decline over soil water content largely controls soil respiration dynamics in a Mediterranean woodland. *Agricultural and Forest Meteorology* **333**.

Rösch C, Bothe H. **2005**. Improved assessment of denitrifying, N2-fixing, and total-community bacteria by terminal restriction fragment length polymorphism analysis using multiple restriction enzymes. *Applied and Environmental Microbiology* **71**: 2026–2035.

Rotthauwe J, Witzel K, Werner L. **1997**. The ammonia monooxygenase structural gene amoA as a functional marker: Molecular fine-scale analysis of natural ammonia-oxidizing populations. *Applied and Environmental Microbiology* **63**: 4704–4712.

Ruess RW, Hendrick RL, Burton AJ, Pregitzer KS, Sveinbjornssön B, Allen MF, Maurer GE. **2003**. Coupling fine root dynamics with ecosystem carbon cycling in black spruce forests of interior Alaska. *Ecological Monographs* **73**: 643–662.

Ruíz-Gómez F, Navarro-Cerrillo RM, Sánchez-Cuesta R, Pérez-de-Luque A. **2015**. Histopathology of infection and colonization of *Quercus ilex* fine roots by *Phytophthora cinnamomi*. *Plant Pathology* **64**: 605–616.

Ruiz-Gómez FJ. **2018a**. Study of the interaction between root rot oomycetes and *Quercus ilex* L. *Doctoral dissertation, Universidad de Cordoba*

Ruíz-Gómez F, Pérez-de-Luque A, Sánchez-Cuesta R, Quero JL, Cerrillo RMN. **2018b**. Differences in the response to acute drought and *Phytophthora cinnamomi* rands infection in *Quercus ilex* L. seedlings. *Forests* **9**: 1–16.

Ruíz-Gómez F, Navarro-Cerrillo R, Reports AP-L-S, 2019 U. **2019a**. Assessment of functional and structural changes of soil fungal and oomycete communities in holm oak declined dehesas through metabarcoding analysis. *Scientific reports* **9**: 1–16.

Ruíz-Gómez FJ, Pérez-de-Luque A, Navarro-Cerrillo RM. **2019b**. The Involvement of *Phytophthora* root rot and drought stress in Holm Oak decline: from ecophysiology to microbiome influence. *Current Forestry Reports* **5**: 251–266.

Sala A, Piper F, Hoch G. **2010**. Physiological mechanisms of drought-induced tree mortality are far from being resolved. *New Phytologist* **186**: 274–281.

San-Emeterio LM, Jiménez-morillo NT, Pérez-ramos IM. **2023**. Changes in soil organic matter molecular structure after five years mimicking climate change scenarios in a Mediterranean savannah. *Science of the Total Environment* **857**.

San-Eufrasio B, Castillejo MÁ, Labella-Ortega M, Ruiz-Gómez FJ, Navarro-Cerrillo RM, Tienda-Parrilla M, Jorrín-Novo J V., Rey MD. **2021**. Effect and Response of *Quercus ilex* subsp. ballota [Desf.] Samp. Seedlings From Three Contrasting Andalusian Populations to Individual and Combined *Phytophthora cinnamomi* and Drought Stresses. *Frontiers in Plant Science* **12**: 1–17.

Sánchez-Cuesta R, Ruiz-Gómez FJ, Duque-Lazo J, González-Moreno P, Navarro-Cerrillo RM. **2021**. The environmental drivers influencing spatio-temporal dynamics of oak defoliation and mortality in dehesas of Southern Spain. *Forest Ecology and Management* **485**.

Sánchez-Cuesta R. **2022**. Patrón espacial de variables bióticas y abióticas implicadas en la mortalidad por podredumbre radical en *Quercus ilex* L . subsp . *ballota* (Desf .) Samp . en el suroeste de la Península Ibérica. *Doctoral dissertation, Universidad de Cordoba*.

Sánchez-Cuesta R, González-Moreno P, Cortés-Márquez A, Navarro-Cerrillo RM, Ruiz-Gómez FJ. **2022**. Soil distribution of *Phytophthora cinnamomi* inoculum in oak afforestation depends on site characteristics rather than host availability. *New Forests*.

Sánchez ME, Caetano P, Ferraz J, Trapero A. **2002**. *Phytophthora* disease of *Quercus ilex* in south-western Spain. *Forest Pathology* **32**: 5–18.

Sanz-Pérez V, Castro-Díez P, Joffre R. **2009**. Seasonal carbon storage and growth in Mediterranean tree seedlings under different water conditions. *Tree Physiology* **29**: 1105–1116.

Sapsford SJ, Paap T, St GE, Treena JH. **2017**. The ‘ chicken or the egg ’: which comes first , forest tree decline or loss of mycorrhizae ? *Plant Ecology* **218**: 1093–1106.

Sardans J, Peñuelas J. **2004**. Increasing drought decreases phosphorus availability in an evergreen Mediterranean forest. *Plant and Soil* **267**: 367–377.

Sardans J, Rodà F, Peñuelas J. **2004**. Phosphorus limitation and competitive capacities of Pinus halepensis and *Quercus ilex* subsp . rotundifolia on different soils. *Plant Ecology* **174**: 305–317.

Sardans J, Peñuelas J, Ogaya R. **2008**. Drought-induced changes in C and N stoichiometry in a *Quercus ilex* Mediterranean forest. *Forest Science* **54**: 513–522.

Scarlett K, Denman S, Clark DR, Forster J, Vanguelova E, Brown N, Whitby C. **2020**.

Relationships between nitrogen cycling microbial community abundance and composition reveal the indirect effect of soil pH on oak decline. *ISME Journal*: 1–13.

Schlesinger WH, Dietze MC, Jackson RB. **2016**. Forest biogeochemistry in response to drought. *Global Change Biology (2016)* **22**: 2318–2328.

Schmied G, Hilmers T, Mellert K, Uhl E, Buness V, Ambs D, Steckel M, Biber P, Muhidin Š, Hoffmann Y, *et al.* 2023. Nutrient regime modulates drought response patterns of three temperate tree species. *Science of the Total Environment* **868**: 161601.

Schulze E-D, Beck E, Buchmann N, Clemens S, Müller-Hohenstein K, Scherer-Lorenzen M. **2019**. *Plant ecology*. Berlin: Springer Nature.

Scott P, Burgess T, Hardy G. **2013**. Globalization and *Phytophthora*. In: Lamour K, ed. *Phytophthora*: A Global Perspective. CPI Group (UK) Ltd, Croydon, 226–232.

Searle PL. **1984**. The Berthelot or Indophenol reaction and its use in the analytical chemistry of nitrogen. A review. *ANALYST* **109**: 549–568.

Serrano MS, Fernández-Rebollo P, De Vita P, Sánchez ME. **2013**. Calcium mineral nutrition increases the tolerance of *Quercus ilex* to *Phytophthora* root disease affecting oak rangeland ecosystems in Spain. *Agroforestry Systems* **87**: 173–179.

Shvaleva A, Siljanen2 H, Correia A, Silva F, Lamprecht R, Lobo-do-Vale R, Bicho C, Fangueiro D, Anderson M, Pereira JS, *et al.* 2015. Environmental and microbial factors influencing methane and nitrous oxide fluxes in Mediterranean cork oak woodlands : trees make a difference. *Frontiers in Microbiology* **6**.

Singh A, Kumar M, Saxena AK. **2020**. Role of microorganisms in regulating carbon cycle in tropical and subtropical soils. In: Ghosh P, Mandal D, Ramakrishnam S, Mahanta S, Mandal B, eds. Carbon Management in Tropical and Sub-Tropical Terrestrial Systems. Singapore: Springer Nature Singapore, 249–263.

Smith P, Cotrufo MF, Rumpel C, Paustian K, Kuikman PJ, Elliott JA, McDowell R, Griffiths RI, Asakawa S, Bustamante M, *et al.* 2015. Biogeochemical cycles and biodiversity as key drivers of ecosystem services provided by soils. *Soil* **1**: 665–685.

Solís-García I, Ceballos-Luna O, Cortazar-Murillo EM, Damaris, Desgarennes Edith G-S, Patiño-Conde V, Guevara-Avendaño E, Méndez-Bravo A, Reverchon F. **2021**. *Phytophthora* root rot modifies the composition of the avocado rhizosphere microbiome and

increases the abundance of opportunistic fungal pathogens. *Frontiers in Microbiology* **11**: 1–15.

Solla A, García L, Pérez A, Cordero A, Cubera E, Moreno G. **2009**. Evaluating potassium phosphonate injections for the control of *Quercus ilex* decline in SW Spain: Implications of low soil contamination by *Phytophthora cinnamomi* and low soil water content on the effectiveness of treatments. *Phytoparasitica* **37**: 303–316.

Solla A, Moreno G, Malewski T, Jung T, Klisz M, Tkaczyk M, Siebyla M, Pérez A, Cubera E, Hrynyk H, *et al.* 2021. Phosphite spray for the control of oak decline induced by *Phytophthora* in Europe. *Forest Ecology and Management* **485**.

Stirbet A, Govindjee. **2011**. On the relation between the Kautsky effect (chlorophyll a fluorescence induction) and Photosystem II: Basics and applications of the OJIP fluorescence transient. *Journal of Photochemistry and Photobiology B: Biology* **104**: 236–257.

Stotz GC, Salgado-Luarte C, Escobedo VM, Valladares F, Gianoli E. **2021**. Global trends in phenotypic plasticity of plants. *Ecology Letters* **24**: 2267–2281.

Strasser RJ, Srivastava A, Tsimilli-Michael M. **2000**. The fluorescence transient as a tool to characterize and screen photosynthetic samples. *Probing Photosynthesis: Mechanism, Regulation & Adaptation*: 443–480.

Strasser RJ, Tsimilli-Michael M, Srivastava A. **2004**. Analysis of the Chlorophyll a Fluorescence Transient. In: 321–362.

Suseela V, Tharayil N, Orr G, Hu D. **2020**. Chemical plasticity in the fine root construct of *Quercus* spp. varies with root order and drought. *New Phytologist* **228**: 1835–1851.

Suz LM, Bidartondo MI, Linde S van der, Kuyper TW. **2021**. Ectomycorrhizas and tipping points in forest ecosystems. *New Phytologist* **231**: 1700–1707.

Szabó I, Bergantino E, Giacometti GM. **2005**. Light and oxygenic photosynthesis: Energy dissipation as a protection mechanism against photo-oxidation. *EMBO Reports* **6**: 629–634.

Tang J, Baldocchi DD, Xu L. **2005**. Tree photosynthesis modulates soil respiration on a diurnal time scale. *Global Change Biology* **11**: 1298–1304.

Tausz M, Wonisch A, Grill D, Morales D, Soledad Jiménez M. **2003**. Measuring antioxidants in tree species in the natural environment: From sampling to data evaluation.

Journal of Experimental Botany **54**: 1505–1510.

Tausz M, Šircelj H, Grill D. **2004**. The glutathione system as a stress marker in plant ecophysiology: Is a stress-response concept valid? In: Journal of Experimental Botany. Oxford Academic, 1955–1962.

Terradas J. **2001**. *Ecología de la vegetación: de la ecofisiología de las plantas a la dinámica de comunidades y paisajes*.

Thaler P, Pagès L. **1998**. Modelling the influence of assimilate availability on root growth and architecture. *Plant and Soil* **201**: 307–320.

Thomas FM. **2008**. Recent advances in cause-effect research on oak decline in Europe. *CAB Reviews: Perspectives in Agriculture, Veterinary Science, Nutrition and Natural Resources* **3**: 1–12.

Toms J, Lesperance M. **2003**. Piecewise regression: A tool for identifying ecological thresholds I. *Ecology* **84**: 2034–2041.

Trubat R, Cortina J, Vilagrosa A. **2012**. Root architecture and hydraulic conductance in nutrient deprived Pistacia lentiscus L. seedlings. *Oecologia* **170**: 899–908.

Trugman A. **2022**. Integrating plant physiology and community ecology across scales through trait-based models to predict drought mortality. *New Phytologist* **234**: 21–27.

Tu Q, Yu H, He Z, Deng Y, Wu L, Nostrand J, Shi Z, Xue K, Yuan T, Wang A, *et al.* 2014. GeoChip 4 : a functional gene-array-based high-throughput environmental technology for microbial community analysis. *Molecular Ecology Resources* **14**: 914–928.

Valladares F, Martinez-Ferri E, Balaguer L, Perez-Corona E, Manrique E. **2000a**. Low leaf-level response to light and nutrients in Mediterranean evergreen oaks: A conservative resource-use strategy? *New Phytologist* **148**: 79–91.

Valladares F, Martinez-Ferri E, Balaguer L, Perez-Corona E, Manrique E. **2000b**. Low leaf-level response to light and nutrients in Mediterranean evergreen oaks: A conservative resource-use strategy? *New Phytologist* **148**: 79–91.

Valladares F, Gianoli E, Gómez JM. **2007**. Ecological limits to plant phenotypic plasticity. *New Phytologist* **176**: 749–763.

Valladares F, Sanchez-Gomez D, Zavala MA. **2006**. Quantitative estimation of phenotypic

plasticity: Bridging the gap between the evolutionary concept and its ecological applications. *Journal of Ecology* **94**: 1103–1116.

Venables WN, Ripley BD. **2002**. Modern Applied Statistics with S. Fourth Edition. Springer, New York. ISBN 0-387-95457-0.

Vicente-Serrano S, Camarero J, C A-M. **2013**. Diverse responses of forest growth to drought time-scales in the northern hemisphere. *Global Ecology and Biogeography* **23**: 1019–1030.

Vidi PA, Kanwischer M, Baginsky S, Austin JR, Csucs G, Dörmann P, Kessler F, Bréhélin C. **2006**. Tocopherol cyclase (VTE1) localization and vitamin E accumulation in chloroplast plastoglobule lipoprotein particles. *Journal of Biological Chemistry* **281**: 11225–11234.

Villar-Salvador P, Planelles R, Oliet J, Juan L, Jacobs DF, González M. **2004**. Drought tolerance and transplanting performance of holm oak (*Quercus ilex*) seedlings after drought hardening in the nursery. *Tree physiology* **24**: 1147–1155.

Vito MRM. **2008**. Segmented: an R Package to Fit Regression Models with Broken-Line Relationships. *R News* **8**: 20–25.

Vivas M, Hernández J, Corcobado T, Cubera E, Solla A. **2021**. Transgenerational induction of resistance to *Phytophthora cinnamomi* in holm oak. *Forests* **12**.

Vranova E, Inze D, Van Breusegem F. **2002**. Signal transduction during oxidative stress. *Journal of Experimental Botany* **53**: 1227–1236.

Walinga I, Van Der Lee JJ, Houba VJG, Van Vark W, Van Der Lee JJ. **1989**. Part 7. In: Plant analysis procedure. Syllabus, 197–200.

Walkley A, Black IA. **1934**. An examination of the Degtjareff method for determining soil organic matter, and a proposed modification of the chromic acid titration method. *Soil Science* **37**: 29–38.

Wambsganss J, Freschet GT, Beyer F, Goldmann K, Prada-Salcedo LD, Scherer-Lorenzen M, Bauhus J. **2021**. Tree species mixing causes a shift in fine-root soil exploitation strategies across European forests. *Functional Ecology* **35**: 1886–1902.

Wang Z, Xue L, Li M, Li C, Li P, Li H. **2021**. Au@SnO2-vertical graphene-based

microneedle sensor for in-situ determination of abscisic acid in plants. *Materials Science and Engineering C* **127**: 112237.

Wei W, Isobe K, Nishizawa T, Zhu L, Shiratori Y, Ohte N, Koba K, Otsuka S, Senoo K. **2015**. Higher diversity and abundance of denitrifying microorganisms in environments than considered previously. *ISME Journal* **9**: 1954–1965.

White HJ, León-Sánchez L, Burton VJ, Cameron EK, Caruso T, Cunha L, Dirilgen T, Jurburg SD, Kelly R, Kumaresan D, *et al.* 2020. Methods and approaches to advance soil macroecology. *Global Ecology and Biogeography* **29**: 1674–1690.

Willaume M, Pagès L. **2006**. How periodic growth pattern and source/sink relations affect root growth in oak tree seedlings. *Journal of Experimental Botany* **57**: 815–826.

Willaume M, Pagès L. **2011**. Correlated responses of root growth and sugar concentrations to various defoliation treatments and rhythmic shoot growth in oak tree seedlings (*Quercus pubescens*). *Annals of Botany* **107**: 653–662.

Willey JM, Sherwood LM, Woolverton C. **2008**. *Prescott,Harley, and Klein's Microbiology*. New York.

Wu X, Rensing C, Han D, Xiao K, Dai Y, Tang Z, Liesack W. **2022**. Genome-Resolved metagenomics reveals distinct phosphorus acquisition strategies between soil microbiomes. *American Society for Microbiology* **7**.

Wujeska A, Bossinger G, Tausz M. **2013**. Responses of foliar antioxidative and photoprotective defence systems of trees to drought: A meta-analysis. *Tree Physiology* **33**: 1018–1029.

Xiao H, Xiao Y, Xu M, Wang Z, Wang L, Wang J, Shi Z. **2022**. Role of autotrophic microbes in organic matter accumulation in soils degraded by erosion. *Land degradation and development* **33**: 2092–2102.

Xiong Y, D'Atri JJ, Fu S, Xia H, Seastedt TR. **2011**. Rapid soil organic matter loss from forest dieback in a subalpine coniferous ecosystem. *Soil Biology and Biochemistry* **43**: 2450–2456.

Yahara H, Tanikawa N, Okamoto M, Makita N. **2019**. Characterizing fine-root traits by species phylogeny and microbial symbiosis in 11 co-existing woody species. *Oecologia* **191**: 983–993.

Yeomans JC, Bremner JM. **1988**. A rapid and precise method for routine determination of organic carbon in soil1. *Communications in Soil Science and Plant Analysis* **19**: 1467–1476.

Zadworny M, Mucha J, Jagodziński AM, Kościelniak P, Łakomy P, Modrzejewski M, Ufnalski K, Żytkowiak R, Comas LH, Rodríguez-Calcerrada J. **2021**. Seedling regeneration techniques affect root systems and the response of *Quercus robur* seedlings to water shortages. *Forest Ecology and Management* **479**: 118552.

Zang U, Goisser M, Häberle K-H, Matyssek R, Matzner E, Borken W. **2014**. Effects of drought stress on photosynthesis, rhizosphere respiration, and fine-root characteristics of beech saplings: A rhizotron field study. *Journal of Plant Nutrition and Soil Science* **177**: 168–177.

Zarco-Tejada PJ, Camino C, Beck PSA, Calderon R, Hornero A, Hernández-Clemente R, Kattenborn T, Montes-Borrego M, Susca L, Morelli M, *et al.* 2018. Previsual symptoms of Xylella fastidiosa infection revealed in spectral plant-trait alterations. *Nature Plants* **4**: 432–439.

Zarter CR, Adams WW, Ebbert V, Cuthbertson DJ, Adamska I, Demmig-Adams B. **2006**. Winter down-regulation of intrinsic photosynthetic capacity coupled with up-regulation of Elip-like proteins and persistent energy dissipation in a subalpine forest. *New Phytologist* **172**: 272–282.

Zheng B, Zhu Y, Sardans J, Peñuelas J, Su Q. **2018**. QMEC : A tool for high-throughput quantitative assessment of microbial functional potential in C , N , P , and S biogeochemical cycling Key. *Science China* **61**: 1451–1462.

Zur A, Ieno E, Smith G. **2016**. *Analysing Ecological Data* (M Gail, K Krickeberg, J Samet, A Tsiatis, and W Wong, Eds.). New York: Springer.

Chapter X

Supplementary material

Table S4.1.. Definition of terms and formulae of the OJIP-test parameters used for the analysis of the chlorophyll *a* fluorescence transients in Figure 5 and Table 1, following the formulas of Strasser et al. (2000, 2004).

Data extracted from the recorded fluorescence transient OJIP		
F_t		Fluorescence at time t after onset of actinic illumination
F_o	$= F_{50\ \mu s}$	Minimal fluorescence intensity at 50 µs, when all reaction centers (RCs) are open
F_j	$=F_{2ms}$	Fluorescence value at 2 ms (J-level)
F_i	$=F_{30ms}$	Fluorescence value at 30 ms (I-level)
F_M	$=F_p=F_{1s}$	Maximal fluorescence intensity, when all RCs are closed
M_0	$4(F_{300\mu s}–F_0)/(F_M–F_0)$	initial slope of the fluorescence transient
S_M	$Area/(F_M-F_o)$	Normalized area (assumed proportional to the number of reduction and oxidation of one Q_A^-molecule during the fast OJIP transient, and therefore related to the number of electron carriers per electron transport chain)
Fluorescence parameters derived from the extracted data		
V_t	$=(F_t-F_0)/(F_M-F_0)$	Relative variable chlorophyll (Chl) fluorescence at time t (from F_0 to F_M)
V_j	$=(F_J-F_O)/(F_M-F_0)$	Relative variable Chl fluorescence at 2 ms (at the J-step)
V_i	$=(F_i-F_O)/(F_M-F_0)$	Relative variable Chl fluorescence at 30 ms (at the I-step)
Specific energy fluxes per RC		
(where TR, ABS and ET denote the trapped, the absorbed excitation energy fluxes and the electron transport rate respectively)		
ABS/RC	$(M_0/V_J)\cdot F_M/(F_M–F_0)$	Specific flux for absorption: absorption flux per RC. Also a measure of PSII apparent antenna size
TRo/RC	M_0/V_J	Specific flux for trapping: trapped energy flux per RC resulting in the reduction of QA to $QA^–$
ETo/RC	$(M_0/V_J)(1–V_J)$	Specific flux for electron transport: electron transport flux per RC
DIo/RC	$(M_0/V_J)(F_0/F_V)$	Specific flux for dissipation: the excitation energy dissipated, mainly as heat and less as fluorescence emission per RC
Quantum yields or flux ratio		
φ_{Po}	F_v/F_M	The maximum quantum yield of primary photochemistry: represents the probability that an absorbed photon is trapped by the RC and used for primary photochemistry.
Ψ_o	$1 - V_J$	The efficiency with which a trapped exciton can move an electron into the electron transport chain further than QA.

φ_{Eo}	$(1-(F_0/F_M)).\ \Psi o$	The quantum yield of electron transport: represents the probability that an absorbed photon moves an electron into the electron transport chain
φ_{Do}	$1-\varphi_{Po}-(F_0/F_M)$	The quantum yield for energy dissipation

PI_{Abs}	$[RC/ABS][TR_0/(ABS-TR_0)][ET_0/(TR_0-ET_0)$	Performance index (potential) for energy conservation from photons absorbed by photosystem II to the reduction of intersystem electron acceptors.

Table S5.1. ANOVA table (type III) of the LMEs in which FRB varied as a function of the different carbohydrate fractions in fine roots, health status and the interaction between the different carbohydrate fractions × health status in holm oak trees.

	FRB		
Model	Df	$\chi 2$	p-value
Intercept	1	6.970	**0.008**
Fine root NSC	1	4.011	**0.045**
Health status	2	9.707	**0.007**
Fine root NSC × Health status	2	10.77	**0.004**
Intercept	1	11.23	**0.000**
Fine root starch	1	6.733	**0.009**
Health status	2	4.743	0.090
Fine root starch × Health status	2	6.253	**0.043**
Intercept	1	3.668	0.055
Fine root soluble sugars	1	0.587	0.443
Health status	2	5.292	0.071
Fine root soluble sugars × Health status	2	6.275	**0.043**

FRB was logarithmically transformed to fulfil assumptions. Abbreviations stand for physiological traits (non-structural carbohydrates, NSC). Also, Df stands for degrees of freedom while the $\chi 2$ symbol stands for the chi-square statistic. Values in bold indicate significant relationships.

Table S5.2. ANOVA table (type III) of the LMEs in which foliage:root parameter ratios (i.e., FRB, FRD, FRL), varied as a function of the soil nutrient availability, health status and the interaction between soil nutrient availability × health status in holm oak trees.

	Foliage:FRB			Foliage:FRD			Foliage:FRL		
Source of variation	Df	$\chi 2$	p-value	Df	$\chi 2$	p-value	Df	$\chi 2$	p-value
Intercept	1	1533.8	0.000	1	12109	0.000	1	2415.1	0.000
Soil nutrient availability	1	3.363	0.066	1	0.741	0.389	1	1.385	0.239
Health status	2	14.348	0.000	2	19.82	0.000	2	6.770	0.033
Soil nutrient availability × Health status	2	10.059	0.006	2	4.437	0.108	2	9.125	0.010

Foliage:root parameter ratios were logarithmically transformed to fulfill assumptions. Abbreviations stand for architectural (fine root branching ratio, FRB) and morphological (fine root diameter, FRD; and fine root length, FRD) root parameters. Also, Df stands for degrees of freedom while the $\chi 2$ symbol stands for the chi-square statistic. Values in bold indicate significant relationships.

Table S6.1. Abbreviation of the soil microbial functional gene and encoded enzyme used in this study. Table are based on Zheng *et al.*, (2018).

Nº	Gen name	Encoded enzyme
1	*abfA*	α-L-arabinofuranosidase
2	*accA*	acetyl-CoA carboxylase carboxyltransferase α subunit
3	*aclB*	ATP-citrate lyase β subunit
4	*acsA*	acetyl-coenzyme A synthetase
5	*acsB*	acetyl-CoA synthase complex β subunit
6	*acsE*	5-methyltetrahydrofolate corrinoid methyltransferase
7	*amoA1*	ammonia monooxygenase α subunit (Archaea)
8	*amoA2*	ammonia monooxygenase α subunit (Bacteria)
9	*amoB*	ammonia monooxygenase β subunit
10	*amyA*	α-amylase
11	*amyX*	pullulanase
12	*apsA*	adenosine-5'-phosphosulfate reductase α subunit
13	*apu*	amylopullulanase
14	*bpp*	β-propeller phytase
15	*cdaR*	carbohydrate diacid regulon transcriptional regulator
16	*cdh*	cellobiose dehydrogenase
17	*cex*	exoglucanase
18	*chiA*	endochitinase
19	*cphy*	ruminal cysteine phytase
20	*dsrA*	sulfite reductase α subunit
21	*dsrB*	sulfite reductase β subunit
22	*exo-chi*	exochitinase
23	*frdA*	fumarate reductase flavoprotein subunit
24	*gcd*	quinoprotein glucose dehydrogenase
25	*gdhA*	glutamate dehydrogenase
26	*glx*	glyoxal oxidase
27	*hao*	hydroxylamine oxidoreductase
28	*hzo*	hydrazine oxidase
29	*hzsA*	hydrazine synthase α subunit
30	*hzsB*	hydrazine synthase β subunit
31	*iso-plu*	Isopullulanase
32	*korA*	2-oxoglutarate ferredoxin oxidoreductase α subunit
33	*lig*	lignin peroxidase
34	*manB*	β- mannanase
35	*mct*	mesaconyl-CoA C1-C4 CoA transferase
36	*mcrA*	methyl-coenzyme M reductase α subunit
37	*mmoX*	methane monooxygenase component A alpha chain
38	*mnp*	manganese peroxidase
39	*mxaF*	methanol dehydrogenase (cytochrome c) subunit 1
40	*naglu*	α-N-acetylglucosaminidase
41	*napA*	periplasmic nitrate reductase
42	*narG*	nitrate reductase α chain
43	*nasA*	assimilatory nitrate reductase catalytic subunit
44	*nifH*	nitrogenase iron protein
45	*nirK1*	nitrite reductase (NO-forming)
46	*nirK2*	nitrite reductase (NO-forming)
47	*nirK3*	nitrite reductase (NO-forming)
48	*nirS1*	nitrite reductase (NO-forming)
49	*nirS2*	nitrite reductase (NO-forming)
50	*nirS3*	nitrite reductase (NO-forming)
51	*nosZ1*	nitrous-oxide reductase

52	*nosZ2*	nitrous-oxide reductase
53	*nxrA*	nitrite oxidoreductase α subunit
54	*pccA*	acetyl/propionyl-CoA carboxylase alpha
55	*pgu*	pectinase/polygalacturonase
56	*phnK*	phosphonate transport system ATP-binding protein
57	*phoD*	alkaline phosphatase D
58	*phoX*	alkaline phosphatase/Pho regulon
59	*pqq-mdh*	methanol/ethanol family PQQ-dependent dehydrogenase
60	*pmoA*	methane/ammonia monooxygenase subunit A
61	*pox*	phenol oxidase
62	*ppk*	polyphosphate kinase
63	*ppx*	exopolyphosphatase
64	*pqqC*	pyrroloquinoline-quinone synthase
65	*rbcL*	ribulose-bisphosphate carboxylase large chain
66	*sga*	glucoamylase
67	*smtA*	succinyl-CoA:(S)- malate CoA transferase
68	*soxY*	sulfur-oxidizing protein
69	*ureC*	urease
70	*xylA*	xylose isomerase
71	*yedZ*	sulfite oxidase
72	16S	ribosomal RNA gene sequence

Table S6.2. Results of the first set of linear mixed-effect models (LMEs) that show the relative abundance of the soil microbial functional genes as a function of the health status (i.e., healthy, susceptible and declining).

	Health Status			p-value	R^2c
Variables	Healthy	Susceptible	Declining		
Carbon hydrolysis					
iso_plu	0.0031±0.0007**a**	0.0069±0.0016**ab**	0.0088±0.0035**b**	**0.01497***	0.2225
lig	0.1395±0.0295**a**	0.162±0.0149**a**	0.2259±0.0291**b**	**0.00003*****	0.3267
pgu	0.0042±0.0005**a**	0.0072±0.0007**b**	0.0053±0.0007**ab**	**0.02087***	0.3264
apu	0.1433±0.0134	0.1488±0.0116	0.1704±0.0149	0.0902	0.1130
glx	0.2113±0.0276**ab**	0.1482±0.017**a**	0.2416±0.0291**b**	**0.00881****	0.3007
abfA	139.0684±9.2285	145.4598±10.9349	155.1957±10.2396	0.19583	0.2465
mnp	2.8141±0.409	2.3855±0.18	2.5316±0.1731	0.61552	0.1230
sga	18.3659±2.4957	15.3421±1.364	16.8432±1.5001	0.5912	0.1618
chiA	0.3797±0.0445	0.3637±0.049	0.3493±0.0587	0.62097	0.4895
cex	3.0547±0.4208	2.5214±0.3965	2.8454±0.6038	0.79056	0.5324
manB	5.2167±0.5447	4.068±0.3335	4.4625±0.4551	0.37462	0.2856
xylA	9.0487±0.6931	8.0477±0.4893	8.6904±0.5283	0.38423	0.0771
amyA	0.0043±0.0022	0.0023±0.0004	0.002±0.0003	0.67155	0.1392
Carbon fixation					
acsB	0.0007±0.0002	0.0011±0.0002	0.0013±0.0002	0.10995	0.2034
accA	0.0023±0.0008	0.0022±0.0003	0.0024±0.0005	0.4842	0.2988
rbcL	133.64±10.16**a**	175.60±13.29**ab**	188.01±17.36**b**	**0.00065*****	0.4850
pccA	0.8191±0.0679	0.908±0.0616	1.0846±0.0961	0.11559	0.2111
smtA	1.8027±0.136**a**	2.4416±0.1754**b**	2.3987±0.2008**b**	**0.01254***	0.1561
aclB	0.2989±0.0294	0.3146±0.0264	0.3675±0.033	0.11961	0.2186
korA	1.3489±0.1535	1.4963±0.1393	2.1853±0.7976	0.09484	0.1199
acsE	10.1292±0.7887	12.104±1.6006	12.6567±1.1266	0.07481•	0.2305
frdA	11.1762±1.8706	13.0574±3.1238	11.6879±1.4341	0.6765	0.4073
acsA	1139.191±112.5979	1000.628±68.34	1180.265±97.1605	0.1002	0.4535
mct	0.2418±0.0184	0.2894±0.0267	0.2744±0.0216	0.30689	0.8991
Methane cycling					
mmoX	0.3292±0.0506**a**	0.326±0.0233**a**	0.5309±0.0897**b**	**0.00308****	0.0917
pqq_mdh	1.8263±0.1769	2.4726±0.907	1.9561±0.2473	0.65071	0.2193
pmoA	1.5924±0.2268	1.2961±0.1156	1.7914±0.5796	0.74619	0.1501
mxaF	5.0973±0.7789**a**	2.843±0.4674**b**	4.3498±0.9399**ab**	**0.03349***	0.2482
Phosphorus cycling					
ppk	0.0033±0.0003**a**	0.0054±0.0005**b**	0.0058±0.0007**b**	**0.00202****	0.2317
pqqC	43.0588±6.1409	36.2675±4.0166	46.4±6.8205	0.28103	0.3732
ppx	2.0473±0.1936**a**	2.5449±0.2925**ab**	2.4981±0.1823**b**	**0.04283***	0.1647
gcd	3.8908±0.3474	3.6848±0.2599	4.5347±0.4142	0.2473	0.2709
phoX	0.0898±0.019	0.0987±0.0259	0.0566±0.0133	0.06155•	0.3379
phoD	141.2534±19.4513	88.4822±10.2453	106.625±12.8122	0.15613	0.5028
phnK	324.499±31.3157	263.9662±19.1754	302.8465±22.2941	0.29731	0.3630
Nitrogen cycling					
amoA1	139.12±24.1298**a**	204.3204±41.61**ab**	233.0673±37.03**b**	**0.02357***	0.3853

nifH	19.7102±4.4438**a**	33.1546±5.8054**ab**	31.0122±5.518**b**	**0.00043**	0.4789
hzsB	0.003±0.0004	0.0072±0.0027	0.0049±0.0007	0.24149	0.0572
gdhA	55.3592±6.5241**a**	67.0413±6.6871**ab**	80.9474±11.0255**b**	**0.00992****	0.2901
nosZ1	0.9536±0.1289**ab**	1.0135±0.1183**a**	1.1501±0.1573**b**	**0.00681****	0.4614
nirS3	0.3537±0.0384**a**	0.4379±0.0237**b**	0.4355±0.0263**b**	**0.02497***	0.1957
nirK1	0.1859±0.0254	0.224±0.0295	0.2315±0.0371	0.13686	0.5286
nosZ2	4.3954±0.4186**a**	4.5234±0.3908**a**	5.5286±0.6223**b**	**0.00946****	0.3504
amoB	0.1015±0.0104	0.086±0.0059	0.1374±0.0206	0.0881•	0.05914
hao	0.1009±0.0869	0.0362±0.009	0.0297±0.0044	0.96943	0.0731
ureC	1149.7317±108.1359	958.1688±60.8789	1111.212±86.7563	0.31492	0.4221
nirS2	0.4783±0.1292	0.3595±0.0635	0.5989±0.2191	0.5741	0.2479
nirS1	0.8102±0.2268	0.5077±0.0781	0.7094±0.2006	0.4622	0.2482
nirK3	11.0054±1.1185	8.3352±0.7031	9.5947±0.915	0.05741•	0.1946
nirK2	1.3397±0.1426	1.0497±0.1293	1.3226±0.2821	0.45319	0.1287
nxrA	6.3155±1.1939**a**	3.117±0.5805**b**	4.0523±0.6942**b**	**0.0028****	0.2681
amoA2	3.0581±0.4803**a**	1.3376±0.2539**b**	1.7233±0.4282**b**	**0.00005*****	0.4021
Sulphur cycling					
dsrB	0.302±0.079**a**	0.8374±0.2239**ab**	0.7423±0.2436**b**	**0.01396**	0.3340
apsA	0.1647±0.0407**a**	0.293±0.0671**ab**	0.3976±0.135**b**	**0.00264**	0.4922
soxY	3.3946±0.6845	3.2781±0.5072	3.8907±0.7752	0.11931	0.4084
dsrA	15.0923±2.7806	17.5109±3.7249	21.3789±6.3913	0.25219	0.2514
yedZ	2.3901±0.2191	2.6482±0.2119	2.7528±0.1952	0.27264	0.2372

Values represent the mean ± standard error of each holm oak category. P-values in bold asterisks (*, p-value < 0.05; **, p-value < 0.01; ***, p-value < 0.001) represent statistically significant differences according to the linear mixed-effects models (LMEs). Points indicates marginally significant differences (•, p-value<0.1). Small caps letters indicate statistically significant differences among categories according to the Tukey multiple pairwise comparisons test. R2c represents the variance explained by the fixed and random effects. Values in bold indicate significant relationships.

Table S6.3. Results of the linear mixed-effect models (LMEs) in which the functional-gene relative abundance of the different biogeochemical cycles: carbon cycling (carbon hydrolysis, carbon fixation, methane metabolism), phosphorus cycling, nitrogen cycling and sulfur cycling were fitted as a function of belowground and aboveground tree compartment.

Belowground effects (PC1)					**Aboveground effects (crown health, PC2)**				
Response	χ^2	Df	p-value	R^2c	Response	χ^2	Df	p-value	R^2c
Carbon hydrolysis									
amyA	0.0056	1	0.9406	0.0667	*amyA*	0.3828	1	0.5361	0.0778
apu	0.1441	1	0.7043	0.1157	*apu*	1.0189	1	0.3128	0.1185
sga	0.1176	1	0.7316	0.1843	*sga*	0.1498	1	0.6987	0.1714
iso_plu	0.3138	1	0.5753	0.1177	*iso_plu*	8.9941	1	**0.0027****	0.2472
abfA	0.9972	1	0.318	0.3061	*abfA*	0.5528	1	0.4572	0.2584
manB	5.0907	1	**0.0241***	0.339	*manB*	0.0562	1	0.8125	0.3094
xylA	0.2316	1	0.6304	0.0635	*xylA*	0.1548	1	0.694	0.0619
cex	5.4948	1	**0.0191***	0.545	*cex*	0.5437	1	0.4609	0.5136
chiA	3.2697	1	0.0706•	0.5287	*chiA*	1.2031	1	0.2727	0.5144
pgu	0.0014	1	0.9704	0.2055	*pgu*	0.0025	1	0.9604	0.2073
lig	1.1419	1	0.2853	0.3777	*lig*	8.4003	1	**0.0038****	0.3731
glx	0.5248	1	0.4688	0.1548	*glx*	0.8111	1	0.3678	0.1468
mnp	0.0208	1	0.8854	0.0964	*mnp*	0.2825	1	0.5951	0.096
Carbon fixation									
accA	0.5462	1	0.4599	0.2106	*accA*	0.3737	1	0.541	0.1712
aclB	0.0037	1	0.9513	0.1651	*aclB*	4.8204	1	**0.0281***	0.1774
acsA	0.0031	1	0.9559	0.4154	*acsA*	2.9667	1	0.085•	0.4084
acsB	0.3066	1	0.5798	0.1269	*acsB*	0.0553	1	0.8142	0.1239
acsE	0.3907	1	0.5319	0.3103	*acsE*	2.9635	1	0.0852•	0.2977
frdA	5.4659	1	**0.0194***	0.5984	*frdA*	4.3632	1	**0.0367***	0.529
korA	0.9152	1	0.3387	0.2183	*korA*	4.9623	1	0.0259	0.1874
mct	1.8756	1	0.1708	0.1463	*mct*	0.13	1	0.7184	0.1404
pccA	0.5625	1	0.4533	0.1088	*pccA*	4.5862	1	**0.0322***	0.1103
rbcL	0.067	1	0.7958	0.5019	*rbcL*	2.9948	1	0.0835•	0.4902
smtA	0.2816	1	0.5957	0.1777	*smtA*	2.5621	1	0.1095	0.2056
Methane metabolism									
mxaF	1.0192	1	0.3127	0.2998	*mxaF*	0.3374	1	0.5614	0.3059
pqq-mdh	0.1163	1	0.7331	0.2799	*pqq_mdh*	0.4514	1	0.5017	0.2613
mmoX	0.2577	1	0.6117	0.0377	*mmoX*	4.9942	1	**0.0254***	0.0937
pmoA	4.5716	1	**0.0325***	0.3326	*pmoA*	0.9192	1	0.3377	0.3099
Phosphorus cycling									
phnK	0.0475	1	0.8276	0.3811	*phnK*	0.5045	1	0.4775	0.3685
phoD	0.7078	1	0.4002	0.5213	*phoD*	0.519	1	0.4713	0.5046
phoX	0.2797	1	0.5969	0.2513	*phoX*	0.2022	1	0.6529	0.2437
gcd	0.4117	1	0.5211	0.2856	*gcd*	1.6995	1	0.1924	0.2447
pqqC	0.0252	1	0.8739	0.4235	*pqqC*	4.8022	1	**0.0284***	0.4315
ppk	1.4028	1	0.2363	0.2079	*ppk*	0.5433	1	0.4611	0.2002
ppx	0.7008	1	0.4025	0.1407	*ppx*	4.4154	1	**0.0356***	0.1308
Nitrogen cycling									
nifH	0.0034	1	0.9535	0.5725	*nifH*	5.7583	1	**0.0164***	0.6266
amoA1	2.0894	1	0.1483	0.4735	*amoA1*	1.6612	1	0.1974	0.4303

amoA2	1.2009	1	0.2731	0.4415	*amoA2*	0.4644	1	0.4956	0.4512
amoB	0	1	0.9952	0.0596	*amoB*	1.4967	1	0.2212	0.0707
hao	0.0114	1	0.9151	0.1495	*hao*	0.7725	1	0.3794	0.1602
nxrA	0.1218	1	0.7271	0.3671	*nxrA*	1.9556	1	0.162	0.5084
nirK1	0.1598	1	0.6893	0.3422	*nirK1*	4.6882	1	**0.0304***	0.4269
nirK2	1.9586	1	0.1617	0.1745	*nirK2*	0.0112	1	0.9157	0.1724
nirK3	0.0432	1	0.8353	0.0965	*nirK3*	0.0312	1	0.8598	0.0943
nirS1	0.0419	1	0.8377	0.1321	*nirS1*	0.5338	1	0.465	0.1457
nirS2	0.3087	1	0.5785	0.1444	*nirS2*	0.8302	1	0.3622	0.1545
nirS3	0.9469	1	0.3305	0.2684	*nirS3*	4.93	1	**0.0264***	0.2716
nosZ1	1.4575	1	0.2273	0.3079	*nosZ1*	2.7739	1	0.0958•	0.3671
nosZ2	0.5656	1	0.452	0.2864	*nosZ2*	3.4222	1	0.0643•	0.3356
ureC	0.2732	1	0.6012	0.4618	*ureC*	0.6352	1	0.4254	0.4443
hzsB	2.0155	1	0.1557	0.0588	*hzsB*	2.3438	1	0.1258	0.0804
gdhA	0.3429	1	0.5582	0.302	*gdhA*	0.7395	1	0.3898	0.3261
Sulfur cycling									
apsA	0	1	0.9953	0.4528	*apsA*	3.1679	1	0.0751•	0.4959
dsrA	0.3509	1	0.5536	0.2304	*dsrA*	0.7366	1	0.3907	0.2616
dsrB	0.0514	1	0.8207	0.3092	*dsrB*	8.0418	1	**0.0046****	0.4154
soxY	0.7846	1	0.3757	0.4418	*soxY*	4.084	1	**0.0433***	0.433
yedZ	0.1469	1	0.7016	0.3245	*yedZ*	4.4571	1	**0.0348***	0.3001

R^2 conditional (R^2_c), indicates the variance explained by the fixed and random effects. Asterisks (*, p-value < 0.05; **, p-value < 0.01) indicate statistically significant effects, while points indicate marginal significant effects (•, p-value <0.1).

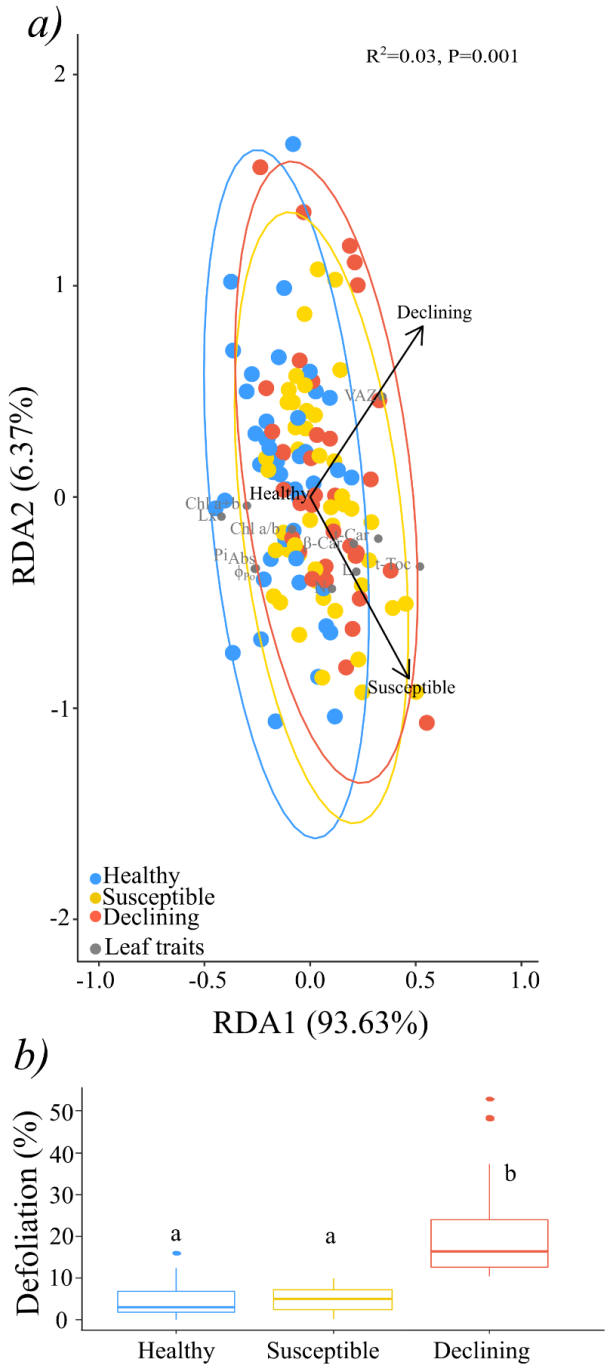

Figure S5.1. Redundancy analysis plot conducted with leaf traits (panel a) and boxplot of defoliation (panel b). Panel a: *i)* chlorophyll a fluorescence induction variables (i.e., photochemical efficiency (φ_{Po}) and potential performance index for energy conservation (Pi_{Abs})), *ii)* pigments variables (total chlorophyll pool (Chl a+b, µmol m^{-2}), a to b chlorophyll ratio (Chl a/b, mol mol^{-1}), neoxanthin (N, mmol mol^{-1} Chl, lutein (L, mmol mol^{-1} Chl), lutein-epoxide (Lx, mmol mol^{-1} Chl), β-carotene (β-Car, mmol mol^{-1} Chl), total xanthophyll pool (VAZ, mmol mol^{-1} Chl)), total carotenoid pool (t-Car, mmol mol^{-1} Chl); and *iii)* total tocopherols (t-Toc, mmol mol^{-1} Chl) using the constrained axes RDA1 and RDA2. Health statuses of the holm oak trees are marked in blue (healthy), yellow (susceptible) and red (declining). Panel b shows boxplots of defoliation (%). Box represents 50% of data (n = 43-53 trees per health status) distribution between the first and the third quartile; the central line represents the median; the upper and below whiskers cover the 1.5 interquartile range. Different letters indicate statistically significant differences between the different health statuses based on the Tukey multiple pairwise comparisons test.

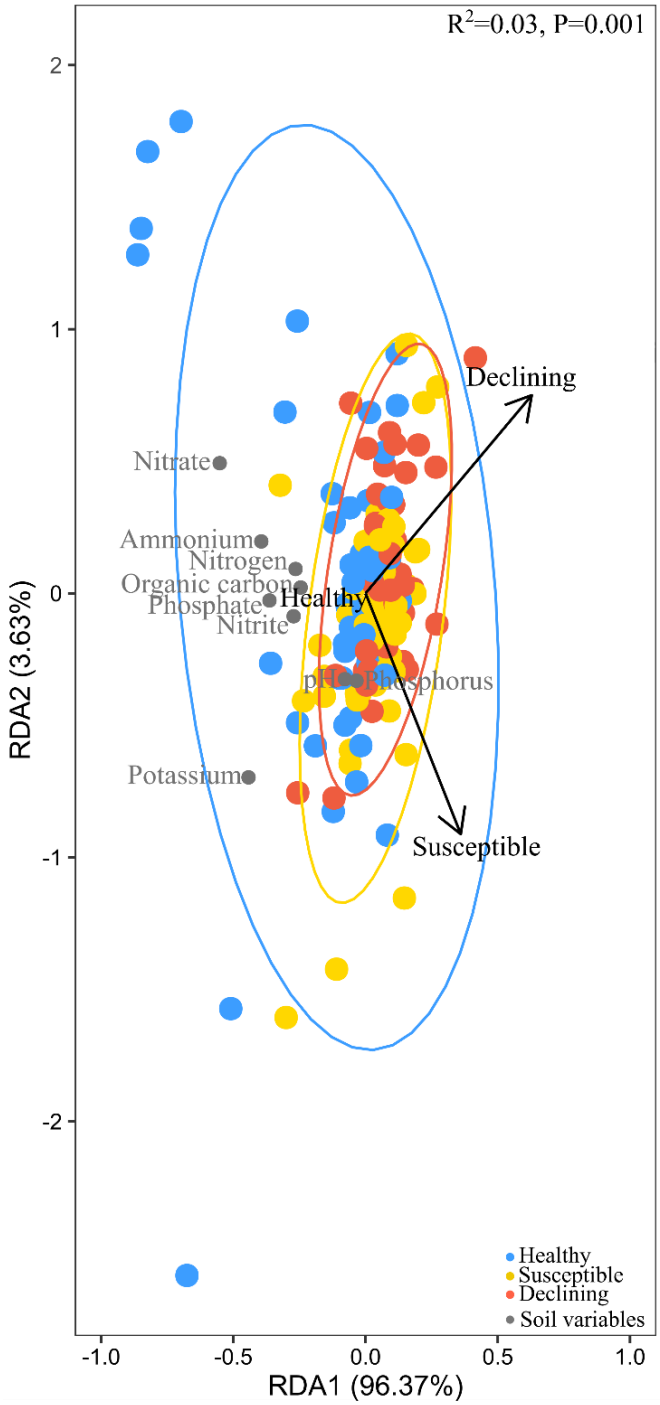

Figure S5.2. Redundancy analysis plot conducted with soil variables. Ammonium, nitrate, nitrite, phosphate, potassium (µg g^{-1}) and organic carbon, nitrogen, phosphorus (%) and pH using the axes RDA1 and RDA 2. Health statuses of the holm oak trees are marked in blue (healthy), yellow (susceptible) and red (declining).

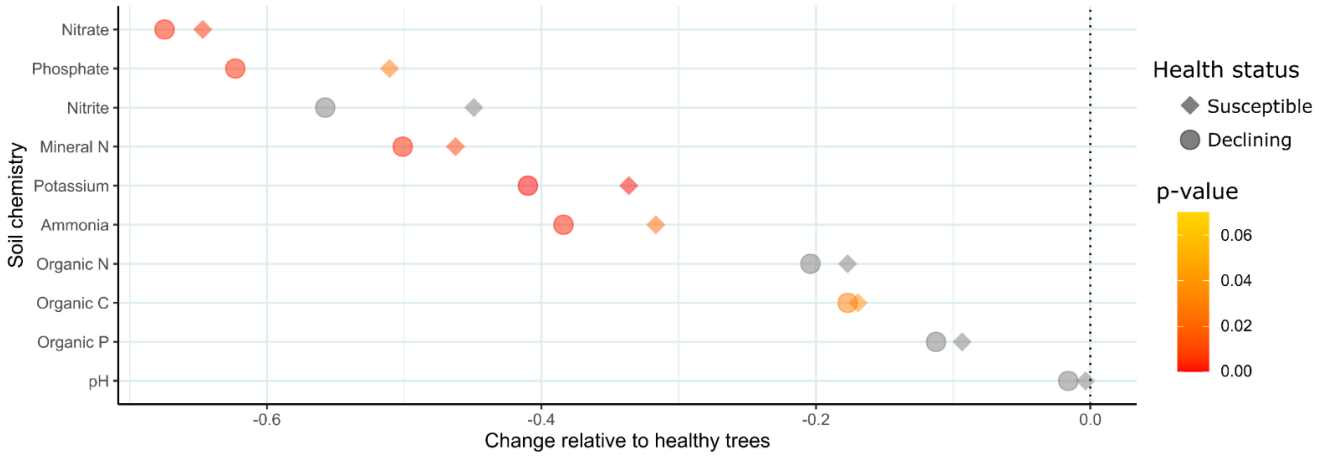

Figure S6.1. Scatter plot showing the change in the soil chemical properties of the susceptible (n=59) and declining (n=49) holm oak trees relative to the healthy (n=54) holm oak trees. Change relative to healthy trees was calculated using the estimated mean of post-hoc tests from the LMEs for each health status. P-values are indicated from red ($p \leq 0.001$) to yellow ($p \leq 0.07$) and they were extracted from the pairwise differences in health status.

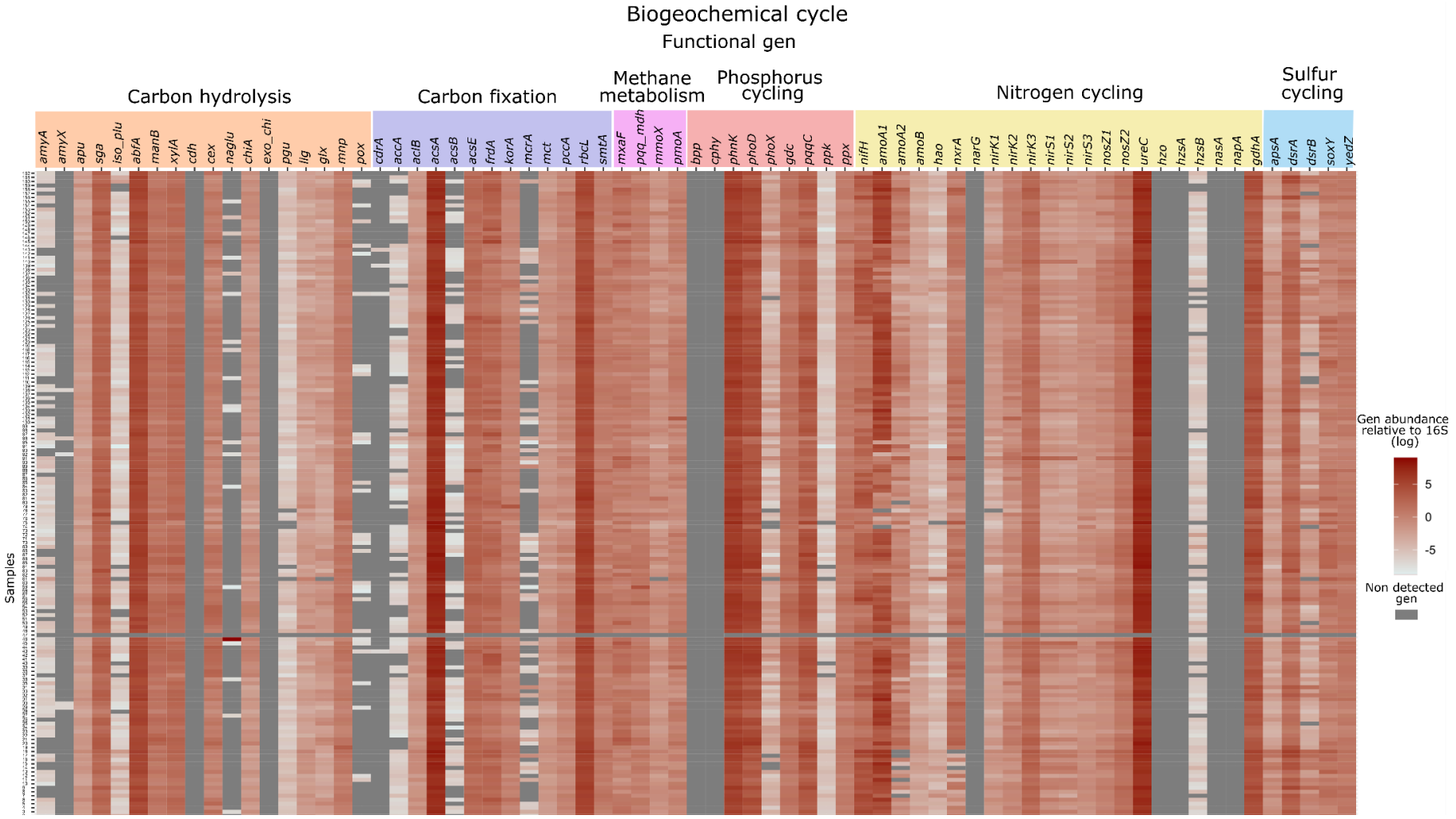

Figure S6.2. Heatmap analyses of gen abundance relative to the 16S rRNA gene. Genes were arranged by their role in the 6 biogeochemical cycles (i.e. carbon hydrolysis and fixation, methane metabolism, phosphorous cycling, nitrogen cycling and sulfur cycling). These values were logarithmically transformed. Gen abundance is represented by the intensity of the colour, with red indicating high abundance and white indicating low abundance. The grey colour indicates non-detected genes. Soil samples for each of the 162 holm oak trees are represented vertically.